

University of Nevada, Reno

**Developmental physiology, nitrogen preference, and estimated biofuel  
production of *Opuntia ficus-indica* (prickly pear cactus) in the United States**

A dissertation submitted in partial fulfillment  
of the requirements for the degree of  
Doctor of Philosophy in Biochemistry

By

Nicholas A. Niechayev

Dr. John C. Cushman / Dissertation Advisor

December 2021

Copyright by Nicholas A. Niechayev 2021

All Rights Reserved



THE GRADUATE SCHOOL

We recommend that the dissertation prepared  
under our supervision by

**Nicholas A. Niechayev**

Entitled

**Developmental physiology, nitrogen preference, and estimated biofuel production of  
*Opuntia ficus-indica* (prickly pear cactus) in the United States**

be accepted in partial fulfillment of the requirements  
for the degree of

DOCTOR OF PHILOSOPHY

John C. Cushman  
*Advisor*

Grant R. Cramer  
*Committee Member*

Claire Heinitz  
*Committee Member*

Ian S. Wallace  
*Committee Member*

Elizabeth Leger  
*Graduate School Representative*

David W. Zeh, Ph. D., Dean,  
*Graduate School*

December, 2021

## Abstract

*Opuntia ficus-indica* (Prickly pear cactus) is a large succulent cactus species that has a long history of agricultural production for carmine dye, fruits, and edible young cladodes. As a CAM plant *O. ficus-indica* uses crassulacean acid metabolism (CAM) which is characterized by assimilation of CO<sub>2</sub> at night, which greatly increases water use efficiency. More recently, *O. ficus-indica* has been recognized as having high biomass and biogas (CH<sub>4</sub>) production values comparable to other large CAM species. *Opuntia eliator*, a closely related tropical epiphyte species, has been shown to predominantly use C<sub>3</sub> photosynthesis in seedlings before switching to CAM photosynthesis. Similarly, young cladodes in *Opuntia ficus-indica* have been shown to predominantly fix CO<sub>2</sub> during the day until they mature. Some plants can also switch to CAM photosynthesis when preferred nitrogen sources (nitrate or ammonium) become limiting and *O. ficus-indica* has been shown to have a slight increase in nitrogen uptake in ammonium vs. nitrate. A field trial, and life cycle assessment has been conducted on biogas production from *O. ficus-indica* in Mexico, but biogas production values in the United States are unknown. Here, measured carbon isotope ratios, 24-hour gas exchange, and tissue acidity in *O. ficus-indica* seedlings and daughter cladodes to determine the occurrence of CAM vs. C<sub>3</sub> photosynthesis. Results demonstrated that *O. ficus-indica* seedlings used predominantly CAM photosynthesis to assimilate CO<sub>2</sub> even under well-watered conditions, while developing cladodes were shown to be sink tissues that switched directly from C<sub>3</sub> photosynthesis to CAM photosynthesis in greenhouse conditions. Here, N preference was



investigated by placing *O. ficus-indica* cladodes in sand culture and providing nutrient solutions with varying amounts of nitrate and ammonium for one month, and measuring differences in growth, biochemistry, and CAM and N-related gene expression. Statistical differences in *O. ficus-indica* growth, chlorophyll content, tissue acidity, soluble sugars, nitrate reductase activity, nitrate and ammonium content, glyoxylic acid content, N:C ratio and relative expression of genes involved N metabolism, and CAM activity were all detected when nitrate and ammonium were varied in sand culture. A life cycle inventory of biogas production from *O. ficus-indica* was built using results from an irrigation field trial that took place in Logandale, NV. Estimated biogas production from *O. ficus-indica* in the United States was 13,004.29-26,877.85 Nm<sup>3</sup> ha<sup>-1</sup> yr<sup>-1</sup> produced from plants receiving 716 mm year<sup>-1</sup> which is comparable to that of actual production values in Mexico.

## Table of Contents

<i>Abstract</i> .....	<i>i</i>
<i>List of Tables</i> .....	<i>v</i>
<i>List of Figures</i> .....	<i>vi</i>
<b>Chapter 1: Introduction</b> .....	<b>1</b>
State of our environment .....	1
Plant photosynthesis .....	2
Crassulacean acid metabolism .....	5
<i>Opuntia ficus-indica</i> .....	10
Estimating <i>Opuntia ficus-indica</i> global productivity.....	12
Nitrogen metabolism in <i>Opuntia ficus-indica</i> .....	14
<i>Opuntia ficus-indica</i> as a biofuel feedstock.....	16
Estimating global impact of <i>Opuntia ficus-indica</i> production pathways.....	17
Developmental physiology, nitrogen preference, and estimates of biofuel production in <i>Opuntia ficus-indica</i> .....	19
Figures .....	20
References.....	22
<b>Chapter 2: Developmental Dynamics of Crassulacean Acid Metabolism (CAM) in <i>Opuntia ficus-indica</i></b> .....	<b>39</b>
Abstract .....	39
Introduction .....	40
<b>Methods</b> .....	<b>46</b>
<i>Opuntia ficus-indica</i> seed collection, cleaning, and germination .....	46
Titratable acidity and isotopic mass spectrometric analysis of <i>O. ficus-indica</i> seedlings.....	48
Seedling gas exchange measurements .....	50
Daughter cladode titratable acidity and isotopic mass spectrometric analysis .....	52
Daughter cladode gas exchange measurements .....	53
Statistical Analysis.....	54
<b>Results</b> .....	<b>57</b>
CAM development in seedlings.....	57
CAM development in daughter cladodes.....	60
<b>Discussion</b> .....	<b>61</b>
<b>Acknowledgments</b> .....	<b>67</b>
<b>Tables</b> .....	<b>68</b>
<b>Figures</b> .....	<b>69</b>
References.....	76
<b>Chapter 3: The nitrogen preference of <i>Opuntia ficus-indica</i>: a sand culture snapshot</b> .....	<b>86</b>

<b>Abstract .....</b>	<b>86</b>
<b>Introduction .....</b>	<b>87</b>
<b>Methods .....</b>	<b>93</b>
Greenhouse experimentation and sample collection.....	93
Growth measurements .....	94
Relative water content.....	94
Chlorophyll content .....	95
Titratable acidity .....	96
Starch content and soluble sugars .....	97
Nitrate reductase activity .....	98
Nitrate content.....	99
Ammonium content Glyoxylic acid content .....	100
Carbon and Nitrogen content .....	101
RT-qPCR of CAM and nitrogen related genes .....	101
Statistical analysis.....	103
<b>Results.....</b>	<b>103</b>
Growth measurements and relative water content. ....	103
Biochemical analyses.....	104
<b>Discussion .....</b>	<b>108</b>
<b>Acknowledgements .....</b>	<b>115</b>
<b>Tables .....</b>	<b>116</b>
<b>Figures .....</b>	<b>121</b>
<b>References.....</b>	<b>145</b>
<b><i>Chapter 4: A life cycle inventory of estimated biogas and bioethanol production from an Opuntia ficus-indica field trial in the United States.....</i></b>	<b><i>156</i></b>
Abstract .....	156
Introduction .....	156
Methods .....	160
Results.....	162
Discussion .....	163
Tables .....	168
Figures .....	170
References.....	173
<b><i>Chapter 5: Concluding Remarks.....</i></b>	<b><i>181</i></b>
Conclusion .....	185
References.....	186
<b><i>Appendix: Supplemental figures for chapter 2.....</i></b>	<b><i>189</i></b>
<b><i>Curriculum vitae .....</i></b>	<b><i>247</i></b>

## List of Tables

### **Chapter 2**

**Table 1:**  $\delta^{13}\text{C}$  ‰ ratio value ranges observed in C3, C4, and CAM. .... 68

**Table 2:** Three-way ANOVA results of Tissue acidity..... 68

### **Chapter 3**

**Table 1:** Recipes for nutrient working solutions. .... 116

**Table 2:** Treatment recipes..... 116

**Table 3:** The factorial  $\text{NO}_3^-$  and  $\text{NH}_4^+$  design. .... 117

**Table 4:**List of primers..... 117

**Table 5:** One-way ANOVA results of growth and relative water content..... 117

**Table 6:** One-way ANOVA results of biochemistry measurements ..... 119

**Table 7:** One-way ANOVA results of relative gene expression ..... 119

### **Chapter 4**

**Table 1:** *Opuntia ficus-indica* life cycle inventory and biofuel production.....168

## List of Figures

### Chapter 1

<b>Figure 1:</b> A simplified model of CAM .....	20
--	----

### Chapter 2

<b>Figure 1:</b> Daughter cladode chamber and seedling germination .....	69
--	----

<b>Figure 2:</b> Seedling tissue acidity and $\delta^{13}\text{C}$ ‰.....	70
---	----

<b>Figure 3:</b> Well watered PAR 100 gas exchange .....	71
--	----

<b>Figure 4:</b> Dry PAR 100 seedling gas exchange .....	72
--	----

<b>Figure 5:</b> PAR 300 seedling gas exchange .....	73
--	----

<b>Figure 6:</b> Daughter cladode tissue acidity and $\delta^{13}\text{C}$ ‰ .....	74
--	----

<b>Figure 7:</b> Daughter cladode gas exchange .....	75
--	----

### Chapter 3

<b>Figure 1:</b> Cladode length.....	121
--------------------------------------	-----

<b>Figure 2:</b> Cladode width.....	121
-------------------------------------	-----

<b>Figure 3:</b> Cladode Thickness.....	122
---	-----

<b>Figure 4:</b> New cladode number.....	123
--	-----

<b>Figure 5:</b> Primary root number.....	123
---	-----

<b>Figure 6:</b> Average primary root Length. ....	124
--	-----

<b>Figure 7:</b> Relative water content. ....	124
---	-----

<b>Figure 8:</b> Chlorophyll content combined. ....	125
---	-----

<b>Figure 9:</b> Chlorophyll a + b content.....	126
---	-----

<b>Figure 10:</b> Chlorophyll a content. ....	126
---	-----

<b>Figure 11:</b> Chlorophyll b content. ....	127
---	-----

<b>Figure 12:</b> Titratable acidity (pH 7) .....	127
<b>Figure 13:</b> Titratable acidity (pH 8.4). .....	128
<b>Figure 14:</b> Starch content. ....	129
<b>Figure 15:</b> Soluble sugars.....	130
<b>Figure 16:</b> Glucose content. ....	131
<b>Figure 17:</b> Fructose content.....	131
<b>Figure 18:</b> Sucrose content.....	132
<b>Figure 19:</b> Nitrate reductase activity.....	132
<b>Figure 20:</b> Nitrate content. ....	133
<b>Figure 21:</b> Ammonium content.....	133
<b>Figure 22:</b> Glyoxylic acid content.....	134
<b>Figure 23:</b> N:C ratio. ....	134
<b>Figure 24:</b> Percent carbon. ....	135
<b>Figure 25:</b> Percent Nitrogen.....	135
<b>Figure 26:</b> N metabolism, and CAM related relative gene expression. ....	136
<b>Figure 27:</b> Relative expression of aluminum-activated malate transporter (ALMT).....	137
<b>Figure 28:</b> Relative expression of phosphoenolpyruvate carboxylase (PPC1)..	138
<b>Figure 29:</b> Relative expression of phosphoenolpyruvate carboxylase kinase (PPCK).....	139
<b>Figure 30:</b> Relative expression of nitrate reductase (NR).....	139
<b>Figure 31:</b> Relative expression of nitrite reductase (NiR) .....	140
<b>Figure 32:</b> Relative expression of glutamate synthase (GOGAT) .....	141

<b>Figure 33:</b> Relative expression of asparagine synthase (AS).....	141
<b>Figure 34:</b> Relative expression of glutamate dehydrogenase (GDH460) .....	142
<b>Figure 35:</b> Relative expression of GDH (GDH201910) .....	143
<b>Figure 36:</b> Relative expression of glutamine synthase (GS30900).....	143
<b>Figure 37:</b> Relative expression of glutamine synthetase (GS94700).....	144
<b><u>Chapter 4</u></b>	
<b>Figure 1:</b> Opuntia Spp. productivity under varying irrigation inputs. ....	170
<b>Figure 2:</b> Nevada Overton power district energy source break down. ....	171
<b>Figure 3:</b> Contribution of different fuels to the electricity mix in Mexico. ....	172
<b>Chapter 2 Supplemental Figures 1-62</b> .....	189

## Chapter 1

# Introduction

## State of our environment

Conveniences of the 21<sup>st</sup> century have made it easy to forget the connections between our environment and the commodities upon which we depend. The reality is that overall socio-economic performance is nested in the sustainable production of natural products from our ecological systems (Purvis et al., 2019). Ecological systems can be defined by the species composition at any point in time (Oliver et al., 2015), and human caused changes in climate, land use, and habitat quality can cause biodiversity loss to an extent that ecological systems might never return to prior equilibrium states.

Today, human activity is pushing the limits on nine proposed planetary boundaries (Steffen et al., 2015; O'Neill et al., 2018) that directly and indirectly have detrimental effects on ecological systems around the globe. These boundaries include climate change, biosphere integrity, land use changes, freshwater availability, biogeochemical flows (nitrogen and phosphorous cycles), ocean acidification, atmospheric aerosol loading, stratospheric ozone depletion, and the introduction of novel entities, such as invasive or genetically modified species, and chemicals with unknown effects. In the current state, high-risk boundaries of genetic diversity loss, phosphorus release, and nitrogen release have already been crossed.

Currently, global deserts, or regions where total surface water loss exceeds the surface water gain through precipitation, make up close to 40% of global land



area (Warner, 2009). Approximately 50% of the global land area is considered arid, semi-arid, or dry sub-humid (Zika and Erb, 2009). Desertification, or the process by which fertile grounds become desert due to deforestation, drought, and detrimental agricultural practices are now affecting an estimated one fifth of the global population (Geist, 2017). Global climate change in particular is projected to increase drought intensity by 30%, and result in a 5-fold increase in water demand in the 21<sup>st</sup> century (Naumann et al., 2018). In addition, climate change in combination with intense water use is causing a reduction in ground water stores (Cuthber et al., 2019). Agriculture accounts for 70% of global water demand (McDaniel et al., 2017), even though 95% of all crops are rainfed (Hadebe et al., 2017). Globally, 11% of croplands, and 10% of grass lands used for agriculture and livestock production are vulnerable to a reduction in water availability, particularly in Africa, Europe, and Asia (Fitton et al., 2019). In addition, each degree-Celsius increase in global mean temperature would also, on average, reduce global yields of wheat by 6.0%, rice by 3.2%, maize by 7.4%, and soybean by 3.1% (Zhao et al., 2017).

### Plant photosynthesis

Of all the natural products that humans depend upon, those derived from agriculture are perhaps the most fundamental. Plants provide building materials for homes (Berge, 2007), fibers for textiles (Xu-fu, 2003), medicinal drug discoveries (Süntar, 2020), sources of bioenergy (Reid et al., 2020), food and fodder, and many other products that are economically valuable and crucial for a

high quality of life. Additionally, plants play a role in maintaining global greenhouse gases, as land use changes associated with deforestation, logging, and modern cultivation practices caused a net CO<sub>2</sub> release of 1.5 +/- 0.7 Gt of C yr<sup>-1</sup> into the atmosphere from 1990 to 2005 (Le Quéré et al., 2009). However, an estimated annual 10<sup>11</sup> tons of global atmospheric carbon is also fixed by an enzyme known as D-ribulose-1,5-bisphosphate carboxylase/oxygenase (RUBISCO) by C<sub>3</sub> photosynthetic plant species (Hennacy and Jonikas, 2020). Thus, fixation by plant capture an estimated 25% of global carbon emissions

In traditional C<sub>3</sub> photosynthesis, RUBISCO combines ribulose-1,5-bisphosphate with a single molecule of CO<sub>2</sub> to form a six-carbon molecule that is quickly hydrolyzed into two molecules of 3-phosphoglycerate (Taiz et al., 2015). The resulting 3-phosphoglycerate molecules enter the Calvin-Benson-Bassham cycle, which ultimately regenerates more ribulose-1,5-bisphosphate to continue CO<sub>2</sub> assimilation by RUBISCO. Globally, an estimated 85% of all plants use C<sub>3</sub> photosynthesis, 5% use C<sub>4</sub> photosynthesis, and the remaining 10% use CAM photosynthesis (Kumar et al., 2017).

While most plants use C<sub>3</sub> photosynthesis, there are several trade-offs to using primarily RUBISCO for CO<sub>2</sub> assimilation. The first is that RUBISCO will occasionally fix O<sub>2</sub> instead of CO<sub>2</sub>, which forms 2-phosphoglycolate (Busch, 2020). 2-Phosphoglycolate is converted into glyoxylate, which must be shuttled between the chloroplast, peroxisome, and mitochondria to be metabolized in an energetically costly process known as photorespiration. The second is that RUBISCO discriminates against the fixation of CO<sub>2</sub> containing C<sup>13</sup> isotopes

(O'Leary, 1988) except under water-limited conditions in which stomata are closed, in which case RUBISCO fixes all remaining CO<sub>2</sub> readily available (Leavitt et al., 2007). The third is the relative size of RUBISCO (560 kDa) and abundance of making up 30% of soluble protein and 25% of total leaf nitrogen (von Caemmerer and Quick, 2000), which requires a considerable N demand to maintain non-limiting RUBISCO concentrations. The fourth is the inherently slow catalytic turnover rate of about 3.5 s<sup>-1</sup> per catalytic site at saturated CO<sub>2</sub> levels (Hennacy and Jonikas, 2020). Lastly, RUBISCO requires light for activation, and therefore, can only fix CO<sub>2</sub> during the day when sunlight is available.

Both C<sub>4</sub> photosynthetic and CAM pathways avoid the limitations associated with RUBISCO by first assimilating CO<sub>2</sub> into bicarbonate with carbonic anhydrase (CA) and then phosphoenolpyruvate carboxylase (PEPC), which combines the resulting bicarbonate with phosphonyl-pyruvate (PEP) to form oxaloacetate (Cousins et al., 2007; Males and Griffiths, 2017). Compared with RUBISCO, CA/PEPC has a 60-fold higher reaction rate, readily fixes <sup>12</sup>CO<sub>2</sub> and <sup>13</sup>CO<sub>2</sub> isotopes, and does not fix O<sub>2</sub>, suppressing limitations due to photorespiration (Lerman et al., 1974; Lüttge, 2002; Rodrigues et al., 2014). The C<sub>4</sub> photosynthetic pathway is characterized by a specialized interwoven anatomy and biochemistry that concentrates CO<sub>2</sub> into RUBISCO-containing cells eliminating photorespiration (Hatch, 1987). In C<sub>4</sub> photosynthesis, atmospheric CO<sub>2</sub> is fixed in mesophyll cells by CA/PEPC into malate. Malate is then shuttled into bundle sheath cells where it is decarboxylated. The decarboxylated CO<sub>2</sub> is then refixed by RUBISCO as in the normal C<sub>3</sub> photosynthetic pathway.

Interestingly, the C<sub>4</sub> photosynthetic pathway is thought to have beneficial advantages under higher temperatures (Hennacy and Jonikas, 2020) where in C<sub>3</sub> photosynthetic plants CO<sub>2</sub> diffuses more readily out of the cell into large extracellular spaces, leaving a higher ratio of O<sub>2</sub> to be fixed by RUBISCO. In contrast, in C<sub>4</sub> plants, the carbon concentrating mechanisms in the bundle sheath cells limit photorespiration and improve water-use efficiency (WUE) defined as unit carbon gained per unit water lost.

### Crassulacean acid metabolism

CAM photosynthesis also assimilates atmospheric CO<sub>2</sub> with PEPC, but unlike C<sub>4</sub> photosynthesis, the carboxylation and decarboxylation steps are temporally separated by a specialized diel circadian rhythm instead of a spatial separation made possible by specialized Kranz anatomy (Ting, 1985). Rather than opening stomata during the day as C<sub>3</sub> and C<sub>4</sub> photosynthetic plants do, obligate CAM plants keep stomata closed during all or part of the day, and open stomata at night. Nocturnal carbon assimilation is achieved by CA/PEPC, and fixed carbon is ultimately stored in the vacuole as malic acid until daybreak (Figure 1). During the day while stomata are closed, malic acid is transported back into the cytosol where it is decarboxylated by either cytosolic PEP carboxykinase (PEPCK) or NAD(P)-malic enzyme (ME) and freed CO<sub>2</sub> is refixed by RUBISCO in chloroplasts while sunlight is available (Silvera et al., 2010). The carboxylation, decarboxylation, and active transport of organic acids across vacuole membranes requires additional metabolic energy compared with C<sub>3</sub>

photosynthesis (Lüttge, 2002). However, a contemporary computational model has demonstrated that this energy cost may be compensated by the carbon-concentrating mechanism of day time malate decarboxylation, especially under high light scenarios (Shameer et al., 2018). This diel circadian is often described taking place in four different phases, which are:

Phase 1: At (mid)night when stomata are open, CO<sub>2</sub> assimilation is occurring, and malate content is building up.

Phase 2: At dawn when the sun rises; and a small spike of CO<sub>2</sub> assimilation occurs by both CA/PEPC and light activated RUBISCO fixing CO<sub>2</sub> at the same time.

Phase 3: Sun is up, stomata are shut, and CO<sub>2</sub> is not being assimilated while malate content decreases with decarboxylation.

Phase 4: at dusk when the sun is setting, and a brief period of CO<sub>2</sub> assimilation occurs as the stomata open and both CA/PEPC and light activated RUBISCO fixes CO<sub>2</sub> until light is no longer available.

Like C<sub>4</sub> photosynthetic plants, the main evolutionary advantage is an increase in WUE thanks to carbon-concentrating mechanisms and nocturnal CO<sub>2</sub> assimilation. By opening stomata at night, CAM plants are able to fix CO<sub>2</sub> with a 6-fold higher WUE than that of C<sub>3</sub> photosynthetic plants, and a 4-fold higher WUE than that of C<sub>4</sub> photosynthetic plants (Borland et al., 2009). C<sub>4</sub> photosynthesis and CAM are great examples of convergent evolution, as each are estimated to have evolved independently more than 60 times (Heyduk et al., 2019), and CAM in particular has been found in over 400 distinct genera across

36 families (Smith and Winter, 1996; Borland et al., 2009). Large, succulent cells are thought to be a prerequisite to CAM photosynthesis, as large tonoplast capacity is required for overnight storage of malate. The enlarged cells reduce mesophyll surface area that is exposed to intracellular airspace, reducing CO<sub>2</sub> conductance from the leaves compared to most C<sub>3</sub> plant species, although this trend is not observed in all CAM plant species.

Many coadapted traits are found in CAM plants that also enhance WUE and abiotic stress tolerance. Besides tissue succulence which can increase salinity tolerance and WUE, CAM plants can have dense epidermal trichomes, various water storage organs (bromeliad tanks, orchid pseudobulbs), thick cuticles and epidermal waxes, reduced stomatal density, enhanced stomatal responsiveness, and often rectifier like roots that pull away from the soil when dry to reduce water loss, and quickly return after rain (Niechayev et al., 2019; Pereira et al., 2021).

CAM species can also be separated by the type of decarboxylation enzymes and storage carbohydrates used (Christopher and Holtum, 1996, 1998). For decarboxylation, during the day malate that is released into the cytosol from the tonoplast is decarboxylated by either NAD(P)-malic enzyme (i.e., *Cactaceae* and *Agave*), or NAD(P)-malate dehydrogenase (i.e., *Bromeliaceae* and *Liliaceae*). Plants that use NAD(P)-malic enzyme convert the resulting pyruvate into phosphoenolpyruvate using pyruvate orthophosphate dikinase. Alternatively, some plants convert released malate into oxaloacetate with NAD(P)-malate dehydrogenase, and then oxaloacetate is decarboxylated with phosphoenolpyruvate carboxykinase producing CO<sub>2</sub> and phosphoenolpyruvate.

Eudicot CAM plants typically store carbon as starch, whereas monocot CAM species store carbohydrates in the form of fructans; however, many variations on these general themes occur (Christopher and Holtum, 1996, 1998).

The occurrence of facultative CAM plants, or CAM plants that switch from C<sub>3</sub> photosynthesis to CAM under unfavorable conditions, has led to a further understanding in how C<sub>3</sub> plants might have evolved to perform CAM (Winter et al., 2015). The bimodal distribution of <sup>13</sup>C abundance in several plant families (Silvera et al., 2010; Torres-Morales et al., 2020; Messerschmid et al., 2021) demonstrates that facultative CAM plants occur much less often than plants that use only C<sub>3</sub> photosynthesis or CAM with some exceptions. The occurrence of more C<sub>3</sub> photosynthesis or CAM species may be a result of niche availability strongly favoring one pathway or the other (Silvera et al., 2010; Torres-Morales et al., 2020). However, facultative CAM also provides advantages in regions that receive intermittent droughts as well (Leverett et al., 2021). Also, CAM plants have similar cellular anatomy to that of C<sub>3</sub> photosynthesis plants, and would not need to evolve new, specialized cell types to perform CAM as is the case with Kranz anatomy in C<sub>4</sub> photosynthesis species (Silvera et al., 2014). Indeed, evidence suggests that CAM photosynthetic species have been shown to have appeared in the fossil record long before C<sub>4</sub> photosynthetic species (Hennacy and Jonikas, 2020). The C<sub>3</sub> photosynthesis to CAM transition also requires CAM specific isozymes of enzymes that already occur in C<sub>3</sub> photosynthesis plants.

A developmental switch progression from C<sub>3</sub> photosynthesis to CAM has been observed in *Kalanchoe fedtschenkoi*, which initially performs C<sub>3</sub>

photosynthesis in distal young leaves, but the leaves switch to CAM once the leaves mature (Winter et al., 1982). In *Opuntia eliator*, a tropical epiphyte, seedlings predominantly perform C<sub>3</sub> photosynthesis, and assimilate the majority of diel CO<sub>2</sub> at night until subjected to water-deficit stress (Winter and Holtum, 2011). Likewise, very young cladodes of *O. ficus-indica* fix more net CO<sub>2</sub> during the light period than the dark period until subjected to water-deficit stress (Winter et al., 2008) even though *O. ficus-indica* is considered an obligate CAM specie. Developing cladodes have also been shown to be primarily sink tissues that receive carbohydrates from basal cladodes until they are large enough to begin CAM photosynthesis (Wang et al., 1998).

CAM plants that occur in especially arid environments, such as the cactus and agave families, have a higher occurrence of species that only use CAM photosynthesis and are thus commonly referred to as obligate CAM plants (Ehleringer and Osmond, 1989). Obligate CAM species often use CAM photosynthesis early on in development and continue to do so through maturity. Obligate CAM plants typically continue to assimilate CO<sub>2</sub> at night even when conditions become favorable. However, recent findings have shown that when conditions are optimum, the occurrence of CO<sub>2</sub> fixation at dusk and dawn by combined activity CA/PEPC and RUBISCO increases in obligate CAM plants to the point that net daytime assimilation may surpass net nighttime assimilation (Winter et al., 2008; Niechayev et al., 2019). Such findings indicate that while categorizing plants as C<sub>3</sub> photosynthesis, facultative and obligate CAM, the reality is that there is a continuum of CAM plasticity in many species (Silvera et al.,



2010; Winter et al., 2015; Torres-Morales et al., 2020; Messerschmid et al., 2021; Winter and Smith, 2021).

### *Opuntia ficus-indica*

One of the most emblematic, if not notorious obligate CAM plant species is *Opuntia stricta*. Introduced to Australia, it covered more than 25 million acres of land in 80 years and produced 1.5 billion tons of biomass (Osmond et al., 2008; Winter, 2021). Control with environmentally toxic herbicides failed and the cactus moth *Cactoblastis cactorum* proved to be an effective biological control. While highly invasive, *Opuntia ficus-indica* has been shown to have a negligible effect on plant species diversity by creating new favorable habitats for some species, but still altering plant species composition in the highlands of Eritrea (Tesfay and Kreyling, 2021). *Opuntia* spp. center of diversity is in central Mexico (Hernández-Pérez et al., 2009), and as a promiscuous and highly hybridizing plant species, there are currently 81 known varieties (Davis et al., 2019) with widely variable ploidy numbers (Palomino et al., 2016).

*O. ficus-indica* is a eudicot, platyopuntia (flat cladodes between nodes), terrestrial stem succulent with rectifying roots (North and Nobel, 1997), sunken stomata (Toumey, 1895), calcium druse crystals (Contreras-cladodeilla et al., 2011), spines, glochids (Mylo et al., 2021), and thick epidermal waxes and cuticles (Mayer, 2018). *O. ficus-indica* also produces tyrosine-derived betalain pigments instead of flavanol-derived anthocyanins (Smeriglio et al., 2019). Despite the common perception that CAM species are low yielding, *Opuntia*

species have biomass productivity that vary widely from 2.4 to 47.3 Mg ha<sup>-1</sup> yr<sup>-1</sup> (Monjauze and Le Hou  rou, 1965; Garcia de Cort  zar and Nobel, 1992; Dubeux et al., 2006; Cross et al., 2018; Ram  rez-Arpide et al., 2018; Neupane et al., 2021). The upper end of this range exceeds yields of commodity crops that use C<sub>3</sub> or C<sub>4</sub> photosynthetic pathways; productivities of C<sub>4</sub> photosynthetic species grown for biofuels such as maize, switchgrass, and sugarcane range from 5 to 26 Mg ha<sup>-1</sup> yr<sup>-1</sup>, and C<sub>3</sub> photosynthetic species grown for biofuels such as oil palm, poplar, and willow produce between 2-14 Mg ha<sup>-1</sup> yr<sup>-1</sup> (Somerville et al., 2010).

From an economic perspective, *O. ficus-indica* has a rich and entertaining history. When the larva of the cochineal insect (*Dactylopius spp.*), generally considered a pest in modern day agricultural objectives (Mendel et al., 2020), which feeds on *O. ficus-indica*, and releases a deep red compound when crushed that is used to create the rich red dye known as carmine (Phipps, 2010). In the new world, cities conquered by Montezuma paid tribute in cochineal dye. Once the Spanish colonized the Americas, carmine found its way into thousands of paintings and was used to dye clothes all over the world. Spanish control of the carmine trade and production, most interestingly on the Canary Islands (Rowe, 2020), caused the value to become more expensive by weight than gold. Carmine was even used for the red coats in the British army, but only the officer's coats were made with carmine, while the regulars had to settle for dyes made with *Rubia tinctorum* (dyer's madder) (Phipps, 2010).

With the advent of synthetic dyes, the value of carmine diminished, but the global market for prickly pear fruits for beverages and jams, and young

cladodes as vegetables remains today (Davis et al., 2019). More recently, the seed oil of *O. ficus-indica* fruits has been recognized as having a combination of unsaturated fatty acids including high amounts of linoleic acid (Ciriminna et al., 2017; Al-Naqeb et al., 2021), which is commonly found in expensive beauty products such as Argonne oil (Miklavčič et al., 2020). Each fruit contains anywhere between 50 to 300 large seeds.

### *Estimating Opuntia ficus-indica* global productivity.

*O. ficus-indica* ecological physiology and agriculture have been studied for decades. Optimal growing conditions and tolerances are well known (Nobel, 2003). A systems dynamics model of CAM that accurately predicts diel CAM expression as an output (i.e., organic acid buildup, CO<sub>2</sub> assimilation) from measured biochemical and physiological inputs has been validated (Owen and Griffiths, 2013). Two separate mathematical models have been developed for estimating the potential productivity of *O. ficus-indica* in any given region. The first is an environmental productivity index (EPI) model first developed by (Nobel and Hartsock, 1984). This simple model estimates productivity using physiological response experiments that measure total nocturnal malate build-up due to changes in temperature, light, and water. Then, given average monthly climate data, the model can be used to calculate estimates of actual productivity in any given region. A newer, photo3 model, developed by (Hartzell et al., 2018) considers the soil-plant air continuum by incorporating the Farquhar model (Farquhar et al., 1980), and modifies it for a whole CAM plant by including CAM

circadian rhythm oscillator inputs, plant water storage, and atmospheric conditions; and considering soil-plant-atmosphere continuum as hydraulic fluxes in a convenient resistor-capacitor fashion.

The EPI model's strength is in its simplicity, as photosynthetic, hydraulic, and soil parameters required for the photo3 model are not necessary nor yet available for many CAM plants, although all inputs needed for *O. ficus-indica* are available and have been used in photo 3 predictions (Hartzell et al., 2018). The multiplicative index parameters make it easy to add parameters such as elevation (Nobel and Hartsock, 1986) and soil nutrients (Nobel, 1989) once those physiological responses are measured. However, the EPI model is based upon a monthly time scale and is limited in that it does not account for the interdependency between factors considered. For example, the PAR response of a given species might change when water is limiting or *vice versa* in ways not considered in the current EPI modeling approach. The Photo3 model, on the other hand, can make predictions on an hourly time scale, be used for C<sub>3</sub> and C<sub>4</sub> photosynthesis crop comparisons, and a comparison of EPI with Photo3 demonstrated that EPI and photo3 predictions can be up to 40% different (Hartzell et al., 2021), pointing out that EPI modeling is likely not the correct model to use when Photo3 estimation is possible.

The EPI model has been used in combination with GIS software to predict the range of *O. ficus-indica* with climate change (Owen and Griffiths, 2014), and the potential growing range is projected to expand in the southern United States. While there are projected range expansions, and *O. ficus-indica* biomass increases

by 40% when CO<sub>2</sub> rates are doubled (Nobel and Israel, 1994), obligate CAM photosynthesis is mostly dependent upon nighttime temperatures (Neales, 1973). Slight increases in nighttime temperatures can reduce stomatal conductance of CAM species and reduce CO<sub>2</sub> assimilation, even under elevated atmospheric CO<sub>2</sub> conditions.

### Nitrogen metabolism in *Opuntia ficus-indica*

While the EPI model developed by Nobel also includes a nutrient index (Nobel, 1989), the nutrient index is not species specific, and does not differentiate between nitrogen sources. Nitrogen metabolism is well understood in C<sub>3</sub> (Baslam et al., 2021) and C<sub>4</sub> photosynthesis plant species (Hirel et al., 2005). However, our current understanding of N metabolism in CAM plants is limited (Pereira and Cushman, 2019). Contemporary studies on CAM and nitrogen nutrition have focused on the link between CAM activity and nitrogen metabolism. Nitrogen assimilation into amino acids occurs in the chloroplasts via the glutamine synthetase and glutamine oxoglutarate aminotransferase (GS/GOGAT) cycle (Rodrigues et al., 2014). CAM plants placed in an increased atmospheric CO<sub>2</sub> concentration have an increase nitrogen uptake. Enzymes and substrates important for the tricarboxylic acid cycle and CAM photosynthesis are also important for nitrogen metabolism and amino acid synthesis. For instance, PEPC has been demonstrated to be important for ammonium assimilation and is directly regulated by quantities of 2-oxoglutarate and citrate synthase activity, both are important for amino acid synthesis. Malic enzyme (ME), and pyruvate orthophosphate dikinase

(PPDK), enzymes responsible for malic acid decarboxylation and phosphoenolpyruvate (PEP) regeneration, respectively, are also important for providing carbon skeletons and metabolic energy for amino acid synthesis.

Contemporary studies on CAM and nitrogen nutrition have focused on the link between CAM activity and nitrogen metabolism. Nitrogen assimilation into amino acids occurs in the chloroplasts via the GS/GOGAT cycle (Rodrigues et al., 2014; Pereira and Cushman, 2019).

As is true for all plant species, variations in the preference of nitrogen source are known, whether it is ammonium, nitrate, or urea (Habteselassie et al., 2013; Wan et al., 2014; Hachiya and Sakakibara, 2017). In *K. blossfeldiana*, CAM expression has been shown to increase when plants are given more nitrate than ammonium, and when both nitrate and ammonium are absent or limiting (1 mM) (Ota, 1988). In *Kalanchoe spp.*, CAM expression decreases when both ammonium and nitrate are supplied in high abundance (>5 mM), both together and separately presumably due to ammonium and nitrate toxicities (Pereira et al., 2017). Proton transport in tonoplasts mediating nocturnal organic acid storage in *K. laxiflora* and *K. delagoensis* is influenced by inorganic nitrogen sources, wherein low nitrate concentration increased nocturnal organic-acid accumulation, whereas the opposite was true in high nitrate concentrations (Pereira et al., 2017). The authors explain that this is likely due to an inhibition of tonoplast ATPase with high nitrate concentrations that corresponds to an increase in anionic species, which requires extra active proton pumping to maintain a beneficial electrochemical gradient. Collectively, these results demonstrate that in

*Kalanchoe spp.*, CAM is highly expressed when plants are cultivated on soils with nitrate rather than ammonium, and when nitrogen in general is limiting, although the exact favorable amounts and preferences for ammonium *versus* nitrate varies from species to species (Hachiya and Sakakibara, 2017; Islam et al., 2020)

Several studies have documented the productivity of *O. ficus-indica* under different fertilizer treatments in the field (Garcia de Cortázar and Nobel, 1992; Dubeux et al., 2006; Sánchez et al., 2012; Nkoi et al., 2021) and the commercial N input is between 50–100 kg ha<sup>-1</sup> year<sup>-1</sup> (Davis et al., 2019). However, these studies were conducted with a wide variety of N sources, soil types, and production goals (*e.g.*, fruit, cladodes, seeds, and methane production). In one study, *O. ficus-indica* initially took up more N when given ammonium than nitrate, and therefore, *O. ficus-indica* likely has a slight preference for ammonium, but can fix either form of N (Vázquez et al., 2000).

### *Opuntia ficus-indica* as a biofuel feedstock

With the addition of aerobic pre-treatments, methane yields from bioenergy crops can be increased. Nine-hours of aerobic pre-treatment of *O. ficus-indica* cladodes using cow rumen fluids caused methane yields to increase 123% with a maximum yield of 0.72 L/kg volatile solid (Myovela et al., 2019). Further studies need to be conducted to assess the economic viability of *Opuntia* spp. as a biogas resource, but initial estimates seem to hold great promise. For example, annual electrical power generated globally from methane gas (about 5 PW) could be generated from CAM plants (*e.g.*, *O. ficus-indica*) on 100–380 Mha of semi-

arid land or between 4% and 15% of such currently available land area (Mason et al. 2015). An evaluation of methane production from representative species of five different CAM genera (e.g., *Ananas comosus*, *Agave angustifolia*, *Euphorbia virosa*, *Kalanchoe daigremontiana*, and *Opuntia fragilis*) showed that *A. angustifolia* produced the highest methane yields and that biomethane yields were similar to those obtained from maize biomass (Lueangwattanapong et al., 2020). The CAM species *Euphorbia tirucalli* and *O. ficus-indica* are able to produce 1791 m<sup>3</sup> and 1860 m<sup>3</sup> of methane from 1 ha of land planted at high planting densities, respectively (Krümpel et al., 2020). Addition of microbes found in the soil of an *O. ficus-indica* plantation, in particular, *Pectobacterium cacticida*, and *Enterobacter sp.*, were shown to digest *O. ficus indica* cladodes and have pectinase activity (Blair et al., 2021). These studies suggest that low-lignin CAM species can serve as highly attractive bioenergy feedstocks for biorefinery industries. The highest reported cellulosic ethanol production value from *O. ficus-indica* is 2.6% v/w (Kuloyo et al., 2014), which is much lower than *Agave tequiliana*, as the higher total soluble solid fraction in juice content, and higher total dry mass make *A. tequilana* more suitable for ethanol production (Yang et al., 2015).

### Estimating global impact of *Opuntia ficus-indica* production pathways

The environmental impact of a crop can vary depending upon the pollutant release associated with required land-use changes, conversion efficiencies to desired products, transportation, and other factors. Life cycle assessment (LCA)



models are a common tool for assessing the overall emissions produced from initial planting to final production and transport to market (Yan et al., 2011). In order to be able to compare the results of LCA results from different crops, most LCA calculations follow a standardized frame work (ISO) in what goal and scope definitions are first defined, second a life cycle inventory of all agricultural production inputs and outputs, then a life cycle impact assessment that determines the net emission produced per unit energy generated, and finally an interpretation of the results. A complete LCA of *Opuntia-ficus indica* biogas production with cow manure has been conducted using the results of actual field production values in Mexico (Ramírez-Arpide et al., 2018). The authors tested a scenario in which convention farming techniques were used with synthetic fertilizer, and an organic farming method, in which cow manure was used as fertilizer had energy return on investment values of 8.1 to 12.4 respectively. They found that the organic farming system decreased the overall environmental impact, but increased the released acids, and eutrophication (nitrogen pollution) on the field site. Overall, there was a 2.3% reduction in global warming potential and a 1.7% reduction in photochemical ozone creation potential (Ramírez-Arpide et al., 2018; Ramírez-Arpide et al., 2018).

With increased drought and temperatures associated with climate change, *O. ficus-indica* appears to have substantial potential as a fuel, feed, fodder and secondary products in the United States. Currently, collective *O. ficus-indica* products are worth an estimated \$2520 million year<sup>-1</sup> globally (Davis et al., 2019). *O. ficus-indica* growing operations could be combined photovoltaic arrays

where water used to clean the panels also irrigates plants (Cushman et al., 2015), and reduce greenhouse gas emissions and generation of ozone deteriorating pollutants while creating a new source of energy (Ramírez-Arpide et al., 2018).

### Developmental physiology, nitrogen preference, and estimates of biofuel production in *Opuntia ficus-indica*

This dissertation is divided into five independent chapters. The second investigates whether or not C<sub>3</sub> photosynthesis is used in developing seedlings and daughter cladodes before switching to CAM photosynthesis, the third investigates responses of *O. ficus-indica* growth, biochemistry, and expression of CAM and nitrogen-related genes under variation in provided nitrate and ammonium concentrations in sand culture, and the fourth chapter outlines ongoing life cycle assessment efforts of theoretical biogas and bioethanol production from *O. ficus-indica* using ground-truth results from a long-term irrigation trial conducted in the United States. These three studies provide novel insights into the relative contribution of C<sub>3</sub> photosynthesis to the high productivity observed for *O. ficus-indica*, which nitrate vs. ammonium ratios are optimum for *O. ficus-indica* productivity while limiting run-off of unused N, estimations of biogas and bioethanol production in the United States, and lastly, a final chapter that provides a brief synthesis of the findings.

## Figures

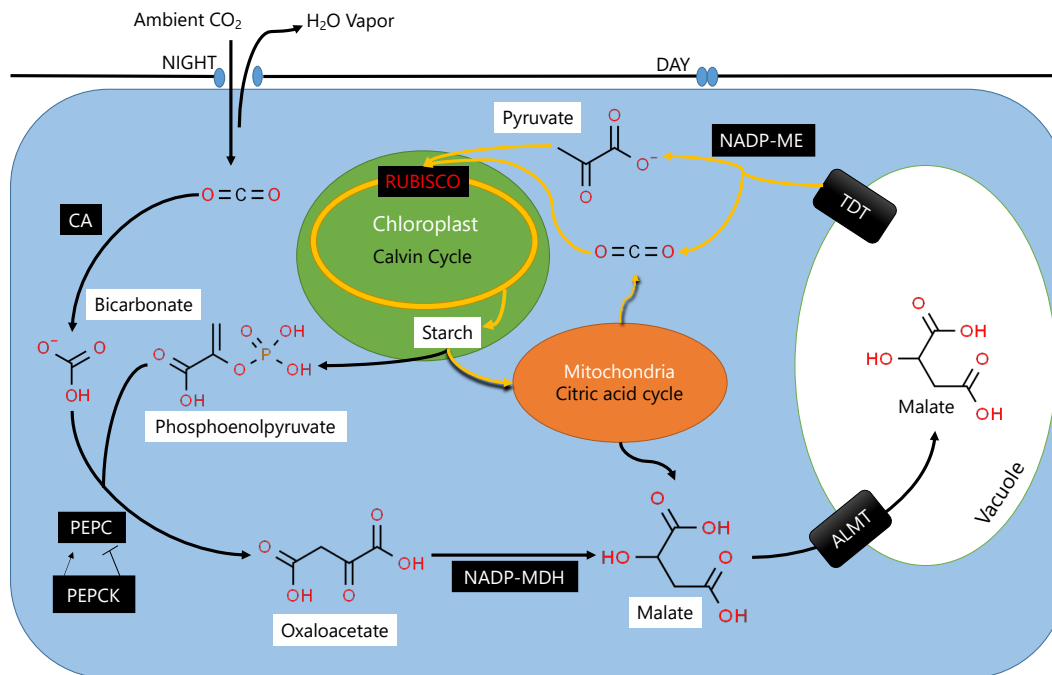


**Figure 1:** A simplified model of CAM with the black arrows representing fluxes at night, and the yellow arrows representing fluxes during the day.  $\text{CO}_2$  entering the cell through nocturnally open stomata is converted into bicarbonate by carbonic anhydrase (CA) followed by fixation into phosphoenolpyruvate (PEP) into oxaloacetate (OAA) by a CAM-specific phosphoenolpyruvate carboxylase (PEPC) isozyme (Nimmo, 2000; Boxall et al., 2017). This PEPC is constitutively expressed with its malate inhibition relieved through phosphorylation by a dedicated, circadian controlled phosphoenolpyruvate carboxylase kinase (PPCK) (Hartwell et al., 1999; Taybi et al., 2000). The resulting OAA is converted malate by malate dehydrogenase and shuttled into the vacuole by a putative aluminum malate transporter (ALMT) (Borland et al., 2016; Pereira et al., 2017) for storage until sunlight is available. During the day, stored malate is released from the vacuole through a tonoplast decarboxylation transporter (TDT), and

decarboxylated by NAD(P)-malic enzyme (Winter and Smith, 2021). The released CO<sub>2</sub> is then fixed by the Calvin-Benson-Bassham cycle by ribulose-1,5-bisphosphate carboxylase/oxygenase (RUBISCO) as in the C<sub>3</sub> photosynthetic pathway. All chemical structures were sourced from chemspider.com.

## References

- Al-Naqeb G, Fiori L, Ciolli M, Aprea E** (2021) *Prickly Pear Seed Oil*  
Extraction, Chemical Characterization and Potential Health Benefits.  
*Molecules* **26**: 5018
- Baslam M, Mitsui T, Sueyoshi K, Ohyama T** (2021) Recent advances in carbon  
and nitrogen metabolism in C<sub>3</sub> plants. *International Journal of Molecular  
Sciences* **22**: 318
- Berge B** (2007) *Ecology of building materials*. Routledge
- Blair BB, Yim WC, Cushman JC** (2021) Characterization of a microbial  
consortium with potential for biological degradation of cactus pear  
biomass for biofuel. *Heliyon* **7**: e07854
- Borland AM, Griffiths H, Hartwell J, Smith JAC** (2009) Exploiting the  
potential of plants with crassulacean acid metabolism for bioenergy  
production on marginal lands. *Journal of Experimental Botany* **60**: 2879–  
2896
- Borland AM, Griffiths H, Hartwell J, Smith JAC** (2009) Exploiting the  
potential of plants with crassulacean acid metabolism for bioenergy  
production on marginal lands. *Journal of Experimental Botany* **60**: 2879-  
2896
- Borland AM, Guo HB, Yang X, Cushman JC** (2016) Orchestration of  
carbohydrate processing for crassulacean acid metabolism. *Current  
Opinion in Plant Biology* **31**: 118–124

- Boxall SF, Dever LV, Knerova J, Gould PD, Hartwell J (2017)**  
Phosphorylation of phosphoenolpyruvate carboxylase is essential for maximal and sustained dark CO<sub>2</sub> fixation and core circadian clock operation in the obligate crassulacean acid metabolism species *Kalanchoe fedtschenkoi*. *The Plant Cell* **29**: 2519–2536
- Busch FA (2020)** Photorespiration in the context of Rubisco biochemistry, CO<sub>2</sub> diffusion and metabolism. *The Plant Journal* **101**: 919-939
- Chomthong M, Griffiths H (2020)** Model approaches to advance crassulacean acid metabolism system integration. *The Plant Journal* **101**: 951–963
- Christopher JT, Holtum JAM (1996)** Patterns of carbohydrate partitioning in the leaves of Crassulacean acid metabolism species during deacidification. *Plant Physiology* **112**: 393–399
- Christopher JT, Holtum JAM (1998)** Carbohydrate partitioning in the leaves of *Bromeliaceae* performing C<sub>3</sub> photosynthesis or Crassulacean acid metabolism. *Australian Journal of Plant Physiology* **25**: 371–376
- Ciriminna R, Bongiorno D, Scurria A, Danzi C, Timpanaro G, Delisi R, Avellone G, Pagliaro M (2017)** Sicilian *Opuntia ficus-indica* seed oil: Fatty acid composition and bio-economical aspects. *European Journal of Lipid Science and Technology* **119**: 1700232
- Contreras-cladodeilla M, Pérez-Torrero E, Hernández-Urbiola MI, Hernández-Quevedo G, del Real A, Rivera-Muñoz EM, Rodríguez-García ME (2011)** Evaluation of oxalates and calcium in nopal cladodes

(*Opuntia ficus-indica* var. *redonda*) at different maturity stages. Journal of Food Composition and Analysis **24**: 38–43

- Cousins AB, Baroli I, Badger MR, Ivakov A, Lea PJ, Leegood RC, von Caemmerer S** (2007) The role of phosphoenolpyruvate carboxylase during C<sub>4</sub> photosynthetic isotope exchange and stomatal conductance. Plant Physiology **145**: 1006-10017
- Cross P, Mukarakate C, Nimlos M, Carpenter D, Donohoe BS, Mayer JA, Cushman JC, Neupane B, Miller GC, Adhikari S** (2018) Fast Pyrolysis of *Opuntia ficus-indica* (Prickly Pear) and *Grindelia squarrosa* (Gumweed). Energy & Fuels **32**: 3510–3518
- Cushman JC, Davis SC, Yang X, Borland AM** (2015) Development and use of bioenergy feedstocks for semi-arid and arid lands. Journal of Experimental Botany **66**: 4177–4193
- Cuthber MO, Gleeson T, Moosdorf N, Befus KM, Schneider A, Hartmann J, Lehner B** (2019) Global patterns and dynamics of climate–groundwater interactions. Nature Climate Change **9**: 137
- Davis SC, Simpson J, Vega G, Del Carmen K, Niechayev NA, Tongerlo EV, Castano NH, Dever LV, Búrque A** (2019) Undervalued potential of crassulacean acid metabolism for current and future agricultural production. Journal of Experimental Botany **70**: 6521–6537
- Dubeux JJCB, Ferreira dos Santos MVF, de Andrade Lira M, Coreiro dos Santos D, Farias I, Lima LE, Ferreira RLC** (2006) Productivity of *Opuntia ficus-indica* (L.) Miller under different N and P fertilization and

plant population in north-east Brazil. *Journal of Arid Environments* **67**: 357–372

**Ehleringer JR, Osmond CB** (1989) Stable isotopes. *In* PW Rundel, ed, *Plant physiological ecology*. Chapman and Hall, London, pp 255-280

**Farquhar GD, von Caemmerer S, Berry JA** (1980) A biochemical model of photosynthetic CO<sub>2</sub> assimilation in leaves of C<sub>3</sub> species. *Planta* **149**: 78–90

**Fitton N, Alexander P, Arnell N, Bajzelj B, Calvin K, Doelman J, Gerber JS, Havlik P, Hasegawa T, Herrero M** (2019) The vulnerabilities of agricultural land and food production to future water scarcity. *Global Environmental Change* **58**: 101944

**Garcia de Cortázar V, Nobel PS** (1992) Biomass and fruit production for the prickly pear cactus *Opuntia ficus-indica*. *Journal of the American Society for Horticultural Science* **117**: 568–562

**Geist H** (2017) *The causes and progression of desertification*. Routledge

**Habteselassie MY, Xu L, Norton JM** (2013) Ammonia-oxidizer communities in an agricultural soil treated with contrasting nitrogen sources. *Frontiers in Microbiology* **4**: 326

**Hachiya T, Sakakibara H** (2017) Interactions between nitrate and ammonium in their uptake, allocation, assimilation, and signaling in plants. *Journal of Experimental Botany* **68**: 2501-2512



- Hadebe S, Modi A, Mabhaudhi T** (2017) Drought tolerance and water use of cereal crops: a focus on sorghum as a food security crop in sub-Saharan Africa. *Journal of Agronomy and Crop Science* **203**: 177-191
- Hartwell J, Nimmo GA, Wilkins MB, Jenkins GL, Nimmo HG** (1999) Phosphoenolpyruvate carboxylase kinase is a novel protein kinase regulated at the level of gene expression. *The Plant Journal* **20**: 333-342
- Hartzell S, Bartlett MS, Inglese P, Consoli S, Yin J, Porporato A** (2021) Modelling nonlinear dynamics of Crassulacean acid metabolism productivity and water use for global predictions. *Plant, Cell & Environment* **44**: 34-48
- Hartzell S, Bartlett MS, Porporato A** (2018) Unified representation of the C<sub>3</sub>, C<sub>4</sub>, and CAM photosynthetic pathways with the Photo3 model. *Ecological Modelling* **384**: 173–187
- Hatch MD** (1987) C<sub>4</sub> photosynthesis: a unique blend of modified biochemistry, anatomy and ultrastructure. *Biochimica et Biophysica Acta (BBA)-Reviews on Bioenergetics* **895**: 81-106
- Hennacy JH, Jonikas MC** (2020) Prospects for engineering biophysical CO<sub>2</sub> concentrating mechanisms into land plants to enhance yields. *Annual Review of Plant Biology* **71**: in press
- Hernández-Pérez R, Noa-Carrazana JC, Gaspar R, Mata P, Flores-Estévez N** (2009) Detection of phytoplasma on indian fig (*Opuntia ficus-indica Mill*) in Mexico central region. In *OnLine Journal of Biological Sciences* **9**: 62–66

**Heyduk K, Moreno-Villena JJ, Gilman IS, Christin P-A, Edwards EJ (2019)**

The genetics of convergent evolution: insights from plant photosynthesis.

Nature Reviews Genetics **20**: 485-493

**Hirel B, Martin A, Tercé-Laforgue T, Gonzalez-Moro MB, Estavillo JM**

(2005) Physiology of maize I: A comprehensive and integrated view of

nitrogen metabolism in a C<sub>4</sub> plant. Physiologia Plantarum **124**: 167-177

**Islam S, Islam R, Kandwal P, Khanam S, Proshad R, Kormoker T, Tusher**

**TR (2020)** Nitrate transport and assimilation in plants: a potential review.

Archives of Agronomy and Soil Science: 1-18

**ISO T 207 (2006)** ISO 14040: 2006 environmental management—life cycle

assessment—principles and framework. ISO, Switzerland

**Krümpel J, George T, Gasston B, Francis G, Lemmer A (2020)** Suitability of

*Opuntia ficus-indica* (L) Mill. and *Euphorbia tirucalli* L. as energy crops

for anaerobic digestion. Journal of Arid Environments **174**: 104047

**Kuloyo OO, du Preez JC, del Prado García-Aparicio M, Kilian SG, Steyn L,**

**Görgens J (2014)** *Opuntia ficus-indica* cladodes as feedstock for ethanol

production by *Kluyveromyces marxianus* and *Saccharomyces cerevisiae*.

World Journal of Microbiology and Biotechnology **30**: 3173–3183

**Kumar V, Sharma A, Soni JK, Pawar N (2017)** Physiological response of C<sub>3</sub>,

C<sub>4</sub> and CAM plants in changeable climate. The Pharma Innovation **6**: 70

**Le Quéré C, Raupach MR, Canadell JG, Marland G, Bopp L, Ciais P,**

**Conway TJ, Doney SC, Feely RA, Foster P (2009)** Trends in the sources

and sinks of carbon dioxide. Nature Geoscience **2**: 831-836

**Leavitt SW, Chase TN, Rajagopalan B, Lee E, Lawrence PJ, Woodhouse CA**

(2007) Southwestern US drought maps from pinyon tree-ring carbon isotopes. *In*. Wiley Online Library

**Lerman J, Deleens E, Nato A, Moyses A** (1974) Variation in the carbon isotope

composition of a plant with Crassulacean acid metabolism. *Plant Physiology* **53**: 581-584

**Leverett A, Castaño NH, Ferguson K, Winter K, Borland AM** (2021)

Crassulacean acid metabolism (CAM) supersedes the turgor loss point (TLP) as an important adaptation across a precipitation gradient, in the genus *Clusia*. *Functional Plant Biology* **48**: 703-716

**Lueangwattanapong K, Ammam F, Mason PM, Whitehead C, McQueen-**

**Mason SJ, Gomez LD, Smith JA, Thompson IP** (2020) Anaerobic digestion of Crassulacean Acid Metabolism plants: exploring alternative feedstocks for semi-arid lands. *Bioresource Technology* **297**: 122262

**Lüttge U** (2002) CO<sub>2</sub>-concentrating: consequences in crassulacean acid

metabolism. *Journal of Experimental Botany* **53**: 2131–2142

**Males J, Griffiths H** (2017) Stomatal biology of CAM plants. *Plant Physiology*

**174**: 550–560

**Mason PM, Glover K, Smith JAC, Willis KJ, Woods J, Thompson IP** (2015)

The potential of CAM crops as a globally significant bioenergy resource: moving from 'fuel or food' to 'fuel and more food'. *Energy and Environmental Science* **8**: 2320–2329

- Mayer JA** (2018) *Opuntia ficus-indica*: a climate-resilient biomass feedstock for low-input drylands agriculture. University of Nevada, Reno
- McDaniel RL, Munster C, Nielsen-Gammon J** (2017) Crop and location specific agricultural drought quantification: Part III. Forecasting water stress and yield trends. *Transactions of the ASABE* **60**: 741-752
- Mendel Z, Protasov A, Vanegas-Rico JM, Lomeli-Flores JR, Suma P, Rodríguez-Leyva E** (2020) Classical and fortuitous biological control of the prickly pear cochineal, *Dactylopius opuntiae*, in Israel. *Biological Control* **142**: 104157
- Messerschmid TF, Wehling J, Bobon N, Kahmen A, Klak C, Los JA, Nelson DB, dos Santos P, de Vos JM, Kadereit G** (2021) Carbon isotope composition of plant photosynthetic tissues reflects a Crassulacean Acid Metabolism (CAM) continuum in the majority of CAM lineages. *Perspectives in Plant Ecology, Evolution and Systematics*: 125619
- Miklavčič MB, Taous F, Valenčič V, Elghali T, Podgornik M, Strojnik L, Ogrinc N** (2020) Fatty Acid Composition of Cosmetic Argan Oil: Provenience and Authenticity Criteria. *Molecules* **25**: 4080
- Monjauze A, Le Houérou HN** (1965) Le rôle des *Opuntia* dans l'économie agricole nord-africaine. *Bulletin de l'Ecole Nationale Supérieure d'Agronomie de Tunis* **8–9**: 8–164
- Mylo MD, Hesse L, Masselter T, Leupold J, Drozella K, Speck T, Speck O** (2021) Morphology and Anatomy of Branch–Branch Junctions in *Opuntia*

*ficus-indica* and *Cylindropuntia bigelovii*: A Comparative Study

Supported by Mechanical Tissue Quantification. *Plants* **10**: 2313

**Myovela H, Mshandete AM, Imathiu S** (2019) Enhancement of anaerobic batch digestion of spineless cacti (*Opuntia ficus indica*) feedstock by aerobic pre-treatment. *African Journal of Biotechnology* **18**: 12–22

**Naumann G, Alfieri L, Wyser K, Mentaschi L, Betts RA, Carrao H, Spinoni J, Vogt J, Feyen L** (2018) Global changes in drought conditions under different levels of warming. *Geophysical Research Letters* **45**: 3285–3296

**Neales TF** (1973) The effect of night temperature on CO<sub>2</sub> assimilation, transpiration, and water use efficiency in *Agave americana* L. *Australian Journal of Biological Sciences* **26**: 705–714

**Neupane D, Mayer JA, Niechayev NA, Bishop CD, Cushman JC** (2021) Five-year field trial of the biomass productivity and irrigation response of prickly pear cactus (*Opuntia spp.*) as a bioenergy feedstock for arid lands. *Global Change Biology: Bioenergy* **13**: 719–741

**Niechayev NA, Jones AM, Rosenthal DM, Davis SC** (2019) A model of environmental limitations on production of *Agave americana* L. grown as a biofuel crop in semi-arid regions. *Journal of Experimental Botany* **70**: 6549–6559

**Niechayev NA, Pereira PN, Cushman JC** (2019) Understanding trait diversity associated with crassulacean acid metabolism (CAM). *Current Opinion in Plant Biology* **49**: 74–85

- Nimmo HG** (2000) The regulation of phosphoenolpyruvate carboxylase in CAM plants. *Trends in Plant Science* **5**: 75-80
- Nkoi V, Wit Md, Fouche H, Coetzer G, Hugo A** (2021) The Effect of Nitrogen Fertilization on the Yield, Quality and Fatty Acid Composition of *Opuntia ficus-indica* Seed Oil. *Sustainability* **13**: 10123
- Nobel PS** (1989) A nutrient index quantifying productivity of Agaves and Cacti. *Journal of Applied Ecology* **26**: 635–645
- Nobel PS** (2003) *Environmental biology of agaves and cacti*. Cambridge University Press
- Nobel PS, Hartsock TL** (1984) Physiological responses of *Opuntia ficus-indica* to growth temperature. *Physiologia Plantarum* **60**: 98-105
- Nobel PS, Hartsock TL** (1986) Temperature, water, and PAR influences on predicted and measured productivity of *Agave deserti* at various elevations. *Oecologia* **68**: 181–185
- Nobel PS, Israel AA** (1994) cladode development, environmental responses of CO<sub>2</sub> uptake, and productivity for *Opuntia ficus-indica* under elevated CO<sub>2</sub>. *Journal of Experimental Botany* **45**: 295–303
- North GB, Nobel PS** (1997) Drought-induced changes in soil contact and hydraulic conductivity for roots of *Opuntia ficus-indica* with and without rhizosheaths. *Plant and Soil* **191**: 249–258
- O'Leary MH** (1988) Carbon isotopes in photosynthesis. *Bioscience* **38**: 328-336
- Oliver TH, Heard MS, Isaac NJ, Roy DB, Procter D, Eigenbrod F, Freckleton R, Hector A, Orme CDL, Petchey OL** (2015) Biodiversity

and resilience of ecosystem functions. *Trends in ecology & evolution* **30**: 673-684

- Osmond B, Tom Neales T, Stange G** (2008) Curiosity and context revisited: crassulacean acid metabolism in the Anthropocene. *Journal of Experimental Botany* **59**: 1489–1502
- Ota K** (1988) Stimulation of CAM photosynthesis in *Kalanchoë blossfeldiana* by transferring to nitrogen-deficient conditions. *Plant Physiology* **87**: 454-457
- Owen NA, Griffiths H** (2013) A system dynamics model integrating physiology and biochemical regulation predicts extent of crassulacean acid metabolism (CAM) phases. *New Phytologist* **200**: 1116–1131
- Owen NA, Griffiths H** (2014) Marginal land bioethanol yield potential of four crassulacean acid metabolism candidates (*Agave fourcroydes*, *Agave salmiana*, *Agave tequilana* and *Opuntia ficus-indica*) in Australia. *Global Change Biology: Bioenergy* **6**: 687–703
- O’Neill DW, Fanning AL, Lamb WF, Steinberger JK** (2018) A good life for all within planetary boundaries. *Nature sustainability* **1**: 88-95
- Palomino G, Martínez J, Méndez I, Muñoz-Urías A, Cepeda-Cornejo V, Pimienta-Barrios E** (2016) Nuclear genome size, ploidy level and endopolyploidy pattern in six species of *Opuntia* (Cactaceae). *Caryologia* **69**: 82-89
- Pereira PN, Cushman JC** (2019) Exploring the relationship between crassulacean acid metabolism (CAM) and mineral nutrition with a special focus on nitrogen. *International Journal of Molecular Sciences* **20**: 4363

- Pereira PN, Niechayev NA, Blair BB, Cushman JC** (2021) Climate change responses and adaptations in crassulacean acid metabolism (CAM) plants. *In* KM Becklin, DA Way, TD Sharkey, eds, Photosynthesis, Respiration, and Climate Change, Vol 48. Springer, Dordrecht
- Pereira PN, Smith JAC, Mercier H** (2017) Nitrate enhancement of CAM activity in two *Kalanchoë* species is associated with increased vacuolar proton transport capacity. *Physiologia Plantarum* **160**: 361-372
- Phipps E** (2010) *Cochineal red: the art history of a color*, Vol 63. Metropolitan Museum of Art
- Purvis B, Mao Y, Robinson D** (2019) Three pillars of sustainability: in search of conceptual origins. *Sustainability Science* **14**: 681-695
- Ramírez-Arpide FR, Demirer GN, Gallegos-Vázquez C, Hernández-Eugenio G, Santoyo-Cortés VH, Espinosa-Solares T** (2018) Life cycle assessment of biogas production through anaerobic co-digestion of nopal cladodes and dairy cow manure. *Journal of Cleaner Production* **172**: 2313–2322
- Ramírez-Arpide FR, Demirer GN, Gallegos-Vázquez C, Hernández-Eugenio G, Santoyo-Cortés VH, Espinosa-Solares T** (2018) Life cycle assessment of biogas production through anaerobic co-digestion of nopal cladodes and dairy cow manure. *Journal of Cleaner Production* **172**: 2313-2322
- Reid WV, Ali MK, Field CB** (2020) The future of bioenergy. *Global Change Biology* **26**: 274-286



- Rodrigues MA, Freschi L, Pereira PN, Mercier H** (2014) Interactions between nutrients and crassulacean acid metabolism. *In Progress in botany*. Springer, pp 167-186
- Rowe A** (2020) Global cochineal production: scale, welfare concerns, and potential interventions.
- Shameer S, Baghalian K, Cheung CM, Ratcliffe RG, Sweetlove LJ** (2018) Computational analysis of the productivity potential of CAM. *Nature Plants* **4**: 165–171
- Silvera K, Neubig KM, Whitten WM, Williams NH, Winter K, Cushman JC** (2010) Evolution along the crassulacean acid metabolism continuum. *Functional Plant Biology* **37**: 995-1010
- Silvera K, Santiago LS, Cushman JC, Winter K** (2010) Incidence of crassulacean acid metabolism in the Orchidaceae derived from carbon isotope ratios: a checklist of the flora of Panama and Costa Rica. *Botanical Journal of the Linnean Society* **163**: 194–222
- Silvera K, Winter K, Rodriguez BL, Albion RL, Cushman JC** (2014) Multiple isoforms of phosphoenolpyruvate carboxylase in the Orchidaceae (subtribe Oncidiinae): implications for the evolution of crassulacean acid metabolism. *Journal of Experimental Botany* **65**: 3623–3636
- Smeriglio A, Bonasera S, Germanò MP, D'Angelo V, Barreca D, Denaro M, Monforte MT, Galati EM, Trombetta D** (2019) *Opuntia ficus-indica* (L.) Mill. fruit as source of betalains with antioxidant, cytoprotective, and anti-angiogenic properties. *Phytotherapy Research* **33**: 1526-1537

- Smith JAC, Winter K** (1996) Taxonomic distribution of crassulacean acid metabolism. *In* SJAC Winter K, ed, Crassulacean Acid Metabolism. Biochemistry, Ecophysiology and Evolution. Springer-Verlag, Berlin, pp 427–436
- Somerville C, Youngs H, Taylor C, Davis SC, Sp L** (2010) Feedstocks for lignocellulosic biofuels. *Science* **329**: 790–792
- Steffen W, Richardson K, Rockström J, Cornell SE, Fetzer I, Bennett EM, Biggs R, Carpenter SR, De Vries W, De Wit CA** (2015) Planetary boundaries: Guiding human development on a changing planet. *Science* **347**
- Sánchez J, Sánchez F, Curt MD, Fernández J** (2012) Assessment of the bioethanol potential of prickly pear (*Opuntia ficus-indica* (L.) Mill.) biomass obtained from regular crops in the province of Almeria (SE Spain). *Israel Journal of Plant Sciences* **60**: 301–318
- Süntar I** (2020) Importance of ethnopharmacological studies in drug discovery: role of medicinal plants. *Phytochemistry Reviews* **19**: 1199-1209
- Taiz L, Zeiger E, Møller IM, Murphy A** (2015) Plant physiology and development. Sinauer Associates Incorporated
- Taybi T, Patil S, Chollet R, Cushman JC** (2000) A minimal Ser/Thr protein kinase circadianly regulates phosphoenolpyruvate carboxylase activity in CAM-induced leaves of *Mesembryanthemum crystallinum*. *Plant Physiology* **123**: 1471–1482

- Tesfay YB, Kreyling J** (2021) The invasive *Opuntia ficus-indica* homogenizes native plant species compositions in the highlands of Eritrea. *Biological Invasions* **23**: 433-442
- Ting I** (1985) Crassulacean acid metabolism. *Annual Review of Plant Physiology* **36**: 595-622
- Torres-Morales G, Lasso E, Silvera K, Turner BL, Winter K** (2020) Occurrence of crassulacean acid metabolism in Colombian orchids determined by leaf carbon isotope ratios. *Botanical Journal of the Linnean Society* **193**: 431-477
- Toumey JW** (1895) Vegetal dissemination in the genus *Opuntia*. *Botanical Gazette* **20**: 356-361
- von Caemmerer S, Quick WP** (2000) Rubisco: physiology in vivo. *In* *Photosynthesis*. Springer, pp 85-113
- Vázquez CG, Sáenz EO, Alvarado RV, García FZ** (2000) Absorción de nitrato y amonio por plantas de nopal en hidroponía. *Terra Latinoamericana* **18**: 133-139
- Wan R, Yang Y, Sun W, Wang Z, Xie S** (2014) Simazine biodegradation and community structures of ammonia-oxidizing microorganisms in bioaugmented soil: impact of ammonia and nitrate nitrogen sources. *Environmental Science and Pollution Research* **21**: 3175-3181
- Wang N, Zhang H, Nobel PS** (1998) Carbon flow and carbohydrate metabolism during sink-to-source transition for developing cladodes of *Opuntia ficus-indica*. *Journal of Experimental Botany* **49**: 1835-1843

- Warner TT** (2009) Desert meteorology. Cambridge University Press
- Winter K** (2021) Diversity of CAM plant photosynthesis (crassulacean acid metabolism): a tribute to Barry Osmond. *Functional Plant Biology* **48**: iii-ix
- Winter K, Foster JG, Schmitt MR, Edwards GE** (1982) Activity and quantity of ribulose biphosphate carboxylase- and phosphoenolpyruvate carboxylase-protein in two Crassulacean acid metabolism plants in relation to leaf age, nitrogen nutrition, and point in time during a day/night cycle. *Planta* **154**: 309–317
- Winter K, Garcia M, Holtum JAM** (2008) On the nature of facultative and constitutive CAM: environmental and developmental control of CAM expression during early growth of *Clusia*, *Kalanchoë*, and *Opuntia*. *Journal of Experimental Botany* **59**: 1829–1840
- Winter K, Holtum J** (2011) Drought-stress-induced up-regulation of CAM in seedlings of a tropical cactus, *Opuntia elatior*, operating predominantly in the C<sub>3</sub> mode. *Journal of Experimental Botany* **62**: 4037-4042
- Winter K, Holtum JA, Smith JAC** (2015) Crassulacean acid metabolism: a continuous or discrete trait? *New phytologist* **208**: 73-78
- Winter K, Holtum JAM, Smith JAC** (2015) Crassulacean acid metabolism: a continuous or discrete trait? *New Phytologist* **208**: 73–78
- Winter K, Smith JAC** (2021) CAM photosynthesis: the acid test. *New Phytologist*

- Xu-fu Z** (2003) Study on the Relationship and Development of the Agriculture Textile Material with Textile Industry [J]. *Sichuan Textile Technology* **4**: 10-15
- Yan X, Tan DKY, Inderwildi OR, Smith JAC, King DA** (2011) Life cycle energy and greenhouse gas analysis for agave-derived bioethanol. *Energy Environmental Science* **4**: 3110–3121
- Yang L, Carl S, Lu M, Mayer JA, Cushman JC, Tian E, Lin H** (2015) Biomass characterization of *Agave* and *Opuntia* as potential biofuel feedstocks. *Biomass and Bioenergy* **76**: 43–53
- Zhao C, Liu B, Piao S, Wang X, Lobell DB, Huang Y, Huang M, Yao Y, Bassu S, Ciais P** (2017) Temperature increase reduces global yields of major crops in four independent estimates. *Proceedings of the National Academy of Sciences* **114**: 9326-9331
- Zika M, Erb KH** (2009) The global loss of net primary production resulting from human-induced soil degradation in drylands. *Ecological Economics* **69**: 310–318

## Chapter 2

## Developmental Dynamics of Crassulacean Acid Metabolism (CAM) in *Opuntia ficus-indica*

Nicholas Niechayev<sup>1</sup>, Jesse A. Mayer, John C. Cushman<sup>1</sup>

<sup>1</sup>*Department of Biochemistry and Molecular Biology, University of Nevada, Reno, NV 89557-0330 USA*

### Abstract

Large agricultural species of cactus pear (*Opuntia ficus-indica*) show great potential for food, feed, and biofuel production in semi-arid and arid regions across the globe. However, the developmental basis of *O. ficus-indica* productivity in terms of its use of C<sub>3</sub> photosynthesis and crassulacean acid metabolism (CAM) remains poorly understood. Utilization of the C<sub>3</sub> photosynthetic pathway early in development might explain the high productivity of this obligate CAM species. The developmental progression of CAM was assessed in seedlings and cladodes developing on mature plants by titratable acidity,  $\delta^{13}\text{C}$  carbon isotopic ratios, and daily gas exchange measurements. Titratable acidity of seedlings revealed a significant buildup of nocturnal tissue acidity in cladodes and cotyledons 75 days after germination. Fifty-day-old seedlings showed  $\delta^{13}\text{C}$  ‰ values of  $-18.15 \pm 0.31$  typical of weak CAM plants. CO<sub>2</sub> assimilation occurred at dusk and night (phases 1 and 4) in seedlings, with predominant net CO<sub>2</sub> assimilation occurring at night once the primary cladode reached 5 cm in size. Slightly higher titratable acidity and  $\delta^{13}\text{C}$  ‰ values

indicative of CAM was observed in seedling cladodes compared to cotyledons. In daughter cladodes, nocturnal titratable acidity build-up began to increase when cladodes were approximately 5 cm in height and peaked at 20 cm in height. Isotopic mass spectrometric analysis revealed  $\delta^{13}\text{C}$  ‰ mean values between -14.77 ‰ and -15.30 ‰ (typical of CAM plants) regardless of cladode size. Daily 24-hour gas exchange measurements showed that the net daily  $\text{CO}_2$  uptake was negative until cladodes were greater than 10 cm in length and that  $\text{CO}_2$  uptake occurs primarily at night under greenhouse conditions. Collectively, these results suggest that developing *O. ficus-indica* cladodes begin as respiring carbon sink tissues that do not perform CAM and then begin to use CAM once cladodes reach 5 cm in length. Overall, these results demonstrate that CAM photosynthesis is the dominant form of carbon assimilation for *O. ficus-indica* even at the earliest stages of development.

## Introduction

Crassulacean acid metabolism is an alternative mode of photosynthesis in which stomata open at night for carbon uptake and transpiration instead of during the day, as is the case in  $\text{C}_3$  and  $\text{C}_4$  photosynthetic plants. CAM results in a four- to six-fold increase water-use efficiency (WUE) relative to  $\text{C}_4$  and  $\text{C}_3$  photosynthetic species, respectively (Borland et al., 2009). CAM plants use carbonic anhydrase (CA) and phosphoenolpyruvate carboxylase (PEPC) for the initial fixation of  $\text{CO}_2$  at night in addition to ribulose-1,5-bisphosphate carboxylase-oxygenase (RUBISCO), which has a much lower reaction rate, is a

larger enzyme, discriminates against CO<sub>2</sub> containing C<sup>13</sup> isotopes, and occasionally fixes O<sub>2</sub> forming 2-phosphoglycolate, a product that must be regenerated back to 3-phosphoglycerate using photorespiration, an energetically wasteful process, before reentering the Calvin-Benson-Bassham cycle. Along with superior WUE, the carbon concentrating mechanism of CAM confers higher sun fleck capture efficiency to *Aechmea magdalenae*, which occupies lower canopy, light-limited environments (Skillman and Winter, 1997). CAM also confers a competitive advantage to plants occupying habitats where daytime ambient CO<sub>2</sub> levels and soil water may be limited as has been shown for the semi-aquatic *Isoetes* genus (Keeley, 1981, 1983; Pedersen et al., 2011; Yang and Liu, 2015).

Some plant species also occur as C<sub>3</sub> photosynthesis-CAM intermediates known as facultative CAM plant species (Cushman and Bohnert, 1999; Borland et al., 2011; Winter et al., 2015). Several facultative CAM species perform C<sub>3</sub> photosynthesis, CAM, or switch between C<sub>3</sub> photosynthesis and CAM in response to salinity (Bohnert et al., 2001), temperature (Nievola et al., 2005), nutrient deficiencies (Rodrigues et al., 2014) including changes in N source (Pereira et al., 2017), and changes in osmotic potentials (Cushman and Borland, 2002). Facultative CAM species are thought to exist as an evolutionary transitional state between C<sub>3</sub> photosynthetic and CAM as they tend to occur at lower frequencies than plant species using only C<sub>3</sub> photosynthesis or CAM (Silvera et al., 2010; Winter et al., 2015; Heyduk et al., 2019). However, the ability to switch between C<sub>3</sub> photosynthesis and CAM photosynthesis also provides fitness



advantages in environments where daily water input is unpredictable (Cushman and Bohnert, 1999), or in regions that experience only brief periods of seasonal drought (Leverett et al., 2021). The transition from  $C_3$  photosynthesis to CAM can also be developmental (Winter et al., 2011). For example, the first leaflets of a growing *Kalanchoe fedtschenkoi* perform  $C_3$  photosynthesis, whereas more mature leaves transition developmentally to CAM (Winter et al., 1982).

In past studies, dawn/dusk tissue acidity,  $C^{12}:C^{13}$  isotope ratio, and diel gas exchange measurements have been used to survey the amount of CAM occurring across a multitude of plant species (Messerschmid et al., 2021). Nocturnal stomatal conductance, fixation of  $CO_2$  by PEPC, and accumulation and decarboxylation cycles of malate are all traits not unique to CAM plant species (Winter et al., 2015). However, the linked nocturnal acid accumulation with PEPC carbon assimilation is indicative of CAM (Ting, 1985) and has been used as a proxy of productivity for CAM plant species by measuring the changes in dawn to dusk acidity build-up with changes in environment (Nobel and Hartsock, 1983; Nobel, 2010). Fixation of  $CO_2$  containing  $^{12}C$  and  $^{13}C$  isotopes by PEPC in CAM vs. mostly  $CO_2$  containing  $^{12}C$  fixed by RUBISCO in the  $C_3$  photosynthetic pathway means that the measured ratio of  $^{12}C:^{13}C$  in a tissue sample can be used to reveal how much CAM activity was occurring over the lifetime of the plant (O'Leary, 1988; Silvera et al., 2010). Lastly, diel gas exchange measurements can be performed to the rate and duration of  $CO_2$  assimilation over the course of a whole day (Chomthong and Griffiths, 2020).

Diel CO<sub>2</sub> uptake in CAM plants is often described in four separate phases over a period of 24 hours (Dittrich et al., 1973; Osmond, 1978; Owen and Griffiths, 2013; Chomthong and Griffiths, 2020). Phase 1 begins in the dark when stomata are open, and CO<sub>2</sub> is fixed by CA and PEPC into a 4-carbon acid, usually malate, that is ultimately stored in the vacuole overnight. Phase 2 happens as the sun begins to rise, and stomata are still open, resulting in a sharp spike of CO<sub>2</sub> fixation by combined activities of both CA/PEPC and light-activated RuBisCO. Phase 3 occurs mid-day when there is full sunlight, and net CO<sub>2</sub> assimilation is generally naught as stomata are shut during this time. During phase 3, malate is released into the mesophyll cytosol, and is decarboxylated by NAD(P)-malic enzyme into pyruvate and CO<sub>2</sub>, which both enter the Calvin-Benson-Bassham cycle as in the normal C<sub>3</sub> photosynthetic pathway. Lastly, phase 4 begins at dusk, with another spike of CO<sub>2</sub> fixation as the stomata begin to open due to a decline in mesophyll CO<sub>2</sub>, and CA/PEPC and RUBISCO both fix carbon as the sun sets.

CAM plant species that are adapted to xeric regions, such as *Opuntia ficus-indica*, are often described as obligate or constitutive CAM plants, which only utilize CAM in mature tissues for the duration of their life cycle, and under all abiotic conditions (Kluge and Ting, 1978; Osmond, 1978; Nobel, 1988; Winter et al., 2008). Cactus pear (*O. ficus-indica*) is a large photosynthetic stem succulent with large flat cladodes between each node (a platyopuntia *spp.*) with a rich agricultural history and center of diversity in central and southern Mexico (Griffith, 2004; Majur et al., 2012). The combined high growth rate, WUE, clonal propagation, and interspecific promiscuous breeding with other *Opuntia* cultivars

has contributed to its success for the agricultural production of edible cladodes, fruits, and fodder, and as a noxious weed in arid and semi-arid regions around the globe (DeFelice, 2004). More recently, *O. ficus-indica* has been recognized for methane (Mason et al., 2015; Krümpel et al., 2020) and bioethanol (Kuloyo et al., 2014) production, and cosmetic and cooking oil production from over 200 large seeds per fruit (El Mannoubi et al., 2009; Ciriminna et al., 2017).

Investigation of the use of C<sub>3</sub> photosynthesis vs. CAM in *Opuntia elatior*, a tropical epiphyte related to *O. ficus-indica* revealed that seedlings fixed the majority of CO<sub>2</sub> during the day, and only fixed more CO<sub>2</sub> at night when the plants were exposed to drought (Winter and Holtum, 2011). When the cotyledons initially emerged, 24-hour gas exchange was similar to that of C<sub>3</sub> photosynthesis plants in that all carbon was fixed during the day, and none of the phases of CAM were evident. As the central cladode emerged, seedling gas exchange patterns began to show all four phases of CAM, but CO<sub>2</sub> was predominantly fixed during phase 2 and 3, when light was available. Titratable acidity also increased with age, but more so with drought. *O. ficus-indica* seeds have been germinated under laboratory conditions (Altare et al., 2006; Khan, 2006; Podda et al., 2017; Mokotjomela et al., 2021). However, the degree of C<sub>3</sub> photosynthesis vs. CAM in the desert adapted *O. ficus-indica* seedlings has yet to be investigated.

Changes in *O. ficus-indica* cladode diel CO<sub>2</sub> uptake have been tested with changes in light (Nobel and Hartsock, 1983), temperature (Nobel and Hartsock, 1984), addition of gibberellic acid (De la Barrera and Nobel, 2004), fruit production (Nobel, 2000), in mother (base) cladodes with and without daughter

(distal) cladodes under water-deficit stress conditions, under shaded conditions (Pimienta-Barrios et al., 2007), under elevated CO<sub>2</sub> and light levels (Cui and Nobel, 1994; Nobel and Israel, 1994; North et al., 1995), soil volume (Nobel et al., 1994), detached cladodes (Raveh and Nobel, 1999), and in one- and two-year-old cladodes on fully grown plants in the field (Liguori et al., 2013). In general, *O. ficus-indica* diel gas exchange primarily occurs in phase 1 with the only change being a reduction in the rate and duration of gas exchange and nocturnal acidity build-up when conditions are unfavorable. Brief periods of CO<sub>2</sub> assimilation during phase 3 and 4 have been recorded in favorable conditions, but sharp spikes of CO<sub>2</sub> assimilation in phase 2 and 4 have generally not been observed in this species. *O. ficus-indica* cladodes begin as sink tissues when they emerge and become source tissues about 27 days after emergence (Wang et al., 1998). As the daughter cladodes grow, they initially show more CO<sub>2</sub> respiration than assimilation, an increase in carbohydrate-metabolism enzyme activities related to sink tissues at day 14, a gradual increase in nocturnal malate build-up, and initially import more carbon from mother cladodes. Interestingly, PEPC and RUBISCO activities were found to decrease as the cladodes grew, but this relationship was explained as being tied with decreasing cellular pH. Young cladodes (referred to as very young) from *O. ficus-indica* showed an increase in net CO<sub>2</sub> uptake in both the light and dark periods at a very similar magnitude as the cladode grew, and only when cladodes were water-deficit stressed did they show that net nocturnal CO<sub>2</sub> uptake overtook net daily CO<sub>2</sub> uptake (Winter et al., 2008). Net CO<sub>2</sub> uptake in the light increased when cladodes were re-watered, but

never was equal to or greater than nocturnal CO<sub>2</sub> uptake again after re-watering. The authors concluded that categorization of facultative and constitutive CAM may be convenient, but the reality is that CAM expression in plants is regulated on a continuum and not necessarily along strict categories of activity.

In this study, we investigated the occurrence of C<sub>3</sub> photosynthesis and CAM as *O. ficus-indica* seedlings and developing daughter cladodes grow by measuring dawn/dusk tissue acidity, <sup>12</sup>C and <sup>13</sup>C isotopes, and 24-hour gas exchange. The objective was to determine if the obligate CAM species *O. ficus-indica* only uses CAM photosynthesis in developing tissues, or if C<sub>3</sub> photosynthesis plays a part in the high growth rate observed in this species.

## Methods

### *Opuntia ficus-indica* seed collection, cleaning, and germination

To produce seeds for experimentation, four-year-old *O. ficus-indica* plants were transferred from 11.3 l pots to 50 l pots in 4:1 ratio of Sunshine MVP soil mix (Sun Gro Horticulture, Agawam, MA) and natural play sand (SAKRETE, Charlotte NC) in the University of Nevada, Reno valley road greenhouse complex. Plants were given 200 g of Osmocote (N-P-K of 14-14-14) as fertilizer and 8 grams of systemic insecticide treatment (Marathon® 1% Granular, OHP) every 6 months to control for thrips. Standard greenhouse conditions with natural light were approx. 1,100-1,500 μmol m<sup>-2</sup> s<sup>-1</sup> and temperature ranged from 28-32 °C day/17-18 °C night. In May, flowers were cross pollinated using cotton swabs. Over the proceeding months, fully mature fruits were collected for seed extraction. Seed extraction was performed by first removing the peel with a razor

blade. The excess pulp was separated by hand, and the remaining seed/pulp mix was placed in a steel mesh colander (2133, Norpro 3 1/4 inch) and rinsed. Seeds were then placed in 500 ml beakers (one per fruit) filled with distilled water at room temperature with a stir bar. Seeds were rinsed in the colander and placed back in beakers with fresh distilled water daily over a period of several days until all of the pectin had been removed from the seeds. At this point, seeds were folded in a paper towel, placed in a drawer to dry, and then placed into appropriately labeled 50 ml Falcon tubes (352070, Corning). Cleaned seeds were allowed to age at least two years before germination.

Prior to planting, seeds were sterilized in a solution containing 10% v/v bleach and 0.5% v/v Triton X-100. Seeds were placed in this sterilizing solution with at least 10 ml of solution per seed. The seeds remained in the sterilizing solution for at least 10 minutes with stirring. After sterilization, seeds were moved into a laminar flow hood while still in solution and poured into a sterilized steel colander. Seeds were then washed with three rounds of sterile, autoclaved water, one round of 200 proof ethanol (V1016, Koptec), and allowed to dry.

After drying, seeds were clipped with sterile nail clippers (Revlon) to allow the germination media to make contact with the embryo. Nail clippers were used to carefully remove the seedcoat from the radicle side of the seed and along the outer edge while avoiding crushing or cutting of the embryo (Figure 1B). Two to three clips were necessary to give enough room for the emerging seedling to emerge from the seed coat. Clipped seeds were then submerged in germination media containing either 3.0% w/v sucrose, 0.6% w/v Phyto agar (PTP01-1KG,

Caisson Labs), 0.5% w/v Murashige & Skoog medium with Gamborg's B5 vitamins (M404, PytoTechnology Laboratories), and 10 mM gibberellic acid (G-120-50, Gold Biotechnology Inc.) or the same media containing no sucrose in 25 x 100 mm sterile polycarbonate Petri dishes (89107-632, VWR). Petri dishes containing clipped seeds in germination media were then placed in a tissue culture growth chamber (AR-7522, Perceival Scientific, Inc. Derry, IA) set at 16/8 day/night cycles held at 24 °C and  $\sim 80 \mu\text{mol m}^{-2} \text{s}^{-1}$  provided by fluorescent lamps. The percentage and timing of germination was recorded. After a two-week period, germinated seedlings were either transferred into plates containing 3.0% w/v sucrose, 0.6% w/v Phytoagar, 0.5% Murashige & Skoog medium with Gamborg's B5 vitamins, and no gibberellic acid, or the same media without sucrose.

Titrateable acidity and isotopic mass spectrometric analysis of *O. ficus-indica* seedlings.

*O. ficus-indica* seedlings were destructively sampled after 30-days, 50-days, 75-days, and 100-days post germination for tissue acidity and carbon isotope measurements. For both measurements, seedlings were harvested and separated into cladode and cotyledon tissues, which were then weighed. For tissue acidity, seedlings were harvested at dusk and dawn and immediately flash frozen in liquid N<sub>2</sub>. The acidity was then analyzed using a modified protocol from Gehrig et al., 2005. Briefly, samples were placed in 25 ml beakers with 20 ml of 50% v/v methanol and heated until 10 ml volume was lost to ensure that all

methanol was boiled off, and that the water reached a minimum of 80 °C. Boiled samples were cooled to room temperature and brought back to 10 ml with deionized water. For each sample the initial pH was recorded and then titrated to a pH = 7 for malate equivalent, 8.4 and 10 in case the previous pH points were missed. All samples were titrated with 5 mM KOH.

The H<sup>+</sup> equivalent was calculated using the equation:

$$H = v * \left( \frac{0.01}{w} \right) * 1000$$

Where: H = H<sup>+</sup> equivalent, v = volume at pH in consideration, and w = fresh weight of the sample.

The difference between the average H<sup>+</sup> equivalent at dusk and at dawn was equal to the amount of malate (pH = 7) built up over night.

Samples collected for isotopic spectrometric analysis were collected at noon on the correct age after germination described above, dried for 72 hours in a LabConCo Freeze Dry System (Freezone 18), and pulverized using a Benchmark D2400 BeadBlaster Microtube Homogenizer. Between two and three mg of tissue was then loaded into tins (041070, Costech Analytical Technologies Inc., Valencia, CA), placed into a 96-well plate, and shipped to either the Facility for Isotope Ratio Mass Spectrometry (FIRMS) located at the University of California, Riverside (<https://ccb.ucr.edu/facilities/firms>) or the UC Davis, Stable Isotope Facility (SIF) at University of California, Davis



(<http://icpms.ucdavis.edu/facilities-procedures>) for the analysis of the ratio of  $^{12}\text{C}$  and  $^{13}\text{C}$  isotopes in each sample using Vienna Pee Dee Belemnite (VPDB) as the reference standard.

### Seedling gas exchange measurements

After germination, and an approximate one-month period in media that did not contain GA, seedlings with fully emerged cotyledons were transferred to 65 mm LI-COR pots (610-09646, LI-COR Environmental) with autoclaved Sunshine MVP soil mix (Sun Gro Horticulture, Agawam, MA) for gas-exchange experiments. Once the seedlings were potted, the entire pot with plant was placed in a plastic container with about 3 cm deep sterilized water to allow the soil to take up water through the drainage holes and maintain field capacity without changing the soil level or physical structure (Figure 1C). Plants were kept on a custom-built fluorescent light rack and moved closer or farther away from the light source to maintain either a PAR of 100 or 300  $\mu\text{mol m}^{-2} \text{s}^{-1}$  depending on the experiment. The dates that seeds were placed in germination media, transferred to regular media, transferred to soil, and measured in the LI-COR portable photosynthesis system were all recorded. Just prior to gas exchange measurements, size of cotyledons, central cladode, and stem height were measured, and several pictures were taken from both side and top views.

In the first experiment, gas exchange was recorded over a 48-hour period in two separate 24-hour measurements using the LI-COR 6400XT portable photosynthesis system with the whole plant *Arabidopsis* chamber with clear top

attached. In the first measurement, the LI-COR mixer was set to hold the sample chamber  $\text{CO}_2$  at  $400 \mu\text{mol mol}^{-1}$ , the flow rate was set to  $500 \mu\text{mol s}^{-1}$ , leaf fan to fast (setting 5), block temperature was set to  $20^\circ\text{C}$ , and the photosynthetically active radiation (PAR) at plant level was  $100 \mu\text{mol m}^{-2} \text{s}^{-1}$  with a 12-hour day/night photoperiod. The auto program (auto log 2) was set to log photo once every 5 minutes for 1440 minutes and match after every log. Desiccant (2088701, LI-COR) and soda lime (9964-090, LI-COR Biosciences) were changed every 3-4 hours. Humidity was held between 50-70% within the sample period.

Interference from root respiration was avoided by using a LI-COR 6400 exhaust set up that forces airflow down through the soil by restricting 50% percent of the exhaust flow (Figure 2 in: <https://www.licor.com/documents/891w0pf0ooypx3wgfmmr>). The air forced down into the soil was pushed out of six small holes made with a hot needle about 6 cm down from the lip of the pots. Before beginning the second measurement, the exhaust valve was turned to restrict air flow by 100% to force air down through the soil, and the flow was set to the maximum with desiccant on full scrub for one hour until the soil in the pot was fully dried. Pots were weighed before and after drying as the weight difference between wet and dry soil in the 65 mm pots was found to be approximately 30 g in a preliminary trial. A second, dry measurement, was then run in which all the above conditions were the same, except humidity and soil moisture were at 0%.

Another gas exchange experiment was conducted using a different set of seedlings. All settings were kept the same with the exception that seedlings were

acclimated and measured at a PAR of  $300 \mu\text{mol m}^{-2} \text{s}^{-1}$  at the plant level, and each measurement was only conducted for 24-hours on well-watered seedlings only. During this time the LI-COR 6400XT software malfunctioned, and a LI-COR 6800 with 6800-17 small plant chamber (Figure 1-2 in: <https://www.licor.com/documents/eg2bp3sqbr4a97wjwhvupgigqter9zic>) was used instead following factory guidelines, with flow rate of  $800 \mu\text{mol s}^{-1}$ , pressure valve set to 0.2 kPa, relative air humidity to 50%, sample  $\text{CO}_2$  to  $400 \mu\text{mol mol}^{-1}$ , fan speed of 10,000 rpm, and a block temperature of  $20 \text{ }^\circ\text{C}$ . The auto log logged data was collected once every 300 seconds for 1440 minutes with matching after each log point. The LI-COR 6800 also uses a system for pushing air down through the soil, but instead of holes in the side of the pot, a silicon exhaust cup was attached to the bottom of the pot. This cup has a nipple that is opened or closed until the measured leak value of 20% is achieved.

#### Daughter cladode titratable acidity and isotopic mass spectrometric analysis

To determine daily nocturnal acidity build-up in daughter cladodes, 4-year-old *O. ficus-indica* individuals in 11.3-l pots within the University of Nevada, Reno greenhouse were selected for analysis. A 10 mm Fisherbrand Cork Borer was used to take punches of cladodes within different size categories ranging from 2-35 cm in length. In May of 2016 tissues were collected at the appropriate dusk and dawn times and immediately weighed and flash frozen for later titratable acidity analysis. Titratable acidity was measured and calculated

exactly as described above in the titratable acidity of *O. ficus-indica* seedlings section.

A second set of samples was also taken in May of 2017 at noon from the same size categories using a 10 mm cork borer. These samples were weighed, and immediately lyophilized. The freeze-dried samples were then pulverized with a bead beater, and 2 to 3 mg of each sample was prepared for shipment to the FIRMS or SIF facility as described above for *O. ficus-indica* seedlings.

#### Daughter cladode gas exchange measurements

To measure the rate and duration of photosynthesis in growing daughter cladodes, emerging 2.5 cm cladodes were placed in a custom clear Plexiglass chamber (30cm tall and 17cm wide cylinder, Figure 1A; Tripp Plastics, Reno, NV) connected to the LI-COR 6400XT. The node of the daughter cladode was flush with the base of the chamber, and puddy (21-601, Ideal Industries) was used to seal any air gaps around the node. For this experiment the LI-COR mixer was set to hold the reference chamber CO<sub>2</sub> at 400  $\mu\text{mol mol}^{-1}$ , the flow rate was set to 700  $\mu\text{mol s}^{-1}$ , leaf fan to fast (setting 5), block temperature was set to 25 °C, and the ambient PAR was measured with the LI-COR 6400XT external light sensor placed in a level position above the chamber with puddy. At the beginning of each measurement, the length of the cladode was measured by looking across a measured grid on each side of the custom chamber, and then the LI-COR 6400XT was set to auto log ever 10 minutes for 1440 minutes while matching once ever 30 minutes. Measurements were repeated daily until the cladode grew too large to fit

in the chamber (about 15 cm in length).  $\Delta\text{CO}_2$  was calculated by subtracting the sample chamber  $\text{CO}_2$  (PPM) from the reference chamber  $\text{CO}_2$  concentration. All cladodes were measured when new cladodes were flushing between April 3<sup>rd</sup> and June 22<sup>nd</sup> in 2017.

In an attempt to separate out variation due to changing conditions within the greenhouse (standard daytime greenhouse conditions with natural light at approx. 1,100-1,500  $\mu\text{mol m}^{-2} \text{s}^{-1}$  and temperature at 28-32 °C day/17-18 °C night with gradual sunup and sundown), 24-hour gas exchange of a growing daughter cladode on an *O. ficus-indica* individual grown under growth chamber conditions was also measured. The growth chamber (AR 75L, Percival Scientific, Derry, IA.) was set to the known optimum temperature of 25 °C/15 °C day/night temperature with a 12-hour day night cycle, and a measured canopy PAR level of 366  $\mu\text{mol m}^{-2} \text{s}^{-1}$ .

### Statistical Analysis

All plots and statistical analysis for this study were performed in PRISM 9 software (Graphcladode Software), except for plots and calculations for cladode length growth rate, which were performed using Excel software (Microsoft, Inc.).

Seedling titratable acidity samples were grouped by tissue type (cotyledon or cladode), samples taken at dawn vs. dusk, and age (30, 50, 75, and 100 days after germination) and plotted together in a grouped column graph. A three-way analysis of variance (ANOVA) was performed to determine if any significant variance was due to differences in tissue type, time of day, and age or any

interactions among these variables. Welch's *t*-test was conducted to determine if significant differences were evident in nocturnal tissue acidity within each tissue type collected at dusk and dawn for each age group (eight independent comparisons). The sample size varied from five to ten within each group.

Seedling  $\delta^{13}\text{C}$  isotope ratios were grouped by tissue type, and age (30, 50, 75, and 100 days after germination) and plotted together in a grouped column graph ( $n = 6$ ). A two-way ANOVA was run to see if any significant variance in  $\delta^{13}\text{C} \text{ ‰}$  vs. VPDB (Vienna Pee Dee Belemnite) occurred due to differences in tissue type and age, or an interaction between tissue type and age. Welch's *t*-test was used to determine if significant differences in  $\delta^{13}\text{C} \text{ ‰}$  vs. VPDB occurred between tissue types within each age group (4 independent comparisons).

Daughter cladode tissue acidity was grouped into eight different size categories (0-2.5, 2.5-5, 5-10, 10-15, 15-20, 20-25, 25-30, and 30-35 cm) in cladode height with separate dawn and dusk tissue acidity measured in each category. Welch's *t*-tests were performed to determine if a statistical difference occurred between dawn and dusk acidity in each category (8 independent comparisons). The minimum sample size was 2 and max of 6.

Daughter C isotope ratios were grouped into 9 size categories of 0-2, 2-4, 4-6, 6-8, 10-12, 12-14, 14-16 cm and adult cladodes with an  $n=6$ . cladodes in the adult category were fully matured cladodes towards the base of the plant that were 35 cm or more in length. A one-way ANOVA was conducted to determine if any variance in measured  $\delta^{13}\text{C} \text{ ‰}$  vs. VPDB occurred across the size categories. A

follow up Tukey's multiple comparisons test was used to reveal any groupings among size categories in relation to measured  $\delta^{13}\text{C}$  ‰ vs. VPDB.

Gas exchange results for seedlings grown in watered conditions under a PAR of  $100 \mu\text{mol m}^{-2} \text{s}^{-1}$ , dry conditions under a PAR of  $100 \mu\text{mol m}^{-2} \text{s}^{-1}$ , watered conditions under a PAR of  $300 \mu\text{mol m}^{-2} \text{s}^{-1}$ , and daughter cladodes in a custom transparent Plexiglas chamber were analyzed independently using the same analysis. All 24-hour measurements for each individual seedling or cladode were plotted together with y-axis being the photosynthesis rate ( $\mu\text{mol CO}_2 \text{ m}^{-2} \text{ s}^{-1}$  for seedlings and  $\Delta\text{CO}_2$  (ppm) for daughter cladodes) and x-axis as time (h:m:s). All of the 24-hour measurements were aligned to the time point in which the attached light sensor recorded a PAR of  $0 \mu\text{mol m}^{-2} \text{ s}^{-1}$ . Then, an area under the curve (AUC) analysis was performed for each of the 24-hour measurements and categorized by cladode length, which was the calculated total diel carbon assimilated for each cladode length measured (net  $\mu\text{mol CO}_2 \text{ m}^{-2}$  for seedlings and net ppm  $\text{CO}_2$  for daughter cladodes). Afterward, each plot was split into only light periods or dark periods (approximately 12 hours each). The AUC of the light period plots reflected the total carbon assimilated in the light, and the AUC of the dark period plots reflected the total carbon assimilated at night. Lastly, the calculated diel, light, and dark total carbon assimilated were all plotted together vs. measured cladode length for each measurement for each experiment to visualize trends in carbon fixation as *O. ficus-indica* cladodes grew.

To determine the growth rate of the central cladode in seedlings, the measured cladode length and combined cotyledon length was plotted vs. days

after germination. The rate of seedling cladode length increase was found to briefly decrease as the cotyledons began to senesce. So, the center cladode length growth rate was calculated by determining the slope of the plotted line before cotyledon senescence began, which was determined by photographs and the initial decrease and reduction in combined cotyledon length vs. days after germination. These values were averaged together for the PAR 100 seedlings ( $n = 4$ ) and the PAR 300 seedlings ( $n = 4$ ). These experiments were not directly comparable because PAR 100 seedlings had intermittent drying for the dry experiment, while PAR 300 seedlings were well watered for the duration of the experiment, but a standard  $t$ -test was used to measure for significant difference of average cladode length growth between the PAR 100 and PAR 300 experiments regardless.

To determine growth rate of daughter cladodes during the sample period, the length of each daughter cladode was plotted with the day it was sampled. The slope of the line was used to calculate cladode growth rate and averaged across all measured daughter cladodes ( $n = 5$ ) except for the daughter cladode measured under growth chamber conditions.

## Results

### CAM development in seedlings

Seedling age, tissue type, and time of day all had a highly significant effect on titratable acidity (Table 1) with the interaction of days after germination with tissue type also having a significant effect on tissue acidity variance (Table 1). No significant difference in seedling tissue acidity of cotyledons collected at



dusk vs. cotyledons collected at dawn was evident until 75 days after germination, and this difference was not significant again until 100 days after germination (Figure 2A). No significant difference in seedling tissue acidity of cladodes collected at dusk vs. cladodes collected at dawn until 75 days after germination was detected, and this significant difference persisted 100 days after germination (Figure 2A). Mean  $\delta^{13}\text{C}$  ‰ ratio values for of cotyledons (-18.43 ‰) and cladodes (-17.53 ‰) were not significantly different 50 days after germination (Figure 2B). While these values were not indicative of strong CAM, they were well within the range of CAM species (O’Leary, 1988; Messerschmid et al., 2021)

In the watered PAR 100 gas exchange experiments, there was an increase in duration and rate of  $\text{CO}_2$  fixation during phase 1 and 4, but not 2 and 3 as the central cladode grew (Figure 3A, Sup. Figures 1-6). Total net carbon assimilated in well-watered seedling grown under PAR 100 was negative during the dark and diel periods until the central cladode reached 5 cm in height (Figure 3B, Supplemental Figures 7-11). Net carbon assimilation in the light period was higher than the dark period (but still negative), until the central cladode was 4 cm in height, at which point net carbon fixation during the dark period surpassed the light period and increased steadily (Figure 3B). Seedlings grown under dry conditions under PAR 100 also showed an increase in  $\text{CO}_2$  assimilation duration and rate during phases 1 and 4, but not phases 2 and 3 (Figure 4A, Supplemental Figures 12-15). However, the amount of  $\text{CO}_2$  fixed in these phases was diminished compared to seedlings grown under well-watered conditions under PAR 100 (Figure 3A, B). The net diel  $\text{CO}_2$  assimilation in seedlings grown under

dry conditions under PAR 100 was negative until the cladodes reached 5 cm in height (Figure 4B, Supplemental Figures 17-20). The net nocturnal CO<sub>2</sub> assimilation was less than the net day CO<sub>2</sub> assimilation rate until the cladodes reached 5 cm in height, at which point the net CO<sub>2</sub> assimilated during the night surpassed the daytime fixation (Figure 4B).

Seedlings grown under well-watered conditions under PAR 300 showed a longer duration and higher rate of CO<sub>2</sub> assimilation in phases 1 and 4 (Figure 5A, Supplemental Figures 26-33) than that of seedling grown under well-watered conditions with PAR 100 (Figure 4A) and seedlings grown under dry under PAR 100 (Figure 3A). As observed for seedlings grown under PAR 100 under either well-watered or dry conditions, PAR 300 seedlings exhibited neither CO<sub>2</sub> assimilation in phase 2, nor obvious CO<sub>2</sub> assimilation during phase 3 (Figure 5A). Initially, most of the daily net CO<sub>2</sub> assimilated by seedlings under PAR 300 was fixed during the day in phase 4, but the nocturnal net CO<sub>2</sub> assimilated in phase 1 increased steadily (Figure 5B). A noticeable decrease in both daytime, and especially nighttime CO<sub>2</sub> assimilation was apparent as the cotyledons began to senesce from the seedlings under PAR 300 (Supplemental Figures 34-37). However, the occurrence of cotyledons senescing and falling off the seedlings was not frequent or consistent enough to make any clear-cut statements about this phenomenon. Unlike seedlings grown under PAR 300, seedlings grown under PAR 100 did experience cotyledon senescence during the sample period, but the cotyledons never fell off within the sampling time frame. The average cladode height growth rate was 0.101 (+/- 0.017) and 0.124 (+/- 0.027) cm/day for

seedlings grown under PAR 100 and PAR 300, respectively, but these rates were not significantly different ( $P$  value = 0.2078).

#### CAM development in daughter cladodes

Tissue samples taken from daughter cladodes revealed no significant difference in dusk/dawn tissue acidity until the cladodes grew to a height of 2.5-5 cm (Figure 6A). This difference in dusk/dawn tissue acidity increased as cladodes grew larger (Figure 6A). The average  $\delta^{13}\text{C}$  ‰ ratio values for daughter cladodes ranged between  $-16.1 \pm 0.7$  in adult cladodes, and  $-14.7 \pm 0.3$  in cladodes 12-14 cm in height, which is typical of strong CAM (Figure 6B) (O'Leary, 1988). For daughter cladodes undergoing development with heights in size ranges of 0-2, 2-4, 4-6, 10-12, and 12-14 cm, the  $\delta^{13}\text{C}$  ‰ ratio values ( $-17.08$  to  $-14.02$ ) were slightly less negative, but also typical of strong CAM (Figure 6B).

Initially, daughter cladodes showed no recognizable phases in  $\text{CO}_2$  uptake over the 24-hour measurement period (Figure 7A). However, as the cladodes grew, the net diel, nocturnal, and daytime  $\text{CO}_2$  assimilated first decreased, and then increased (Figure 7B). CAM phases 1, 2, and 4 periods of  $\text{CO}_2$  assimilation in daughter cladodes increased as the cladodes grew larger in size (Figure 7A). Notably, no net positive diel  $\text{CO}_2$  assimilation was detected until the daughter cladodes reached 7 cm in height or greater (Figure 7B). Both net nocturnal and daytime  $\text{CO}_2$  assimilation increased as the daughter cladodes reached 15 cm (Figure 7A, B), although this trend was not seen in every cladode measured (Figure 7B, Supplemental Figures 42-46). Within the sample period, daughter cladodes showed a linear growth trend in relation to cladode height with an

average growth of 1.00 cm ( $\pm$  0.22) per day (Supplemental Figures 53-57). The daughter cladode measured on the plant grown under growth chamber conditions showed net positive diel and light period CO<sub>2</sub> assimilation, with net negative nocturnal assimilation at 8.5 cm in height (Supplemental figure 59), and both net light and dark period CO<sub>2</sub> fixation increased with the same magnitude as the cladode height increased. The growth chamber-grown daughter cladode showed clear periods of assimilation during phase 1 and 4, but only small, brief spikes of assimilation in phase 2 (Supplemental Figure 58). The measured cladode also had a linear gain in cladode height of 1.16 cm per day (Supplemental Figure 60).

## Discussion

Unlike the tropical epiphyte *O. elatior* seedlings measured in Winter et al., 2011, *O. ficus-indica* seedlings showed no initial C<sub>3</sub> photosynthetic CO<sub>2</sub> assimilation pattern, which was active all day long during phase 3 when only cotyledons were present (Figure 3A, 4A, & 5A). Initial net diel CO<sub>2</sub> fixation was negative in seedlings grown under PAR 100 (Figure 2B & 2B), and initially positive in seedlings grown under PAR 300 (Figure 5B). While the rate and duration of CO<sub>2</sub> fixation during phase 1 and 3 increased as the seedlings grew, phase 2 CO<sub>2</sub> assimilation at dawn measured in *O. elatior* seedlings was not observed in any of the *O. ficus-indica* seedling gas exchange experiments. These differences are likely due to *O. ficus-indica* being a terrestrial species adapted to especially arid regions, while the epiphytic *O. eliator* is adapted to the canopy under more humid conditions.

While gas exchange measurements of *O. ficus-indica* seedling grown under dry conditions with PAR 100 did not mimic conditions of prolonged drought, they showed the non-acclimated response in quickly dried soil. While the seedlings fixed less overall CO<sub>2</sub> under dry experiment, CO<sub>2</sub> assimilation in phases 1 and 4 were still visible (Figure 4A). Net positive fixation of CO<sub>2</sub> was apparent as cladodes reached 5 cm in height (Figure 4B), and the majority of CO<sub>2</sub> was fixed at night (Figure 4A & B), demonstrating that photosynthesis continues for at least one day, even when the soil was completely dried. Repeating this experiment with prolonged drought and re-watering would be useful as *O. elatior* was shown to switch from mostly daytime CO<sub>2</sub> assimilation to nighttime assimilation when subjected to water-deficit stress for several days, and switch back when watered (Winter and Holtum, 2011). However, *O. ficus-indica* seedlings fixed CO<sub>2</sub> predominantly at night after 5 cm in length in all gas exchange experiments, suggesting that unlike *O. elatior*, *O. ficus-indica* predominantly uses CAM.

Number of days after germination, time of day, and tissue type all had a significant effect on measured tissue acidity in seedlings (Table 1). High tissue acidity of *O. ficus-indica* seedling cotyledons and cladodes at both dawn and dusk only 30-days after germination (Figure 2A) may have been a response to the gibberellic acid treatment (Swanson and Jones, 1996) used in the initial media germination recipe, although this has yet to be well demonstrated in many plant, let alone a cactus species. Like many constitutive CAM plant species, *O. ficus-indica* seedlings demonstrated an early onset of CAM documented through tissue acidity measurements (Altesor, 1993; Loza-Cornejo et al., 2003; Hernández-

González and Villarreal, 2007) as both the primary cladode and cotyledons had significantly higher tissue acidity at dawn than dusk 75 days after germination. However, this dawn/dusk difference was no longer significant in cotyledons at day 100 as they senesced, whereas the cladode dusk/dawn acidity remained significantly different as they continued to grow.

No difference in the timing, frequency (Supplemental Figure 61), or isotopic  $^{12}\text{C}$ : $^{13}\text{C}$  ratio in seedling tissues was detected in *O. ficus-indica* grown on media containing sucrose vs. no sucrose. Collectively, *O. ficus-indica* seedlings displayed a mean germination rate of 63% using the methods outlined in this report. Other studies have also reported high germination rates when using nail clippers in combination with gibberellic acid treatment (Podda et al., 2017), and chemical scarification with concentrated  $\text{H}_2\text{SO}_4$  or  $\text{H}_2\text{O}_2$  for a few minutes (Altare et al., 2006; Khan, 2006). The latter method was found to be more challenging, as  $\text{H}_2\text{SO}_4$  damaged many embryos within two minutes of application, and scarified germination rates were near zero in our hands. Interestingly, the fungal species *Penicillium chrysogenum*, *Phoma medicaginis*, and *Trichoderma koningii*, and *Trichoderma harzianum* have all been shown to promote germination in *O. streptacantha*, *O. robusta*, and *O. leucotricha* (Delgado-Sánchez et al., 2011; Delgado-Sánchez et al., 2013) and may be helpful for improving germination rates in *O. ficus-indica* as well.

A high occurrence of tricotyledonous seedlings, a three-cotyledon trait known to be caused by only a few mutated genes in *Arabidopsis thaliana*, was measured, but the molecular basis in *O. ficus-indica* is unknown (Khan, 2006).

Within our batch, we observed only one tricotyledonous seedling (Supplemental Figure 62B). Other *O. ficus-indica* seedling oddities were observed, such as several seedlings that had roots emerging from the point at which the central cladode connects with the hypocotyl (Supplemental Figure 62A), possibly for anchoring the central cladode to the ground when cotyledons are lost. We also observed two unfused seedlings germinate out of a single seed (Supplemental Figure 62C). Monozygotic polyembryony is common in angiosperms (Tisserat et al., 1979; Filonova et al., 2002). Two to three *O. ficus-indica* seedlings have been grown from single seeds in the past (Vélez-Gutierrez and Rodríguez-Garay, 1996), and gibberellic acid, used here, has been shown to promote polyembryony in *O. ficus-indica* (Kaaniche-Elloumi et al., 2013). We also observed one seedling with two fused cladodes connected to a single hypocotyl (Supplemental Figure 62D), and another that produced cotyledons that did not senesce, but failed to produce a central cladode. While these abnormal growth forms deserve further study and are a reflection of the genetic diversity of the particular seedlings used in this study, only intact, normal phenotypes were used for experimentation in this study.

Young, developing *O. ficus-indica* daughter cladodes had an increase in nocturnal tissue acidity build-up between 2.5 and 5.0 cm in length (Figure 6A),  $^{12}\text{C}:^{13}\text{C}$  ratios within the range of typical CAM regardless of size (Figure 6B), and an initial net negative dip in both light and dark fixation of  $\text{CO}_2$  before emergence of a net positive assimilation in both the light and dark periods (Figure 7B) with the increase of carbon gain during phases 1, 2 and 4 (Figure 7A). Collectively,

these results support the notion that as daughter cladodes emerge from mother cladodes, they initially start as sink tissues that metabolize resources partitioned from mature parts of the plant, releasing more CO<sub>2</sub> than fixed by either CA/PEPC or RUBISCO. These results are consistent with Wang et al., 1998 who found that daughter cladodes did not have a positive net CO<sub>2</sub> uptake until 20 days after initial appearance, that the sink-to-source transition is characterized by an increase in nocturnal malate build-up, that daughter cladodes imported carbohydrates from mother cladodes until 25 days after emergence, and was accompanied by a strong increase in sucrose synthase and hexokinase enzyme activities, which are linked to breakdown of carbohydrates from source tissues. The 24-hour gas exchange measurements in Wang et al., 1998 showed brief periods of phase 4 assimilation, and primarily phase 1 assimilation of CO<sub>2</sub> when the cladodes reached 28-days of age, while our results clearly showed increasing CO<sub>2</sub> assimilation in phase 1, 2, and 4 in growing daughter cladodes (Figure 7A).

While the greenhouse grown plants did not exhibit a net positive diel carbon assimilation until the cladodes reached about 10 cm in length (Figure 11B), this trend was not observed for all cladodes measured (Supplemental Figure 47-48). However, the daughter cladode measured on the *O. ficus-indica* individual grown in the growth chamber showed higher daytime than nighttime net CO<sub>2</sub> assimilation (Supplemental Figure 59), and both daytime and nighttime net CO<sub>2</sub> assimilation increased at a similar magnitude as the cladode grew, which was also observed by Winter et al., 2008 in lab conditions with similar PAR level. Unlike the greenhouse, the growth chamber daughter cladode had consistent light



intensity during the light period and optimal day night temperatures. The resulting duration and rate of CO<sub>2</sub> fixation during phase 4 was much higher (Supplemental Figure 58) than that observed in greenhouse grown plants (Figure 7A, Supplemental Figures 42-46), which were likely limited in the amount of CO<sub>2</sub> that could be fixed during phase 3 and 4 by a gradual reduction of light at dusk, and gradual increase in light at dawn respectively. Curiously, while phase 4 was dramatically increased in the growth chamber grown plant, a strong increase in phase 2 vs. greenhouse plants was not observed (Supplemental Figure 58). More experimentation under growth chamber conditions is needed to make meaningful comparisons, but the greenhouse grown plants likely better represent cladode growth dynamics of plants grown under field conditions.

In this study, an early, significant build-up of nocturnal tissue acidity, typical CAM <sup>12</sup>C: <sup>13</sup>C ratios, and primarily nocturnal net CO<sub>2</sub> assimilation in *O. ficus-indica* seedlings all indicate the use of CAM in cotyledons and cladodes shortly after germination. In addition, *O. ficus-indica* daughter cladodes emerge as sink tissues that release more CO<sub>2</sub> through respiration than fixed by photosynthesis and begin to assimilate CO<sub>2</sub> both at night and briefly during dawn and dusk. These results show that seedlings use CAM photosynthesis early in development, and C<sub>3</sub> photosynthesis is not the predominantly used form of photosynthesis even under well-watered conditions. These findings also show that developing cladodes of *O. ficus-indica* begin as sink tissues, and switch to CAM after reaching about 5 cm in length, and fix CO<sub>2</sub> predominantly at night under greenhouse condition, but predominantly during the day under artificial

conditions with a continuous light level throughout the day.  $C_3$  photosynthesis does not appear to contribute to the high productivity observed in *O. ficus-indica* in developing tissues.

### Acknowledgments

This research was funded in part by Nevada Agricultural Experimental Station (NEV-0377, NEV-0380) and National Institute of Food and Agriculture (NIFA), U.S. Department of Agriculture, Sustainable Bioenergy and Bioproducts Challenge Area (Award #2018-68005-27924). We would like to thank Charli Faris, Eileen Rodriguez, Lisa Petrusa, and Nathan King for their assistance in running 24-hour gas exchange measurements on seedlings.

## Tables

**Table 1:**  $\delta^{13}\text{C}$  ‰ ratio value ranges observed for different modes of photosynthesis adapted from (O'Leary, 1988).

$\delta^{13}\text{C}$ ‰ values in C <sub>3</sub> , C <sub>4</sub> , and CAM plants.				
C <sub>3</sub> Photosynthesis Plants	C <sub>4</sub> Photosynthesis Plants	Typical CAM Plants	Strong CAM Plants	Weak CAM Plants
-25 to -29	-12 to -16	-10 to -20	-11	-28

**Table 2:** 3-way ANOVA results of Tissue acidity ( $\mu\text{mol H}^+$  / g f.w.) of cotyledons sampled at dusk and dawn, and cladodes at dusk and dawn at 30, 50, 75, and 100 days after germination.

Source of Variation	% of total variation	P value	P value summary	Significant?
Days after germination	10.87	<0.0001	****	Yes
Cotyl vs. cladode	9.076	<0.0001	****	Yes
Dusk vs. Dawn	15.84	<0.0001	****	Yes
Days after germination x Cotyl vs. cladode	3.636	0.0428	*	Yes
Days after germination x Dusk vs. Dawn	2.46	0.1337	ns	No
Cotyl vs. cladode x Dusk vs. Dawn	1.018	0.1275	ns	No
Days after germination x Cotyl vs. cladode x Dusk vs. Dawn	1.327	0.3848	ns	No

## Figures

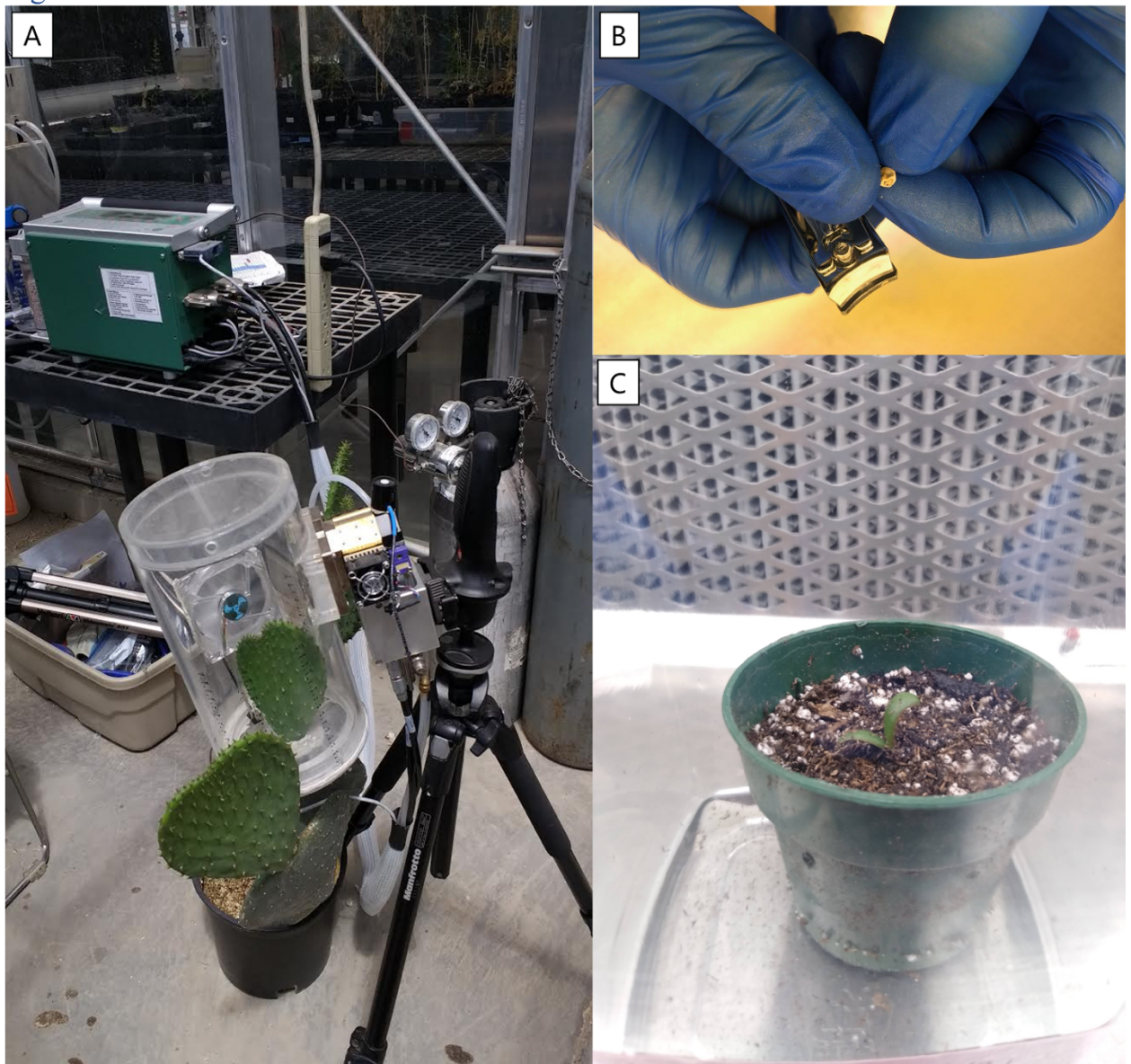


**Figure 1:** *Opuntia ficus-indica* daughter cladode gas exchange and seedling germination. **A:** The custom-built gas exchange chamber for measuring 24-hour gas exchange of *Opuntia ficus-indica* daughter cladodes as they grow. **B:** A 2-year-old *O. ficus-indica* seed with the seed coat clipped enough that the embryo can make contact with germination media containing gibberellic acid, and so the embryo has enough room to leave the seed coat. **C:** Between seedling gas

exchange experiments, seedlings were kept in 65 mm LI-COR pots in a plastic container with water in the bottom. Notice the holes in the sides of the pots for root respiration air flow to be pushed out of during measurements with the LI-COR 6400XT whole *Arabidopsis* chamber exhaust restriction set up.

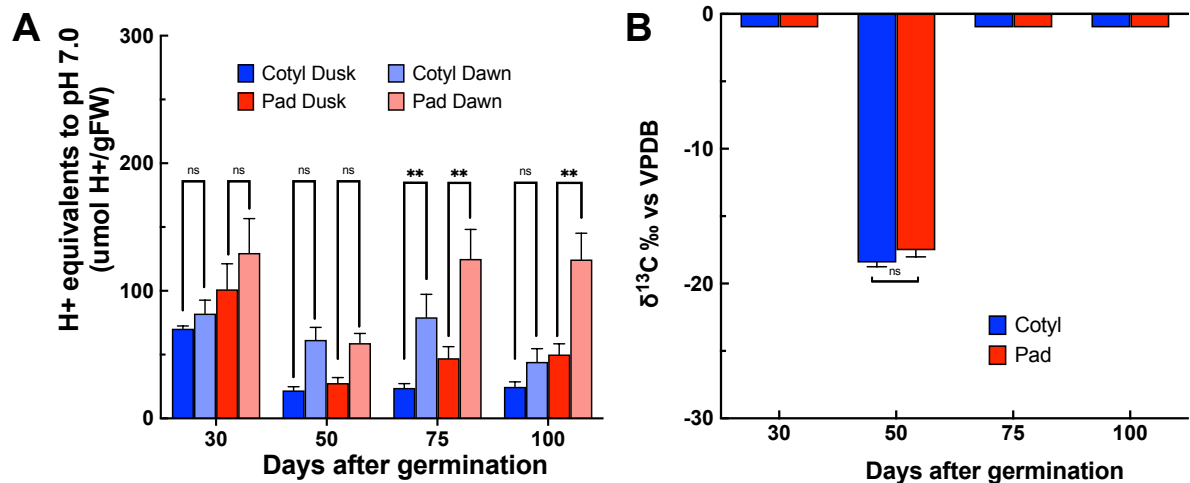


**Figure 2:** Seedling tissue acidity and  $\delta^{13}\text{C}$ . **A:** Tissue acidity ( $\mu\text{mol H}^+ / \text{g f.w.}$ ) of cotyledons sampled at dusk (dark blue bars) and dawn (light blue bars); and cladodes at dusk (dark red bars) and dawn (light red bars) at 30, 50, 75, and 100 days after germination. The significance comparisons are the results of independent Welch's paired  $t$ -tests ( $p < 0.05$ ) where 'ns' is not significant and '\*\*' is  $p < 0.0021$ , where  $n=5-10$ . **B:** Measured  $^{12}\text{C}:^{13}\text{C}$  isotope ratio ( $\delta^{13}\text{C} \text{ ‰ vs. VPDB}$ ) of seedling cotyledons (blue bars) and central cladode (red bars) at 30, 50, 75, and 100 days after germination. Isotope ratio values for 30, 75, and 100 days (all shown as values of  $-1 \delta^{13}\text{C} \text{ ‰ vs. VPDB}$ ) after germination are still being analyzed at UC Davis and are not included in this dissertation. The significance

comparisons are the results of independent Welch's paired  $t$ -tests ( $p < 0.05$ ) where 'ns' is not significant,  $n = 6$ .

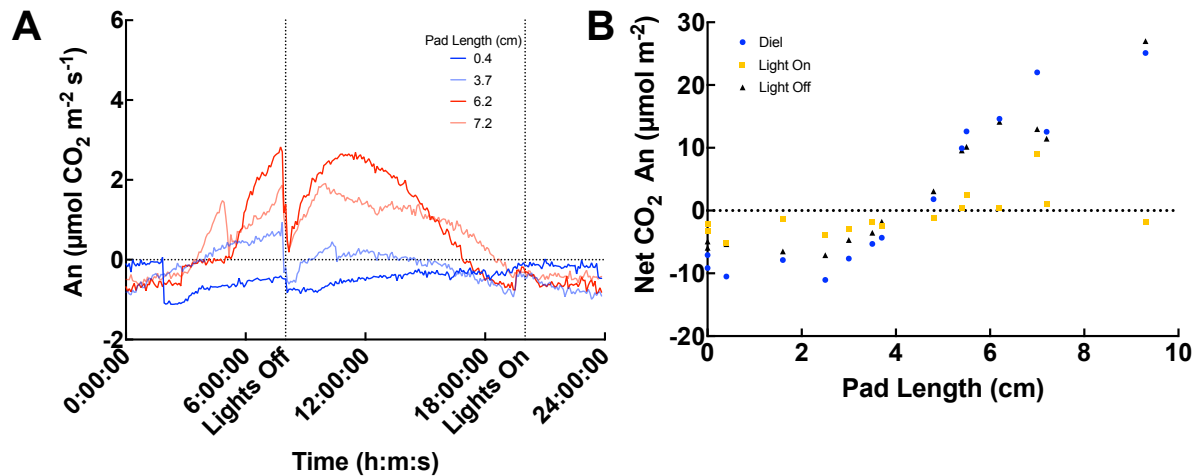


**Figure 3:** Well-watered PAR 100 gas exchange. **A:** 24-hour gas exchange measurements of *O. ficus-indica* seedling 3 (see Supplemental Figures 1-5 for all PAR 100 watered seedlings) grown at a PAR of  $100 \mu\text{mol m}^{-2} \text{ s}^{-1}$  at  $20^\circ \text{C}$  in well-watered conditions as the central cladode grows (dark blue to light blue to light red to dark red). The assimilation rate ( $\mu\text{mol CO}_2 \text{ m}^{-2} \text{ s}^{-1}$ ) was logged every 5 minutes. **B:** The combined diel (blue circles), light (yellow squares), and dark (black triangles) net assimilated  $\text{CO}_2$  ( $\mu\text{mol m}^{-2}$ ) vs. cladode length (cm) in all seedlings grown at PAR of  $100 \mu\text{mol m}^{-2} \text{ s}^{-1}$  at  $20^\circ \text{C}$  in well-watered conditions.

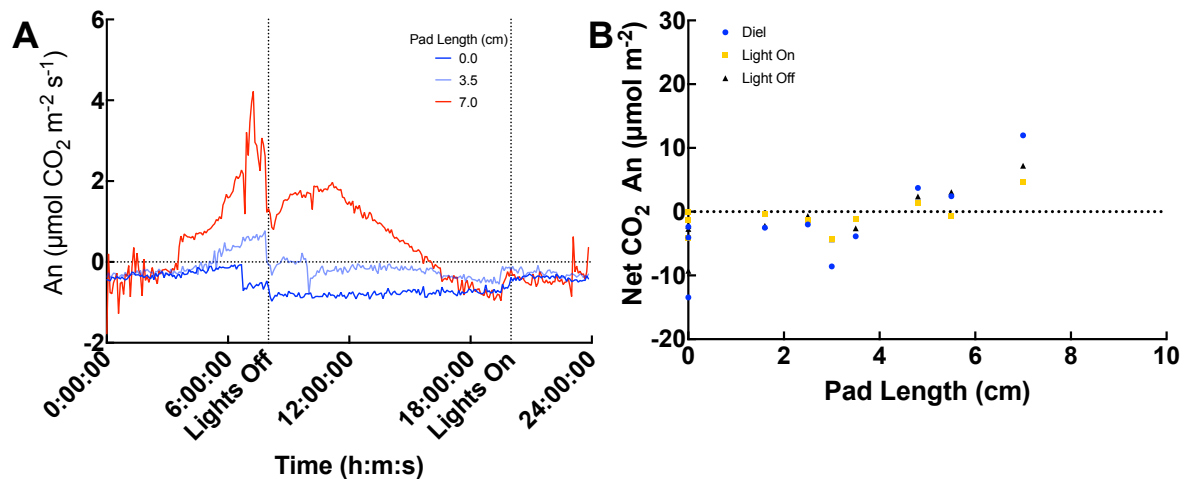


**Figure 4:** Dry PAR 100 seedling gas exchange **A:** 24-hour gas exchange measurements of *O. ficus-indica* seedling 5 (see Supplemental Figures 12-15 for all Dry PAR 100 seedlings) grown at a PAR of  $100 \mu\text{mol m}^{-2} \text{ s}^{-1}$  at  $20^\circ \text{C}$  in well-watered conditions as the central cladode grows (dark blue to light blue to light red to dark red). The assimilation rate ( $\mu\text{mol CO}_2 \text{ m}^{-2} \text{ s}^{-1}$ ) was logged every 5 minutes. Each measurement was taken after allowing the soil to completely dry out for one day. **B:** The combined diel (blue line), light (yellow line), and dark (black line) net assimilated  $\text{CO}_2$  ( $\mu\text{mol m}^{-2}$ ) vs. cladode length (cm) in all seedlings grown at PAR of  $100 \mu\text{mol m}^{-2} \text{ s}^{-1}$  at  $20^\circ \text{C}$  after drying out for one day.

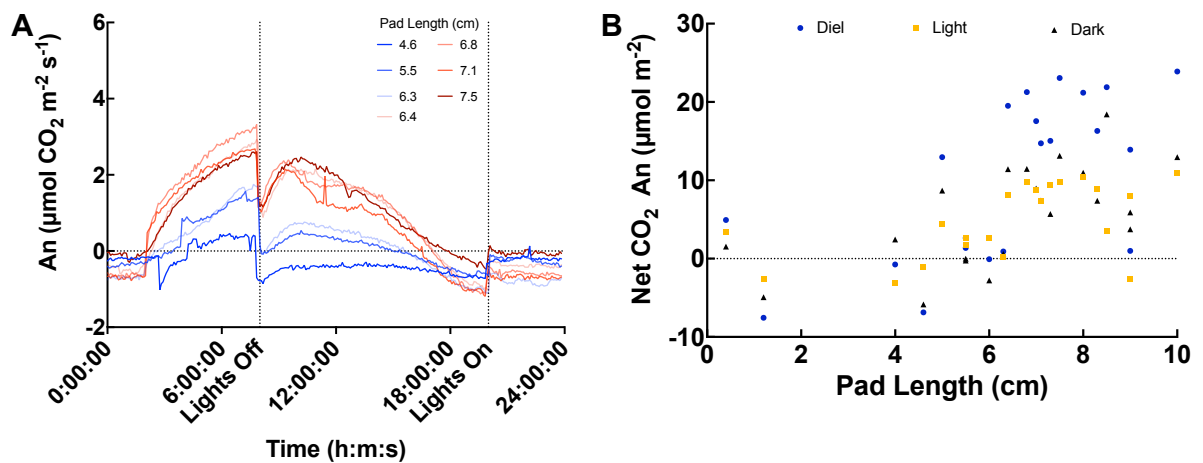


**Figure 5:** PAR 300 seedling gas exchange. **A:** 24-hour gas exchange measurements of *O. ficus-indica* seedling 8 (see Supplemental Figures 26-33 for all PAR 300 seedlings) grown at a PAR of  $300 \mu\text{mol m}^{-2} \text{ s}^{-1}$  at  $20^\circ \text{C}$  in well-watered conditions as the central cladode grows (Dark blue to light blue to light red to dark red). The assimilation rate ( $\mu\text{mol CO}_2 \text{ m}^{-2} \text{ s}^{-1}$ ) was logged every 5 minutes. **B:** The combined diel (blue triangle), light (yellow circle), and dark (black square) net assimilated  $\text{CO}_2$  ( $\mu\text{mol m}^{-2}$ ) vs. cladode length (cm) in all seedlings grown at PAR of  $300 \mu\text{mol m}^{-2} \text{ s}^{-1}$  at  $20^\circ \text{C}$  in well-watered conditions.



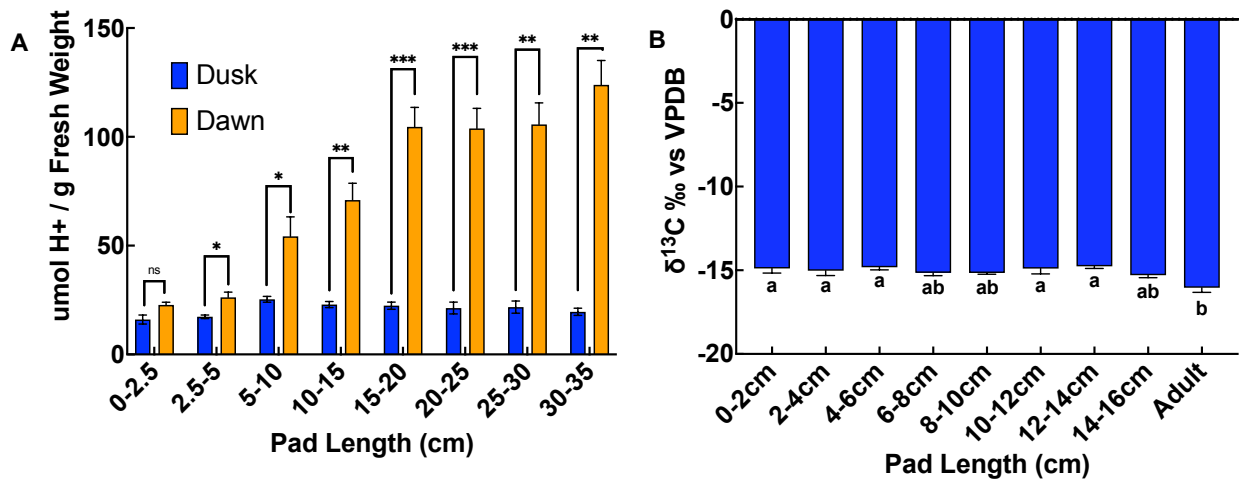


**Figure 6:** Daughter cladode tissue acidity and  $\delta^{13}\text{C}$ . **A:** Tissue acidity ( $\mu\text{mol H}^+ / \text{g f.w.}$ ) of *O. ficus-indica* daughter cladode tissues collected at dusk (blue bars) and dawn (orange bars). The significance comparisons are the results of independent Welch's paired *t*-tests ( $p < 0.05$ ) where 'ns' is not significant, '\*' is  $p < 0.0332$ , '\*\*' is  $p < 0.0021$ , and '\*\*\*' is  $p < 0.0002$ , error bars represent standard error ( $n = 2-6$ ). **B:** Measured  $^{12}\text{C}:^{13}\text{C}$  isotope ratio ( $\delta^{13}\text{C} \text{ ‰ vs. VPDB}$ ) of seedling cotyledons (blue bars) and central cladode (red bars) at 30, 50, 75, and 100 days after germination. The letters indicate grouping of compared means by Tukey's test ( $p < 0.05$ ), error bars represent standard error ( $n = 6$ ). For both figures, samples were taken from 4-year-old plants grown under standard greenhouse conditions with natural light at approx.  $1,100-1,500 \mu\text{mol m}^{-2} \text{ s}^{-1}$  and temperature at  $28-32 \text{ }^\circ\text{C}$  day/ $17-18 \text{ }^\circ\text{C}$  night

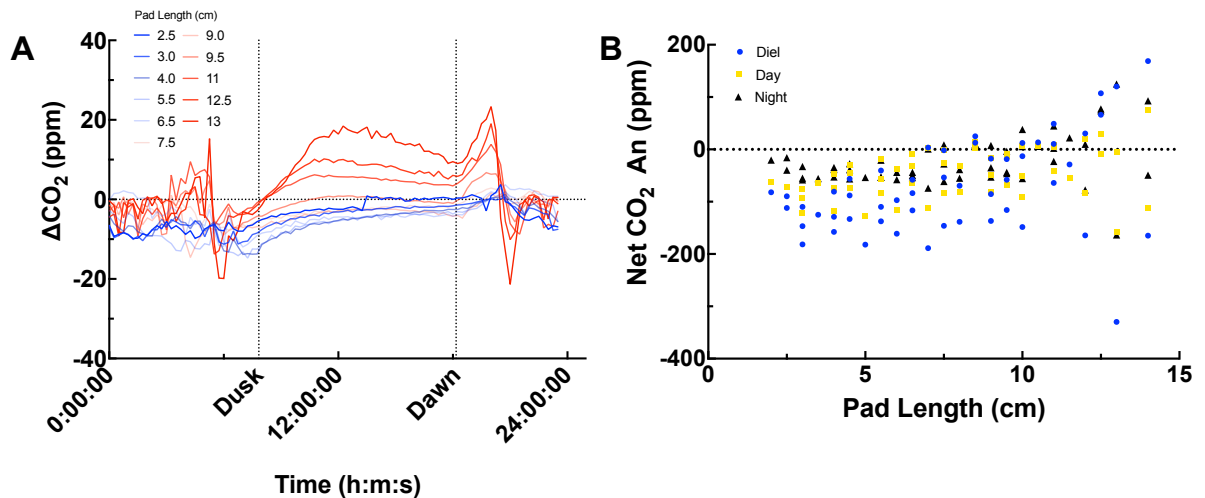


**Figure 7:** Daughter cladode gas exchange. **A:** 24-hour gas exchange measurements of *O. ficus-indica* daughter cladode 4 (see Supplemental Figures 42-46 for all daughter cladodes) in the custom-built chamber as the cladode grows (dark blue to light blue to light red to dark red) under standard greenhouse conditions with natural light at approx.  $1,100\text{-}1,500\ \mu\text{mol m}^{-2}\ \text{s}^{-1}$  and temperature at  $28\text{-}32\ ^\circ\text{C}$  day/ $17\text{-}18\ ^\circ\text{C}$  night. The  $\Delta\text{CO}_2$  (ppm) is equal to the sample chamber subtracted by the reference chamber and was logged every 10 minutes. **B:** Combined diel (blue circle), light (yellow square), and dark (black triangle) net assimilated CO<sub>2</sub> (ppm) vs. cladode length (cm) in *O. ficus-indica* daughter cladodes grown under standard greenhouse conditions with natural light at approx.  $1,100\text{-}1,500\ \mu\text{mol m}^{-2}\ \text{s}^{-1}$  and temperature at  $28\text{-}32\ ^\circ\text{C}$  day/ $17\text{-}18\ ^\circ\text{C}$  night.

## References

- Altare M, Trione S, Guevara JC, Cony M** (2006) Stimulation and promotion of germination in *Opuntia ficus-indica* seeds. Journal of the Professional Association for Cactus Development **8**: 91-100
- Altesor A** (1993) Changes in the photosynthetic metabolism during the early ontogeny in four cactus species. Acta oecol **13**: 777-785
- Bohnert HJ, Ayoubi P, Borchert C, Bressan RA, Burnap RL, Cushman JC, Cushman MA, Deyholos M, Fischer R, Galbraith DW, Hasegawa PM, Jenks M, Kawasaki S, Koiwa H, Kore-eda S, Lee BH, Michalowski CB, Misawa E, Nomura M, Ozturk M, Postier B, Prade R, Song CP, Tanaka Y, Wang H, Zhu JK** (2001) A genomics approach towards salt stress tolerance. Plant Physiology and Biochemistry **39**: 295-311
- Borland AM, Barerra-Zambrano VA, Ceusters J, Shorrocks K** (2011) The photosynthetic plasticity of crassulacean acid metabolism: an evolutionary innovation for sustainable productivity in a changing world. New Phytologist **191**: 619–633
- Borland AM, Griffiths H, Hartwell J, Smith JAC** (2009) Exploiting the potential of plants with crassulacean acid metabolism for bioenergy production on marginal lands. Journal of Experimental Botany **60**: 2879-2896
- Chomthong M, Griffiths H** (2020) Model approaches to advance crassulacean acid metabolism system integration. The Plant Journal **101**: 951–963
- Ciriminna R, Bongiorno D, Scurria A, Danzi C, Timpanaro G, Delisi R, Avellone G, Pagliaro M** (2017) Sicilian *Opuntia ficus-indica* seed oil:

Fatty acid composition and bio-economical aspects. *European Journal of Lipid Science and Technology* **119**: 1700232

- Cui M, Nobel PS** (1994) Gas exchange and growth responses to elevated CO<sub>2</sub> and light levels in the CAM species *Opuntia ficus-indica*. *Plant, Cell & Environment* **17**: 935–944
- Cushman JC, Bohnert HJ** (1999) Crassulacean acid metabolism: Molecular genetics. *Annual Review of Plant Physiology and Plant Molecular Biology* **50**: 305–322
- Cushman JC, Borland AM** (2002) Induction of Crassulacean acid metabolism by water limitation. *Plant Cell & Environment* **25**: 295–310
- De la Barrera E, Nobel PS** (2004) Carbon and water relations for developing fruits of *Opuntia ficus-indica* (L.) Miller, including effects of drought and gibberellic acid. *Journal of Experimental Botany* **55**: 719–729
- DeFelice MS** (2004) Prickly pear cactus, *Opuntia spp.* – A spine-tingling tale. *Weed Technology* **18**: 869–877
- Delgado-Sánchez P, Jiménez-Bremont JF, de la Luz Guerrero-González M, Flores J** (2013) Effect of fungi and light on seed germination of three *Opuntia* species from semiarid lands of central Mexico. *Journal of Plant Research* **126**: 643–649
- Delgado-Sánchez P, Ortega-Amaro M, Jiménez-Bremont J, Flores J** (2011) Are fungi important for breaking seed dormancy in desert species? Experimental evidence in *Opuntia streptacantha* (Cactaceae). *Plant Biology* **13**: 154–159

- Dittrich P, Campbell WH, Black CC** (1973) Phosphoenolpyruvate carboxykinase in plants exhibiting crassulacean acid metabolism. *Plant Physiology* **52**: 357–361
- El Mannoubi I, Barrek S, Skanji T, Casabianca H, Zarrouk H** (2009) Characterization of *Opuntia ficus-indica* seed oil from Tunisia. *Chemistry of Natural Compounds* **45**: 616-620
- Filonova L, Von Arnold S, Daniel G, Bozhkov P** (2002) Programmed cell death eliminates all but one embryo in a polyembryonic plant seed. *Cell Death & Differentiation* **9**: 1057-1062
- Griffith MP** (2004) The origins of an important cactus crop, *Opuntia ficus-indica* (Cactaceae): new molecular evidence. *American Journal of Botany* **91**: 1915-1921
- Hernández-González O, Villarreal OB** (2007) Crassulacean acid metabolism photosynthesis in columnar cactus seedlings during ontogeny: the effect of light on nocturnal acidity accumulation and chlorophyll fluorescence. *American Journal of Botany* **94**: 1344-1351
- Heyduk K, Hwang M, Albert V, Silvera K, Lan T, Farr K, Chang T-H, Chan M-T, Winter K, Leebens-Mack J** (2019) Altered gene regulatory networks are associated with the transition from C<sub>3</sub> to crassulacean acid metabolism in *Erycina* (Oncidiinae: Orchidaceae). *Frontiers in plant science* **9**: 2000
- Kaaniche-Elloumi N, Jedidi E, Mahmoud K, Chakroun A, Jemmali A** (2013) Gibberellic acid application and its incidence on *in vitro* somatic

embryogenesis and fruit parthenocarpy in an apomictic cactus pear (*Opuntia ficus-indica* (L.) Mill.) clone. In VIII International Congress on Cactus Pear and Cochineal 1067, pp 225-230

**Keeley JE** (1981) *Isoetes howellii*: a submerged aquatic CAM plant? American Journal of Botany **68**: 420–424

**Keeley JE** (1983) Crassulacean acid metabolism in the seasonally submerged aquatic *Isoetes howellii*. Oecologia **58**: 57–62

**Khan D** (2006) Some seed and seedling characteristics (tricotyledony) of *Opuntia ficus-indica* (L.) Mill.(Cactaceae). Intern. J. Biol. & Biotech **3**: 795-800

**Kluge M, Ting IP** (1978) Crassulacean acid metabolism, Vol 30. Springer-Verlag, Berlin

**Krümpel J, George T, Gasston B, Francis G, Lemmer A** (2020) Suitability of *Opuntia ficus-indica* (L) Mill. and *Euphorbia tirucalli* L. as energy crops for anaerobic digestion. Journal of Arid Environments **174**: 104047

**Kuloyo OO, du Preez JC, del Prado García-Aparicio M, Kilian SG, Steyn L, Görgens J** (2014) *Opuntia ficus-indica* cladodes as feedstock for ethanol production by *Kluyveromyces marxianus* and *Saccharomyces cerevisiae*. World Journal of Microbiology and Biotechnology **30**: 3173–3183

**Leverett A, Castaño NH, Ferguson K, Winter K, Borland AM** (2021) Crassulacean acid metabolism (CAM) supersedes the turgor loss point (TLP) as an important adaptation across a precipitation gradient, in the genus *Clusia*. Functional Plant Biology **48**: 703-716

- Liguori G, Inglese G, Pernice F, Sortino G, Inglese P (2013)** CO<sub>2</sub> uptake of *Opuntia ficus-indica* (L.) Mill. whole trees and single cladodes, in relation to plant water status and cladode age. Italian Journal of Agronomy **8**: e3-e3
- Loza-Cornejo S, Terrazas T, López-Mata L, Trejo C (2003)** Características morfo-anatómicas y metabolismo fotosintético en plántulas de *Stenocereus queretaroensis* (Cactaceae): su significado adaptativo. Interciencia **28**: 83-89
- Majur LC, Puente R, Griffith MP, Judd WS, Soltis PS, Soltis DE (2012)** Phylogeny of *Opuntia* ss (Cactaceae): clade delineation, geographic origins, and reticulate evolution. American Journal of Botany **99**: 847–864
- Mason PM, Glover K, Smith JAC, Willis KJ, Woods J, Thompson IP (2015)** The potential of CAM crops as a globally significant bioenergy resource: moving from 'fuel or food' to 'fuel and more food'. Energy and Environmental Science **8**: 2320–2329
- Messerschmid TF, Wehling J, Bobon N, Kahmen A, Klak C, Los JA, Nelson DB, dos Santos P, de Vos JM, Kadereit G (2021)** Carbon isotope composition of plant photosynthetic tissues reflects a Crassulacean Acid Metabolism (CAM) continuum in the majority of CAM lineages. Perspectives in Plant Ecology, Evolution and Systematics: 125619
- Mokotjomela TM, Thabethe V, Downs C (2021)** Comparing germination metrics of *Opuntia ficus-indica* and *O. robusta* between two sets of bird

species (Pied Crows and two smaller species). *Acta Oecologica* **110**: 103676

**Nievola C, Kraus J, Freschi L, Souza B, Mercier H** (2005) Temperature determines the occurrence of CAM or C<sub>3</sub> photosynthesis in pineapple plantlets grown in vitro. *In Vitro Cellular & Developmental Biology-Plant* **41**: 832-837

**Nobel P** (2000) Cactus physiological ecology, emphasizing gas exchange of *Platyopuntia* fruits. *In* IV International Congress on Cactus Pear and Cochineal 581, pp 143-150

**Nobel PS** (1988) Environmental biology of agaves and cacti. Cambridge University Press, New York

**Nobel PS** (2010) Desert wisdom/Agaves and Cacti: CO<sub>2</sub>, water, and climate change. iUniverse, New York, NY

**Nobel PS, Cui M, Miller PM, Luo Y** (1994) Influences of soil volume and an elevated CO<sub>2</sub> level on growth and CO<sub>2</sub> exchange for the Crassulacean acid metabolism plant *Opuntia ficus-indica*. *Physiologia Plantarum* **90**: 173-180

**Nobel PS, Hartsock TL** (1983) Relationships between photosynthetically active radiation, nocturnal acid accumulation, and CO<sub>2</sub> uptake for a Crassulacean acid metabolism plant, *Opuntia ficus-indica*. *Plant Physiology* **71**: 71-75

**Nobel PS, Hartsock TL** (1984) Physiological responses of *Opuntia ficus-indica* to growth temperature. *Physiologia Plantarum* **60**: 98-105



- Nobel PS, Israel AA** (1994) cladode development, environmental responses of CO<sub>2</sub> uptake, and productivity for *Opuntia ficus-indica* under elevated CO<sub>2</sub>. *Journal of Experimental Botany* **45**: 295–303
- North GB, Moore TL, Nobel PS** (1995) cladode development for *Opuntia ficus-indica* (Cactaceae) under current and doubled CO<sub>2</sub> concentrations. *American Journal of Botany* **82**: 159–166
- Osmond CB** (1978) Crassulacean acid metabolism: a curiosity in context. *Annual Review of Plant Physiology* **29**: 379–414
- Owen NA, Griffiths H** (2013) A system dynamics model integrating physiology and biochemical regulation predicts extent of crassulacean acid metabolism (CAM) phases. *New Phytologist* **200**: 1116–1131
- O’Leary M** (1988) Carbon isotope in photosynthesis. *Bioscience* **38**: 328–336
- Pedersen O, Rich SM, Pulido C, Cawthray GR, Colmer TD** (2011) Crassulacean acid metabolism enhances underwater photosynthesis and diminishes photorespiration in the aquatic plant *Isoetes australis*. *New Phytologist* **190**: 332–339
- Pereira PN, Smith JAC, Mercier H** (2017) Nitrate enhancement of CAM activity in two *Kalanchoë* species is associated with increased vacuolar proton transport capacity. *Physiologia Plantarum* **160**: 361–372
- Pimienta-Barrios E, Castillo-Cruz I, Zañudo-Hernández J, Méndez-Morán L, Nobel PS** (2007) Effects of shade, drought and daughter cladodes on the CO<sub>2</sub> uptake by cladodes of *Opuntia ficus-indica*. *Annals of applied biology* **151**: 137–144

- Podda L, Santo A, Leone C, Mayoral O, Bacchetta G** (2017) Seed germination, salt stress tolerance and seedling growth of *Opuntia ficus-indica* (Cactaceae), invasive species in the Mediterranean Basin. *Flora* **229**: 50-57
- Raveh E, Nobel PS** (1999) CO<sub>2</sub> uptake and water loss accompanying vernalization for detached cladodes of *Opuntia ficus-indica*. *International journal of plant sciences* **160**: 92-97
- Rodrigues MA, Freschi L, Pereira PN, Mercier H** (2014) Interactions between nutrients and crassulacean acid metabolism. *In Progress in Botany*. Springer, pp 167-186
- Silvera K, Neubig KM, Whitten WM, Williams NH, Winter K, Cushman JC** (2010) Evolution along the crassulacian acid metabolism continuum. *Functional Plant Biology* **37**: 995–1010
- Silvera K, Santiago LS, Cushman JC, Winter K** (2010) Incidence of crassulacean acid metabolism in the Orchidaceae derived from carbon isotope ratios: a checklist of the flora of Panama and Costa Rica. *Botanical Journal of the Linnean Society* **163**: 194–222
- Skillman JB, Winter K** (1997) High photosynthetic capacity in a shade-tolerant crassulacean acid metabolism plant (implications for sunfleck use, nonphotochemical energy dissipation, and susceptibility to photoinhibition). *Plant Physiology* **113**: 441-450
- Swanson SJ, Jones RL** (1996) Gibberellic acid induces vacuolar acidification in barley aleurone. *The Plant Cell* **8**: 2211-2221

- Ting IP** (1985) Crassulacean acid metabolism. Annual Review of Plant Physiology **36**: 595–622
- Tisserat B, Esan E, Murashige T** (1979) Somatic embryogenesis in angiosperms. Horticultural reviews **1**: 1-78
- Vélez-Gutierrez C, Rodríguez-Garay B** (1996) Microscopic analysis of polyembryony in *Opuntia ficus-indica*. Journal of the Professional Association for Cactus Development **1**: 39-48
- Wang N, Zhang H, Nobel PS** (1998) Carbon flow and carbohydrate metabolism during sink-to-source transition for developing cladodes of *Opuntia ficus-indica*. Journal of Experimental Botany **49**: 1835-1843
- Winter K, Garcia M, Holtum JAM** (2008) On the nature of facultative and constitutive CAM: environmental and developmental control of CAM expression during early growth of *Clusia*, *Kalanchoë*, and *Opuntia*. Journal of Experimental Botany **59**: 1829–1840
- Winter K, Holtum JA, Smith JAC** (2015) Crassulacean acid metabolism: a continuous or discrete trait? New phytologist **208**: 73-78
- Winter K, Holtum JAM** (2011) Drought-stress-induced up-regulation of CAM in seedlings of a tropical cactus, *Opuntia elatior*, operating predominantly in the C<sub>3</sub> mode. Journal of Experimental Botany **62**: 4037–4042
- Winter K, Holtum JAM, Smith JAC** (2015) Crassulacean acid metabolism: a continuous or discrete trait? New Phytologist **208**: 73–78

**Yang T, Liu X** (2015) Comparing photosynthetic characteristics of *Isoetes sinensis* Palmer under submerged and terrestrial conditions. *Scientific Reports* **5**: 17783

## Chapter 3

### The nitrogen preference of *Opuntia ficus-indica*: a sand culture snapshot.

Nicholas A. Niechayev, Paula N. Pereira, & John C. Cushman

#### Abstract

Cactus pear (*Opuntia-ficus indica* (L.) Mill.) is an important agricultural crassulacean acid metabolism (CAM) species that has been gaining popularity as a source of food, forage, fodder, secondary products, and as a biofuel feedstock. The preferred source of nitrogen for this species, whether it be nitrate ( $\text{NO}_3^-$ ), ammonium ( $\text{NH}_4^+$ ), or a combination of both, is not well understood. This chapter summarizes the investigation into the nitrate and ammonium preference of cladodes grown in sand culture with distilled water for one month and given a cross-factorial nutrient solution of 0.0, 2.5, 5.0, and 10.0 mmol of nitrate and/or ammonium for a month. Physiological measures were assessed including cladode growth, relative water content, chlorophyll, tissue acidity, soluble sugars, starch, nitrate, ammonium, glyoxylic acid, nitrate reductase activity, and nitrogen and carbon content. Relative steady-state transcript abundance of genes that encode enzymes involved in N metabolism and CAM were also determined. Significant differences were found in all measured variables except for cladode length, relative water content, and carbon content. Cladodes provided with only distilled water produced no new cladodes, showed increased starch content, decreased soluble sugar content, and increased tissue acidity. Furthermore, these control

cladodes showed increased steady-state mRNA expression of the CAM-related genes encoding aluminum-activated malate transporter (ALMT) and phosphoenolpyruvate carboxylase (PEPC) and higher steady-state mRNA expression of the nitrogen metabolism-related genes including glutamine oxoglutarate aminotransferase (Fd-GOGAT), glutamate dehydrogenase (NADH-GDH460), glutamine synthetase 2 (GS2), but lower expression of asparagine synthetase (AS) than nutrient supplied cladodes.

## Introduction

Contemporary climate models predict that both the severity and duration of drought caused by anthropogenic climate change will increase worldwide by the mid to late 21<sup>st</sup> century (Naumann et al., 2018; Pokhrel et al., 2021). The resulting depletion of ground water stores is already having a direct effect on agricultural production, especially in the southwestern United States. With climate change, the habitable zones of many plant species are shifting (Feeley et al., 2020). Large agricultural crassulacean acid metabolism (CAM) species such as those within the *Agave* and *Opuntia* genus, are projected to have range expansions with climate change due to their many adaptations to xeric regions around the globe (Owen and Griffiths, 2014). *Opuntia-ficus indica* (L.) Mill. is well adapted to long periods of extreme drought due to stem succulence, extremely thick cuticle, root retention, and CAM photosynthesis (Davis et al., 2019). This species has a rich history of traditional uses for food, forage, fodder, and profitable secondary products (Stintzing and Carle, 2005). More recently, it's

potential as biofuel feedstock, especially in the production of methane, has been recognized (Yang et al., 2015; do Nascimento Santos et al., 2016; Calabrò et al., 2018; Krümpel et al., 2020).

As an obligate CAM species, *O. ficus-indica* fixes most of its required carbon at night. CO<sub>2</sub> entering the cell through nocturnally open stomata (Males and Griffiths, 2017) is converted into bicarbonate by carbonic anhydrase followed by fixation into phosphoenolpyruvate (PEP) into oxaloacetate (OAA) by a CAM-specific phosphoenolpyruvate carboxylase (PEPC) isozyme (Nimmo, 2000; Boxall et al., 2017). This PEPC is constitutively expressed with its malate inhibition relieved through phosphorylation by a dedicated, circadian controlled phosphoenolpyruvate carboxylase kinase (PPCK) (Hartwell et al., 1999; Taybi et al., 2000). The resulting OAA is converted malate by malate dehydrogenase and shuttled into the vacuole by a putative aluminum malate transporter (ALMT) (Borland et al., 2016; Pereira et al., 2017) for storage until sunlight is available. During the day, stored malate is released from the vacuole, and decarboxylated by NAD(P)-malic enzyme (Winter and Smith, 2021) or phosphoenolpyruvate carboxykinase (PEPCK). Storage of malate, and thereby CAM activity can be quantified by measuring the titratable acidity difference in tissue samples collected at dusk and dawn (Cushman et al., 2008). The released CO<sub>2</sub> is then fixed by the Calvin-Benson-Bassham cycle by ribulose-1,5-bisphosphate carboxylase/oxygenase (RUBISCO) as in the C<sub>3</sub> photosynthetic pathway.

One advantage of CAM photosynthesis is the high concentration of CO<sub>2</sub> within the mesophyll cells during the day thanks to malate decarboxylation

coupled with stomata closure (Osmond, 1978; Cockburn et al., 1979; von Caemmerer and Griffiths, 2009). In the presence of high intercellular CO<sub>2</sub> concentrations, RUBISCO fixes more CO<sub>2</sub> into 3-phosphoglycerate (3-PGA) while reducing the amount of O<sub>2</sub> fixed into 2-phosphoglycolate (2-PGA). 2-PGA is converted into glyoxylate, which must be shuttled between the chloroplast, peroxisome, and mitochondria to be metabolized in an energy costly process known photorespiration (Busch, 2020). CAM photosynthesis has been shown to reduce photorespiration in plants (Cushman and Bohnert, 1997; Lüttge et al., 2012), as photorespiration is often considered a wasteful process that limits productivity, although it is also considered to be a process that may balance ATP and NAD(P)H concentrations under excess energy conditions, and a process for shuttling carbon-containing compounds between vesicles for nitrogen assimilation (Busch, 2020). Another advantage of CAM is high water-use efficiency (WUE). CAM plants are often recognized as having a 6-fold greater WUE than that of C<sub>3</sub> photosynthesis plants, and a 4-fold greater WUE than that of C<sub>4</sub> photosynthetic species (Borland et al., 2009) thanks in part to reduced transpiration from nocturnal stomatal conductance, and many co-adapted traits that both further enhance CAM and WUE (Niechayev et al., 2019).

While nitrogen (N) metabolism in C<sub>3</sub> and C<sub>4</sub> photosynthesis species is well studied, a robust understanding of N metabolism in CAM plants is lacking (Pereira and Cushman, 2019). Plants can take up N in the form of inorganic nitrate (NO<sub>3</sub><sup>-</sup>) and ammonium (NH<sub>4</sub><sup>+</sup>) (Hachiya and Sakakibara, 2017), and in organic N forms such as urea (CO(NH<sub>2</sub>)<sub>2</sub>) and released biological matter, which is



often decomposed into ammonium by microbial communities in the soil (Habteselassie et al., 2013; Wan et al., 2014). Nitrate and ammonium interact with one another within the soil and can limit or enhance total N uptake in plants depending on the abundance and ratio of these two oppositely charged molecules (Hachiya and Sakakibara, 2017). In addition, soils containing too much nitrate or ammonium can alter plant cellular pH, which causes detrimental changes in basic cellular functions such as osmosis, diffusion, membrane stability, and enzyme activities (Feng et al., 2020). In most standard nutrient solutions, nitrate and ammonium are present in the millimolar range in a 1:1 ratio for ionic charge balance, or with more nitrate than ammonium (Smith et al., 1983; De Rijck and Schrevens, 1998) as there are many ammonium-sensitive plant species (Britto and Kronzucker, 2002). The optimal nitrate and ammonium concentrations for any given plant species is dictated by adaptation to a specific environment (Houlton et al., 2007; Wang and Macko, 2011). Dry, nitrate rich landscapes, plants tend to prefer nitrate, whereas wet, ammonium rich landscape, plants tend to prefer ammonium. Some species might adapt to changes in nitrate and ammonium availability in the soil within only a few generations, although the rate at which plants can adapt to new nitrogen sources appears to vary among domesticated crop species. (Daryanto et al., 2019), and was shown to be limited in wild African grass species (Wang and Macko, 2011).

In CAM plants, inorganic nitrate and ammonium can be assimilated into roots directly by enzymes, and then transported to mesophyll cells for fixation into amino acids (Pereira and Cushman, 2019). Root uptake is regulated by

ammonium transporters (AMT) and nitrate transporters (NRT). Nitrate is reduced to nitrite ( $\text{NO}_2^-$ ) by nitrate reductase (NR) with NADH or ferredoxin (Fdx) reducing power in roots or shoots, respectively. Nitrite is highly oxidized and needs to be transported and/or reduced to ammonia ( $\text{NH}_3$ ) by nitrite reductase (NiR) with Fdx in the stroma of shoot cells or NADH reducing power in the stroma of root cells. Glutamine synthetase (GS) combines ammonium with an acyl phosphate intermediate into glutamine in the chloroplast. Glutamine is then converted to 2-glutamate by glutamine oxoglutarate aminotransferase (GOGAT). Alternatively, ammonium can be converted to carbamoyl phosphate by carbamoyl phosphate synthetase which is ATP dependent. In the mitochondria, NAD-glutamate dehydrogenase (NAD-GDH) can convert  $\text{NH}_4^+$  directly into glutamate by combining with 2-oxoglutarate and using NAD(P)H reducing power. Glutamine and ammonium can also be converted into asparagine by asparagine synthetase (AS) in ATP-rich regions of the cytosol.

Several studies have documented the productivity of *O. ficus-indica* under different fertilizer treatments in the field (Garcia de Cortazar and Nobel, 1992; Dubeux et al., 2006; Sánchez et al., 2012; Nkoi et al., 2021) and the commercial N input is between  $50\text{--}100 \text{ kg ha}^{-1} \text{ year}^{-1}$  (Davis et al., 2019). However, these studies were conducted with a wide variety of N sources, soil types, and production goals (e.g., fruit, cladodes, seeds, and methane production); and did not reveal the nitrate and ammonium preferences of *O. ficus-indica*. Interestingly, a 4-fold increase in nocturnal acidity in *O. ficus-indica* was observed when chlorophyll content increased 3-fold, and higher chlorophyll content was observed

in seedlings grown in concentrated Hoagland's solution over six months (Nobel, 1983). A nutrient index was developed to estimate productivity given different nutrient availabilities for cacti and agave species (Nobel et al., 1987), but this model is not species specific and does not specify between nitrate and ammonium for N input. To our knowledge, the only study that investigated nitrate vs. ammonium preference in *O. ficus-indica* was performed by (Vázquez et al., 2000). Through measuring nitrate and ammonium depletion from the sand, the authors found that plants initially took up more N when given ammonium than nitrate after 5, 10, and 15 days of treatment, but this difference was not significant after 20 days. Furthermore, plants accumulated significantly more biomass in the above ground tissue, and slightly more on average in root tissue when plants were given nitrate. The authors concluded that in hydroponic conditions, *O. ficus-indica* absorbed more N when supplied with nitrate than with ammonium, and when supplied with nitrate, the plants showed increased biomass production.

In this study, the response *O. ficus-indica* to varying amounts of nitrate vs. ammonium was investigated in a sand culture experiment. Mature cladodes were planted in pots containing sand, watered with distilled H<sub>2</sub>O for a month, and then given one of 16 different nutrient treatments with modified Hoagland's nutrient solution that varied in nitrate and ammonium concentrations in a cross-factorial design, as well as a continued distilled H<sub>2</sub>O treatment. After one month of applying nutrient treatments growth, relative water content, chlorophyll, tissue acidity, soluble sugars, starch, nitrate, ammonium, glyoxylic acid, nitrate reductase activity, nitrogen, carbon, and relative transcript abundance of genes

that code for enzymes involved in N metabolism and CAM were all measured in an attempt to gain an understanding of how *O. ficus-indica* responded to differences in nitrate and ammonium availability.

## Methods

### Greenhouse experimentation and sample collection

Prior to planting, 102 mature daughter cladodes were collected from 4-year-old *O. ficus-indica* plants located in the Valley Road Greenhouse Complex at the University of Reno, Nevada. The original mature plants were grown in three-gallon pots containing a 3:1 ratio of Sunshine MVP soil mix (Sun GroHorticulture, Bellevue, WA, USA) and decomposed granite with the cladode placed about 5 cm into the soil. Plants were watered once or twice a week depending on season, treated monthly with both a Miracle Gro<sup>®</sup> fertilizer (Scott's MiracleGro, Inc., Marysville, OH, USA) as well as insecticide treatment (Marathon<sup>®</sup> 1% Granular, OHP, Mainland, PA, USA) every six months, and repotted on an annual basis. The collected daughter cladodes were allowed to callus for two weeks under greenhouse shaded conditions to prevent infection upon planting. Cladodes were then planted in 11.3 L plastic pots containing a base layer of gravel and the remaining volume with sand (Sandbox Play Sand, Quikrete, Atlanta, GA) sterilized via autoclave set to a 40-minute dry cycle at 121°C and 15 PSI. All plants received 1L of distilled H<sub>2</sub>O for 1 month prior to applying nutrient treatments to allow for acclimation and to leech any mineral nutrients out of the sand. After acclimation, 6 cladodes were randomly selected

for each nutrient treatment, and the position of each cladode within the greenhouse was also randomized to mitigate for any possible differences in greenhouse microclimate. Under standard greenhouse conditions, the natural light was approximately  $1,100\text{-}1,500 \mu\text{mol m}^{-2} \text{s}^{-1}$  and temperature was  $28\text{-}32 \text{ }^{\circ}\text{C}$  day/ $17\text{-}18 \text{ }^{\circ}\text{C}$  night.

The experiment was conducted in a cross-factorial design with respect to nitrate and ammonium concentrations (Table 5). Each treatment received 1L, twice a week, of an assigned modified full Hoagland's solution with 0.0, 2.5, 5.0, or 10.0 mMol of nitrate and/or ammonium that was adjusted to  $\text{pH} = 5.7\text{-}5.8$  (Supplemental 1 for exact nutrient recipe of each treatment). In addition, a 17<sup>th</sup> treatment, which only received 1L of distilled H<sub>2</sub>O twice a week, was included as a negative control. After one month of applying treatments, cladodes were collected to measure various parameters detailed below.

#### Growth measurements

cladode length, width, new cladode number, root length, and root number were all measured before beginning treatments (after the 1-month acclimation treatment), and after the one-month treatment period. Center cladode thickness was also measured with a digital caliper (IP54 caliper, Baleigh Industrial, Manitowoc, WI) after the treatment period.

#### Relative water content

A 2-cm diameter cork bore was used to collect tissue from each cladode for relative water content. Fresh samples were immediately weighed and submerged in distilled water for 24 hours. After soaking, tissues were weighed again to acquire the turgid weight. Lastly, samples were dried for 72 hours in a freeze drier (7755030, Labconco, Kansas City, MO) and weighed again to acquire the dry weight. The relative water content was calculated as:

$$RWC (\%) = \left( \frac{f - d}{t} - d \right) * 100(\%)$$

Where  $f$  is fresh weight,  $t$  is turgid weight, and  $d$  is dry weight all in grams.

#### Chlorophyll content

Chlorophyll content was determined using a protocol modified from (Ni et al., 2009). 300 mg of frozen and ground tissue was placed into 15 ml Falcon tubes (430791, Corning, Corning, NY) and mixed with 5 ml of 80% acetone in the dark. Samples were then centrifuged at 3000  $x$  g at 4° C for 15 min and preserving the supernatant. Samples were loaded into disposable cuvettes and the absorbance at 663nm for chlorophyll a (Ca) and 645 nm for chlorophyll b (Cb) was measured using a Thermo Scientific nanodrop 2000 spectrophotometer. The chlorophyll content was calculated as:

$$Ca (mg/g \text{ sample}) = (12.7 * A - 2.69 * B) * \frac{v}{1000} * w$$

$$Cb (mg/g \text{ sample}) = (22.9 * B - 4.86 * A) * \frac{v}{1000} * w$$

$$Ca + b (mg/g \text{ sample}) = (8.02 * A + 20.20 * B) * \frac{v}{1000} * w$$

Where  $A$  is absorbance at 663 nm,  $B$  is absorbance at 645 nm,  $v$  is volume of extract in ml, and  $w$  is weight of the sample in g.

#### Titrateable acidity

To determine the nocturnal acid stored overnight within treatments, between 0.844-2.886 g fresh weight material was collected with a 2-cm diameter cork bore at dusk and dawn from each cladode with and flash frozen with liquid nitrogen. The titrateable acidity was determined using a modified protocol (Gehrig et al., 2005). Collected tissue was ground in a mortar and pestle containing liquid nitrogen. 0.5 g of freeze-ground tissue from each sample was placed in pre-chilled 15 ml conical tubes. 10 ml of 50% methanol was added to each sample, and the top volume point marked with a marker. A small hole was made in the cap of each tube, and samples were boiled in an 80 °C water bath for 10 minutes. After boiling, samples were brought back to the marked level with distilled H<sub>2</sub>O and centrifuged at 3,000  $\times$  g for 10 minutes. The decanted supernatant was then placed into 50 ml beakers and titrated to a pH of 7.0 for malate equivalent, and 8.4 for citrate equivalent with 10 mM KOH. The H<sup>+</sup> equivalent at 7.0 and 8.4 was calculated by:

$$H^+ \text{ equivalent}(\mu\text{mol } H^+ / \text{gFW}) = w \left( \frac{0.01}{v} \right) * 1000$$

Where  $w$  is fresh weight of sample in grams,  $v$  is volume of 10 mM KOH added in ml.

For each sample, the total nocturnal buildup of malate and citrate was calculated by subtracting the dusk sample  $H^+$  equivalent from the dawn sample  $H^+$  equivalent.

#### Starch content and soluble sugars

The soluble sugars, glucose, fructose, and sucrose and non-soluble starch contents were analyzed exactly as specified (Gomez et al., 2007). To summarize, 10 mg of freeze ground tissue underwent a methanol extraction and chloroform phase separation. The top phase containing soluble sugars, and the lower phase containing starch were separated for appropriate analysis. The soluble sugar fraction was analyzed by conducting sequential enzyme assays that measure the production of NADH at 340 nm in a SpectraMax M5 multi-mode microplate reader (17000, SpectraMax, San Jose, CA) after the addition of glucose-6-phosphate dehydrogenase (10165875001, Sigma-Aldrich, St. Louis, MO) for glucose content, hexokinase (11426362001, Sigma-Aldrich, St. Louis, MO) and phosphogluco isomerase (10128139001, Sigma-Aldrich, St. Louis, MO) for fructose content, and  $\beta$ -fructosidase (14504, Sigma-Aldrich, St. Louis, MO) for sucrose content. The lower starch containing phase was hydrolyzed into glucose monomers by first autoclaving, and then the application of an amylglucosidase (11202332001, Sigma-Aldrich, St. Louis, MO) treatment. The freed glucose monomers were then determined by measuring the production of NADH at 340 nm after the addition of glucose-6-phosphate dehydrogenase (10165875001, Sigma-Aldrich, St. Louis, MO) as in the soluble sugar assay.



### Nitrate reductase activity

NR activity assays, roots were collected from each cladode and the cortex was removed by hand before recording fresh weight. Prior to experimentation, a phosphate buffer was made by combining 500 ml of 0.1 M  $\text{KH}_2\text{PO}_4$  with 400 ml of 0.1 M NaOH and adding more of 0.1 M NaOH until  $\text{pH} = 7.5$  was achieved. 1 l of an incubation buffer was made by adding 970 ml of the phosphate buffer with 30 ml of *n*-propanol, and 100 mM  $\text{KNO}_3$ . The incubation buffer was heated in a water bath for 20 minutes at 30 °C and then placed in a 60 Sonic Dismembrator (F60, Fisher Scientific, San Diego, CA) and vacuum pump for 15 minutes to eliminate  $\text{O}_2$  from the solution. The incubation solution void of  $\text{O}_2$  was then kept in a water bath at 30 °C until fresh tissue was collected.

Approximately 0.5 g of *O. ficus-indica* cortex free root tissue was placed into 15 ml glass tubes. Six ml of the  $\text{O}_2$ -free incubation buffer was added to each sample and all samples were placed into a vacuum chamber for two 1-minute rounds to promote infiltration of tissues with incubation solution. All samples were kept in the dark or under foil for the remainder of the experiment to prevent nitrate degradation by light. 1 ml of incubation buffer from each sample was then pipetted into 2 ml microtubes to represent time point 0 (T0). T0 tubes were incubated at room temperature for one hour. The remaining samples were incubated for 1 hour in a 30 °C water bath, and 1 ml was transferred to a second set of tubes to represent the 60-minute time point (T60). 1 ml of  $\text{O}_2$ -free incubation buffer was added in a separate microtube as a blank for

spectrophotometer readings and final calculation. In each microtube from the T0, T60, and blank, 30  $\mu$ l of 1% sulfanilamide in 3 M HCl was added and vortexed. Then, 300  $\mu$ l of 0.02% of N-(1-Naphthyl) ethylenediamine dihydrochloride in reagent water was added and vortexed, and samples were allowed to incubate for 30 min at room temperature. Lastly, samples were loaded into quartz cuvettes and measured at 540 nm in a Thermo Scientific nanodrop 2000 spectrophotometer using the appropriate buffer blank. A 345 mg  $\text{NaNO}_2$  in 500 ml water solution was diluted to make 0, 1, 2, 4, 8, and 16  $\mu\text{M}$   $\text{NO}_2^-/\text{l}$  standard solutions.

The reaction rate of nitrate reductase in solution was calculated by first converting T0 and T60 to concentration to  $\mu\text{M}$  using the equation of the best fit line of the standard absorbance readings. This calculated concentration was normalized by dividing it by the initial sample weight. Lastly, subtracting the normalized T0 concentration from the T60 concentration gave the  $\mu\text{M}$   $\text{NO}_2^-$  produced per gram fresh weight of sample per hour by NR.

#### Nitrate content

Nitrate content was determined using a modified protocol (Cataldo et al., 1975). Briefly, 20 mg of freeze-dried tissue was resuspended in distilled water and incubated at 45  $^{\circ}\text{C}$  for 1 hour. Samples were then mixed and centrifuged at 5,000  $\times g$  for 15 min. 0.2 ml of supernatant was placed into a 50 ml flask with 5% salicylic acid in concentrated  $\text{H}_2\text{SO}_4$  for 20 min at room temperature. 19 ml of 2 N NaOH was added to each sample to adjust  $\text{pH} \geq 12$ . Flasks were gently vortexed for 5 minutes and 100  $\mu$ l of each sample was loaded into a 96-well clear

polycarbonate, flatbottom microliter plate (3364, Corning, Corning, NY) and the absorbance was measured at 410 nm using a SpectraMax M5 multi-mode microplate reader (17000, SpectraMax, San Jose, CA). Samples were compared to a set of 8 standards containing between 0 and 60 mg of  $\text{NO}_3^-$  using a  $\text{KNO}_3^-$  standard solution and normalized by sample dry weight.

#### Ammonium content Glyoxylic acid content

Ammonium and glyoxylic acid content were quantified following (Bräutigam et al., 2007). About 50 mg of homogenized freeze-dried tissue was collected from each cladode. Samples were mixed with 1 ml of 100 mM HCl with 500  $\mu\text{l}$  of chloroform in 2 ml test tubes. Samples were then centrifuged at 12,000  $\times g$  for 5 minutes at 8 °C. The aqueous phase was transferred to a new set of test tubes containing 50 mg of acid-washed activated charcoal, mixed by elution, and centrifuged again at 20,000  $\times g$  for 5 minutes in 8 °C. 200  $\mu\text{l}$  of the charcoal washed supernatant went into the glyoxylate assay, and 200  $\mu\text{l}$  went into the ammonium assay workflows.

The glyoxylate samples were combined with 20  $\mu\text{l}$  of a 1% (v/v) solution of phenylhydrazine in 100 mM HCl and incubated at 95 °C in a hot water bath for 2 minutes and immediately cooled on ice for 6 minutes. 100  $\mu\text{l}$  of concentrated HCl was added to each sample. 225  $\mu\text{l}$  of each sample was loaded into a well of a 96-well clear flatbottom microliter plate, and the absorbance at 520 nm was measured exactly at 4, 5, and 6 minutes after the additions of 25  $\mu\text{l}$  of 1.6%  $\text{K}_3\text{Fe}(\text{CN})_6$  solution using a SpectraMax M5 multi-mode microplate reader.

The 200  $\mu\text{l}$  of ammonium samples were diluted 1:1 with 100 mM HCl. 20  $\mu\text{L}$  of this solution was mixed with 100  $\mu\text{L}$  of 1% (w/v) phenol, 0.005% (w/v) sodium nitroprusside solution in water, and 100  $\mu\text{L}$  of 1% (v/v) sodium hypochlorite and 0.5% (w/v) sodium hydroxide. All samples were then incubated at 37 °C for 30 minutes, and the absorbance at 520 nm was measured in a SpectraMax M5 multi-mode microplate reader. Concentrations were calculated with the equation of a linear curve with 12 ammonium standards between 0- and 20-mM concentrations of ammonium sulfate.

#### Carbon and Nitrogen content

Total carbon and nitrogen content were determined by loading approximately 50 mg of ground freeze-dried tissue from each cladode into clay crucibles (2203-828, Leco, St. Joseph, MI) for elemental analysis with a Leco 928 combustion analyzer (Leco, St. Joseph, MI). Results were normalized on a weight basis and presented as the ratio of unit N per unit C (N:C Ratio).

#### RT-qPCR of CAM and nitrogen related genes

In order to measure the expression of CAM and nitrogen metabolism-related genes within treatments, plant tissue was collected at noon with a 2 cm diameter cork bore from each cladode and then immediately frozen in liquid  $\text{N}_2$  and ground to a fine powder using a mortar and pestle. 100 mg of ground frozen tissue was used for RNA extraction using a modified Qiagen RNeasy Plant Mini Kit (Qiagen Cat. No. 79254) protocol that included the addition DNase digestion,

and Fruit-Mate (9192, Takara Bio Inc., Kusatsu, Shiga, Japan), a proprietary non-ionic polymer that binds to polysaccharides and polyphenols. The addition of Fruit-Mate was necessary to perform RNA extractions on *O. ficus-indica* due to the naturally occurring high pectin content (Goycoolea and Cárdenas, 2003). RNeasy kit protocol was followed exactly as specified by the manufacturer with the addition of 1 ml of Fruit-Mate to the samples in step 2, and on-column DNase digestion using the RNase-free DNase kit as specified by Qiagen. The RNA concentration was measured with the Thermo Scientific nanodrop 2000 spectrophotometer, and potential RNA degradation during the extraction was checked by electrophoretic separation on a 1% agarose gel with Qiagen RNA sample loading dye (74904, Qiagen). cDNA of the extracted RNA transcripts was generated following iScript™ Reverse Transcription Supermix for RT-qPCR protocol (1708840, Bio-Rad Laboratories, Hercules, CA).

For RT-qPCR analysis, primers were designed for *O. ficus-indica* genes related to CAM and nitrogen metabolism shown in Table 1. Real-time quantification was done following the SsoAdvanced Universal SYBR Green Supermix (172-5271, Bio-Rad Laboratories, Hercules, CA) protocol. The relative amounts of cDNA in each sample were determined on the basis of the threshold cycle (Ct) for each PCR product and normalized to both UBQ10 (Op\_ fin19) and ACTIN7 (Op\_ fin88560) Ct values (Pfaffl, 2001, 2004). Predicted localization of the final product of each gene was estimated by first translating the cDNA sequence to protein sequence using the Expasy translate tool (<https://web.expasy.org/translate/>). Then, the resulting protein sequence was

analyzed using LOCALIZER software (<http://localizer.csiro.au/>) to generate a subcellular localization prediction (Sperschneider et al., 2017).

### Statistical analysis

All raw data input and calculations described above were performed in Microsoft Excel. Analysis of variance for one factor One-Way ANOVA, Tukey test ( $\alpha = 0.05$ ), and boxplots with letters for significance were conducted in RStudio using datasets, ggplot2, multcompView, and dplyr packages. Graphcladode software was used to plot group bar graphs of soluble sugars, and chlorophyll content along with standard error.

## Results

### Growth measurements and relative water content.

No statistical differences were found in cladode length among the nitrate and ammonium treatments before and after the treatment period (Table 5), nor separate groupings among treatments (Figure 1). There was a significant difference in regard to cladode width among treatments (Table 5) both before treatment measurements, and the diH<sub>2</sub>O treatment which had the lowest average widths, whereas the 5.0 + 2.5 (mMol Nitrate + Ammonium) and 10.0 + 5.0 treatments having the highest average widths (Figure 2). A highly significant difference in cladode thickness among treatments (Table 5) was found with the lowest treatment averages being diH<sub>2</sub>O and 0.0 + 0.0 (Figure 3). Treatments with the largest average cladode thickness were 5.0 + 2.5 and 2.5 + 10.0 (Figure 3).

Difference in average number of new cladodes was highly significant among treatments (Table 5) and all nitrogen treatments had an average new cladode number above 0 (Figure 4) and 2.5 + 5.0, 0.0 + 10.0, and 2.5 + 10.0 all having the highest average new cladode number of 2, and before treatment samples, and diH<sub>2</sub>O had no new cladodes. Primary root number was highly significantly different (Table 5) among treatments, and root number was also significantly different among treatments (Table 5). Treatments 0.0 + 0.0 and 0.0 + 10.0 had the highest average root numbers (Figure 5), whereas 10.0 + 0.0 had the highest average root length (Figure 6).

Relative water content averaged between 67.8 and 77.1% among treatments and no significant difference among treatments was found (Table 5, Figure 7).

## Biochemical analyses

### *Chlorophyll*

A slightly significant difference in Chlorophyll a + b content was observed among treatments (Table 6). However, no treatments were individually grouped by Tukey's test (Figure 8 and 9) with the maximum average combined in the 10.0 + 5.0 treatment, and the lowest in the 0.0 + 2.5 treatment. Chlorophyll a content showed a significant difference among treatments (Table 6), but all treatments were grouped together as well (Figure 8 and 10) with the maximum average content evident in the 10.0 + 5.0 treatment and the lowest in the 0.0 + 2.5 treatment. Chlorophyll b content showed an extremely significant difference

among treatments (Table 6) with the highest average content in the 0.0 + 10.0 treatment, and lowest in the 0.0 + 5.0 treatment (Figure 8 and 11).

#### *Titrateable acidity*

Dawn-dusk delta H<sup>+</sup> to pH 7.0 (μmol/gFW) showed a significant difference among treatments (Table 6) with the highest tissue acidity measured in the diH<sub>2</sub>O treatment (Figure 12). Dawn-dusk delta H<sup>+</sup> from pH 7.0 to pH 8.4 (μmol/gFW) also showed a significant difference among treatments (Table 6), with the highest average tissue acidity evident in the 5.0 + 5.0 treatment (Figure 12).

#### *Starch and sugar*

Starch content among treatments showed a significant difference (Table 6), with the highest measured content in the diH<sub>2</sub>O treatment (Figure 13). All treatments showed consistently higher average fructose than glucose, and glucose than sucrose (Figure 15, 16, 17, & 18). Individually, all three soluble sugars were statistically different among treatments (Table 5), with the highest concentrations in the 0.0 + 2.5 treatment, and the lowest in the diH<sub>2</sub>O treatment.

#### *Nitrate reductase activity*

Preliminary results demonstrated that *O. ficus-indica* roots have a higher NR activity (average of 171.0 nmoles NO<sub>2</sub>/g fw/h) than cladode chlorenchyma (21 nmoles NO<sub>2</sub>/g fw/h) and hydrenchyma (16 nmoles NO<sub>2</sub>/g fw/h) tissues. Roots



with cortex tissues were also shown to have less NR activity than that of roots with the cortex physically removed before analysis. Nitrate reductase (NR) activity measured in the roots of the plants submitted to different treatments was significantly different (Table 6). The highest NR activity was measured in the 10.0 + 2.5 treatment, while the lowest was observed in the 2.5 + 5.0 and diH<sub>2</sub>O treatments (Figure 19).

#### *Nitrate, ammonium, and glyoxylic acid*

Nitrate and ammonium content showed significant differences among treatments (Table 6), with the highest recorded average nitrate content in the 10.0 + 0.0 treatment, and lowest in the 0.0 + 2.5 treatment (Figure 20). On the other hand, the 5.0 + 10.0 treatment showed the highest average ammonium content, while the 2.5 + 0.0 treatment presented the lowest (Figure 21). Glyoxylic acid content was significantly different among treatments (Table 6). The diH<sub>2</sub>O treatment had the highest average glyoxylic acid content (Figure 22), but with a wide sample variance (2.0 to 5.5  $\mu\text{mol}/\text{mg}$  sample).

#### *Nitrogen and carbon*

Nitrogen:Carbon ratio (N:C) among treatments was significantly different (Table 6). Interestingly, while the percent C was not significantly different (Table 6, Figure 24), the percent N (Figure 25) showed a significant difference (Table 6) with the highest percent N in the 10.0 + 2.5 treatment and N:C ratio occurring in the 5.0 + 10.0 treatment.

*mRNA abundance of CAM and nitrogen metabolism-related genes*

All measured relative expression levels for each gene were significantly different among treatments (Table 7, Figure 26). Of the CAM enzymes surveyed, the steady-state transcript abundance of ALMT and PPC1 were the highest in the diH<sub>2</sub>O treatment (Figure 26, 27 and 28). In contrast, the relative steady-state transcript abundance of PPCK was highest in the 0.0 + 2.5 and 2.5 + 5.0 treatments, and lowest in the 0.0 + 0.0 treatment (Figure 26 & 29).

For N metabolism genes relative steady-state transcript abundance for NR was the significantly increased in the 10.0 + 0.0 and 10.0 + 2.5 treatments and the lowest in the 0.0 + 10.0 treatment (Figure 26 & 30). Nitrite Reductase (NiR) steady-state transcript abundance was highest in the 10.0 + 10.0 treatment, and lowest in 0.0 + 10.0 treatment (Figure 26 & 31). GOGAT steady-state transcript abundance was significantly increased in the 10.0 + 10.0 and diH<sub>2</sub>O treatments, and lowest in the 5.0 + 10.0 treatment (Figure 26 & 32). AS steady-state transcript abundance was highest in the 0.0 + 5.0 treatment and lowest in the 5.0 + 10.0 treatment (Figure 26 & 33). GDH460 steady-state transcript abundance was highest in the 2.5 + 5.0 treatment, and lowest in 5.0 + 0.0 treatment (Figure 26 & 34). GDH201910 steady-state transcript abundance was highest in the 2.5 + 10.0 treatment, and lowest in the diH<sub>2</sub>O (Figure 26 & 35). Lastly, GS30900 showed no significant difference steady-state transcript abundance among the treatments (Figure 26 & 36). In contrast, GS94700 had about a 3-fold higher steady-state

transcript abundance in diH<sub>2</sub>O than that of all of the other treatments (Figure 26 & 37).

## Discussion

All treatments put on new cladodes with the exception of diH<sub>2</sub>O treatment controls (Figure 4). The formation of new biomass might have affected the measured concentration of nitrate and ammonium due to mobilization of nutrients between source tissue in mother cladodes and sink tissue in daughter cladodes (Marschnert et al., 1997). In *O. ficus-indica* chlorophyll content has been shown to increase with increasing amounts of nitrate (Nerd and Nobel, 1995), and to decrease under high light and elevated CO<sub>2</sub> conditions (Cui and Nobel, 1994). The differences observed in combined chlorophyll content among treatments was slightly significant (Table 6, Figure 8 and 9), with the difference in chlorophyll a (Figure 8 & 10) and b (Figure 8 & 11) being more significant among treatments. In most plants, including *O. ficus-indica*, limited N in the soil promotes root growth (Vázquez et al., 2000; Kiba and Krapp, 2016). An increase in average root length (Figure 6) with less N was not obvious, but the primary root number was higher in the 0.0 + 0.0 treatment (Figure 5). Cladode width (Figure 2) and cladode length (Figure 1) did not vary greatly among treatments, but cladode thickness did (Figure 3). Curiously, cladode thickness has been shown to correlate strongly with relative water content (Scalisi et al., 2016), but relative water content did not vary among treatments within this experiment (Figure 7).

In *O. ficus-indica*, fructose, glucose, and sucrose levels make up 35%, 32%, and 33% of the relative sugar content, respectively, found in chlorenchyma, and 44%, 43%, and 13%, respectively, in the parenchyma under well-watered conditions (Nerd and Nobel, 1991). Homogenized samples (combined chlorenchyma and parenchyma) were analyzed for soluble sugar analysis. We found that average fructose content was higher than glucose content in all nitrate vs. ammonium treatments (Figure 15), and sucrose content was minimal (< 2.5 mg/mg sample) in all treatments (Figure 18). Interestingly, no measured soluble sugar content was observed in the diH<sub>2</sub>O control treatment samples (Figures 15,16,17, and 18). The control treatment samples also had the highest starch content (Figure 14). These observations suggest that under nutrient limiting conditions, *O. ficus-indica* is likely storing soluble sugars by conversion into starch until nutrient availability becomes more favorable, as has been seen in other plant species (Christopher and Holtum, 1996; Rosa et al., 2009; Tao et al., 2013; Tao et al., 2017)

Vázquez *et al.* (2000) observed a significantly higher uptake of N from sand in *O. ficus-indica* given nitrate vs. ammonium until 20 days after application, at which time the authors suggested that a significant difference was not seen because most of the supplied N had been taken up from the sand. The authors also measured higher above and below ground biomass when *O. ficus-indica* was provided with nitrate vs. ammonium. Our results complement these former results in demonstrating that percentage N appears to be slightly higher in *O. ficus-indica* cladodes when plants were supplied with only nitrate vs. only ammonium in the

2.5 + 0.0 vs. 0.0 + 2.5, and 5.0 + 0.0 vs. 0.0 + 5.0 treatments. However, no statistically significant differences were observed in the 10.0 + 0.0 vs. 0.0 + 10.0 treatments (Figure 25). In addition, *O. ficus-indica* results showed a higher percentage of N when supplied with both nitrate and ammonium except in the 10.0 + 5.0 treatment (Figure 25), which might be a result of nitrate toxicity (Islam et al., 2020). Nitrate and ammonium content in cladodes were both significantly different across treatments (Figure 20 and 21), but understanding these differences is complicated by the fact that ammonium and nitrate are readily interconvertible in both the roots and cladodes (Krapp, 2015; Taiz et al., 2015).

Prior to this study, nitrate reductase activity and nitrate content had been measured in *O. ficus-indica* cladodes and roots under both field and glasshouse conditions (Nerd and Nobel, 1995). Both Nerd and Nobel, 1995 and this study demonstrated increased nitrate content in cladodes (Figure 20), and NR activity in roots (Figure 19) when given nitrate concentrations were increased. However, our study revealed that NR activity did not always increase when both nitrate and ammonium were present, specifically in the 2.5 + 2.5, 2.5 + 5.0, and 2.5 + 10.0 treatments (Figure 19). NR activity was observed under higher nitrate concentration when compared to ammonium concentration, which is likely explained by the fact that  $\text{NO}_3^-$  is the substrate for NR. Nerd and Nobel, 1995 also found the highest NR activity in new cladodes vs. that in basal cladodes, and roots, which had the least amount of NR activity. Conversely, in preliminary measurements, we found that root tissue had the highest amount of NR activity compared with both chlorenchyma and parenchyma cladode tissues (data not

shown). This difference is likely because cortical root tissue was removed before conducting NR activity assays, and Nerd and Nobel 1995 used intact roots for measurements. NR in the roots reduces nitrate to nitrite using ferredoxin reducing power prior to transport to photosynthetic tissues, while the nitrate reductase in photosynthetic tissues uses NADH reducing power (Pereira and Cushman, 2019). The NR activity measured in this study likely represents the conversion of nitrate to nitrite before being converted into ammonium by nitrate reductase prior to being assimilated into amino acids or transported to the shoots, while NR activity in cladodes is likely linked to the conversion of nitrate to nitrite just prior to assimilation into amino acids via the GOGAT cycle in plastids (Krapp, 2015). Thus, in *O. ficus-indica*, both root and cladode NR activities increased with an increase in supplied nitrate (Figure 19) (Nerd and Nobel, 1995).

As in facultative CAM plants, which have the ability to switch from C<sub>3</sub> photosynthesis to CAM photosynthesis under unfavorable conditions, a switch to CAM has been demonstrated in (Winter et al., 2015) when either high concentrations of an unfavorable N source is present, and/or when a favorable source of N is limited (Pereira and Cushman, 2019). As an obligate CAM plant, *O. ficus-indica* is expected to increase CO<sub>2</sub> uptake by CAM as has been shown in other cactaceae species (Nobel, 1983). Indeed, steady-state transcript abundance for PEPC1 increased when ammonium increased in the 0.0 + 2.5, 0.0 + 5.0, 0.0 + 10.0 treatments and when nitrate increased in the 2.5 + 0.0, 5.0 + 0.0, 10.0 + 0.0 treatments (Figure 28), although this trend was not apparent in the combined nitrate and ammonium treatments. ALMT steady-state transcript abundance was

also higher in 0.0 + 5.0 and 10.0 + 10.0, (Figure 27). An increase in ALMT with increases in N might translate to an increase in transport of malate in and out of tonoplasts within these treatments, as metabolism in general may be increased in this situation (Kovermann et al., 2007). No obvious trends were recognized in PPCK steady-state transcript abundance among treatments in relation to nitrate and ammonium concentrations (Figure 29) even though there were significant differences among treatments for PPCK steady-state transcript abundance.

Interestingly, diH<sub>2</sub>O control plants showed the highest accumulation of organic acids (malate + citrate) (Figure 12), and relative expression of ALMT (Figure 27) and PPC1 genes (Figure 29), which suggests that CAM increased without nutrient supplementation. However, organic acid build-up in the diH<sub>2</sub>O treatment might also be due, in part, to a stress response (Lopez-Bucio et al., 2000), rather than an increase in net CO<sub>2</sub> fixation, which could be revealed by diel gas-exchange measurements (Niechayev et al., 2019). Glyoxylic acid content (Figure 22) was the same across all treatments except for the diH<sub>2</sub>O control supporting the possibility that photorespiration rates in *O. ficus-indica* remained similar regardless of N supply.

NR and NiR from homogenized cladode tissue showed a similar relative expression pattern among treatments (Figures 30 & 31), which was likely because a coordination of both enzymes for the initial fixation of nitrate is required (Sestili et al., 2018). In addition, the steady-state mRNA abundance of these two enzymes has been shown to increase when N supply is increased, especially in the form of nitrate. In the next step of the pathway, GS fixes ammonium into glutamine both

in the cytoplasm through GS1 (GS30900), and chloroplast with GS2 (GS94700) (Bernard and Habash, 2009). The expression of GS30900 and GS94700 were both relatively similar across treatments with the exception that GS94700 showed increased relative steady-state transcript abundance in the diH<sub>2</sub>O control treatment (Figure 37), while GS30900 relative expression was similar in all treatments (Figure 38). This observation suggests that chloroplast GS is upregulated more so than cytosolic GS under nutrient deprivation in *O. ficus-indica*. Likewise, there was also an increase in GOGAT steady-state transcript abundance within the diH<sub>2</sub>O control treatment (Figure 32). GOGAT mRNA expression was also significantly higher in the 10.0 + 10.0 treatment (Figure 32), suggesting that GOGAT expression in *O. ficus-indica* was higher when the most N was supplied, and when nutrient limited. The high relative mRNA expression of GOGAT in the 10.0 + 10.0 treatment was likely due to an increased fixation of glutamine into glutamate with more nitrogen availability, while the high GOGAT relative mRNA expression in the diH<sub>2</sub>O control treatment might be due to glutamate production. Glutamate production has been linked to maintenance of redox homeostasis and ATP production via glycolysis when malate levels are high or NAD-MDH function is lacking (Selinski and Scheibe, 2019), as high malate levels (H<sup>+</sup> equivalent) were also observed in the diH<sub>2</sub>O treatment (Figure 12). Asparagine synthetase steady-state transcript abundance in the cytosol was highest in the 0.0 + 5.0 treatment, but interestingly lower in the high N treatments 10.0 + 10.0, 2.5 + 10.0, 5.0 + 10.0, and the diH<sub>2</sub>O control treatment (Figure 33). Under high concentrations of ammonium, GDH converts ammonium into glutamate



(Skopelitis et al., 2006). In this experiment, the highest steady-state transcript abundance of GDH460 was measured in the 2.5 + 5.0 treatment (Figure 34), and the highest GDH201910 steady-state transcript abundance was observed in the 2.5 + 10.0 treatment (Figure 35). GDH460 showed higher steady-state transcript abundance in the diH<sub>2</sub>O control treatment compared to GDH20190, and both of these genes showed slightly higher steady-state transcript abundance in the 0.0 + 5.0 treatment than the 0+10 treatments, corroborating previous results observed by (Skopelitis et al., 2006).

After one month of acclimating *O. ficus-indica* cladodes to sand culture with diH<sub>2</sub>O and one additional month of varying nitrate and ammonium concentrations in applied nutrients solutions, significant differences were found among treatments for all independent variables measured with the exception of cladode length, relative water content, and percent carbon (Table 5, 6, & 7). Thus, the one-month acclimation and one-month treatment periods were long enough to elicit significant differences in growth, biochemical parameters, and gene expression in *O. ficus-indica*. Obvious trends and best overall nitrate vs. ammonium treatments were not clearly revealed for all the parameters studied perhaps because only a single, terminal measurement was taken. The experimentation described here might have been more informative if several tissue samples had been taken over the 2-month period to reveal a continuum of changes within each treatment. If multiple samples are taken more *O. ficus-indica* individuals may be needed to prevent variation due to destructive sampling for tissue samples. Despite this, these results showed that nutrient limited in *O. ficus-*

*indica* failed to add new cladodes, exhibited increased starch content, near complete reductions in the contents of several soluble sugar, and increased steady-state transcript abundance for ALMT, PPC1, GOGAT, GDH460, and GS genes. Overall, these results demonstrate that fertilizers designed for *O. ficus-indica* production should have either equal parts nitrate and ammonium, or slightly more nitrate than ammonium based upon the results obtained here and suggested by previous literature reports.

### Acknowledgements

This research was funded in part by Nevada Agricultural Experimental Station (NEV-0377, NEV-0380) and National Institute of Food and Agriculture (NIFA), U.S. Department of Agriculture, Sustainable Bioenergy and Bioproducts Challenge Area (Award #2018-68005-27924). I would also like to thank undergraduate researchers Eileen Rodriguez, Charli Faris, and Nathan King as well as our lab manager Lisa Petrusa for their assistance in all steps of the protocol for this project.



**Table 3:** The factorial design to test the response of OFI to understand possible synergistic effects with differences in  $\text{NO}_3^-$  and  $\text{NH}_4^+$  availability. An additional treatment that only received deionized water was included ( $\text{diH}_2\text{O}$ ).

Treatments	0.0mM $\text{NO}_3^-$	2.5mM $\text{NO}_3^-$	5.0mM $\text{NO}_3^-$	10.0mM $\text{NO}_3^-$
0.0mM $\text{NH}_4^+$	0.0mM $\text{NH}_4^+$ 0.0mM $\text{NO}_3^-$	0.0mM $\text{NH}_4^+$ 2.5mM $\text{NO}_3^-$	0.0mM $\text{NH}_4^+$ 5.0mM $\text{NO}_3^-$	0.0mM $\text{NH}_4^+$ 10.0mM $\text{NO}_3^-$
2.5mM $\text{NH}_4^+$	2.5mM $\text{NH}_4^+$ 0.0mM $\text{NO}_3^-$	2.5mM $\text{NH}_4^+$ 2.5mM $\text{NO}_3^-$	2.5mM $\text{NH}_4^+$ 5.0mM $\text{NO}_3^-$	2.5mM $\text{NH}_4^+$ 10.0mM $\text{NO}_3^-$
5.0mM $\text{NH}_4^+$	5.0mM $\text{NH}_4^+$ 0.0mM $\text{NO}_3^-$	5.0mM $\text{NH}_4^+$ 2.5mM $\text{NO}_3^-$	5.0mM $\text{NH}_4^+$ 5.0mM $\text{NO}_3^-$	5.0mM $\text{NH}_4^+$ 10.0mM $\text{NO}_3^-$
10.0mM $\text{NH}_4^+$	10.0mM $\text{NH}_4^+$ 0.0mM $\text{NO}_3^-$	10.0mM $\text{NH}_4^+$ 2.5mM $\text{NO}_3^-$	10.0mM $\text{NH}_4^+$ 5.0mM $\text{NO}_3^-$	10.0mM $\text{NH}_4^+$ 10.0mM $\text{NO}_3^-$

**Table 4:** List of primers designed for RT-qPCR analysis with predicted subcellular localizations.

Gene	Primer	Description	Localized to	Primer Sequence	Annealing Temperature (°C)	Amplicon Lenth (bp)
Op_fin206820	ALMT10	Aluminum Activated Malate Transporter	Mitochondria, Tonoplast	F:TTTCCTATCTGGGCTGGC R:TTTCAAGGGTGTTCGCTTC	56.2	68
Op_fin7190	PPC1	Phosphoenolpyruvate Carboxylase	Cytosol	F:AGGCACATGATGTGATGGA R:CCAATCTCCCAAACTGAAGAA	55.2	150
Op_fin211860	PPCK1	Phosphoenolpyruvate Carboxylase Kinase	Cytosol	F:AACCAGTTTGACGAGCCA R:ATGCCATCTACCGTACCAGC	60	154
Op_fin52570	NR	Nitrate Reductase	Cytosol	F:CCACACTTTGACCCGTGCC R:TCCTGTCCGATTGGCGTA	56.2	87
Op_fin241390	NiR	Nitrite Reductase	Chloroplast	F:ACAATAGGCACCAAGTCC R:GCAACCCATGAAACCGATAT	53.6	151
Op_fin81140	GOGAT	Glutamate Synthase	Chloroplast	F:GTAAAGTTGAACCTGCTCATCTA R:GAACAGATTGGGTGGAATAATC	53.6	124
Op_fin236590	AS	Asparagine Synthase	Cytosol	F:ATCCCACTCCGCTCACTGAAC R:ATCATCATCAAAGGCATTGCG	56.2	88
Op_fin460	GDH	Glutamate Dehydrogenase	Cytosol	F:AGTGGTTAGGGATGAATT R:AAGAAATTGACTTGGAAATTGGA	60	105
Op_fin201910	GDH	Glutamate Dehydrogenase	Cytosol	F:ACCAAGAGATCCACCAAGG R:TTTGTCCCATACAGGTGC	60	123
Op_fin30900	GS	Glutamine Synthetase	Chloroplast	F:GGAATGAAGAAGTTGACTGGA R:GTCGCTAATCGTGGTTGCTC	55.2	82
Op_fin94700	GS	Glutamine Synthetase	Cytosol	F:AATCACCTCGTAGCCACC R:AAGCACCACTCCAGCAATC	55.2	121
Op_fin19060	UBQ10	Ubiquitin	Mitochondria, Cytosol	F:CTTGGATGTTGTAGTCAGC R:GCTCTCAACCTCCAAGT	56.2	150
Op_fin88560	ACTIN7	Actin	Cytosol	F:CACATCTGTTGGAAGGTGC R:ATTTCTTTGCTCATACGGTCAG	53.6	139

**Table 5:** Ordinary one-way analysis (ANOVA) results of growth and relative water content. Significance codes: extremely significant 0 '\*\*\*', highly significant

p<0.001 '\*\*', significant p<0.01 '\*', slightly significant p<0.05 '!', and not significant p>0.05 'NS'.

Independent Variable	N (# within treatment)	DF (Treatment number)	F-value	P-Value	Significance code
cladode Length	3	17	1.569	0.1260	NS
cladode Width	3	17	2.074	0.0326	*
cladode Thickness	6	16	2.678	0.001	**
New cladode #	3	17	2.689	0.0063	**
Primary Root Length	3	17	2.544	0.0091	**
Root Length	3	17	2.097	0.0306	*
Relative water Content	6	16	1.533	0.1070	NS

**Table 6:** Ordinary one-way analysis (ANOVA) results of biochemistry measurements with 6 samples ( $n = 6$ ) in each treatment and 17 treatments (Df = 16) in all. Significance codes: extremely significant 0 '\*\*\*\*', highly significant  $p < 0.001$  '\*\*', significant  $p < 0.01$  '\*', slightly significant  $p < 0.05$  '!', and not significant  $p > 0.05$  'NS'.

Independent Variable	F-Value	p-Value	Significance Code
Chlorophyll a+b	1.674	0.0676	.
Chlorophyll a	1.909	0.0303	*
Chlorophyll b	2.909	0.0007	***
Titrateable Acidity (pH 7)	42.61	<0.0001	***
Titrateable Acidity (pH 7-8.4)	32.67	<0.0001	***
Starch	16.68	<0.0001	***
Glucose	7.189	<0.0001	***
Fructose	6.279	<0.0001	***
Sucrose	4.171	<0.0001	***
NR Activity	26.22	<0.0001	***
Nitrate	9.492	<0.0001	***
Ammonium	12.38	<0.0001	***
Glyoxylic Acid	3.004	0.0001	***
N:C Ratio	24.6	<0.0001	***
Percent C	1.39	0.1634	NS
Percent N	12.65	<0.0001	***

**Table 7:** Ordinary one-way analysis (ANOVA) results of relative gene expression results with 6 samples ( $n = 6$ ) in each treatment and 17 treatments (Df = 16) in all. Significance codes: extremely significant 0 '\*\*\*\*', highly significant  $p < 0.001$  '\*\*', significant  $p < 0.01$  '\*', slightly significant  $p < 0.05$  '!', and not significant  $p > 0.05$  'NS'.

Gene Names	F-Value	p-Value	Significance Code
ALMT	3.319	0.0001	***
PPC1	6.963	<0.0001	***
PPCK	3.460	<0.0001	***
NR	10.290	<0.0001	***
NiR	8.182	<0.0001	***
GOGAT	4.176	<0.0001	***
AS	3.885	<0.0001	***
GDH460	3.773	<0.0001	***
GDH201910	4.068	<0.0001	***
GS30900	1.950	0.0263	*
GS94700	13.490	<0.0001	***

## Figures

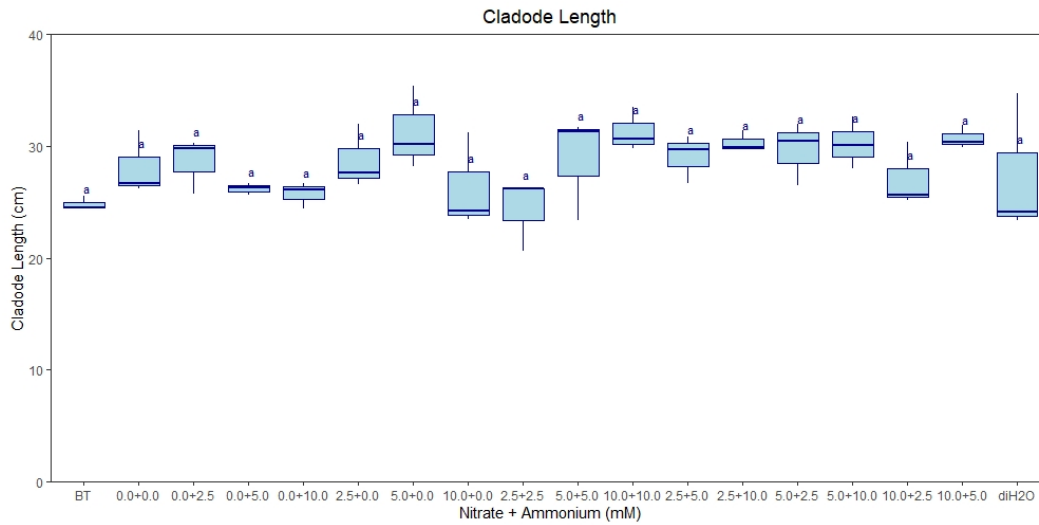


**Figure 2:** cladode length (cm) among treatments ( $n = 3$ ). BT = measurements taken before applying treatments. Treatments are all modified Hoagland's solution with varying amounts of nitrate and ammonium (mMol) and a deionized water treatment (diH<sub>2</sub>O) control. Letters represent the result of Tukey's test ( $\alpha = 0.05$ ).

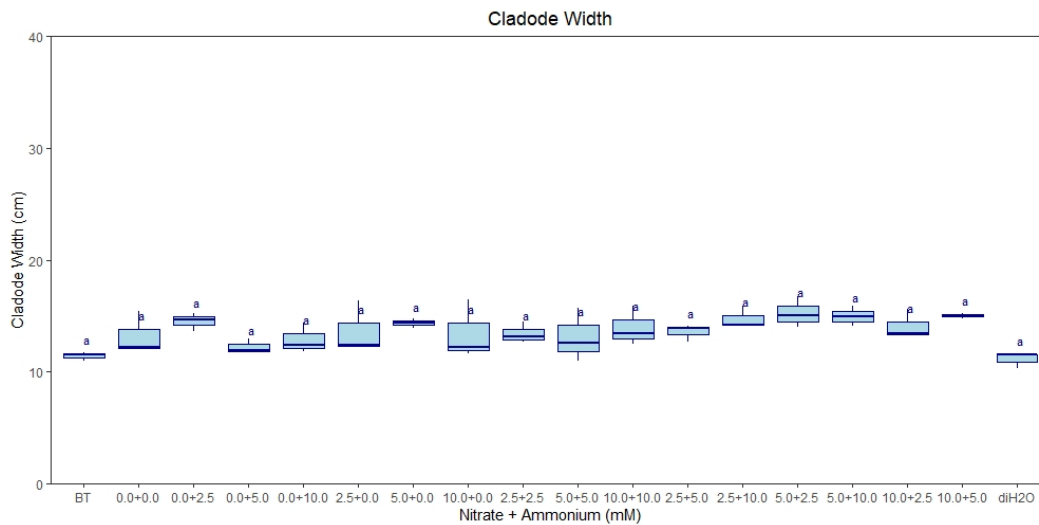


**Figure 2:** cladode width (cm) among treatments ( $n = 3$ ). BT= measurements taken before applying treatments. Treatments are all modified Hoagland's solution with



varying amounts of nitrate and ammonium (mMol) and a deionized water treatment (diH<sub>2</sub>O) control. Letters represent the result of Tukey's test ( $\alpha = 0.05$ ).

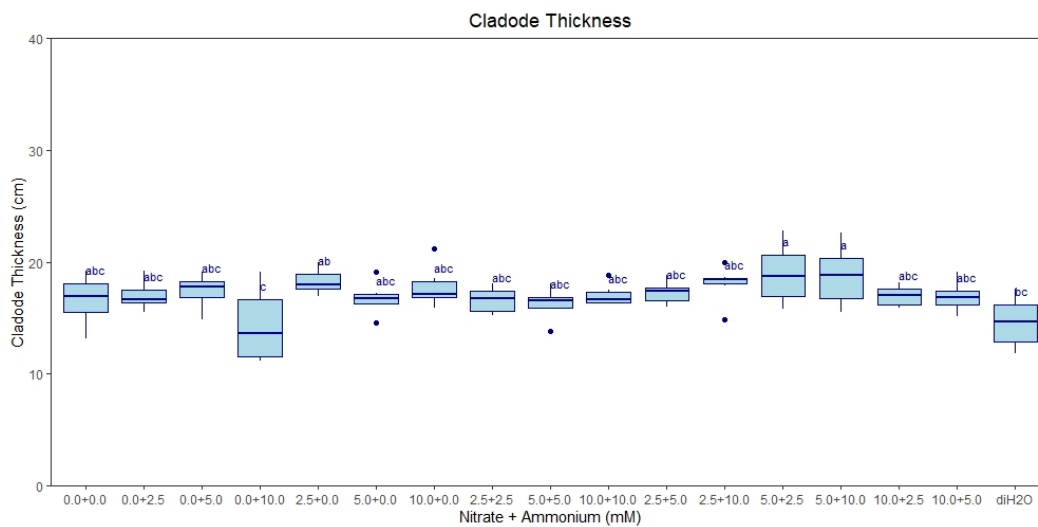


**Figure 3:** cladode Thickness (mm) among treatments (mm) ( $n = 6$ ). Treatments are all modified Hoagland's solution with varying amounts of nitrate and ammonium (mMol) and a deionized water treatment (diH<sub>2</sub>O) control. Letters represent the result of Tukey's test ( $\alpha = 0.05$ ).

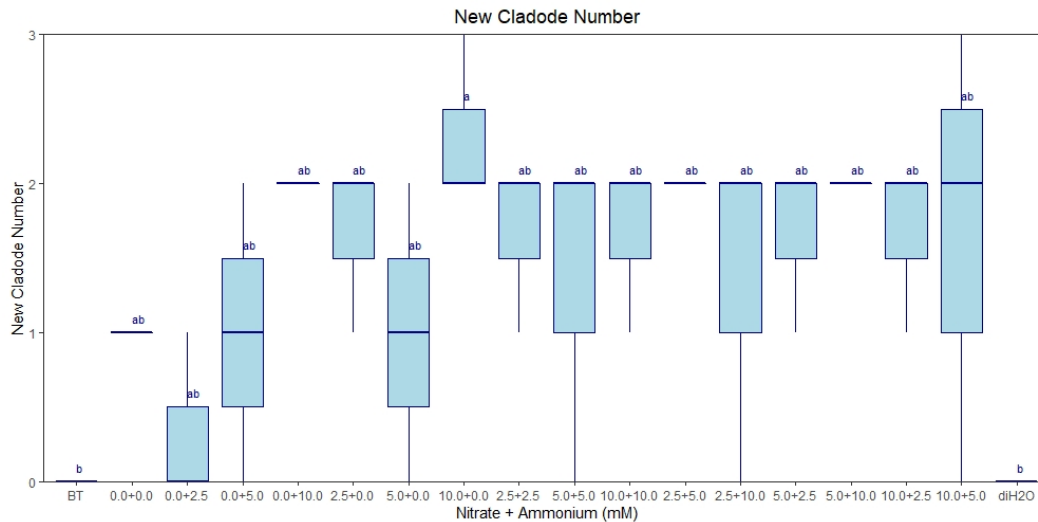


**Figure 4:** New cladode number among treatments ( $n = 3$ ) and before the treatment period (BT). Treatments are all modified Hoagland's solution with varying amounts of nitrate and ammonium (mMol) and a deionized water treatment (diH<sub>2</sub>O) control. Letters represent the result of Tukey's test ( $\alpha = 0.05$ ).

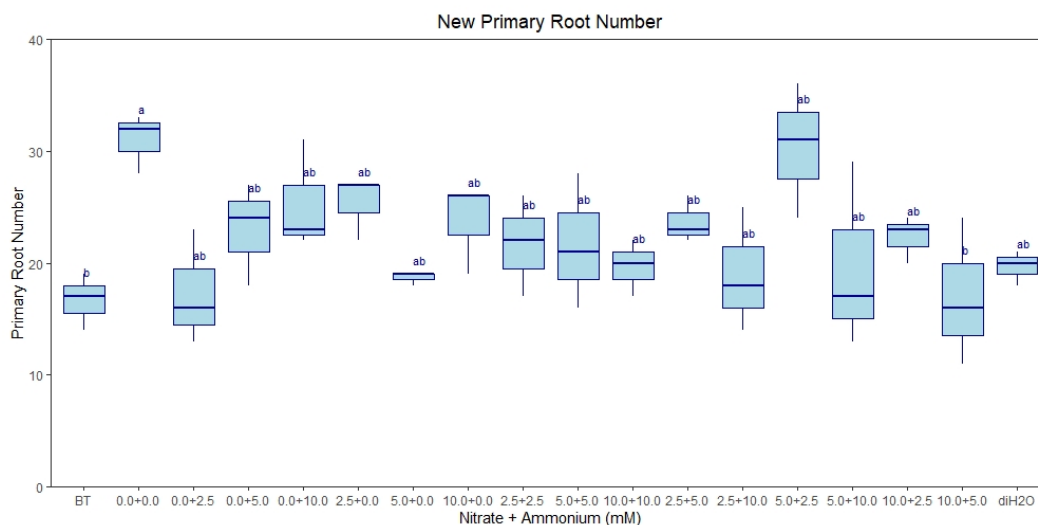


**Figure 5:** Primary root number among treatments ( $n = 3$ ). BT= measurements taken before applying treatments. Treatments are all modified Hoagland's solution with varying amounts of nitrate and ammonium (mMol) and a deionized water treatment (diH<sub>2</sub>O) control. Letters represent the result of Tukey's test ( $\alpha = 0.05$ ).

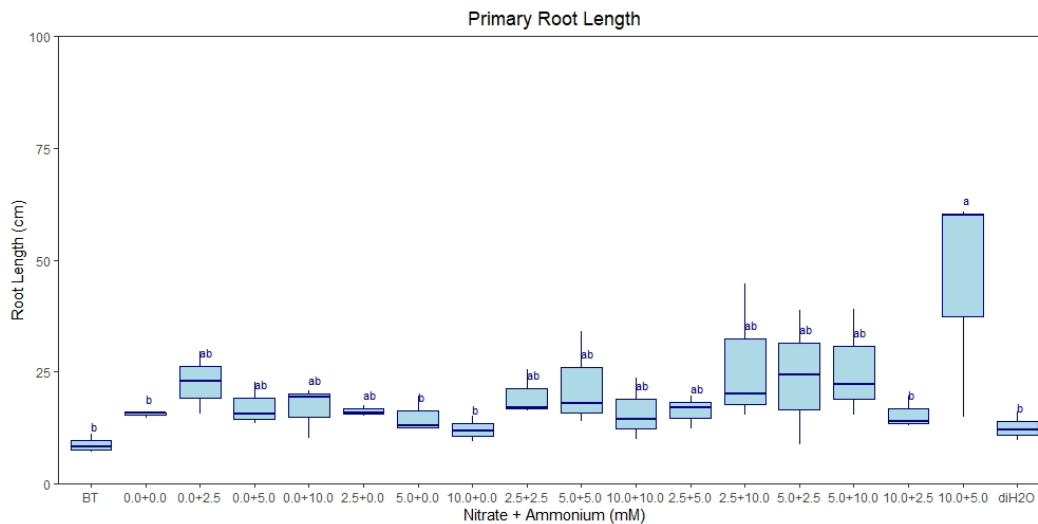


**Figure 6:** Average primary root Length (cm) among treatments ( $n = 3$ ). BT= measurements taken before applying treatments. Treatments are all modified Hoagland's solution with varying amounts of nitrate and ammonium (mMol) and a deionized water treatment (diH<sub>2</sub>O) control. Letters represent the result of Tukey's test ( $\alpha = 0.05$ ).

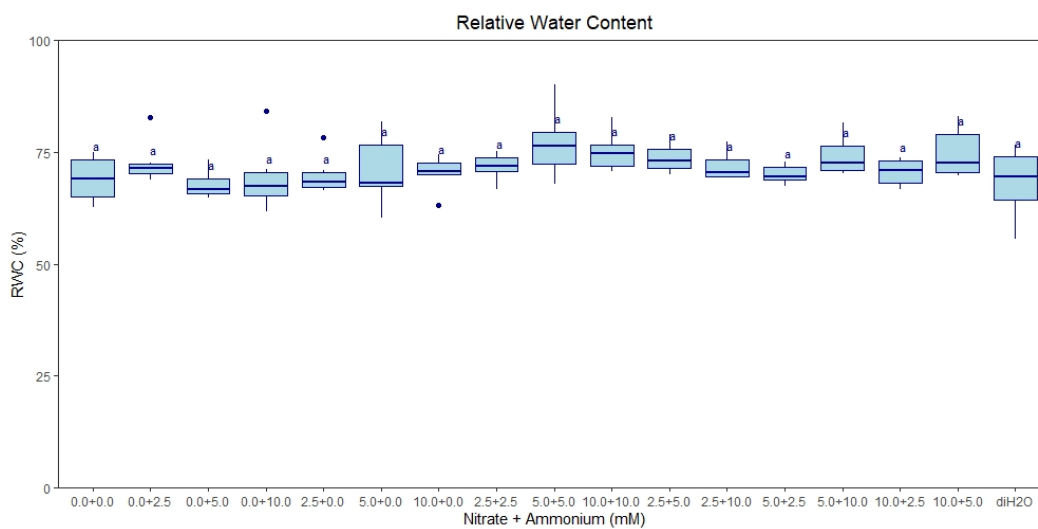


**Figure 7:** Relative water content (%) among treatments ( $n = 6$ ). Treatments are all modified Hoagland's solution with varying amounts of nitrate and ammonium

(mMol) and a deionized water treatment (diH<sub>2</sub>O) control. Letters represent the result of Tukey's test ( $\alpha = 0.05$ ).

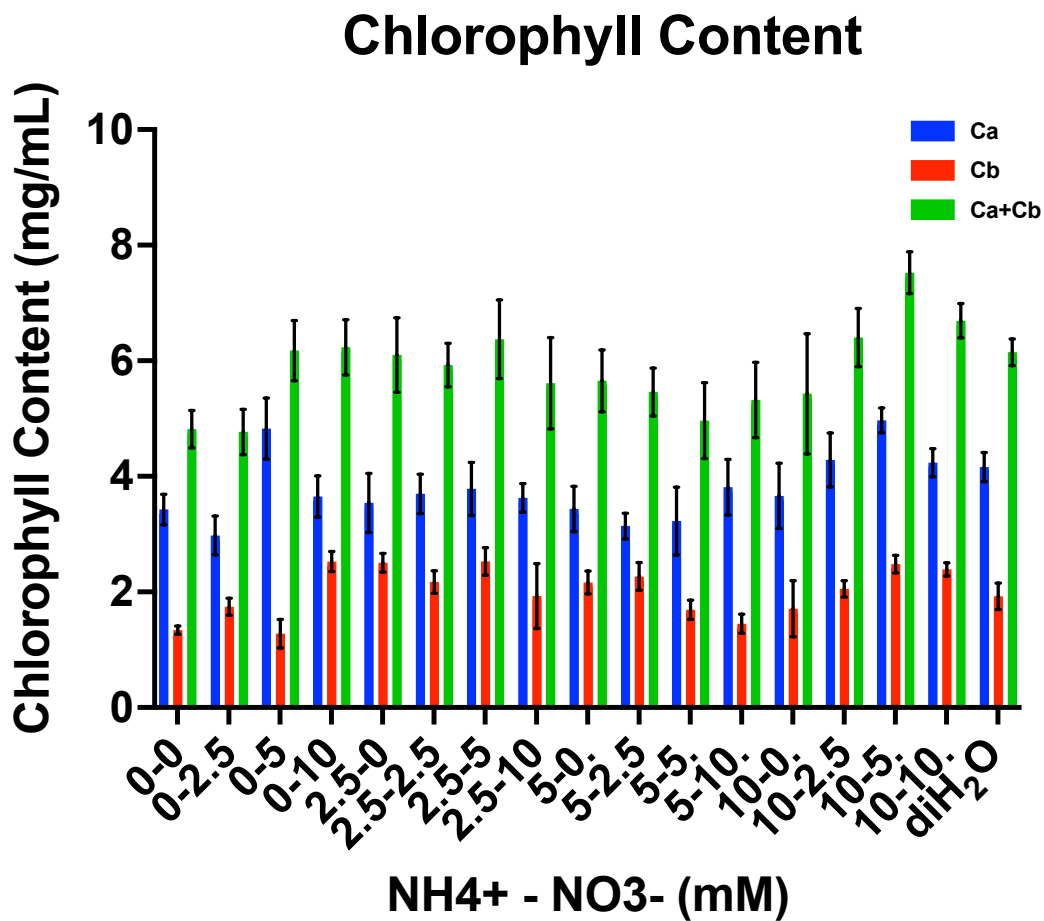


**Figure 8:** Chlorophyll content: Ca (blue), Cb (red), and Ca + Cb (green) content (mg/ml) among treatments ( $n = 6$ ). Treatments are all modified Hoagland's solution with varying amounts of nitrate and ammonium (mMol) and a deionized water treatment (diH<sub>2</sub>O) control. Error bars represent standard error.

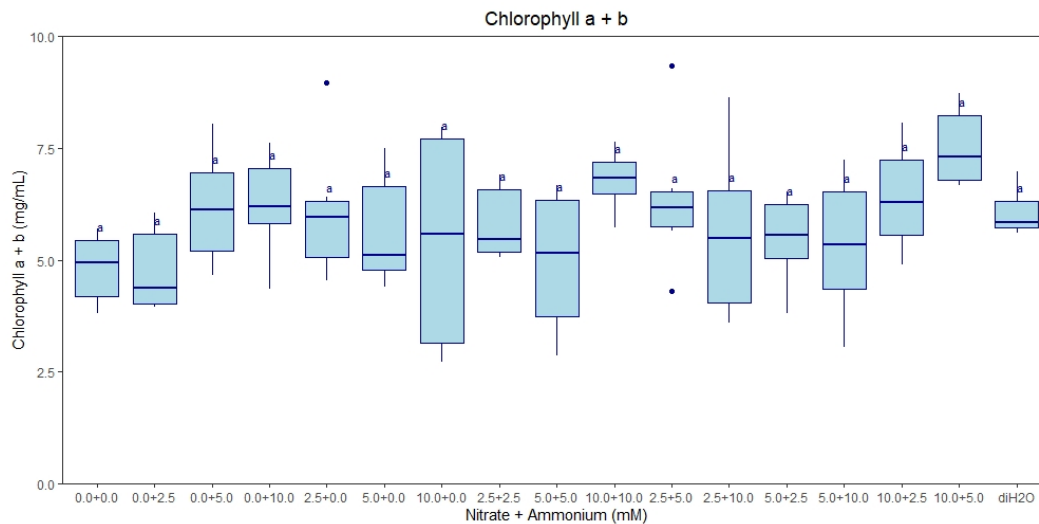


**Figure 9:** Chlorophyll a + b content (mg/ml) among treatments  $n = 6$ . Treatments are all modified Hoagland's solution with varying amounts of nitrate and ammonium (mMol) and a deionized water treatment (diH<sub>2</sub>O) control. Letters represent the result of Tukey's test ( $\alpha = 0.05$ ).

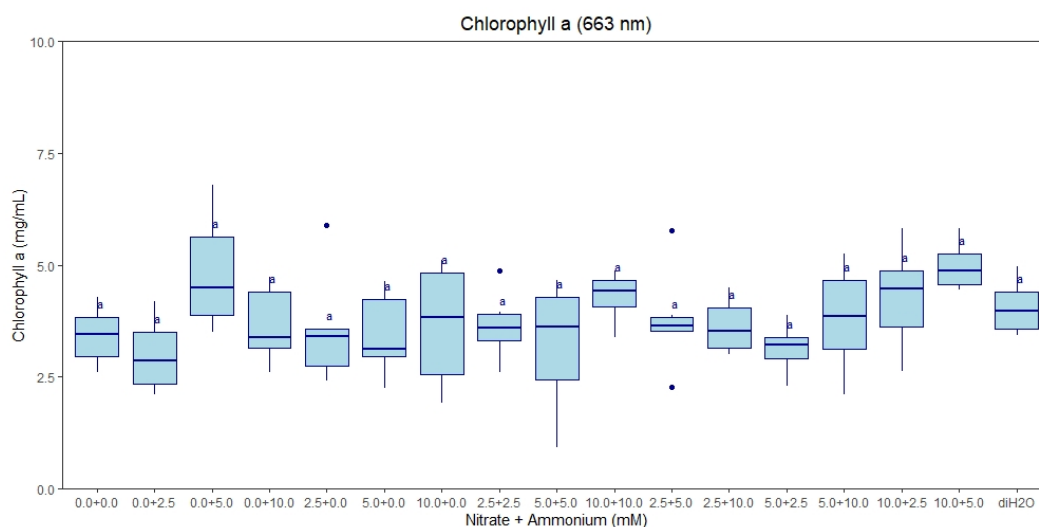


**Figure 10:** Chlorophyll a content (mg/ml) among treatments  $n = 6$ . Treatments are all modified Hoagland's solution with varying amounts of nitrate and ammonium (mMol) and a deionized water treatment (diH<sub>2</sub>O) control. Letters represent the result of Tukey's test ( $\alpha = 0.05$ ).

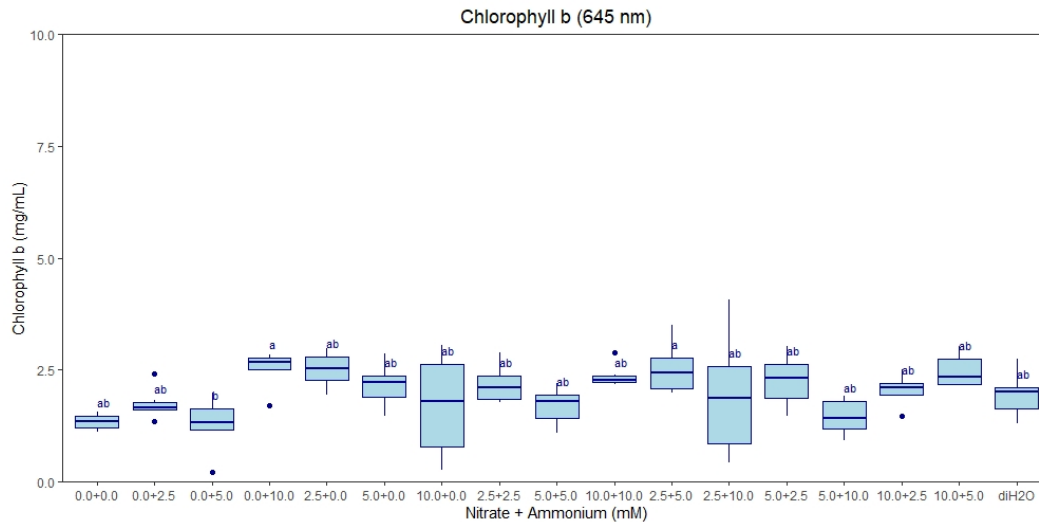


**Figure 11:** Chlorophyll b content (mg/ml) among treatments  $n = 6$ . Treatments are all modified Hoagland's solution with varying amounts of nitrate and ammonium (mMol) and a deionized water treatment (diH<sub>2</sub>O) control. Letters represent the result of Tukey's test ( $\alpha = 0.05$ ).

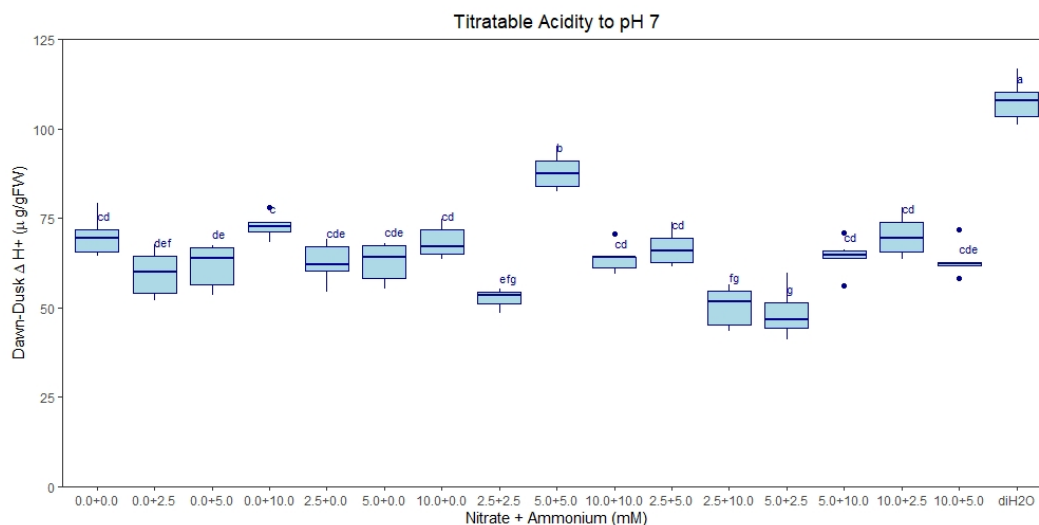


**Figure 12:** Difference between dawn and dusk titrateable tissue to pH 7 (malate equivalent) among treatments ( $n = 6$ ). Treatments are all modified Hoagland's solution with varying amounts of nitrate and ammonium (mMol) and a deionized

water treatment (diH<sub>2</sub>O) control. Letters represent the result of Tukey's test ( $\alpha = 0.05$ ).

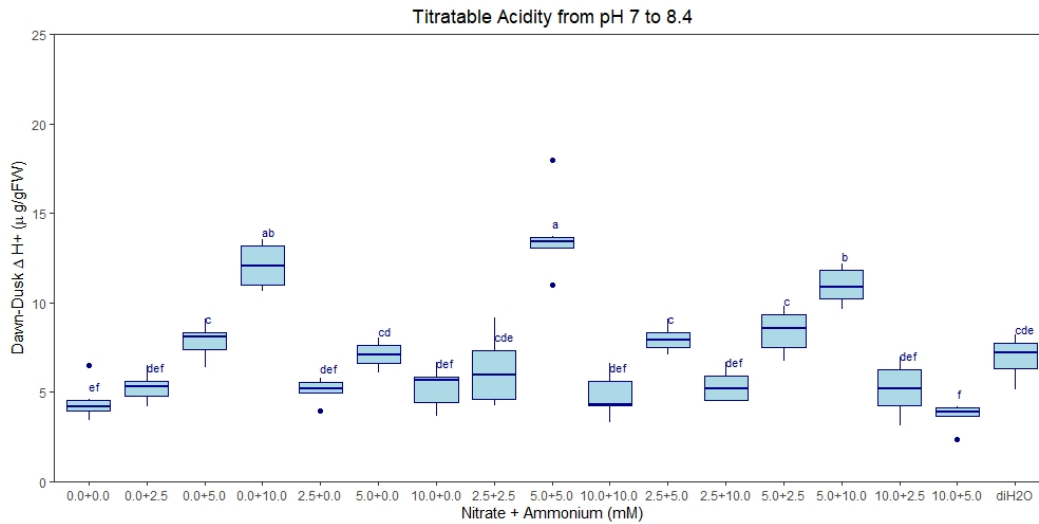


**Figure 13:** Difference between dawn dusk titratable tissue acidity from pH 7 to 8.4 (citrate equivalent) among treatments ( $n = 6$ ). Treatments are all modified Hoagland's solution with varying amounts of nitrate and ammonium (mMol) and a deionized water treatment (diH<sub>2</sub>O) control. Letters represent the result of Tukey's test ( $\alpha = 0.05$ ).

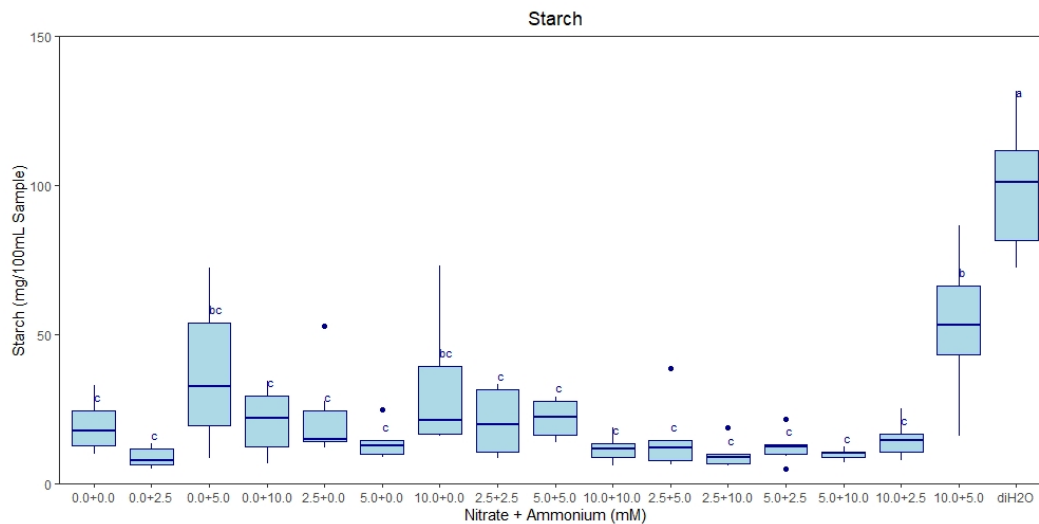


**Figure 14:** Starch content (mg/100ml of sample extract) among treatments ( $n = 6$ ). Treatments are all modified Hoagland's solution with varying amounts of nitrate and ammonium (mMol) and a deionized water treatment (diH<sub>2</sub>O) control. Letters represent the result of Tukey's test ( $\alpha = 0.05$ ).



## Soluble Sugars

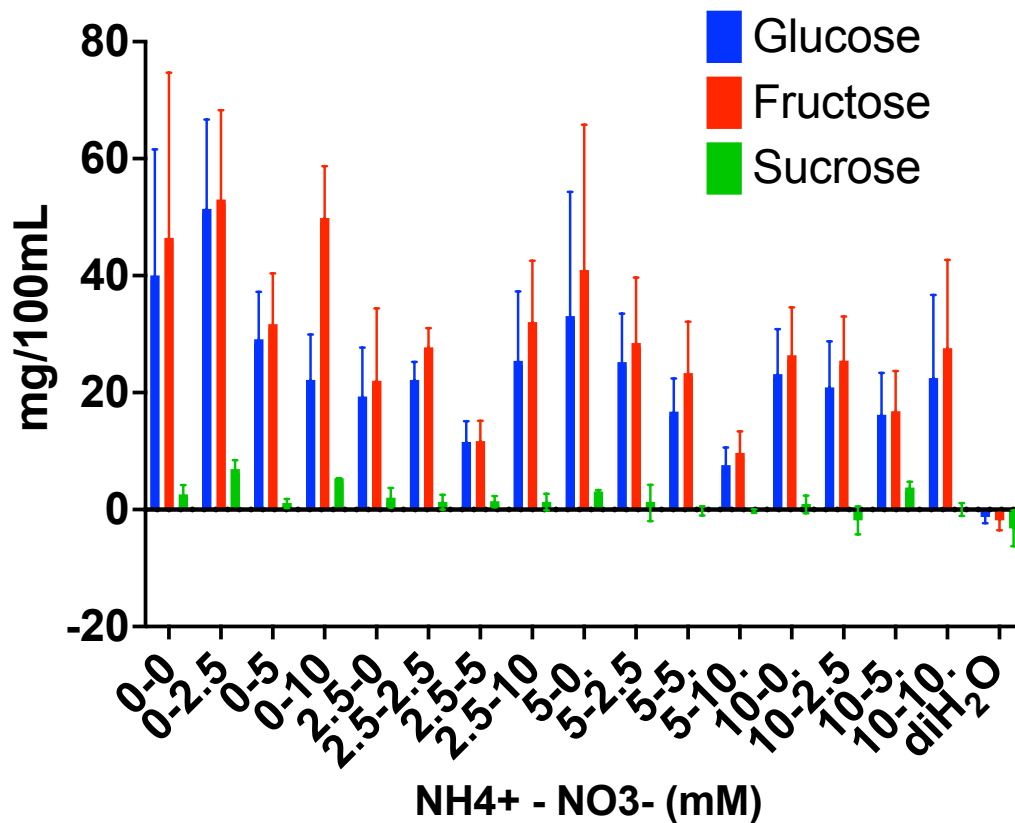


*Figure 15:* Soluble sugars: glucose (blue), fructose (red), and sucrose (green)

content (mg/100 ml sample extract) measured among treatments ( $n = 6$ ).

Treatments are all modified Hoagland's solution with varying amounts of nitrate and ammonium (mMol) and a deionized water treatment (diH<sub>2</sub>O) control. Error bars represent standard error. Negative values represent those calculated below zero by the standard linear equation for each respective sugar.

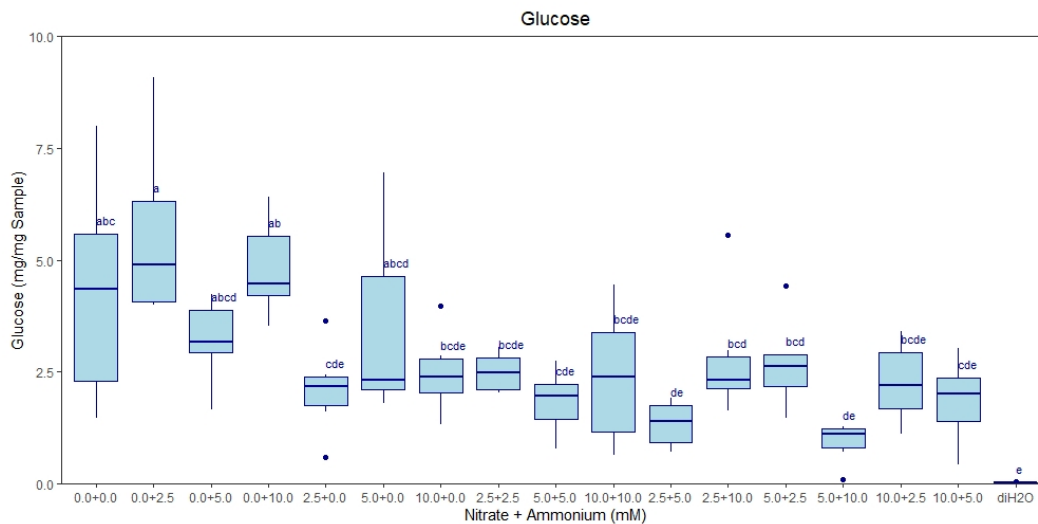


**Figure 16:** Glucose content (mg/mg of sample) among treatments ( $n = 6$ ).

Treatments are all modified Hoagland's solution with varying amounts of nitrate and ammonium (mMol) and a deionized water treatment (diH<sub>2</sub>O) control. Letters represent the result of Tukey's test ( $\alpha = 0.05$ ).

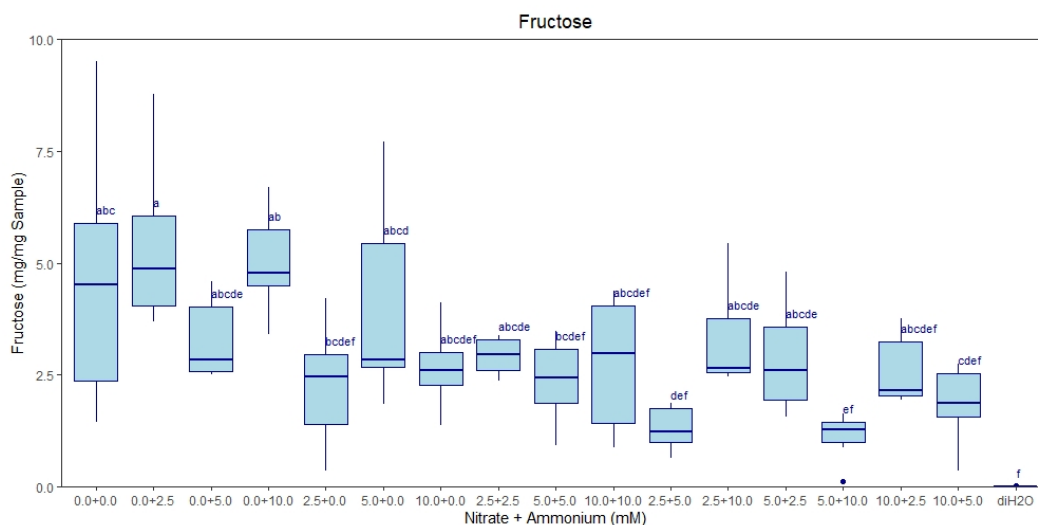


**Figure 17:** Fructose content (mg/mg of sample) among treatments ( $n = 6$ ).

Treatments are all modified Hoagland's solution with varying amounts of nitrate and ammonium (mMol) and a deionized water treatment (diH<sub>2</sub>O) control. Letters represent the result of Tukey's test ( $\alpha = 0.05$ ).

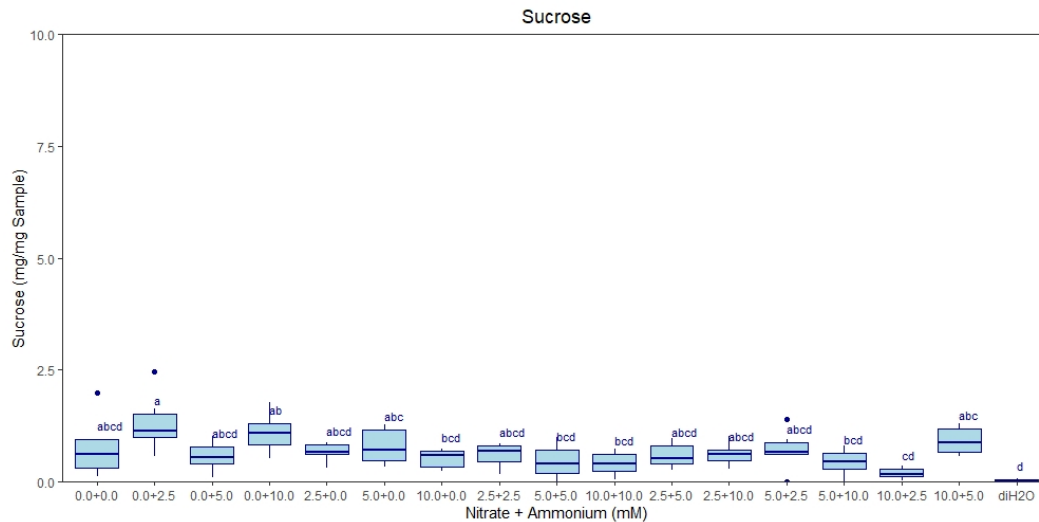


**Figure 18:** Sucrose content (mg/mg of sample) among treatments ( $n = 6$ ).

Treatments are all modified Hoagland's solution with varying amounts of nitrate and ammonium (mMol) and a deionized water treatment (diH<sub>2</sub>O) control. Letters represent the result of Tukey's test ( $\alpha = 0.05$ ).

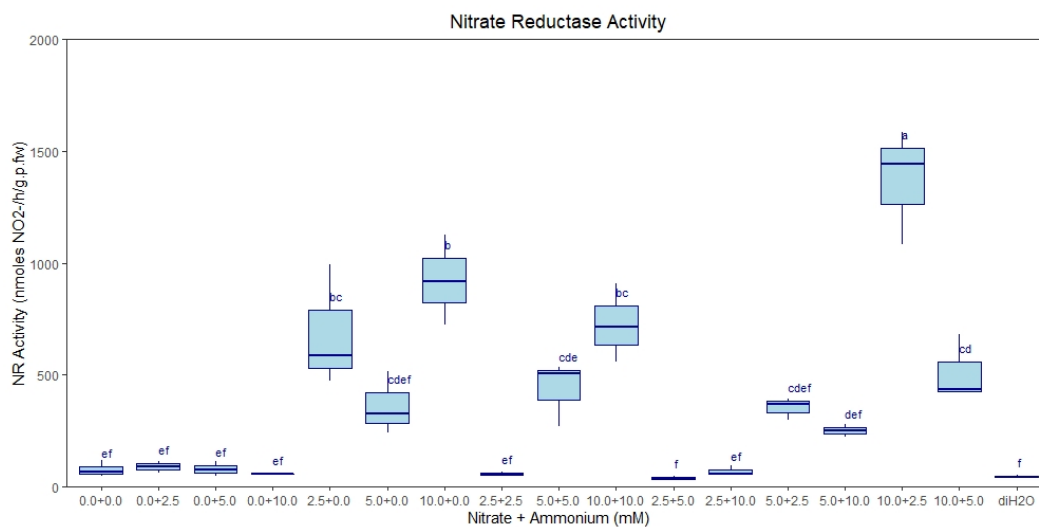


**Figure 19:** Nitrate reductase activity (nmol NO<sub>2</sub><sup>-</sup> fixed/hour/gram fresh weight) among treatments ( $n = 3$ ). Treatments are all modified Hoagland's solution with varying amounts of nitrate and ammonium (mMol) and a deionized water treatment (diH<sub>2</sub>O) control. Letters represent the result of Tukey's test ( $\alpha = 0.05$ ).

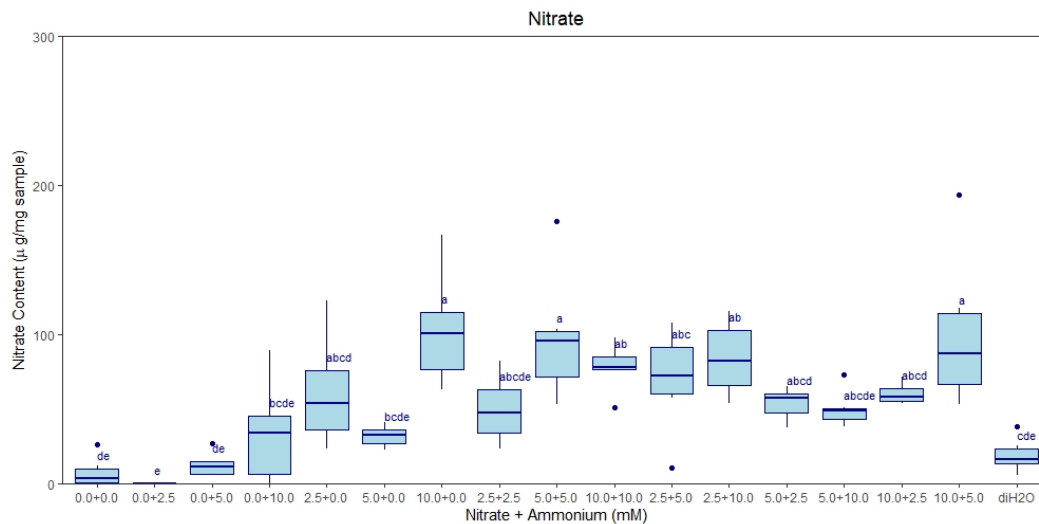


**Figure 20:** Nitrate content ( $\mu\text{g}/\text{mg}$  of sample) among treatments ( $n = 6$ ).

Treatments are all modified Hoagland's solution with varying amounts of nitrate and ammonium (mMol) and a deionized water treatment ( $\text{diH}_2\text{O}$ ) control. Letters represent the result of Tukey's test ( $\alpha = 0.05$ ).

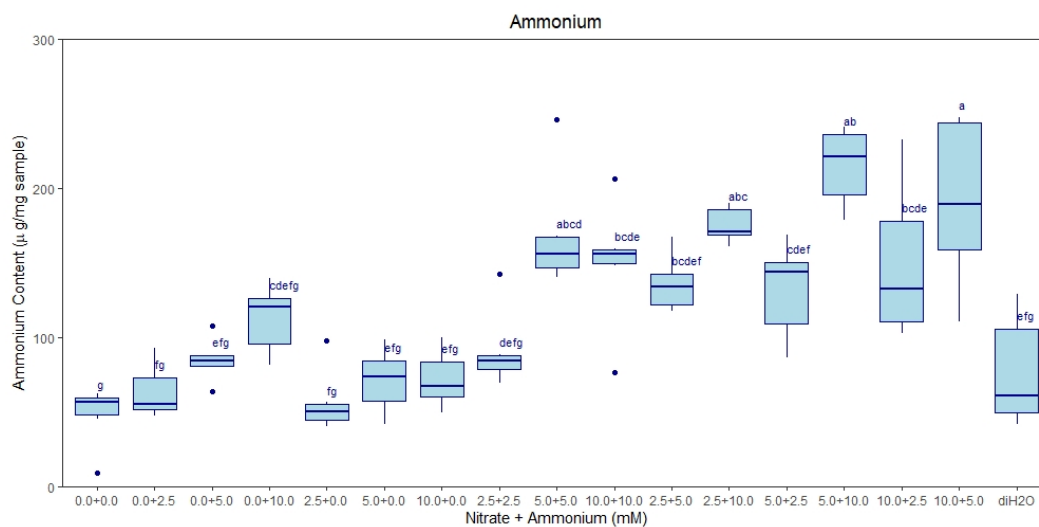


**Figure 21:** Ammonium content ( $\mu\text{Mol}/\text{mg}$  of sample) among treatments ( $n = 3$ ).

Treatments are all modified Hoagland's solution with varying amounts of nitrate and ammonium (mMol) and a deionized water treatment ( $\text{diH}_2\text{O}$ ) control. Letters represent the result of Tukey's test ( $\alpha = 0.05$ ).

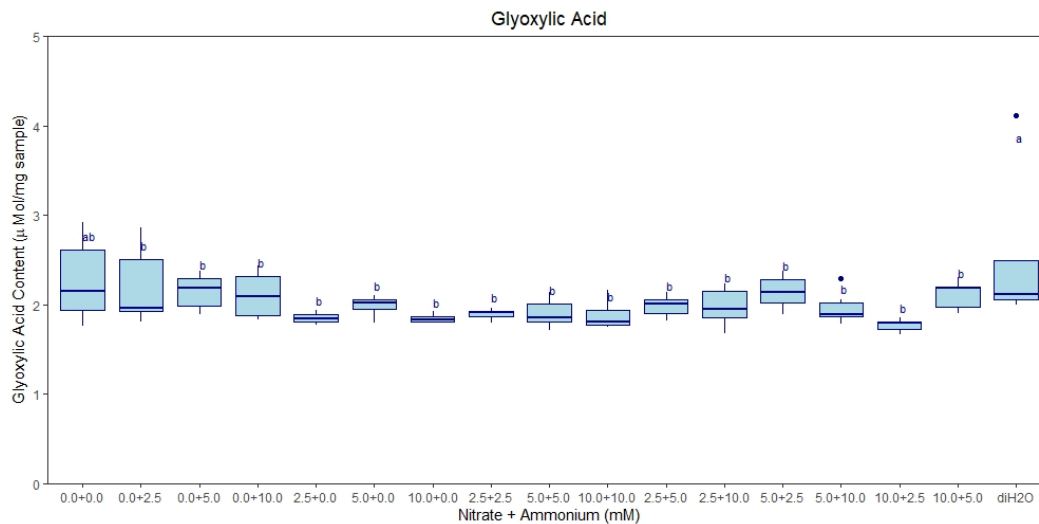


**Figure 22:** Glyoxylic acid content ( $\mu\text{Mol}/\text{mg}$  of sample) among treatments ( $n = 6$ ). Treatments are all modified Hoagland's solution with varying amounts of nitrate and ammonium ( $\text{mMol}$ ) and a deionized water treatment ( $\text{diH}_2\text{O}$ ) control. Letters represent the result of Tukey's test ( $\alpha = 0.05$ ).

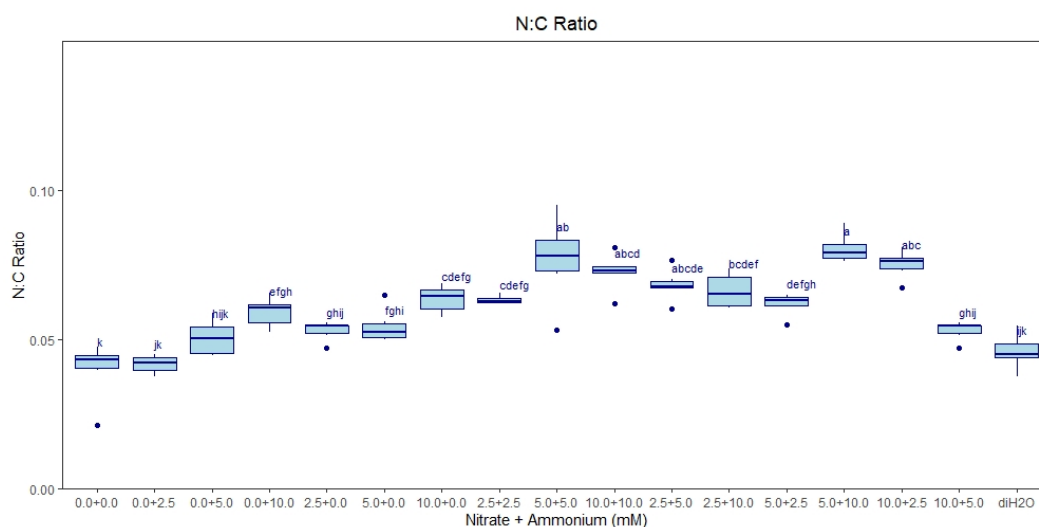


**Figure 23:** N:C ratio among treatments ( $n = 6$ ). Treatments are all modified Hoagland's solution with varying amounts of nitrate and ammonium ( $\text{mMol}$ ) and a deionized water treatment ( $\text{diH}_2\text{O}$ ) control. Letters represent the result of Tukey's test ( $\alpha = 0.05$ ).

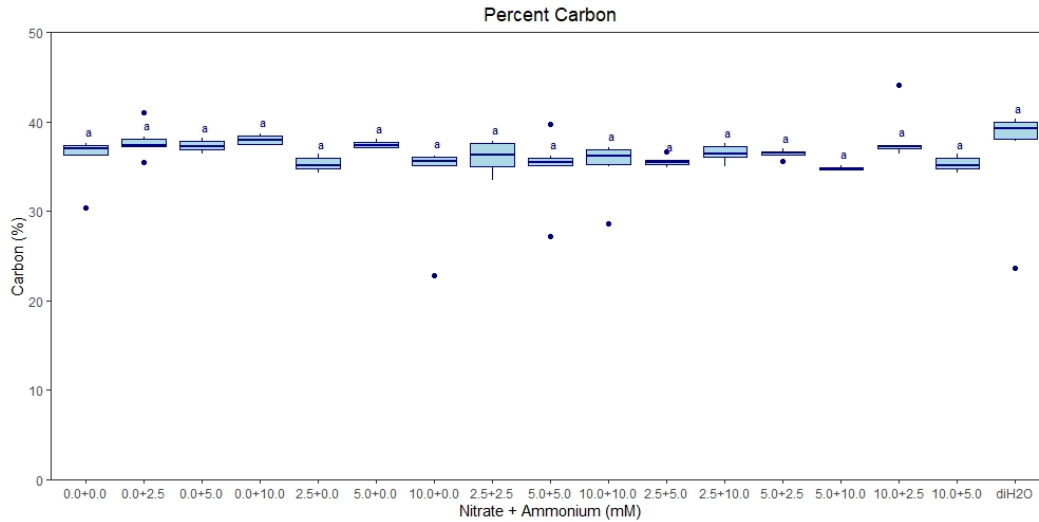


**Figure 24:** Percent carbon (%) among treatments ( $n = 6$ ). Treatments are all modified Hoagland's solution with varying amounts of nitrate and ammonium (mMol) and a deionized water treatment (diH<sub>2</sub>O) control. Letters represent the result of Tukey's test ( $\alpha = 0.05$ ).

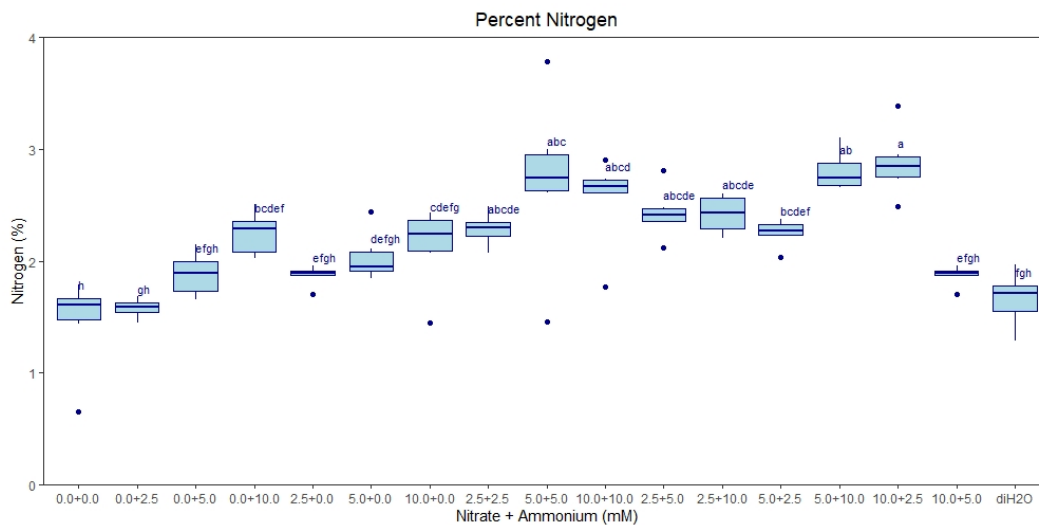


**Figure 25:** Percent Nitrogen (%) among treatments ( $n = 6$ ). Treatments are all modified Hoagland's solution with varying amounts of nitrate and ammonium (mMol) and a deionized water treatment (diH<sub>2</sub>O) control. Letters represent the result of Tukey's test ( $\alpha = 0.05$ ).

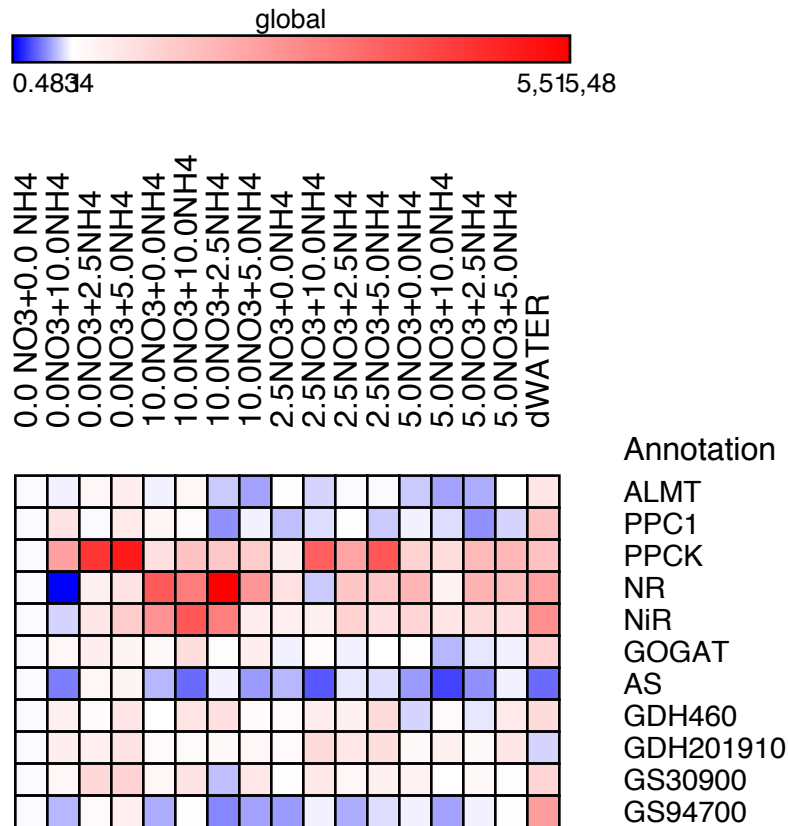


**Figure 26:** Collective heatmap of N metabolism, and CAM related relative gene expression measured through RT-qPCR analysis among nitrate and ammonium treatments (mMol). Genes listed: aluminum activated malate transporter (ALMT), phosphoenolpyruvate carboxylase (PPC1), phosphoenolpyruvate carboxylase kinase (PPCK), nitrate reductase (NR), nitrite reductase (NiR), glutamate synthase (GOGAT), asparagine synthase (AS), glutamate dehydrogenase (GDH), and glutamine synthetase (GS). Relative expression of all genes is normalized to the 0+0 nitrate and ammonium treatment. The color scale represents actin and ubiquitin FPKM normalized  $\log_2$  transformed counts where blue indicates low expression, and red indicates high expression.

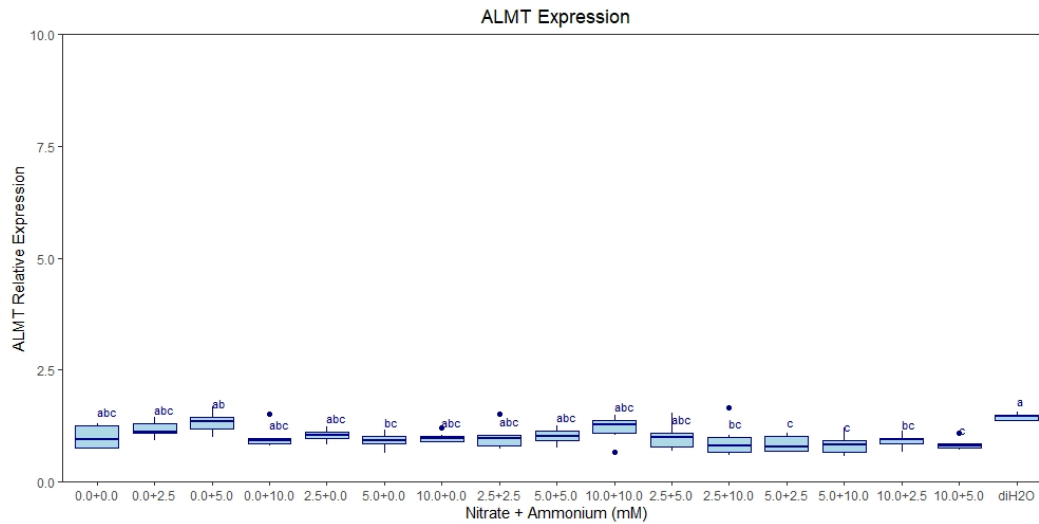


**Figure 27:** Relative expression of aluminum-activated malate transporter (ALMT) among nitrate and ammonium treatments (mM). Relative expression of ALMT in all treatments is normalized to average ALMT expression in the 0+0 nitrate and ammonium treatment. All values represent the average actin and ubiquitin FPKM normalized  $\log_2$  transformed counts. Letters represent the result of Tukey's test ( $\alpha=0.05$ ). ( $n = 6$ )



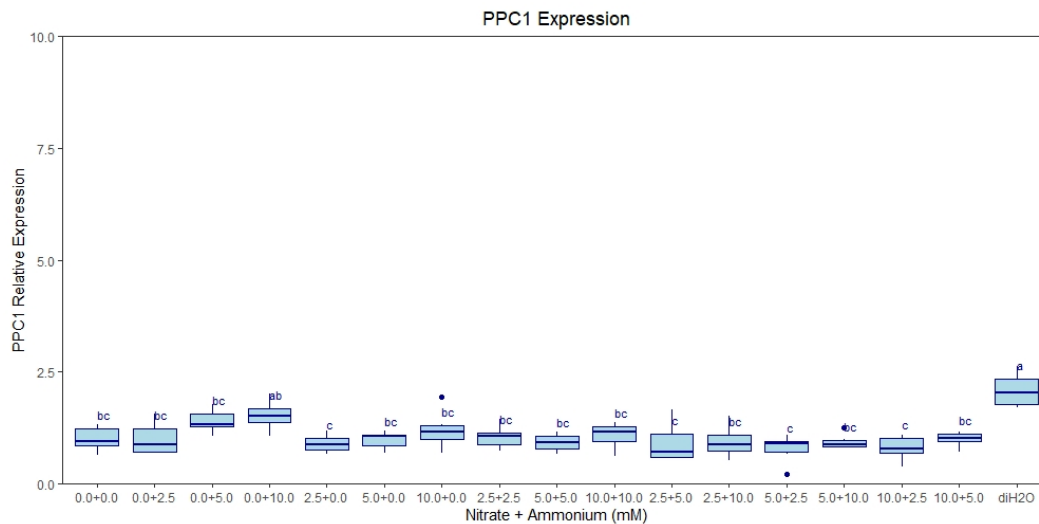


**Figure 28:** Relative expression of phosphoenolpyruvate carboxylase (PPC1) among nitrate and ammonium treatments (mM). Relative expression of PPC1 in all treatments is normalized to the average PPC1 expression in the 0+0 nitrate and ammonium treatment. All values represent the average actin and ubiquitin FPKM normalized  $\log_2$  transformed counts. Letters represent the result of Tukey's test ( $\alpha = 0.05$ ). ( $n = 6$ )

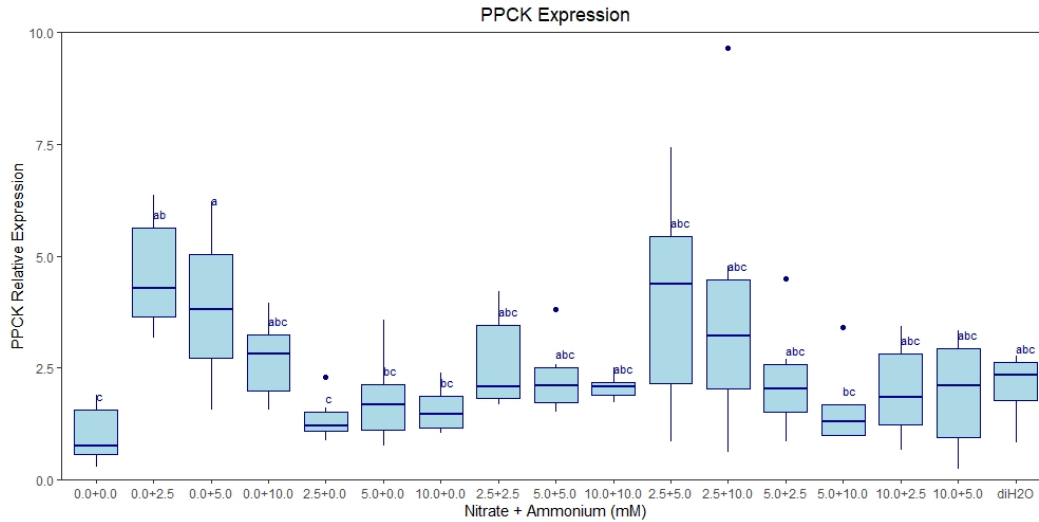


**Figure 29:** Relative expression of phosphoenolpyruvate carboxylase kinase (PPCK) among nitrate and ammonium treatments. Relative expression of PPCK in all treatments is normalized to the average PPCK expression in the 0+0 nitrate and ammonium treatment. All values represent the average actin and ubiquitin FPKM normalized  $\log_2$  transformed counts. Letters represent the result of Tukey's test ( $\alpha = 0.05$ ). ( $n=6$ )

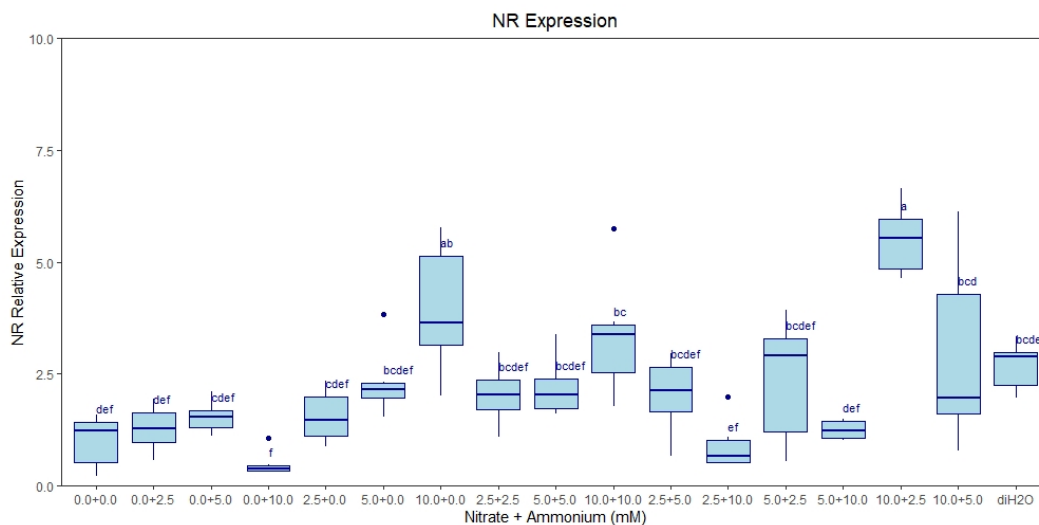


**Figure 30:** Relative expression of nitrate reductase (NR) among nitrate and ammonium treatments. Relative expression of NR in all treatments is normalized

to the average NR expression in the 0+0 nitrate and ammonium treatment. All values represent the average actin and ubiquitin FPKM normalized  $\log_2$  transformed counts. Letters represent the result of Tukey's test ( $\alpha = 0.05$ ). ( $n = 6$ )

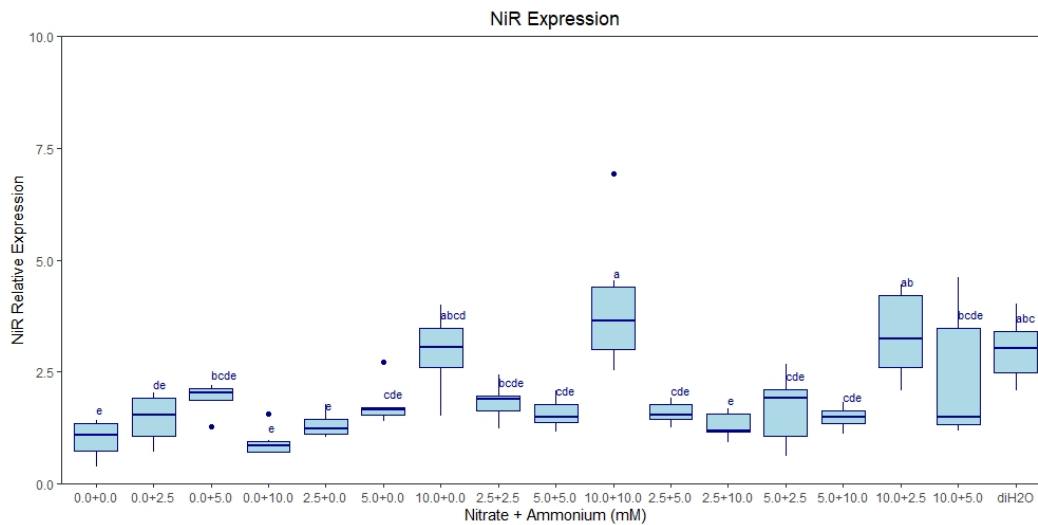


**Figure 31:** Relative expression of nitrite reductase (NiR) among nitrate and ammonium treatments. Relative expression of NiR in all treatments is normalized to the average NiR expression in the 0+0 nitrate and ammonium treatment. All values represent the average actin and ubiquitin FPKM normalized  $\log_2$  transformed counts. Letters represent the result of Tukey's test ( $\alpha = 0.05$ ). ( $n = 3$ )

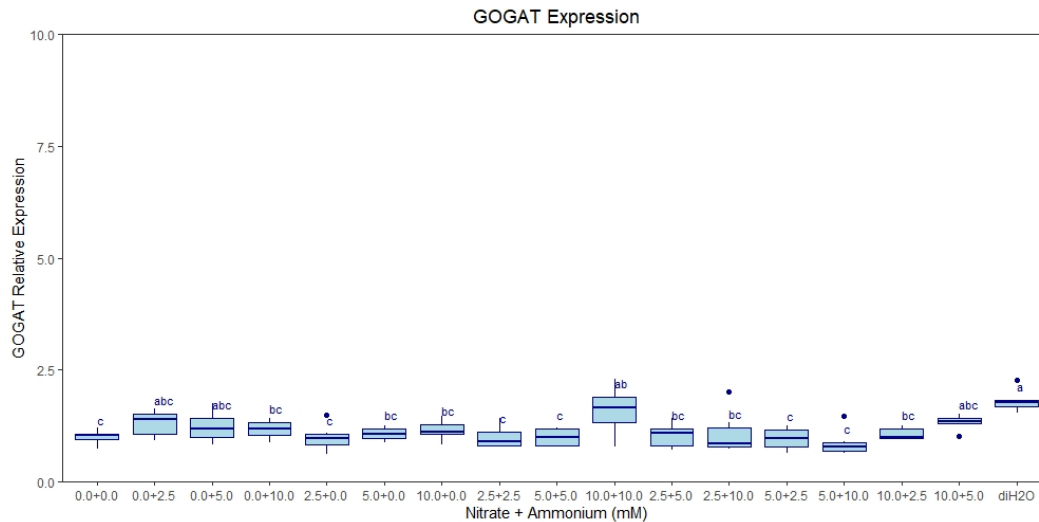


**Figure 32:** Relative expression of glutamate synthase (GOGAT) among nitrate and ammonium treatments. Relative expression of GOGAT in all treatments is normalized to the average GOGAT expression in the 0+0 nitrate and ammonium treatment. All values represent the average actin and ubiquitin FPKM normalized  $\log_2$  transformed counts. Letters represent the result of Tukey's test ( $\alpha = 0.05$ ). ( $n = 3$ )

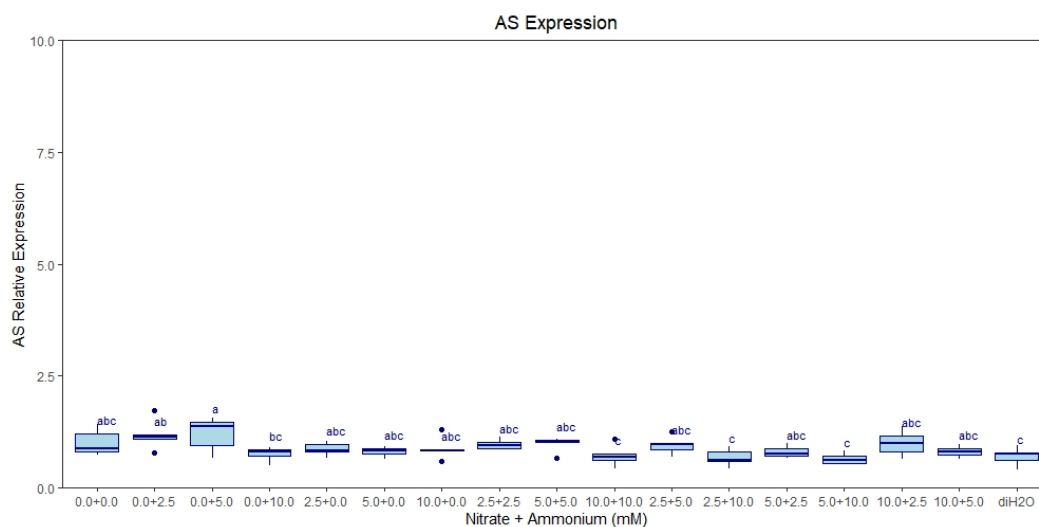


**Figure 33:** Relative expression of asparagine synthase (AS) among nitrate and ammonium treatments. Relative expression of AS in all treatments is normalized

to the average AS expression in the 0+0 nitrate and ammonium treatment. All values represent the average actin and ubiquitin FPKM normalized  $\log_2$  transformed counts. Letters represent the result of Tukey's test ( $\alpha = 0.05$ ). ( $n = 6$ )

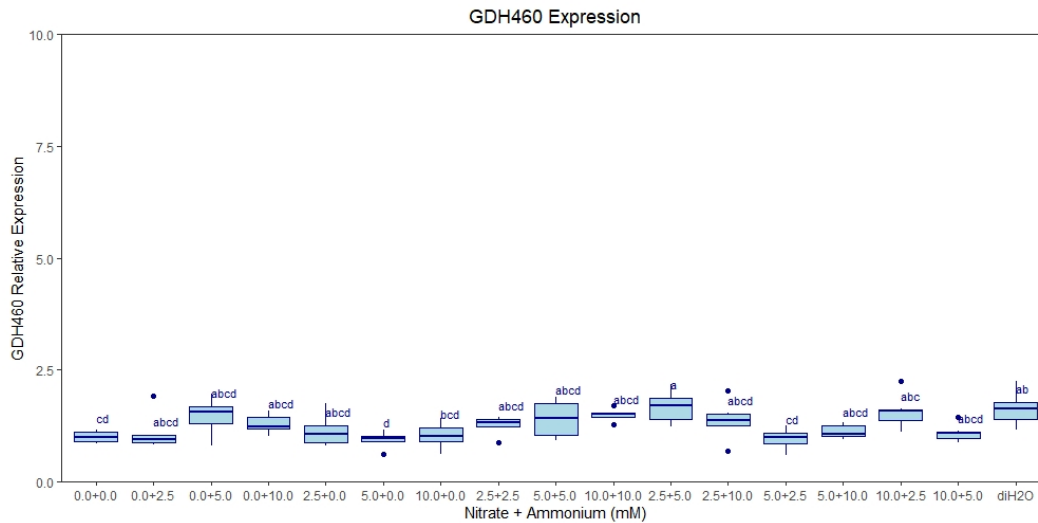


**Figure 34:** Relative expression of glutamate dehydrogenase (GDH460) among nitrate and ammonium treatments. Relative expression of GDH460 in all treatments is normalized to the average GDH460 expression in the 0+0 nitrate and ammonium treatment. All values represent the average actin and ubiquitin FPKM normalized  $\log_2$  transformed counts. Letters represent the result of Tukey's test ( $\alpha = 0.05$ ). ( $n = 6$ )

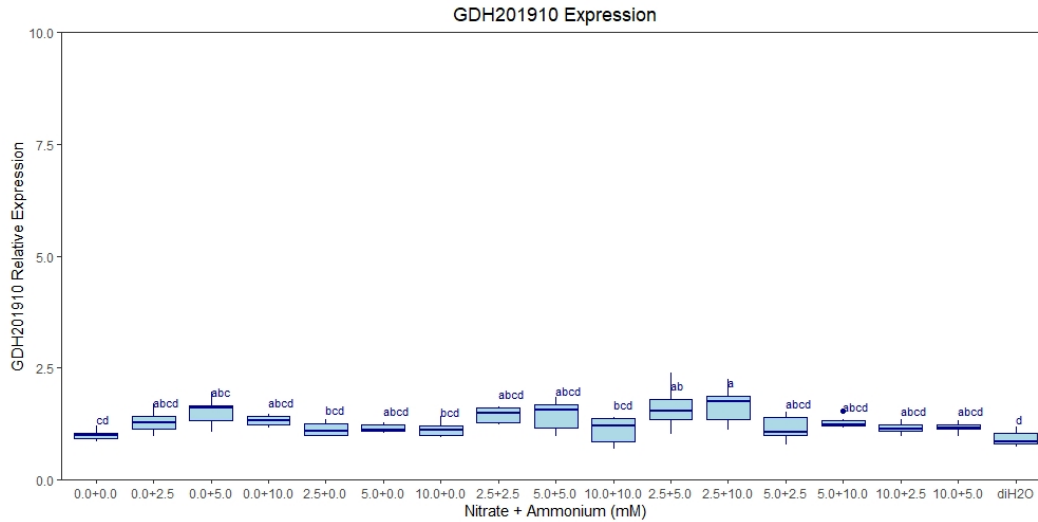


**Figure 35:** Relative expression of GDH (GDH201910) among nitrate and ammonium treatments. Relative expression of GDH201910 in all treatments is normalized to the average GDH201910 expression in the 0+0 nitrate and ammonium treatment. All values represent the average actin and ubiquitin FPKM normalized  $\log_2$  transformed counts. Letters represent the result of Tukey's test ( $\alpha = 0.05$ ). ( $n = 6$ )

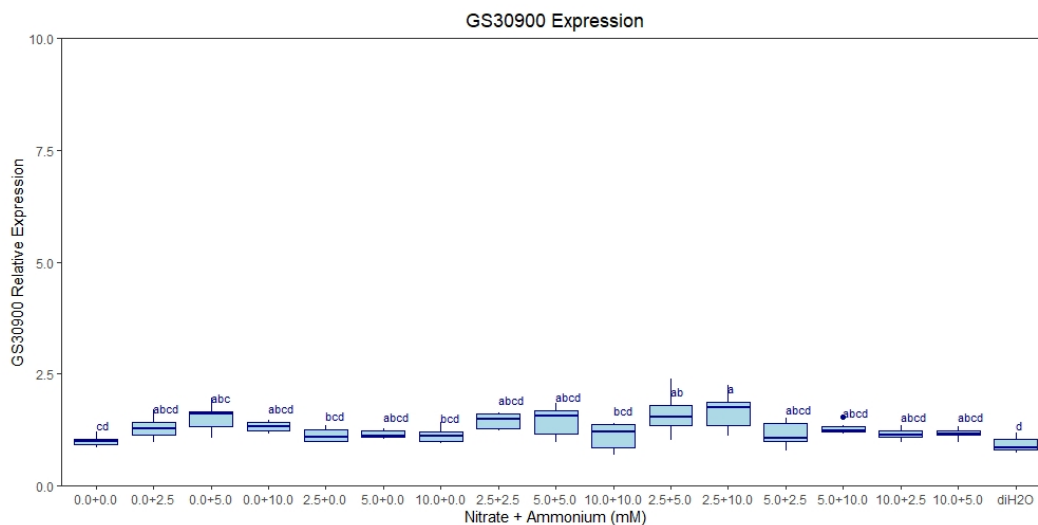


**Figure 36:** Relative expression of glutamine synthase (GS30900) among nitrate and ammonium treatments. Relative expression of GS30900 in all treatments is

normalized to the average GS30900 expression in the 0+0 nitrate and ammonium treatment. All values represent the average actin and ubiquitin FPKM normalized  $\log_2$  transformed counts. Letters represent the result of Tukey's test ( $\alpha = 0.05$ ). ( $n = 6$ )

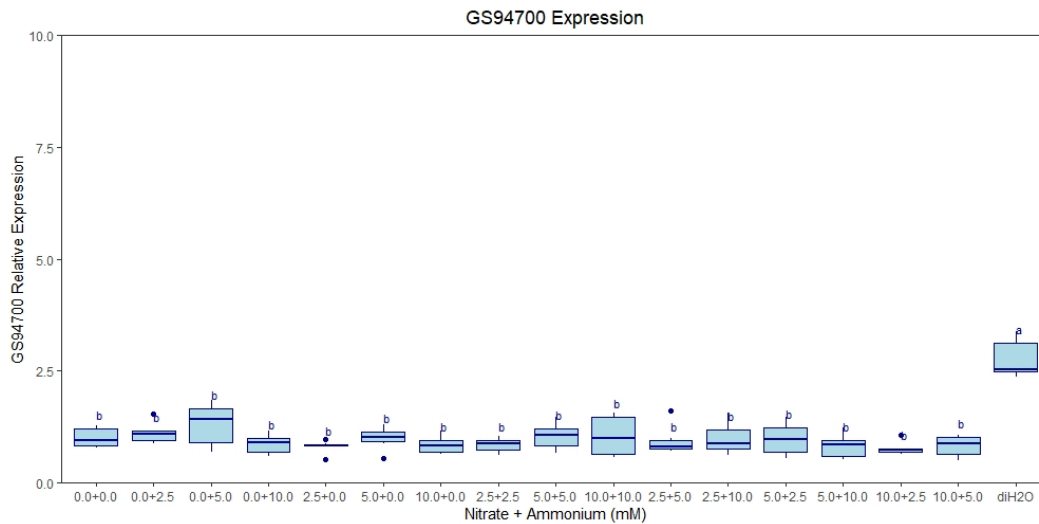


**Figure 37:** Relative expression of glutamine synthetase (GS94700) among nitrate and ammonium treatments. Relative expression of GS94700 in all treatments is normalized to the average GS94700 expression in the 0+0 nitrate and ammonium treatment. All values represent the average actin and ubiquitin FPKM normalized  $\log_2$  transformed counts. Letters represent the result of Tukey's test ( $\alpha = 0.05$ ). ( $n = 6$ )

## References

- Bernard SM, Habash DZ** (2009) The importance of cytosolic glutamine synthetase in nitrogen assimilation and recycling. *New Phytologist* **182**: 608-620
- Borland AM, Griffiths H, Hartwell J, Smith JAC** (2009) Exploiting the potential of plants with crassulacean acid metabolism for bioenergy production on marginal lands. *Journal of Experimental Botany* **60**: 2879–2896
- Borland AM, Guo HB, Yang X, Cushman JC** (2016) Orchestration of carbohydrate processing for crassulacean acid metabolism. *Current Opinion in Plant Biology* **31**: 118–124
- Boxall SF, Dever LV, Knerova J, Gould PD, Hartwell J** (2017) Phosphorylation of phosphoenolpyruvate carboxylase is essential for maximal and sustained dark CO<sub>2</sub> fixation and core circadian clock operation in the obligate crassulacean acid metabolism species *Kalanchoe fedtschenkoi*. *The Plant Cell* **29**: 2519–2536
- Britto DT, Kronzucker HJ** (2002) NH<sub>4</sub><sup>+</sup> toxicity in higher plants: a critical review. *Journal of plant physiology* **159**: 567-584
- Bräutigam A, Gagneul D, Weber AP** (2007) High-throughput colorimetric method for the parallel assay of glyoxylic acid and ammonium in a single extract. *Analytical biochemistry* **362**
- Busch FA** (2020) Photorespiration in the context of Rubisco biochemistry, CO<sub>2</sub> diffusion and metabolism. *The Plant Journal* **101**: 919-939



- Calabrò PS, Catalán E, Folino A, Sánchez A, Komilis D** (2018) Effect of three pretreatment techniques on the chemical composition and on the methane yields of *Opuntia ficus-indica* (prickly pear) biomass. *Waste Management & Research* **36**: 17–29
- Cataldo D, Maroon M, Schrader LE, Youngs VL** (1975) Rapid colorimetric determination of nitrate in plant tissue by nitration of salicylic acid. *Communications in soil science and plant analysis* **6**: 71-80
- Christopher JT, Holtum JAM** (1996) Patterns of carbohydrate partitioning in the leaves of Crassulacean acid metabolism species during deacidification. *Plant Physiology* **112**: 393–399
- Cockburn W, Ting IP, Sternberg LO** (1979) Relationships between stomatal behavior and internal carbon-dioxide concentrations in crassulacean acid metabolism plants. *Plant Physiology* **63**: 1029–1032
- Cui M, Nobel PS** (1994) Gas exchange and growth responses to elevated CO<sub>2</sub> and light levels in the CAM species *Opuntia ficus-indica*. *Plant, Cell & Environment* **17**: 935–944
- Cushman JC, Agarie S, Albion RL, Elliot SM, Taybi T, Borland AM** (2008) Isolation and characterization of mutants of common ice plant deficient in Crassulacean acid metabolism. *Plant Physiology* **147**: 228–238
- Cushman JC, Bohnert HJ** (1997) Molecular genetics of crassulacean acid metabolism. *Plant Physiology* **113**: 667-676

- Daryanto S, Wang L, Gilhooly III WP, Jacinthe P-A** (2019) Nitrogen preference across generations under changing ammonium nitrate ratios. *Journal of Plant Ecology* **12**: 235-244
- Davis SC, Simpson J, Vega G, Del Carmen K, Niechayev NA, Tongerlo EV, Castano NH, Dever LV, Búrque A** (2019) Undervalued potential of crassulacean acid metabolism for current and future agricultural production. *Journal of Experimental Botany* **70**: 6521–6537
- De Rijck G, Schrevens E** (1998) Comparison of the mineral composition of twelve standard nutrient solutions. *Journal of Plant Nutrition* **21**: 2115-2125
- do Nascimento Santos T, Dutra ED, do Prado AG, Leite FC, de Souza RD, dos Santos DC, de Abreu CA, Simões DA, de Moraes JMA, Menezes RS** (2016) Potential for biofuels from the biomass of prickly pear cladodes: Challenges for bioethanol and biogas production in dry areas. *Biomass and Bioenergy* **85**: 215–222
- Dubeux JJCB, Ferreira dos Santos MVF, de Andrade Lira M, Coreiro dos Santos D, Farias I, Lima LE, Ferreira RLC** (2006) Productivity of *Opuntia ficus-indica* (L.) Miller under different N and P fertilization and plant population in north-east Brazil. *Journal of Arid Environments* **67**: 357–372
- Feeley K, Bravo-Avila C, Fadrique B, Perez T, Zuleta D** (2020) Climate-driven changes in the composition of New World plant communities. *Nature Climate Change* **10**: 965-970

- Feng H, Fan X, Miller AJ, Xu G** (2020) Plant nitrogen uptake and assimilation: regulation of cellular pH homeostasis. *Journal of Experimental Botany* **In press**
- Garcia de Cortazar V, Nobel P** (1992) Biomass and fruit production for the prickly pear cactus *Opuntia ficus-indica*. *Journal of the American Society for Horticultural Science* **117**: 568–562
- Gehrig HH, Wood J, Cushman MA, Virgo A, Cushman JC, Winter K** (2005) Large gene family of phosphoenolpyruvate carboxylase in the Crassulacean acid metabolism plant *Kalanchoe pinnata* (Crassulaceae). *Functional Plant Biology* **32**: 467–472
- Gomez L, Bancel D, Rubio E, Vercambre G** (2007) The microplate reader: an efficient tool for the separate enzymatic analysis of sugars in plant tissues—validation of a micro-method. *Journal of the Science of Food and Agriculture* **87**: 1893-1905
- Goycoolea FM, Cárdenas A** (2003) Pectins from *Opuntia spp.*: a short review. *Journal of the Professional Association for Cactus Development* **5**: 17–29
- Habteselassie MY, Xu L, Norton JM** (2013) Ammonia-oxidizer communities in an agricultural soil treated with contrasting nitrogen sources. *Frontiers in Microbiology* **4**: 326
- Hachiya T, Sakakibara H** (2017) Interactions between nitrate and ammonium in their uptake, allocation, assimilation, and signaling in plants. *Journal of Experimental Botany* **68**: 2501-2512

- Hartwell J, Nimmo GA, Wilkins MB, Jenkins GL, Nimmo HG (1999)**  
Phosphoenolpyruvate carboxylase kinase is a novel protein kinase regulated at the level of gene expression. *The Plant Journal* **20**: 333-342
- Houlton BZ, Sigman DM, Schuur EA, Hedin LO (2007)** A climate-driven switch in plant nitrogen acquisition within tropical forest communities. *Proceedings of the National Academy of Sciences* **104**: 8902-8906
- Islam S, Islam R, Kandwal P, Khanam S, Proshad R, Kormoker T, Tusher TR (2020)** Nitrate transport and assimilation in plants: a potential review. *Archives of Agronomy and Soil Science*: 1-18
- Kiba T, Krapp A (2016)** Plant nitrogen acquisition under low availability: regulation of uptake and root architecture. *Plant and Cell Physiology* **57**: 707-714
- Kovermann P, Meyer S, Hörtensteiner S, Picco C, Scholz-Starke J, Ravera S, Lee Y, Martinoia E (2007)** The Arabidopsis vacuolar malate channel is a member of the ALMT family. *The Plant Journal* **52**: 1169–1180
- Krapp A (2015)** Plant nitrogen assimilation and its regulation: a complex puzzle with missing pieces. *Current Opinion in Plant Biology* **25**: 115-122
- Krümpel J, George T, Gasston B, Francis G, Lemmer A (2020)** Suitability of *Opuntia ficus-indica* (L) Mill. and *Euphorbia tirucalli* L. as energy crops for anaerobic digestion. *Journal of Arid Environments* **174**: 104047
- Lopez-Bucio J, Nieto-Jacobo MF, Ramirez-Rodriguez V, Herrera-Estrella L (2000)** Organic acid metabolism in plants: from adaptive physiology to

transgenic varieties for cultivation in extreme soils. *Plant Science* **160**: 1-13

**Lüttge U, Beyschlag W, Büdel B, Francis D** (2012) *Progress in Botany* 77. Springer

**Males J, Griffiths H** (2017) Stomatal biology of CAM plants. *Plant Physiology* **174**: 550–560

**Marschnert H, Kirkby EA, Engels C** (1997) Importance of cycling and recycling of mineral nutrients within plants for growth and development. *Botanica Acta* **110**: 265-273

**Naumann G, Alfieri L, Wyser K, Mentaschi L, Betts RA, Carrao H, Spinoni J, Vogt J, Feyen L** (2018) Global changes in drought conditions under different levels of warming. *Geophysical Research Letters* **45**: 3285–3296

**Nerd A, Nobel PS** (1991) Effects of drought on water relations and nonstructural carbohydrates in cladodes of *Opuntia ficus-indica*. *Physiologia Plantarum* **81**: 495-500

**Nerd A, Nobel PS** (1995) Accumulation, partitioning, and assimilation of nitrate in *Opuntia ficus-indica*. *Journal of Plant Nutrition* **18**: 2533-2549

**Ni Z, Kim ED, Ha M, Lackey E, Liu J, Zhang Y, Sun Q, Chen ZJ** (2009) Altered circadian rhythms regulate growth vigour in hybrids and allopolyploids. *Nature* **457**: 327–331

**Niechayev NA, Jones AM, Rosenthal DM, Davis SC** (2019) A model of environmental limitations on production of *Agave americana* L. grown as

- a biofuel crop in semi-arid regions. *Journal of Experimental Botany* **70**: 6549–6559
- Nimmo HG** (2000) The regulation of phosphoenolpyruvate carboxylase in CAM plants. *Trends in Plant Science* **5**: 75-80
- Nkoi V, Wit Md, Fouche H, Coetzer G, Hugo A** (2021) The Effect of Nitrogen Fertilization on the Yield, Quality and Fatty Acid Composition of *Opuntia ficus-indica* Seed Oil. *Sustainability* **13**: 10123
- Nobel PS** (1983) Nutrient levels in cacti—relation to nocturnal acid accumulation and growth. *American Journal of Botany* **70**: 1244-1253
- Nobel PS, Russell C, Felker P, Medina J, Acuna E** (1987) Nutrient relations and productivity of prickly pear cacti. *Agronomy Journal* **79**: 550–555
- Osmond CB** (1978) Crassulacean acid metabolism: a curiosity in context. *Annual Review of Plant Physiology* **29**: 379–414
- Owen NA, Griffiths H** (2014) Marginal land bioethanol yield potential of four crassulacean acid metabolism candidates (*Agave fourcroydes*, *Agave salmiana*, *Agave tequilana* and *Opuntia ficus-indica*) in Australia. *Global Change Biology: Bioenergy* **6**: 687–703
- Pereira PN, Cushman JC** (2019) Exploring the relationship between crassulacean acid metabolism (CAM) and mineral nutrition with a special focus on nitrogen. *International Journal of Molecular Sciences* **20**: 4363
- Pereira PN, Smith JAC, Mercier H** (2017) Nitrate enhancement of CAM activity in two *Kalanchoë* species is associated with increased vacuolar proton transport capacity. *Physiologia Plantarum* **160**: 361-372

- Pfaffl MW** (2001) A new mathematical model for relative quantification in real-time RT-PCR. *Nucleic Acids Research* **29**: e45-e45
- Pfaffl MW** (2004) Quantification strategies in real-time PCR. *AZ of quantitative PCR* **1**: 89-113
- Pokhrel Y, Felfelani F, Satoh Y, Boulange J, Burek P, Gädeke A, Gerten D, Gosling SN, Grillakis M, Gudmundsson L** (2021) Global terrestrial water storage and drought severity under climate change. *Nature Climate Change* **11**: 226-233
- Rosa M, Prado C, Podazza G, Interdonato R, González JA, Hilal M, Prado FE** (2009) Soluble sugars: Metabolism, sensing and abiotic stress: A complex network in the life of plants. *Plant Signaling & Behavior* **4**: 388-393
- Scalisi A, Morandi B, Inglese P, Bianco RL** (2016) cladode growth dynamics in *Opuntia ficus-indica* under drought. *Environmental and Experimental Botany* **122**: 158–167
- Selinski J, Scheibe R** (2019) Malate valves: old shuttles with new perspectives. *Plant Biology* **21**: 21-30
- Sestili F, Roupael Y, Cardarelli M, Pucci A, Bonini P, Canaguier R, Colla G** (2018) Protein hydrolysate stimulates growth in tomato coupled with N-dependent gene expression involved in N assimilation. *Frontiers in Plant Science* **9**: 1233
- Skopelitis DS, Paranychianakis NV, Paschalidis KA, Pliakonis ED, Delis ID, Yakoumakis DI, Kouvarakis A, Pacladodeakis AK, Stephanou EG,**

- Roubelakis-Angelakis KA** (2006) Abiotic stress generates ROS that signal expression of anionic glutamate dehydrogenases to form glutamate for proline synthesis in tobacco and grapevine. *The Plant Cell* **18**: 2767-2781
- Smith GS, Johnston CM, Cornforth IS** (1983) Comparison of nutrient solutions for growth of plants in sand culture. *New Phytologist* **94**: 537–548
- Sperschneider J, Catanzariti A-M, DeBoer K, Petre B, Gardiner DM, Singh KB, Dodds PN, Taylor JM** (2017) LOCALIZER: subcellular localization prediction of both plant and effector proteins in the plant cell. *Scientific Reports* **7**: 1-14
- Stintzing FC, Carle R** (2005) Cactus stems (*Opuntia* spp.): A review on their chemistry, technology, and uses. *Molecular Nutrition and Food Research* **49**: 175–194
- Sánchez J, Sánchez F, Curt M, Fernández J** (2012) Assessment of the bioethanol potential of prickly pear (*Opuntia ficus-indica* (L.) Mill.) biomass obtained from regular crops in the province of Almeria (SE Spain). *Israel Journal of Plant Sciences* **60**: 301–318
- Taiz L, Zeiger E, Møller IM, Murphy A** (2015) *Plant physiology and development*. Sinauer Associates Incorporated
- Tao X, Fang Y, Huang M-J, Xiao Y, Liu Y, Ma X-R, Zhao H** (2017) High flavonoid accompanied with high starch accumulation triggered by nutrient starvation in bioenergy crop duckweed (*Landoltia punctata*). *BMC Genomics* **18**: 1-14



- Tao X, Fang Y, Xiao Y, Jin Y-l, Ma X-r, Zhao Y, He K-z, Zhao H, Wang H-y** (2013) Comparative transcriptome analysis to investigate the high starch accumulation of duckweed (*Landoltia punctata*) under nutrient starvation. *Biotechnology for biofuels* **6**: 1-15
- Taybi T, Patil S, Chollet R, Cushman JC** (2000) A minimal Ser/Thr protein kinase circadianly regulates phosphoenolpyruvate carboxylase activity in CAM-induced leaves of *Mesembryanthemum crystallinum*. *Plant Physiology* **123**: 1471–1482
- von Caemmerer S, Griffiths H** (2009) Stomatal responses to CO<sub>2</sub> during a diel crassulacean acid metabolism cycle in *Kalanchoe daigremontiana* and *Kalanchoe pinnata*. *Plant Cell and Environment* **32**: 567–576
- Vázquez CG, Sáenz EO, Alvarado RV, García FZ** (2000) Absorción de nitrato y amonio por plantas de nopal en hidroponía. *Terra Latinoamericana* **18**: 133-139
- Wan R, Yang Y, Sun W, Wang Z, Xie S** (2014) Simazine biodegradation and community structures of ammonia-oxidizing microorganisms in bioaugmented soil: impact of ammonia and nitrate nitrogen sources. *Environmental Science and Pollution Research* **21**: 3175-3181
- Wang L, Macko SA** (2011) Constrained preferences in nitrogen uptake across plant species and environments. *Plant, Cell & Environment* **34**: 525-534
- Winter K, Smith JAC** (2021) CAM photosynthesis: the acid test. *New Phytologist* .

**Yang L, Carl S, Lu M, Mayer JA, Cushman JC, Tian E, Lin H (2015)**

Biomass characterization of Agave and Opuntia as potential biofuel feedstocks. *Biomass and Bioenergy* **76**: 43–53

## Chapter 4

# A life cycle inventory of estimated biogas and bioethanol production from an *Opuntia ficus-indica* field trial in the United States

Nicholas A. Niechayev & John C. Cushman

## Abstract

Production of biofuels from *Opuntia spp.* could become a source of energy while having net negative CO<sub>2</sub> emissions. The global warming potential of agricultural production systems can be decreased with production of biogas or bioethanol from *Opuntia ficus-indica*. This study evaluates the production of biogas and bioethanol from *O. ficus-indica* in the United States using data from a previously published 5-year field trial in Logandale, Nevada. Biogas production of 13,004.29-26,877.85 Nm<sup>3</sup> ha<sup>-1</sup> yr<sup>-1</sup> could be produced from plants receiving 716 mm year<sup>-1</sup>, and 4082.46-8,532.19 Nm<sup>3</sup> ha<sup>-1</sup> yr<sup>-1</sup> for plants receiving 300 mm ha<sup>-1</sup> year<sup>-1</sup> with a planting density of 1,418 plant ha<sup>-1</sup>. Bioethanol production of 470.87 and 1783.32 Kg ha<sup>-1</sup> yr<sup>-1</sup> could be produced from plants at the same planting density receiving 300 and 716 mm yr<sup>-1</sup>, respectively. The efficiency and bioenergy yields could easily be advanced if planting density were increased and fertilizer, transport, and harvesting methods were optimized.

## Introduction

*Opuntia ficus-indica* (prickly pear cactus) is grown for the production of edible young cladodes, fruits (López, 1995), cattle feed (Mayer and Cushman, 2019), several secondary products, and most recently, biofuels (Yang et al., 2015). Central Mexico is the center of *Opuntia* spp. diversity (Omar et al., 2021), but it is currently grown in arid, semi-arid, and subtropical locations around the globe. Stem succulence, rectifier like roots, thick epidermal waxes, and utilization of crassulacean acid metabolism photosynthesis, a photosynthetic pathway in which carbon is assimilated at night, all confer an extremely high level of water use-efficiency (Nobel, 2003), while still maintaining competitive whole biomass production values between 2.4 to 47.3 Mg ha<sup>-1</sup> yr<sup>-1</sup> (Monjauze and Le Houérou, 1965; Garcia de Cortazar and Nobel, 1992; Dubeux et al., 2006; Guevara et al., 2011; Ramírez-Arpide et al., 2018; Neupane et al., 2021). Overall, *O. ficus-indica* has a recognized global economic value of \$2,520 million year<sup>-1</sup> globally (Davis et al., 2019).

As a cactus species, *Opuntia ficus-indica* operations can be established in the southwestern United States while requiring minimal water input (Neupane et al., 2021). *O. ficus-indica* can also cause increased CO<sub>2</sub> emissions from detrimental land use changes (Bautista-Cruz et al., 2018). In addition, *O. ficus-indica* could be integrated with photovoltaic systems, where water run-off from cleaning of panels is enough to grow plants (Cushman et al., 2015). A 2.6% (w/v) cellulosic bioethanol conversion of cladode hydrosolates has been achieved (Kuloyo et al., 2014), but a minimal conversion efficiency of 4% (w/v) is considered standard for the success of a crop as a bioethanol source. As a biogas

source, *O. ficus-indica* has been demonstrated to contain 78% volatile solids (Calabrò et al., 2018), and a maximum methane production value of 604 NmL/gVS added (Jigar et al., 2011). The addition of cow manure (Calabrò et al., 2018), and cow rumen fluid (Myovela et al., 2019) have both been shown to increase biogas production from *O. ficus-indica*. In addition, inoculation of microbes found degrading decaying cladodes in the soil of *O. ficu-indica* plantations have been shown to increase cladode digestion, due in part to the excretion of pectinase activity (Blair et al., 2021). Ethanol production from *O. ficus-indica* cladodes or fruits of 2.5 to 34.9 g L<sup>-1</sup> have been reported (Retamal et al., 1987; Kuloyo et al., 2014; de Souza Filho et al., 2016; do Nascimento Santos et al., 2016; Alencar et al., 2018; Pérez-Cadena et al., 2018), and biogas (methane) yields of 233 to 325 L kg<sup>-1</sup> have been reported from the anaerobic digestion of *O. ficus-indica* cladodes (Ramos-Suárez et al., 2014; Mason et al., 2015; Calabrò et al., 2018; Ramírez-Arpide et al., 2018; Valenti et al., 2018; Lueangwattanapong et al., 2020).

A complete life cycle assessment (LCA) and life cycle impact assessment (LCIA) of biogas production from *O. ficus-indica* under conventional farming methods using synthetic fertilizer, and an organic farming method using cow manure was conducted in Queretaro, Mexico (Ramírez-Arpide et al., 2018). The authors found that the organic farming scenario with nopal cladode transport, preprocessing by grinding, and mixing in 3:1 mix with cow manure, followed by anaerobic digestion in a covered lagoon anaerobic digester, and closed storage of the digestate for later use in inoculating the digester had the highest energy return

on investment (amount of energy expended to produce a certain amount of net energy) value of 12.41, which was a 12% increase over the conventional farming base line scenario. In addition, global warming potential (a unit of emission of combined climate warming gases) was reduced by 2.3%. However, soil acidification and eutrophication potentials were increased under the organic farming scenarios. In total, in the organic farming plot, 417,130 Kg ha<sup>-1</sup> yr<sup>-1</sup> of biomass was produced with a planting density of 22,988 plant ha<sup>-1</sup>, resulting in the production of 30,068.88 Mg yr<sup>-1</sup> of biogas.

In 2021, an *Opuntia* spp. field trial was conducted in the Logandale, Nevada to determine optimal irrigation inputs for production (Neupane et al., 2021). Within the irrigation treatments of 300, 407, and 716 mm year<sup>-1</sup> water input resulted in a combined average yield of 8.25, 11.16, and 15.52 Mg dry mass ha<sup>-1</sup> year<sup>-1</sup>, respectively, for three different *Opuntia* spp. (Figure 1). Interestingly, *Opuntia cochinellifera*, which has longer oblong shaped cladodes, had lower occurrence of limb breakage due to wind, and accumulated the highest biomass after five years of growth. However, *Opuntia ficus-indica* was more responsive to water inputs and produced higher quantities of fruit with commercial grade fruit quality.

The objective of this study was to generate a life cycle inventory, as well as estimates of biogas and bioethanol production, using the inputs and data collected in the Logandale field trial. The resulting inventory was then used to make comparisons to the inventory and yields published by Ramírez-Arpide et al., 2018. These results were then used to performed complete life cycle assessment

(LCA) of anaerobic biogas and bioethanol fermentation of *O. ficus-indica* in the United States following the International Organization for Standardization framework (ISO) for direct comparisons against other bioenergy, and alternative fuel sources.

## Methods

In 2021 our lab published the results of a five-year field trial of *Opuntia ficus-indica* in the United States (Neupane et al., 2021). This trial tested the above ground biomass production, fruit yield, and limb breakage in three different *Opuntia* spp. in combined precipitation and irrigation levels of 300 to 716 mm year<sup>-1</sup>. A simple comparative life cycle inventory was constructed using the values from this study (Table 1) following the methods of (Ramírez-Arpide et al., 2018), which provided a full LCA of *O. ficus-indica* biogas production from an operation in Queretaro, Mexico.

The annual productivity of *O. ficus-indica* in the 300 to 716 mm year<sup>-1</sup> was calculated by taking the average biomass gained by *O. ficus-indica* between the 4<sup>th</sup> and 5<sup>th</sup> year (Figure 1) (Neupane et al., 2021) and multiplying it by the planting density, as we considered a coppicing operation in which only the cladodes produced after the 4<sup>th</sup> year of growth were used for biogas and ethanol production. A typical household-sized University of Nevada Cooperative Extension (UNCE) building was next to the field site, and grid electricity use of a typical American household was used (eia.gov). The Overton power district generates 25% of its monthly electricity from hydroelectric power from Hoover

damn (Figure 2). The remaining percent of energy generated from natural gas, coal, solar, and wind energy vary from month to month, but typically more than 50% of the electricity generated is from natural gas. Fuel use was estimated by considering transport of harvested cladodes from the field to a transport truck approximated to be 0.2 km ha<sup>-1</sup> of ten trips up and down rows with a compact tractor (John Deere 1023E, 340 Kg carrying capacity, 14.48 Km/L diesel). The transport truck (GMC C7500 Box Truck, 4535.92 Kg carrying capacity, 4.67 Km/L diesel) was then used to transport harvested material to a theoretical covered lagoon anaerobic digester 50 km away for biogas production (Ramírez-Arpide et al., 2018), or a large-scale bioethanol fermentation plant (Kuloyo et al., 2014). The water inputs were the actual irrigation additions without including precipitation with the addition of supplemental water for inoculation of cladodes under digestion.

Theoretical biogas yield was first calculated by using published percent of volatile carbons in *O. ficus-indica* of 78% (Jigar et al., 2011) of 420 NmL/gVS added from adding the raw substrate alone and a high methane yield 604 NmL/gVS added with an acid pretreatment were used to estimate biogas generated in both low and high irrigation treatments per ha (Calabrò et al., 2018). Remaining effluent was estimated by calculating the percent effluent remaining from the methane generation in Ramírez-Arpide et al., 2018, and applying that percent to our own yields. Lastly, the estimated ethanol yield was calculated from a reported 2.6 % (w/v) (Kuloyo et al., 2014) obtained by fermentation of the *O. ficus-indica* cladode hydrolysate by hydrolysis and fermentation and simultaneous



saccharification and fermentation procedures using *Kluyveromyces marxianus* and *Saccharomyces cerevisiae* at 35 and 40 °C.

## Results

The Logandale field site produced an average biomass gain of approximately 12.77 and 40.23 Kg/plant in the 300 to 716 mm year<sup>-1</sup> respectively, while Ramírez-Arpide et al., 2018 produced about 11.47 Kg/plant (Table 1). The Logandale field trial used about 3.5-fold more fertilizer than the conventional farming system in Ramírez-Arpide et al., 2018. Ramírez-Arpide et al., 2018 used slightly less grid electricity (28,271.1 MJ a<sup>-1</sup>), and Mexico currently generates its electricity from natural gas, geothermal, hydro, nuclear, hard coal, fuel oil, and diesel sources (Figure 3). Ramírez-Arpide et al., 2018 used more water (2.07 Kg yr<sup>-1</sup>) than even our highest irrigation treatment (0.580 Kg ha<sup>-1</sup> yr<sup>-1</sup>), and similar diesel fuel use compared to our estimated value for the 716 mm yr<sup>-1</sup> treatment (222.2 vs. 230 L ha<sup>-1</sup> yr<sup>-1</sup>).

The theoretical yield of biogas from *O. ficus-indica* biomass produced in Neupane et al., 2021 was 13,004.293-26,877.85 Nm<sup>3</sup> ha<sup>-1</sup> yr<sup>-1</sup> for plants receiving 716 mm year<sup>-1</sup>, and 4082.46-8,532.19 Nm<sup>3</sup> ha<sup>-1</sup> yr<sup>-1</sup> for plants receiving 300 mm ha<sup>-1</sup> year<sup>-1</sup> (Table 1). This is more methane production per plant than reported in Ramírez-Arpide et al., 2018 (2.87-18.95 Nm<sup>3</sup> yr<sup>-1</sup> plant<sup>-1</sup> vs. 1.308 Nm<sup>3</sup> yr<sup>-1</sup> plant<sup>-1</sup>), but less methane per hectare than the published 30,068.88 Nm<sup>3</sup> ha<sup>-1</sup> yr<sup>-1</sup> value. Estimated effluent values were 2712.39 and 861.02 Kg ha<sup>-1</sup> yr<sup>-1</sup> for the 300 and 716 mm yr<sup>-1</sup>, respectively. Lastly, estimated ethanol production for the Neupane

et al., 2021 field trial was 470.87 and 1783.32 Kg ha<sup>-1</sup> yr<sup>-1</sup> for the 300 and 716 mm yr<sup>-1</sup>, respectively.

## Discussion

Several key differences were apparent between the Logandale field trial and that performed by Ramírez-Arpide et al., 2018 using a conventional farming system scenario. Mainly, the Logandale trial defined differences in production *vs.* irrigation instead of biogas production. Therefore, about 3.5-fold more nitrogen was applied to the plants to avoid limitations in growth due to nutrient availability. A much lower planting density was also used (22,988 *vs.* 1, 418 plants ha<sup>-1</sup>) to insure that no intraspecific competition among individuals occurred and that no interference among irrigation blocks occurred at the field site. Initial field preparation required two rounds of tilling, a perimeter fence for herbivory prevention, and irrigation lines used for delivery of supplemental irrigation water and monthly all Purpose LiquaFeed<sup>®</sup> fertilizer N:P:K 12:4:8 (Scott's MiracleGro, Inc.). Weeds were controlled by hand weeding instead of herbicides, and no pesticides were used. In comparison, Ramírez-Arpide et al., 2018 site preparation involved initial harrowing and plowing and plants were grown for one year before reaching a productive stage for biomass estimates. Furthermore, dry inorganic fertilizer containing urea, triple superphosphate, and potassium chloride were used and weeds and pests were controlled using atrazin and insecticides (unspecified), respectively.

The measured biomass production per plant in the Logandale field trial was higher than the actual field values reported in Ramírez-Arpide et al., 2018. However, these values would likely be similar if planting density and fertilizer inputs were the same (Guimarães et al., 2020). Percentage of volatile carbons and methane production increased when a 3:1 mixture of *O. ficus-indica* with cow manure was used (Jigar et al., 2011). This finding is convenient when considering that *O. ficus-indica* makes for an excellent source of cattle fodder when combined with other feedstocks (Mayer and Cushman, 2019). Therefore, *O. ficus-indica* production and cattle ranching can be combined successfully into a single production system.

Field emissions from the soil were not measured in Neupane et al., 2021. The use of synthetic fertilizers in *O. ficus-indica* were shown to produce net negative methane emissions ( $-1,314.6 \text{ gCH}_4 \text{ ha}^{-1} \text{ a}^{-1}$ ), but more  $\text{N}_2\text{O}$  emissions ( $636 \text{ gN}_2\text{O ha}^{-1} \text{ yr}^{-1}$ ) in the Ramírez-Arpide et al., 2018 trial compared to the organic scenario. The organic scenario in the same field used cow manure for fertilizer, producing a substantial amount of released methane ( $661.5 \text{ g CH}_4 \text{ ha}^{-1} \text{ yr}^{-1}$ ), but less  $\text{N}_2\text{O}$  ( $375.85 \text{ gCH}_4 \text{ ha}^{-1} \text{ yr}^{-1}$ ). Using fertigation to directly apply fertilizer in irrigation lines has also been shown to reduce  $\text{N}_2\text{O}$  emissions compared to granular urea application in *Triticum aestivum* (wheat) and *Brassica napus* (canolla) (Chai et al., 2020), *Lycopersicon esculentum* (tomatoes) (Kennedy et al., 2013), and *Zea mays* (maize) (Tian et al., 2017). As such, the use of fertigation likely did not produce methane emissions, while also reducing  $\text{N}_2\text{O}$  emissions than if granular urea been applied instead.

The Logandale field trial benefitted from having information available on grid electricity sources on a local level from the Overton Power District (opd5.com) (Figure 2), whereas Ramírez-Arpide et al., 2018 used grid electricity sources from the whole country (Figure 3) (Itten et al., 2012). The majority of grid electricity from both operations was sourced from natural gas, which generates about 66 gCO<sub>2</sub>/MJ in the United States (Venkatesh et al., 2011). Hydroelectricity makes up 25% of the grid electricity each month due to close proximity to Hoover dam. Hydroelectric power generates an estimated 23.6 gCO<sub>2</sub>/MJ and 3.0 gCH<sub>4</sub>/MJ as the flow of water is slowed, and organic matter builds up and degrades anerobically (Hertwich, 2013). Solar and wind electricity generation vary from month to month, and must be supplemented by natural during periods when renewable energy production is limited. Southern Nevada recieves a high amount of solar radiation, and a minimum of 9.7 gCO<sub>2</sub>/MJ can be achieved with solar panels (Liu et al., 2015). Advancement of battery technology has also helped to increase the efficiency of wind generation, and 5 gCO<sub>2</sub>/kWh can be achieved with wind power (Alsaleh and Sattler, 2019). Electricity generated in Overton power district most certainly coresponded with less CO<sub>2</sub> emissions than the Mexican power grid (Figure 3) as it uses nuclear (3.3 gCO<sub>2</sub>/MJ), hard coal (303.8 gCO<sub>2</sub>/MJ), fuel oil (267 gCO<sub>2</sub>/MJ) (Santoyo-Castelazo et al., 2011), and diesel in addition to natural gas, wind, and hydroelectricity.

Estimated diesel used for tranportation was higher at the Logandale field site, and the efficiency could have been improved by using a tractor with a larger

carrying capacity although the compact tractor was convenient for navigating narrow rows for research purposes. The CO<sub>2</sub> emissions from the transport truck could be mitigated by primarily using rail ways for transport of cladodes to a centralized digester, as rail transport has the lowest associated CO<sub>2</sub> emissions (Horvath, 2006), although this would require strategic planning of location along a rail line. Current battery powered trucks are a promising form of transportation in regards to CO<sub>2</sub> emissions, but do not significantly improve life-cycle emissions or costs compared to diesel without generating all the energy for operation and manufacturing with biofuels (Sen et al., 2017).

Both the life cycle inventory created here and in Ramírez-Arpide et al., 2018 did not consider the impact of human labor as an input, and including human labor has been shown to have about a 10.2% increase in embodied energy cost estimates in agricultural production pathways (Rocco and Colombo, 2016). In addition, human labor costs are much cheaper in Mexico (Roka and Guan, 2018) and would likely be a major barrier in the competitive biofuel production of *O. ficus-indica* in the United States. As a solution, mechanization of *O. ficus-indica* harvesting for biofuel generation is conceivable with typical farm equipment where the entire above ground biomass is harvested, but specialized machinery would be needed for the coppicing operations outlined here.

In conclusion, these life cycle inventory estimates indicate that theoretical biogas production from *O. ficus-indica* in Logandale, Nevada is comparable to that of actual biogas production values in Mexico, but without the use of herbicides or pesticides. *O. ficus-indica* agriculture, in combination with other

renewable energy sources, could help the United States meet demands for energy sources with reduced net CO<sub>2</sub> emissions. The next step of this study is to follow the methods of Ramírez-Arpide et al., 2018, in creating a complete LCA of *O. ficus-indica* following ISO guidelines (ISO), using OpenLCA software (GreenDelta, 2017), or a similar software (Silva et al., 2017), and the ecoinvent database (Wernet et al., 2016).

## Tables

**Table 1:** A life cycle inventory (LCI) for *Opuntia ficus-indica* grown in an irrigation treatment in Logandale, NV, United States (Neupane et al., 2021).

Parameter	Units	Quantity
<b>Productivity</b>		
Planting Density	Plants ha <sup>-1</sup>	1,418
High Irrigation <i>Ofi</i> productivity (716 mm yr <sup>-1</sup> )	Kg d.w. ha <sup>-1</sup> yr <sup>-1</sup>	57,050
Low Irrigation <i>Ofi</i> productivity (300 mm yr <sup>-1</sup> )	Kg d.w. ha <sup>-1</sup> yr <sup>-1</sup>	18,110
High Irrigation <i>Ofi</i> productivity (716 mm yr <sup>-1</sup> )	Kg f.w. ha <sup>-1</sup> yr <sup>-1</sup>	298848
Low Irrigation <i>Ofi</i> productivity (300 mm yr <sup>-1</sup> )	Kg f.w. ha <sup>-1</sup> yr <sup>-1</sup>	221534
<b>Inputs</b>		
Urea	Kg ha <sup>-1</sup> yr <sup>-1</sup>	875.75
P <sub>2</sub> O <sub>5</sub>	Kg ha <sup>-1</sup> yr <sup>-1</sup>	291.91
K <sub>2</sub> O	Kg ha <sup>-1</sup> yr <sup>-1</sup>	583.83
Mn	Kg ha <sup>-1</sup> yr <sup>-1</sup>	3.65
Chelated Mn	Kg ha <sup>-1</sup> yr <sup>-1</sup>	3.65
Zn	Kg ha <sup>-1</sup> yr <sup>-1</sup>	3.65
Chelated Zn	Kg ha <sup>-1</sup> yr <sup>-1</sup>	3.65
Grid Electricity	MJ ha <sup>-1</sup> yr <sup>-1</sup>	38,574 (Average household eia.gov)
Diesel (716 mm yr <sup>-1</sup> )	L ha <sup>-1</sup> yr <sup>-1</sup>	230
Diesel (300 mm yr <sup>-1</sup> )	L ha <sup>-1</sup> yr <sup>-1</sup>	170
Water (716 mm yr <sup>-1</sup> )	mm ha <sup>-1</sup> yr <sup>-1</sup>	580
Water (300 mm yr <sup>-1</sup> )	mm ha <sup>-1</sup> yr <sup>-1</sup>	164

<b>Theoretical Yield</b>		
Biogas (716 mm yr <sup>-1</sup> )	Nm <sup>3</sup> ha <sup>-1</sup> yr <sup>-1</sup>	1,300-26,877 (Calabrò et al., 2018; Jigar et al., 2011)
Biogas (300 mm yr <sup>-1</sup> )	Nm <sup>3</sup> ha <sup>-1</sup> yr <sup>-1</sup>	4082-8,532 (Calabrò et al., 2018; Jigar et al., 2011)
Effluent (716 mm yr <sup>-1</sup> )	Kg ha <sup>-1</sup> yr <sup>-1</sup>	2712 (Ramírez-Arpide et al., 2018)
Effluent (300 mm yr <sup>-1</sup> )	Kg ha <sup>-1</sup> yr <sup>-1</sup>	861 (Ramírez-Arpide et al., 2018)
Ethanol (716 mm yr <sup>-1</sup> )	Kg ha <sup>-1</sup> yr <sup>-1</sup>	1483 (Kuloyo et al., 2014)
Ethanol (300 mm yr <sup>-1</sup> )	Kg ha <sup>-1</sup> yr <sup>-1</sup>	470.87 (Kuloyo et al., 2014)



## Figures

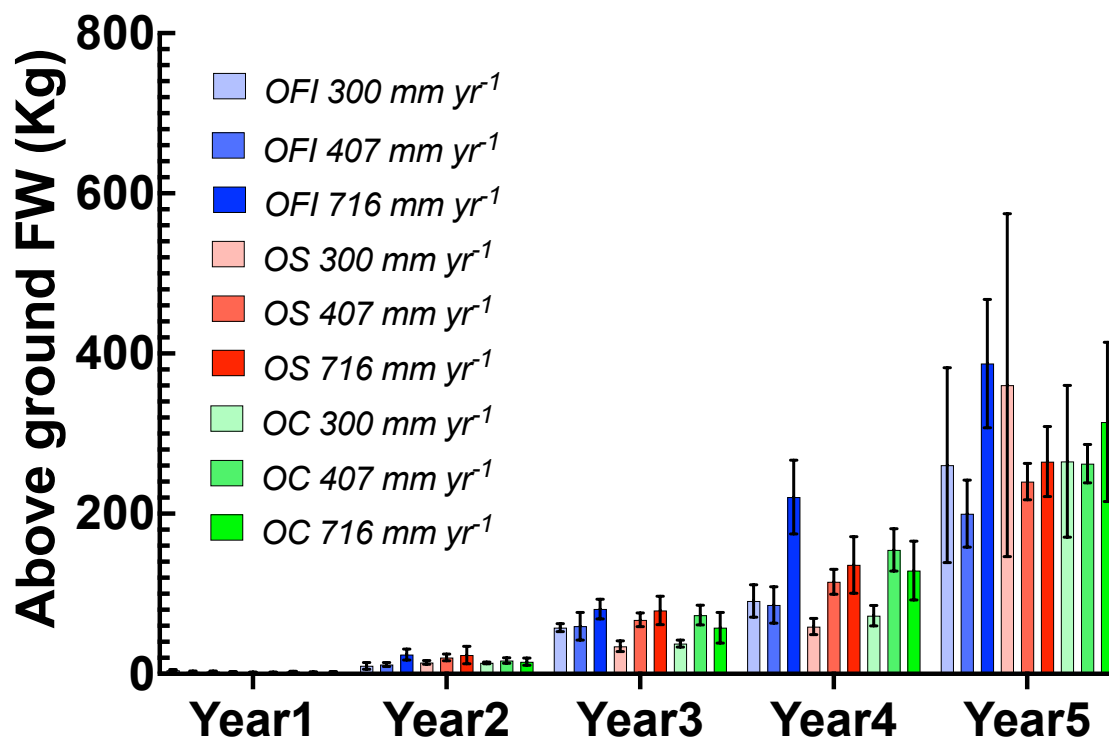


**Figure 1:** *Opuntia spp.* above ground fresh weight (FW) productivity under varying irrigation inputs over 5 years in Logandale, Nevada. Bars represent the average above ground FW biomass (Kg) of cladodes *Opuntia ficus-indica* (OFI: light blue, blue, dark blue), *Opuntia streptacantha* (OS: light red, red, dark red), and *Opuntia cochenillifera* (OC: light green, green, dark green). Error bars represent standard error ( $n = 4$ ). Data sourced from Neupane et al. 2021.

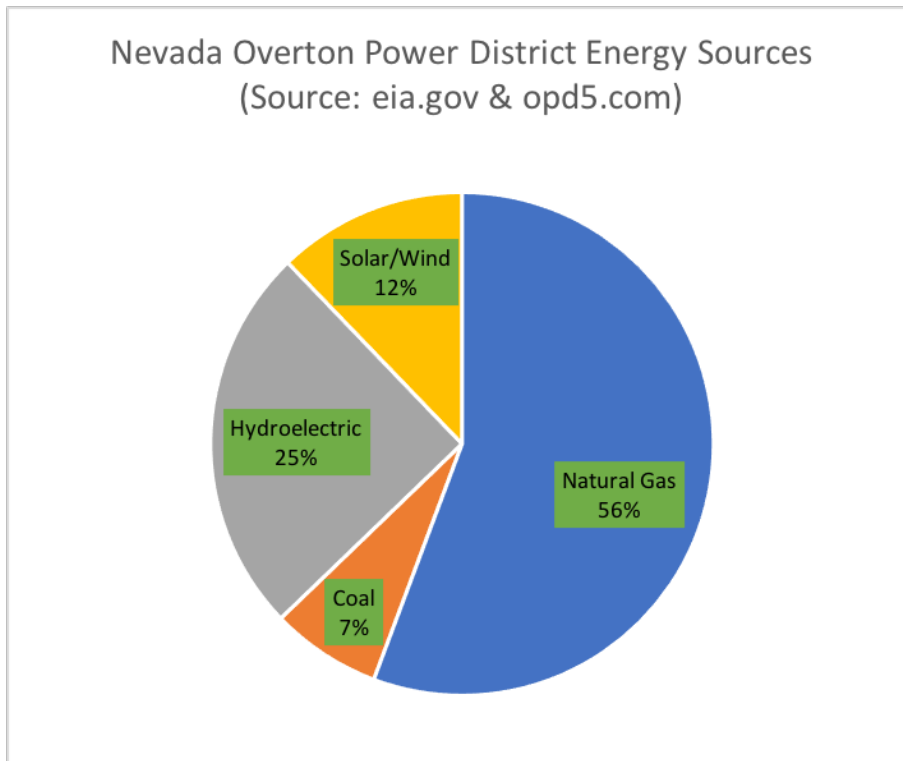


**Figure 2:** Nevada Overton power district energy source break down. (source: eia.gov and opd5.com)

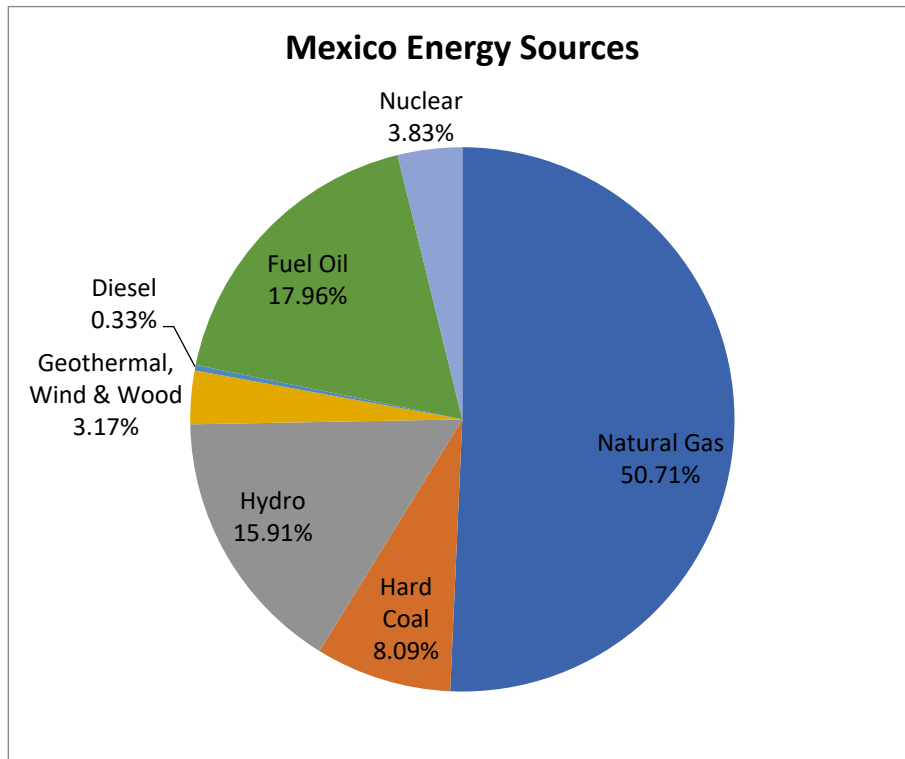


**Figure 3:** Contribution of different fuels to the electricity mix in Mexico. Figure adapted from Ramírez-Arpide et al., 2018

## References

- Alencar BR, Dutra ED, Sampaio EV, Menezes RS, Morais JMA (2018)**  
Enzymatic hydrolysis of cactus pear varieties with high solids loading for bioethanol production. *Bioresource Technology* **250**: 273–280
- Alsaleh A, Sattler M (2019)** Comprehensive life cycle assessment of large wind turbines in the US. *Clean Technologies and Environmental Policy* **21**: 887-903
- Bautista-Cruz A, Leyva-Pablo T, de León-González F, Zornoza R, Martínez-Gallegos V, Fuentes-Ponce M, Rodríguez-Sánchez L (2018)** Cultivation of *Opuntia ficus-indica* under different soil management practices: A possible sustainable agricultural system to promote soil carbon sequestration and increase soil microbial biomass and activity. *Land Degradation & Development* **29**: 38–46
- Blair BB, Yim WC, Cushman JC (2021)** Characterization of a microbial consortium with potential for biological degradation of cactus pear biomass for biofuel. *Heliyon* **7**: e07854
- Calabrò PS, Catalán E, Folino A, Sánchez A, Komilis D (2018)** Effect of three pretreatment techniques on the chemical composition and on the methane yields of *Opuntia ficus-indica* (prickly pear) biomass. *Waste Management & Research* **36**: 17–29
- Chai LL, Hernandez-Ramirez G, Dyck M, Pauly D, Kryzanowski L, Middleton A, Powers L-A, Lohstraeter G, Werk D (2020)** Can

fertigation reduce nitrous oxide emissions from wheat and canola fields?

Science of the Total Environment **745**: 141014

**Cushman JC, Davis SC, Yang X, Borland AM** (2015) Development and use of bioenergy feedstocks for semi-arid and arid lands. Journal of Experimental Botany **66**: 4177–4193

**Davis SC, Simpson J, Vega G, Del Carmen K, Niechayev NA, Tongerlo EV, Castano NH, Dever LV, Búrque A** (2019) Undervalued potential of crassulacean acid metabolism for current and future agricultural production. Journal of Experimental Botany **70**: 6521–6537

**de Souza Filho PF, Ribeiro VT, dos Santos ES, de Macedo GR** (2016) Simultaneous saccharification and fermentation of cactus pear biomass—evaluation of using different pretreatments. Industrial Crops and Products **89**: 425–433

**do Nascimento Santos T, Dutra ED, do Prado AG, Leite FC, de Souza RD, dos Santos DC, de Abreu CA, Simões DA, de Moraes JMA, Menezes RS** (2016) Potential for biofuels from the biomass of prickly pear cladodes: Challenges for bioethanol and biogas production in dry areas. Biomass and Bioenergy **85**: 215–222

**Dubeux JJCB, Ferreira dos Santos MVF, de Andrade Lira M, Coreiro dos Santos D, Farias I, Lima LE, Ferreira RLC** (2006) Productivity of *Opuntia ficus-indica* (L.) Miller under different N and P fertilization and plant population in north-east Brazil. Journal of Arid Environments **67**: 357–372

- Garcia de Cortazar V, Nobel P** (1992) Biomass and fruit production for the prickly pear cactus *Opuntia ficus-indica*. Journal of the American Society for Horticultural Science **117**: 568–562
- Guevara JC, Felker P, Balzarini MG, Páez SA, Estevez OR, Paez MN, Antúnez JC** (2011) Productivity, cold hardiness and forage quality of spineless progeny of the *Opuntia ficus-indica* 1281 x *O. lindheimerii* 1250 cross in Mendoza plain, Argentina. Journal of Professional Association for Cactus Development **13**: 48–62
- Guimarães BVC, Donato SLR, Aspiazú I, Azevedo AM, de Carvalho AJ** (2020) Optimal plot size for experimental trials with *Opuntia* cactus pear. Acta Scientiarum. Technology **42**: e42579-e42579
- Hertwich EG** (2013) Addressing biogenic greenhouse gas emissions from hydropower in LCA. Environmental science & technology **47**: 9604-9611
- Horvath A** (2006) Environmental Assessment of Freight Transportation in the US (11 pp). The International Journal of Life Cycle Assessment **11**: 229-239
- ISO T 207** (2006) ISO 14040: 2006 environmental management—life cycle assessment—principles and framework. ISO, Switzerland
- Itten R, Frischknecht R, Stucki M, Scherrer P, Psi I** (2012) Life cycle inventories of electricity mixes and grid.
- Jigar E, Sulaiman H, Asfaw A, Bairu A** (2011) Study on renewable biogas energy production from cladodes of *Opuntia ficus indica*. ISABB Journal of Food and Agricultural Sciences **1**: 44-48

- Kennedy TL, Suddick EC, Six J** (2013) Reduced nitrous oxide emissions and increased yields in California tomato cropping systems under drip irrigation and fertigation. *Agriculture, Ecosystems & Environment* **170**: 16-27
- Kuloyo OO, du Preez JC, del Prado García-Aparicio M, Kilian SG, Steyn L, Görgens J** (2014) *Opuntia ficus-indica* cladodes as feedstock for ethanol production by *Kluyveromyces marxianus* and *Saccharomyces cerevisiae*. *World Journal of Microbiology and Biotechnology* **30**: 3173–3183
- Liu X, Hoekman SK, Robbins C, Ross P** (2015) Life cycle climate impacts and economic performance of commercial-scale solar PV systems: A study of PV systems at Nevada's Desert Research Institute (DRI). *Solar Energy* **119**: 561-572
- Lueangwattanapong K, Ammam F, Mason PM, Whitehead C, McQueen-Mason SJ, Gomez LD, Smith J, Thompson IP** (2020) Anaerobic digestion of Crassulacean Acid Metabolism plants: exploring alternative feedstocks for semi-arid lands. *Bioresource Technology* **297**: 122262
- López AD** (1995) Use of the fruits and stems of the prickly pear cactus (*Opuntia spp.*) into human food. *Food Science and Technology International* **1**: 65-74
- Mason PM, Glover K, Smith JAC, Willis KJ, Woods J, Thompson IP** (2015) The potential of CAM crops as a globally significant bioenergy resource: moving from 'fuel or food' to 'fuel and more food'. *Energy and Environmental Science* **8**: 2320–2329

- Mayer JA, Cushman JC** (2019) Nutritional and mineral content of prickly pear cactus: A highly water-use efficient forage, fodder and food species. *Journal of Agronomy and Crop Science* **205**: 625–634
- Monjauze A, Le Houérou HN** (1965) Le rôle des *Opuntia* dans l'économie agricole nord-africaine. *Bulletin de l'Ecole Nationale Supérieure d'Agronomie de Tunis* **8–9**: 8–164
- Myovela H, Mshandete AM, Imathiu S** (2019) Enhancement of anaerobic batch digestion of spineless cacti (*Opuntia ficus indica*) feedstock by aerobic pre-treatment. *African Journal of Biotechnology* **18**: 12–22
- Neupane D, Mayer JA, Niechayev NA, Bishop CD, Cushman JC** (2021) Five-year field trial of the biomass productivity and irrigation response of prickly pear cactus (*Opuntia* spp.) as a bioenergy feedstock for arid lands. *Global Change Biology: Bioenergy* **13**: 719–741
- Nobel PS** (2003) *Environmental biology of agaves and cacti*. Cambridge University Press
- Omar AA, ElSayed AI, Mohamed AH** (2021) Genetic Diversity and Ecotypes of *Opuntia* spp. In *Opuntia* spp.: Chemistry, Bioactivity and Industrial Applications. Springer, pp 181-199
- Pérez-Cadena R, Espinosa Solares T, Medina-Moreno SA, Martínez A, Lizardi-Jiménez MA, Téllez-Jurado A** (2018) Production of ethanol by three yeasts in defined media and hydrolyzed cladodes of *Opuntia ficus-indica* var. *Atlixco*. *International Journal of Agriculture and Forestry* **8**: 26–34



- Ramos-Suárez JL, Martínez A, Carreras N** (2014) Optimization of the digestion process of *Scenedesmus* sp. and *Opuntia maxima* for biogas production. *Energy Conversion and Management* **88**: 1263–1270
- Ramírez-Arpide FR, Demirer GN, Gallegos-Vázquez C, Hernández-Eugenio G, Santoy-Cortés VH, Espinosa-Solares T** (2018) Life cycle assessment of biogas production through anaerobic co-digestion of nopal cladodes and dairy cow manure. *Journal of Cleaner Production* **172**: 2313–2322
- Ramírez-Arpide FR, Demirer GN, Gallegos-Vázquez C, Hernández-Eugenio G, Santoyo-Cortés VH, Espinosa-Solares T** (2018) Life cycle assessment of biogas production through anaerobic co-digestion of nopal cladodes and dairy cow manure. *Journal of Cleaner Production* **172**: 2313-2322
- Retamal N, Duran JM, Fernandez J** (1987) Ethanol production by fermentation of fruits and cladodes of prickly pear cactus (*Opuntia ficus-indica* (L.) Miller). *Journal of the Science of Food and Agriculture* **40**: 213–218
- Rocco MV, Colombo E** (2016) Internalization of human labor in embodied energy analysis: Definition and application of a novel approach based on Environmentally extended Input-Output analysis. *Applied Energy* **182**: 590-601
- Roka FM, Guan Z** (2018) Farm labor management trends in Florida, USA-challenges and opportunities. *International Journal of Agricultural Management* **7**: 1-9

- Santoyo-Castelazo E, Gujba H, Azapagic A** (2011) Life cycle assessment of electricity generation in Mexico. *Energy* **36**: 1488-1499
- Sen B, Ercan T, Tatari O** (2017) Does a battery-electric truck make a difference?—Life cycle emissions, costs, and externality analysis of alternative fuel-powered Class 8 heavy-duty trucks in the United States. *Journal of cleaner production* **141**: 110-121
- Silva D, Nunes AO, da Silva Moris A, Moro C, Piekarski TOR** (2017) How important is the LCA software tool you choose Comparative results from GaBi, openLCA, SimaPro and Umberto. *In Proceedings of the VII Conferencia Internacional de Análisis de Ciclo de Vida en Latinoamérica, Medellin, Colombia, pp 10-15*
- Tian D, Zhang Y, Zhou Y, Mu Y, Liu J, Zhang C, Liu P** (2017) Effect of nitrification inhibitors on mitigating N<sub>2</sub>O and NO emissions from an agricultural field under drip fertigation in the North China Plain. *Science of the Total Environment* **598**: 87-96
- Valenti F, Porto SMC, Selvaggi R, Pecorino B** (2018) Evaluation of biomethane potential from by-products and agricultural residues co-digestion in southern Italy. *Journal of Environmental Management* **223**: 834–840
- Venkatesh A, Jaramillo P, Griffin WM, Matthews HS** (2011) Uncertainty in life cycle greenhouse gas emissions from United States natural gas end-uses and its effects on policy. *Environmental Science & Technology* **45**: 8182-8189

**Wernet G, Bauer C, Steubing B, Reinhard J, Moreno-Ruiz E, Weidema B**

(2016) The ecoinvent database version 3 (part I): overview and methodology. *The International Journal of Life Cycle Assessment* **21**: 1218-1230

**Yang L, Carl S, Lu M, Mayer JA, Cushman JC, Tian E, Lin H (2015)**

Biomass characterization of *Agave* and *Opuntia* as potential biofuel feedstocks. *Biomass and Bioenergy* **76**: 43–53

## Chapter 5

### Concluding Remarks

Of the three photosynthetic pathways, CAM confers the highest water-use efficiency (Borland et al., 2009), and often occurs with several co-adapted traits that enhance tolerances to other types of abiotic stress (Niechayev et al., 2019). As a desert-adapted species, *Opuntia ficus-indica* is an obligate CAM species with a remarkable growth rate, tasty fruits, vegetable like young cladodes, cosmetic seed oil, and provides feed for livestock, and shows comparatively high biogas production values (Lueangwattanapong et al., 2020). In a drying world with ever decreasing ground water stores (Naumann et al., 2018), *O. ficus-indica* and other economically important CAM species (Davis et al., 2019) may prove to be vital in maintaining food, energy, and economic security in regions that regularly experience drought. In chapter 2 young tissues in *O. ficus-indica* were shown to use CAM early in development; in chapter 3 plant growth, biochemistry, and N and CAM gene expression is affected by variation in N source; and in chapter 4 potential biofuel production from *O. ficus-indica* in the United States was estimated.

In chapter 2, *O. ficus-indica* seedlings were shown to use CAM photosynthesis early in development, even under well-watered conditions. Seedlings also continued to use CAM photosynthesis to fix CO<sub>2</sub> even when the soil was completely dried out. These findings demonstrated that C<sub>3</sub> photosynthesis does not play a major role in seedling development. However, some daytime fixation of CO<sub>2</sub> does occur at dawn and dusk, especially when light

intensity was increased. In contrast, *O. eliator* (Winter and Holtum, 2011), a tropical epiphyte species was shown to perform C<sub>3</sub> photosynthesis early on with none of the defined CAM phases, and fix CO<sub>2</sub> predominantly during the light period unless under drought conditions. Collectively, these findings demonstrate that the diversity in photosynthetic plasticity in the *Opuntia* genus with tropical species exhibiting more facultative CAM, and xeric species showing more obligate CAM.

*O. ficus-indica* daughter cladodes had previously been demonstrated to act as sink tissues before beginning in CAM photosynthesis (Wang et al., 1998). Our results corroborated these findings, as the isotopic ratios were indicative of typical CAM fixation no matter what size the cladodes were, nocturnal tissue acidity began to build-up early on, and CO<sub>2</sub> assimilation occurred primarily during the dark period. However, this was in contrast with the results of (Winter et al., 2008) who measured higher net CO<sub>2</sub> assimilation during the light period. The same results were observed when *O. ficus-indica* cladodes were measured under optimal conditions in a growth chamber instead of in a greenhouse. Higher daytime net CO<sub>2</sub> assimilation observed in the growth chamber is likely due to constant light conditions that cause a higher fixation of CO<sub>2</sub> before the lights turn off, and after they turn on vs. the greenhouse in which the sun gradually sets and rises, limiting the amount of CO<sub>2</sub> assimilation during twilight. The greenhouse conditions may better represent how *O. ficus-indica* assimilates CO<sub>2</sub> in the field.

In chapter 3, under varying nitrate and ammonia concentrations in sand culture, statistically significant differences in *O. ficus-indica* growth, chlorophyll

content, tissue acidity, soluble sugars, nitrate reductase activity, nitrate and ammonia content, glyoxylic acid content, N:C ratio and relative expression of genes involved N metabolism, and CAM activity were measured. Our deionized water treatment demonstrated that when nutrients are limited growth is hindered, tissue acidity, and starch content is increased, and soluble sugars are no longer present. Within deionized water treatment, cladodes also showed increased steady-state mRNA expression of the CAM-related genes encoding aluminum-activated malate transporter (ALMT) and phosphoenolpyruvate carboxylase (PEPC) and higher steady-state mRNA expression of the nitrogen metabolism-related genes including glutamine oxoglutarate aminotransferase (Fd-GOGAT), glutamate dehydrogenase (NADH-GDH460), glutamine synthetase 2 (GS2), but lower expression of asparagine synthetase (AS) than nutrient supplied cladodes. Altogether, these results suggest that when nutrients are limited, *Opuntia ficus-indica* converts soluble sugars into starch, builds up stored organic acids, and enhances expression of CAM-related genes.

In general, the responses in growth, biochemistry, and gene expression reflected that growth and metabolism were enhanced when more nitrogen was present regardless of whether *O. ficus-indica* was given nitrate or ammonium. (Vázquez et al., 2000) et al. supported this evidence as *O. ficus-indica* cladodes were shown to take up N regardless of being given only nitrate or ammonia, and only had slight increases in N uptake when given ammonium alone. *O. ficus-indica* field operations can be successful with either nitrate (Nerd and Nobel, 1995), ammonium (Nkoi et al., 2021), or urea (Galizzi et al., 2004), as long as soil

pH is kept balanced with N application. In retrospect, it would have been useful to collect samples at multiple timepoints with variation in nitrate and ammonium, although our sample size was already cumbersome for a single timepoint (~112 samples \* 34 independent variables measured). Therefore, repeating the experiment with fewer nitrate and ammonia treatments and/or singling out desired measurements from our methodology, and adding more time points might reveal trends overtime in relation to diversity of N source.

In Chapter 4, beginnings of a life cycle assessment for biogas and bioethanol production from *O. ficus-indica* field trial in the United States (Neupane et al., 2021) was presented in the form of a life cycle inventory. Our inventory mirrored that of a complete life cycle assessment from an *O. ficus-indica* trial in Mexico (Ramírez-Arpide et al., 2018) in order to have the ability to make comparisons between the two trials. Clearly, the United States irrigation trial was not designed with biogas generation in mind, and therefore, had a much higher application of fertilizer, and space between plants. Having plants in optimal nutrient and spacing conditions resulted in higher yields on a per plant basis, but the higher planting density in the Mexican trial resulted in higher overall yield.

Several advantages became apparent when comparing an operation in the United States vs. Mexico. First, being that grid electricity in Southern Nevada is typically produced with more renewable energy sources and less carbon emissions than that of Mexico. Second, the Logandale field trial, herbicides and insecticides were not needed. Both of these advantages would decrease the net carbon release

associated with biogas production from *O. ficus-indica* in the United States. Appearance of *Cactoblastis* (Zimmermann et al., 2004) or *Cochineal* (Moran and Cabby, 1979; Viguera et al., 2007) pests could conceivably happen at any time and require insecticides to be used. *Cochineal* is a problem in our ongoing field trials in Parlier, CA. As a disadvantage, field labor in the United States is much more expensive than Mexico, and competitive unit biogas production per dollar from *O. ficus-indica* would likely require mechanized harvesting.

## Conclusion

*Opuntia ficus-indica* is a highly productive CAM species that can improve food, feed, and fuel security in drought prone regions. As a drought adapted species it predominantly uses CAM throughout development. In regard to N source preferences, *O. ficus-indica* grows slightly better when given slightly more nitrate than ammonium. Finally, estimated biofuel production from *O. ficus-indica* in the United States is comparable to that of actual yields in Mexico, and biogas production from *O. ficus-indica* could be used to produce biofuels with minimal CO<sub>2</sub> emissions associated with land use changes or effects on current food supply.



## References

- Borland AM, Griffiths H, Hartwell J, Smith JAC** (2009) Exploiting the potential of plants with crassulacean acid metabolism for bioenergy production on marginal lands. *Journal of Experimental Botany* **60**: 2879–2896
- Davis SC, Simpson J, Vega G, Del Carmen K, Niechayev NA, Tongerlo EV, Castano NH, Dever LV, Búrque A** (2019) Undervalued potential of crassulacean acid metabolism for current and future agricultural production. *Journal of Experimental Botany* **70**: 6521–6537
- Galizzi FA, Felker P, González C, Gardiner D** (2004) Correlations between soil and cladode nutrient concentrations and fruit yield and quality in cactus pears, *Opuntia ficus-indica* in a traditional farm setting in Argentina. *Journal of Arid Environments* **59**: 115–132
- Lueangwattanapong K, Ammam F, Mason PM, Whitehead C, McQueen-Mason SJ, Gomez LD, Smith JA, Thompson IP** (2020) Anaerobic digestion of Crassulacean Acid Metabolism plants: exploring alternative feedstocks for semi-arid lands. *Bioresource Technology* **297**: 122262
- Moran V, Cabby B** (1979) On the life-history and fecundity of the cochineal insect, *Dactylopius austrinus* De Lotto (Homoptera: Dactylopiidae), a biological control agent for the cactus *Opuntia awantiaca*. *Bulletin of Entomological Research* **69**: 629-636

- Naumann G, Alfieri L, Wyser K, Mentaschi L, Betts RA, Carrao H, Spinoni J, Vogt J, Feyen L** (2018) Global changes in drought conditions under different levels of warming. *Geophysical Research Letters* **45**: 3285–3296
- Nerd A, Nobel PS** (1995) Accumulation, partitioning, and assimilation of nitrate in *Opuntia ficus-indica*. *Journal of Plant Nutrition* **18**: 2533-2549
- Neupane D, Mayer JA, Niechayev NA, Bishop CD, Cushman JC** (2021) Five-year field trial of the biomass productivity and irrigation response of prickly pear cactus (*Opuntia spp.*) as a bioenergy feedstock for arid lands. *Global Change Biology: Bioenergy* **13**: 719–741
- Niechayev NA, Pereira PN, Cushman JC** (2019) Understanding trait diversity associated with crassulacean acid metabolism (CAM). *Current Opinion in Plant Biology* **49**: 74–85
- Nkoi V, Wit Md, Fouche H, Coetzer G, Hugo A** (2021) The Effect of Nitrogen Fertilization on the Yield, Quality and Fatty Acid Composition of *Opuntia ficus-indica* Seed Oil. *Sustainability* **13**: 10123
- Ramírez-Arpide FR, Demirer GN, Gallegos-Vázquez C, Hernández-Eugenio G, Santoy-Cortés VH, Espinosa-Solares T** (2018) Life cycle assessment of biogas production through anaerobic co-digestion of nopal cladodes and dairy cow manure. *Journal of Cleaner Production* **172**: 2313–2322
- Vigueras A, Cibrian-Tovar J, Pelayo-Ortiz C** (2007) Use of botanicals extracts to control wild cochineal (*Dactylopius opuntiae* Cockerell) on cactus pear. *In VI International Congress on Cactus Pear and Cochineal* 811, pp 229-234

- Vázquez CG, Sáenz EO, Alvarado RV, García FZ** (2000) Absorción de nitrato y amonio por plantas de nopal en hidroponía. *Terra Latinoamericana* **18**: 133-139
- Wang N, Zhang H, Nobel PS** (1998) Carbon flow and carbohydrate metabolism during sink-to-source transition for developing cladodes of *Opuntia ficus-indica*. *Journal of Experimental Botany* **49**: 1835-1843
- Winter K, Garcia M, Holtum JAM** (2008) On the nature of facultative and constitutive CAM: environmental and developmental control of CAM expression during early growth of *Clusia*, *Kalanchoë*, and *Opuntia*. *Journal of Experimental Botany* **59**: 1829–1840
- Winter K, Holtum JAM** (2011) Drought-stress-induced up-regulation of CAM in seedlings of a tropical cactus, *Opuntia elatior*, operating predominantly in the C3 mode. *Journal of Experimental Botany* **62**: 4037–4042
- Zimmermann H, Bloem S, Klein H** (2004) Biology, history, threat, surveillance and control of the cactus moth, *Cactoblastis cactorum*. Food and Agriculture Organization of the United Nations (FAO).

Supplemental figures for chapter 2

## Seedling 1 - PAR 100 - Watered

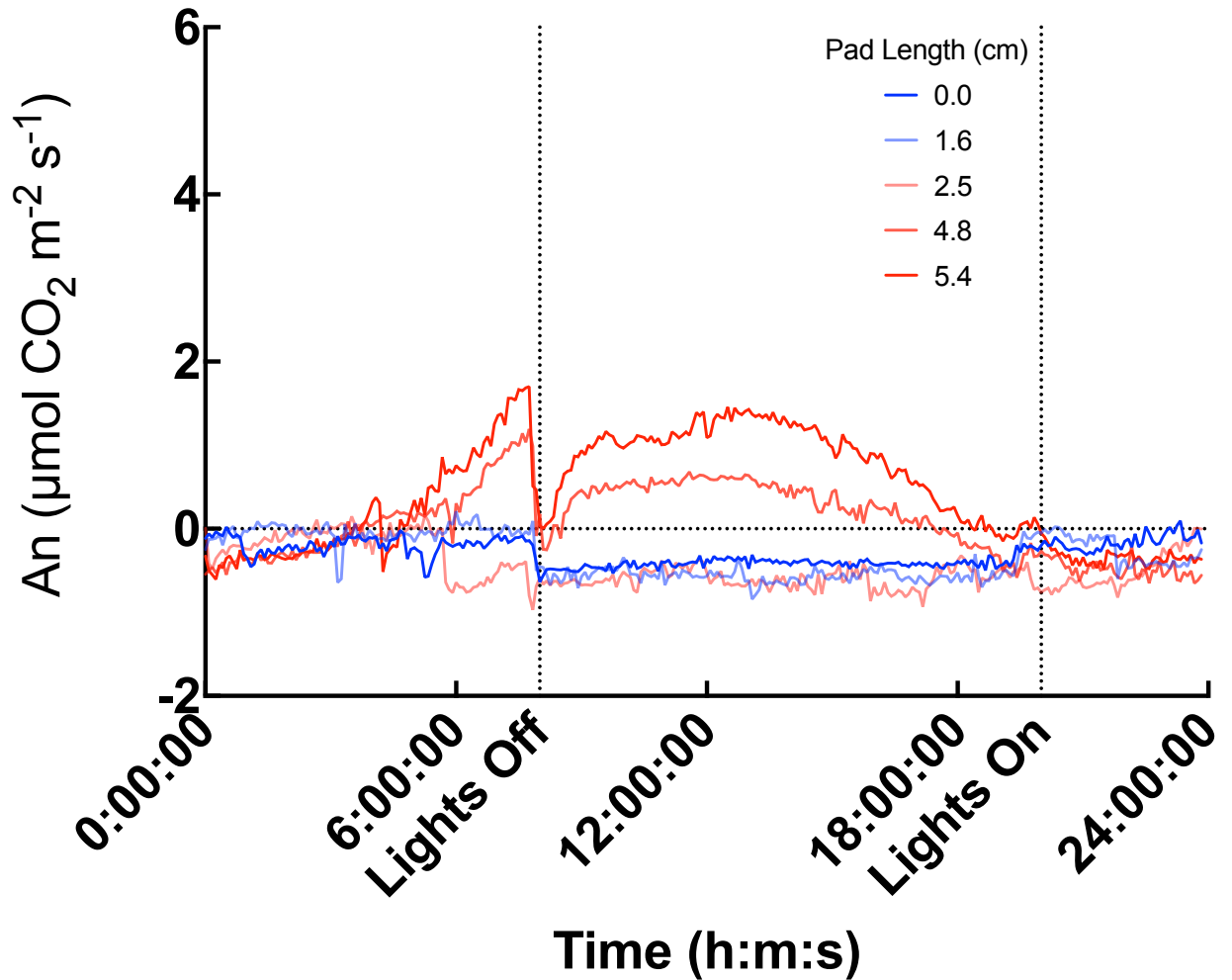


Figure 1: 24-hour gas exchange measurements of *O. ficus-indica* seedling 1 grown at a PAR of  $100 \mu\text{mol m}^{-2} \text{ s}^{-1}$  at  $20^\circ\text{C}$  in well-watered conditions as the central cladode grows (Dark blue to light blue to light red to dark red). The assimilation rate ( $\mu\text{mol CO}_2 \text{ m}^{-2} \text{ S}^{-1}$ ) was logged every 5 minutes.

## Seedling 2 - PAR 100 - Watered

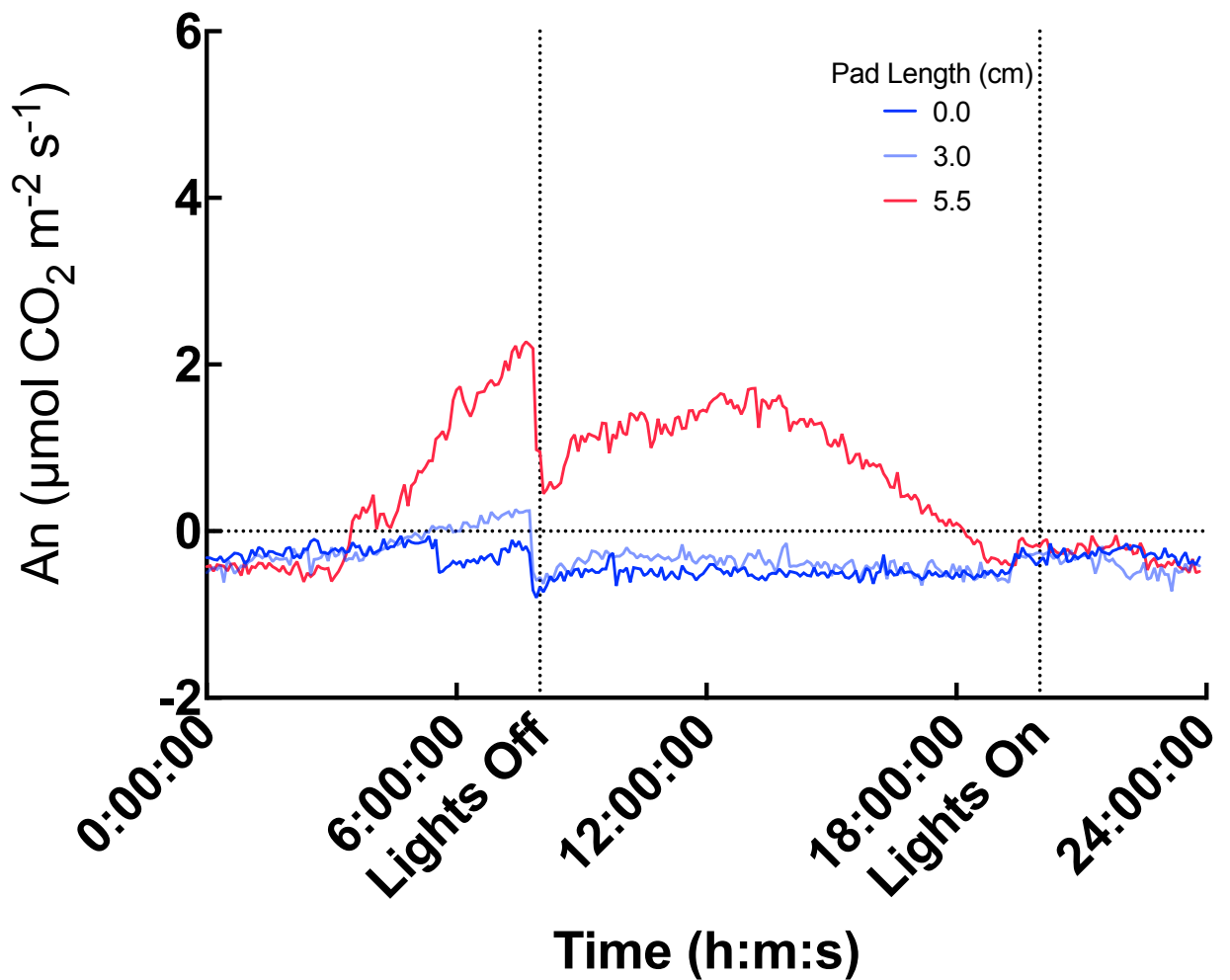


Figure 2: 24-hour gas exchange measurements of *O. ficus-indica* seedling 2 grown at a PAR of  $100 \mu\text{mol m}^{-2} \text{ s}^{-1}$  at  $20^\circ \text{C}$  in well-watered conditions as the central cladode grows (Dark blue to light blue to light red to dark red). The assimilation rate ( $\mu\text{mol CO}_2 \text{ m}^{-2} \text{ S}^{-1}$ ) was logged every 5 minutes.

## Seedling 3 - PAR - Watered

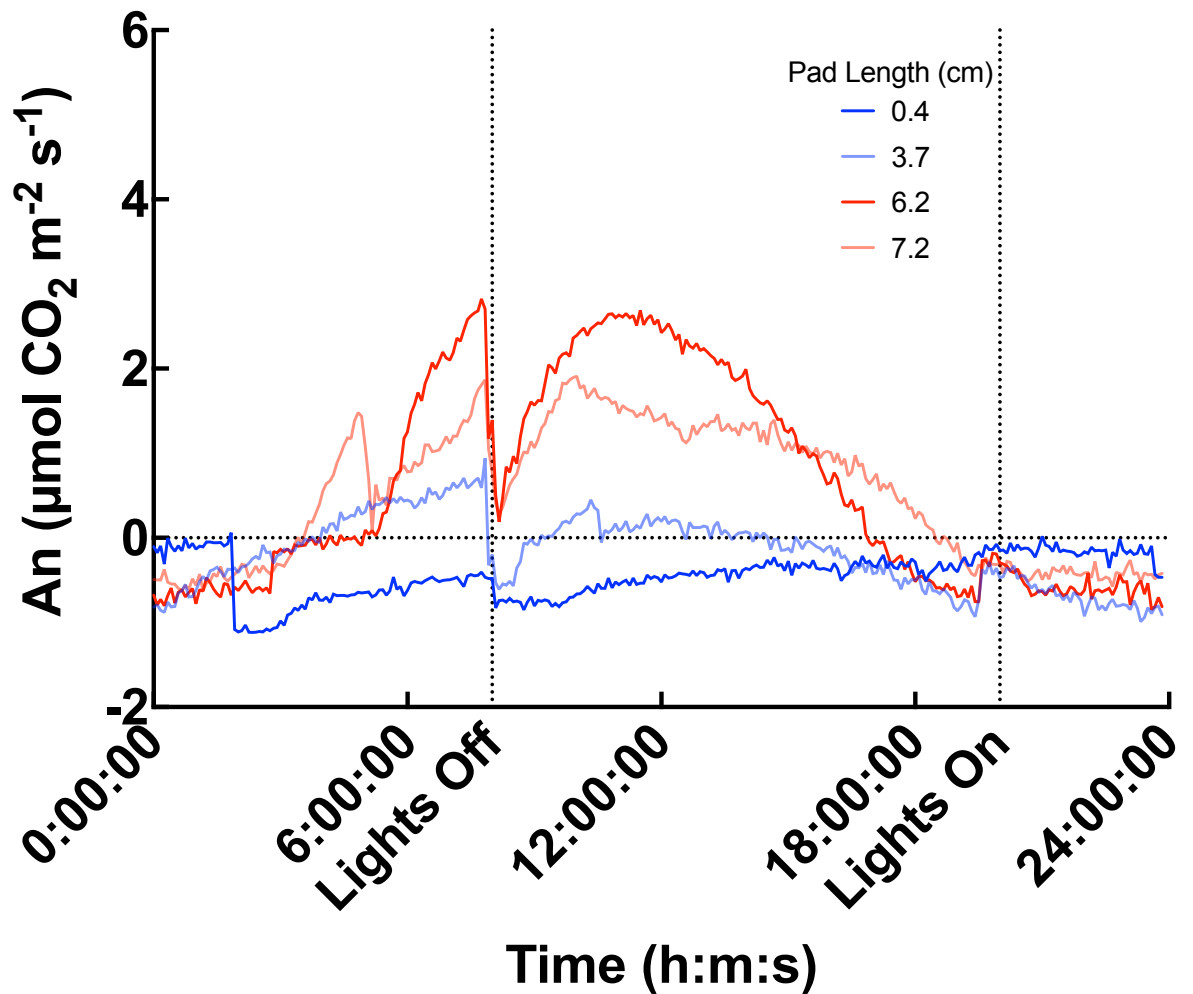


Figure 3: 24-hour gas exchange measurements of *O. ficus-indica* seedling 3 grown at a PAR of  $100 \mu\text{mol m}^{-2} \text{ s}^{-1}$  at  $20^\circ \text{C}$  in well-watered conditions as the central cladode grows (Dark blue to light blue to light red to dark red). The assimilation rate ( $\mu\text{mol CO}_2 \text{ m}^{-2} \text{ S}^{-1}$ ) was logged every 5 minutes.

## Seedling 4 - Par 100 Watered - Chlorosis

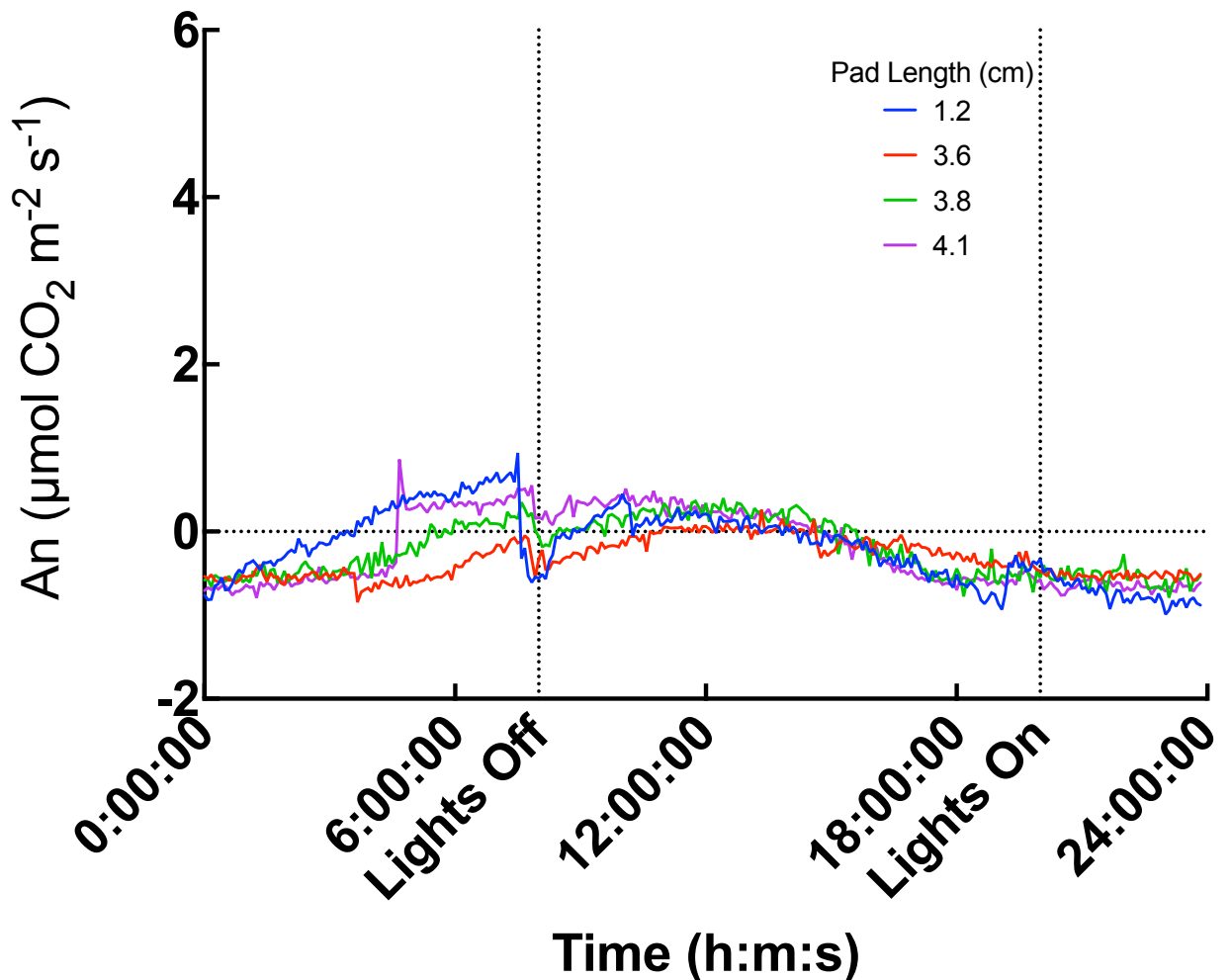


Figure 4: 24-hour gas exchange measurements of *O. ficus-indica* seedling 4 grown at a PAR of  $100 \mu\text{mol m}^{-2} \text{ s}^{-1}$  at  $20^\circ \text{C}$  in well-watered conditions as the central cladode grows (Dark blue to light blue to light red to dark red). The assimilation rate ( $\mu\text{mol CO}_2 \text{ m}^{-2} \text{ S}^{-1}$ ) was logged every 5 minutes. This seedling had chlorosis from tightly packed soil and was not used to calculate the AUC for net gas exchange of well-watered plants in PAR 100.

## Seedling 5 - PAR 100 - Watered

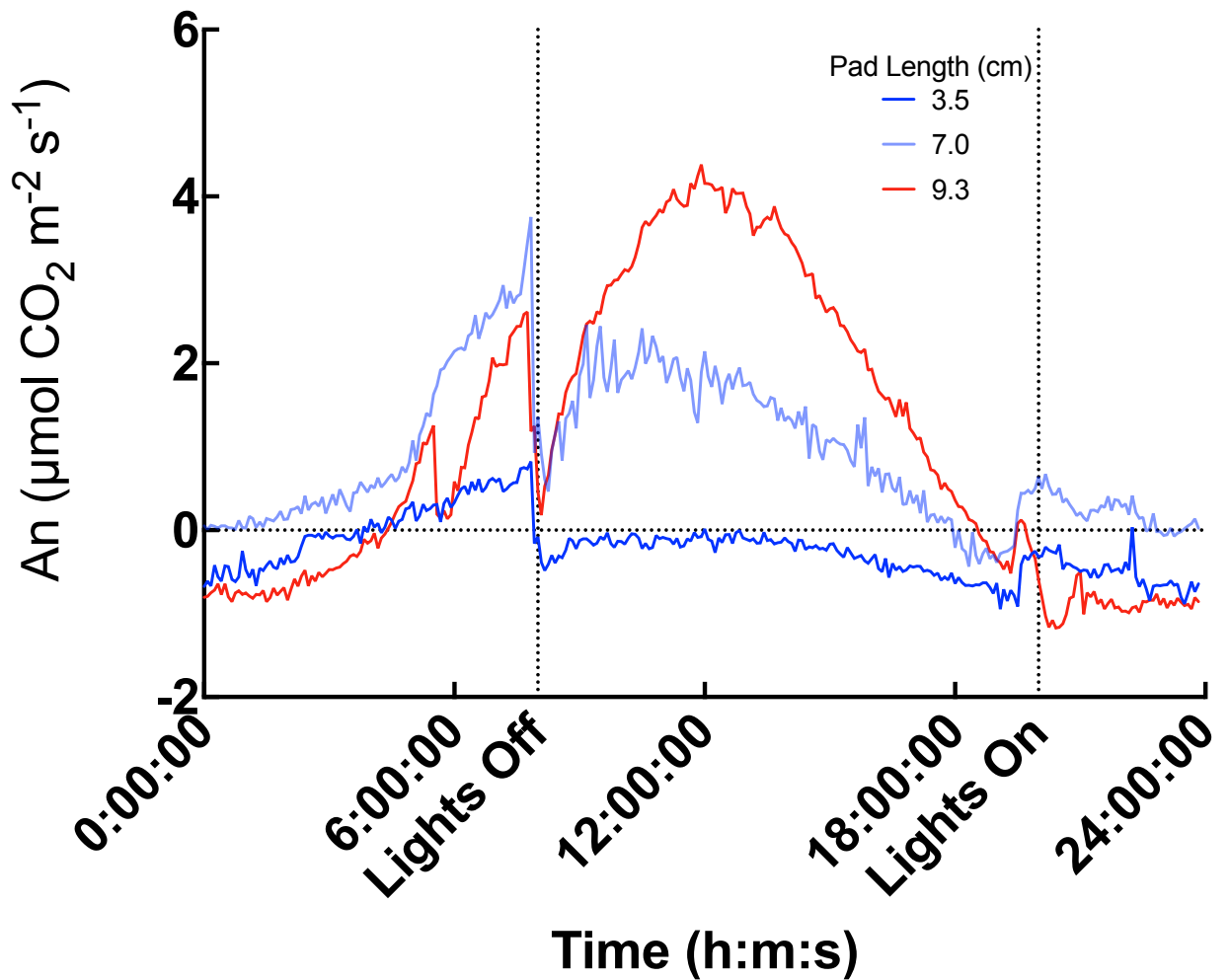
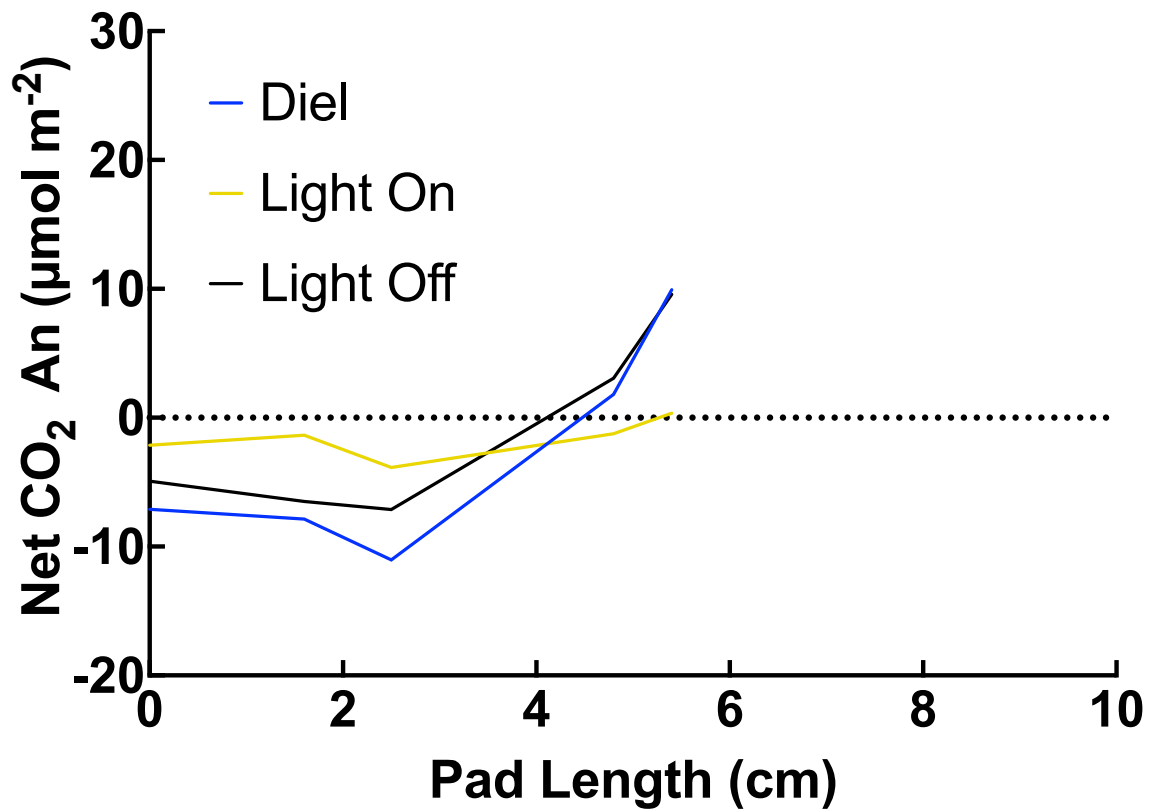


Figure 3: 24-hour gas exchange measurements of *O. ficus-indica* seedling 5 grown at a PAR of  $100 \mu\text{mol m}^{-2} \text{ s}^{-1}$  at  $20^\circ\text{C}$  in well-watered conditions as the central cladode grows (Dark blue to light blue to light red to dark red). The assimilation rate ( $\mu\text{mol CO}_2 \text{ m}^{-2} \text{ S}^{-1}$ ) was logged every 5 minutes.



## Seedling 1 - PAR 100 - Watered



*Figure 6:* The diel (blue line), light (yellow line), and dark (black line) net assimilated CO<sub>2</sub> (µmol m<sup>-2</sup>) vs. cladode length (cm) in seedling 1 grown at PAR of 100 µmol m<sup>-2</sup> s<sup>-1</sup> at 20 °C in well-watered conditions.

## Seedling 2 - Par 100 - Watered

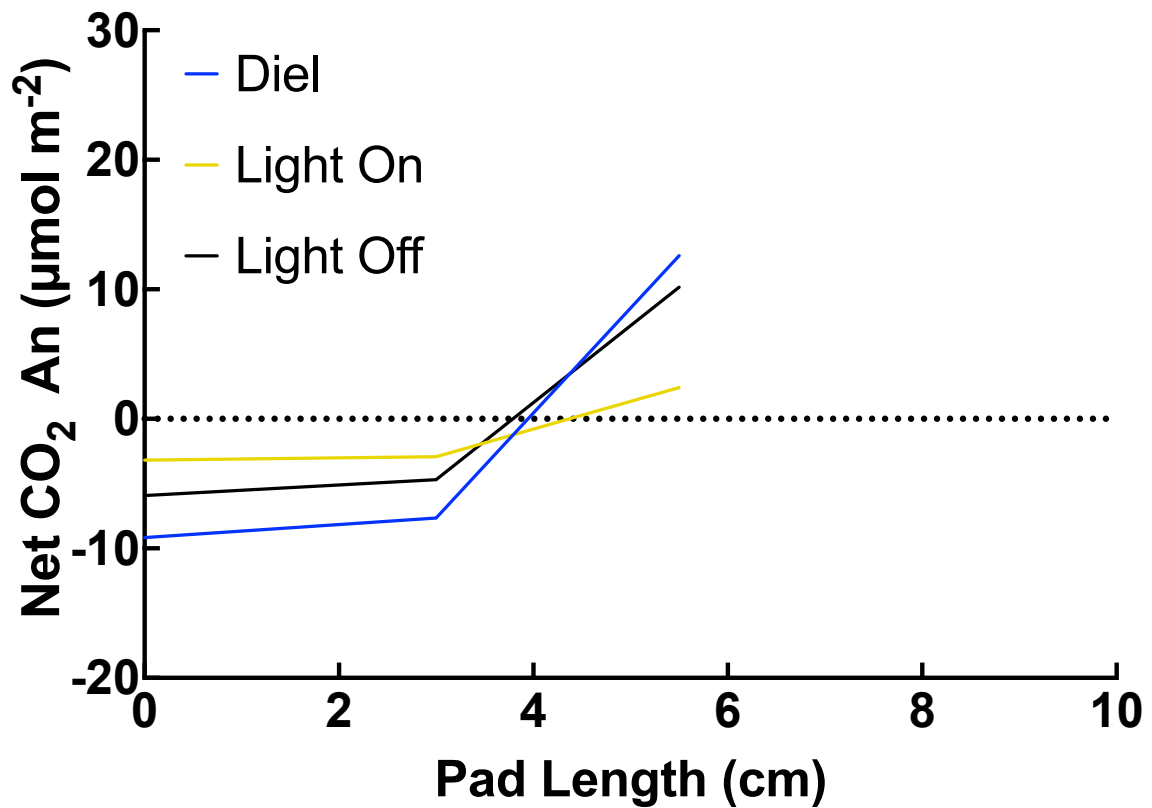


*Figure 7:* The diel (blue line), light (yellow line), and dark (black line) net assimilated CO<sub>2</sub> (µmol m<sup>-2</sup>) vs. cladode length (cm) in seedling 2 grown at PAR of 100 µmol m<sup>-2</sup> s<sup>-1</sup> at 20 °C in well-watered conditions.

### Seedling 3 - PAR 100 - Watered

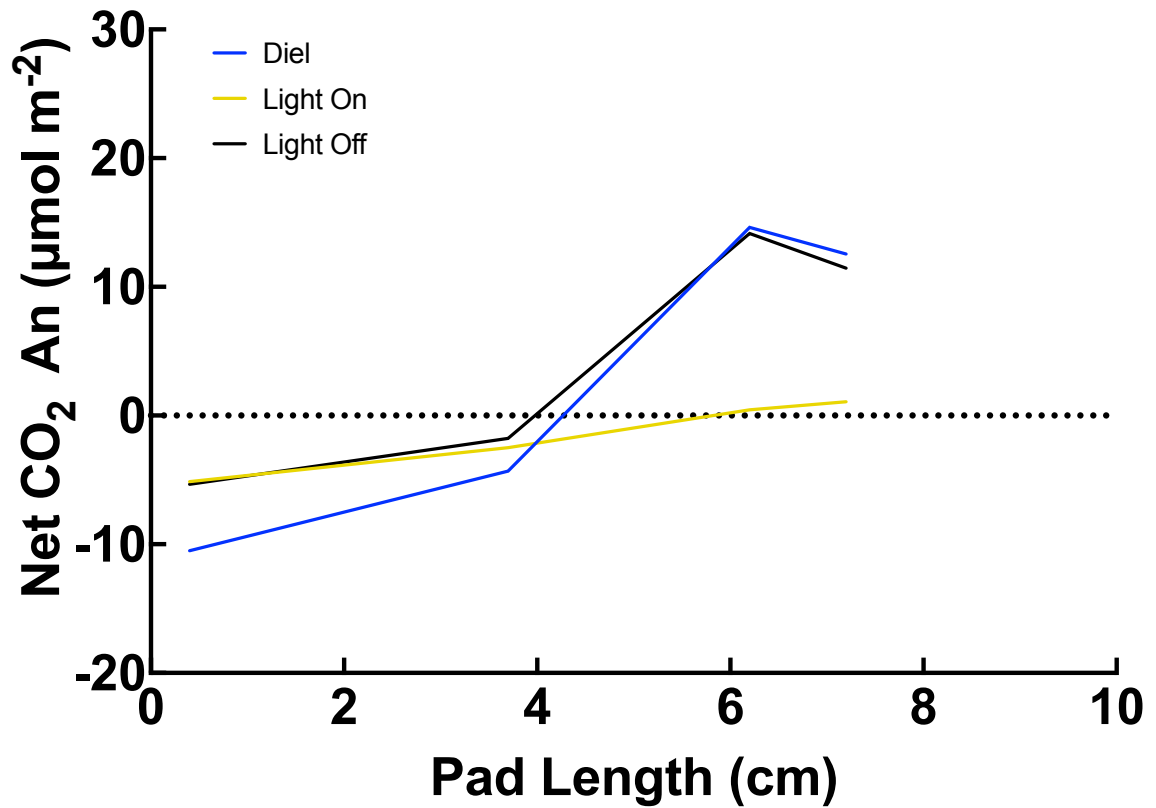


*Figure 8:* The diel (blue line), light (yellow line), and dark (black line) net assimilated CO<sub>2</sub> (µmol m<sup>-2</sup>) vs. cladode length (cm) in seedling 3 grown at PAR of 100 µmol m<sup>-2</sup> s<sup>-1</sup> at 20 °C in well-watered conditions.

## Seedling 4 - PAR 100 Drought - Chlorosis

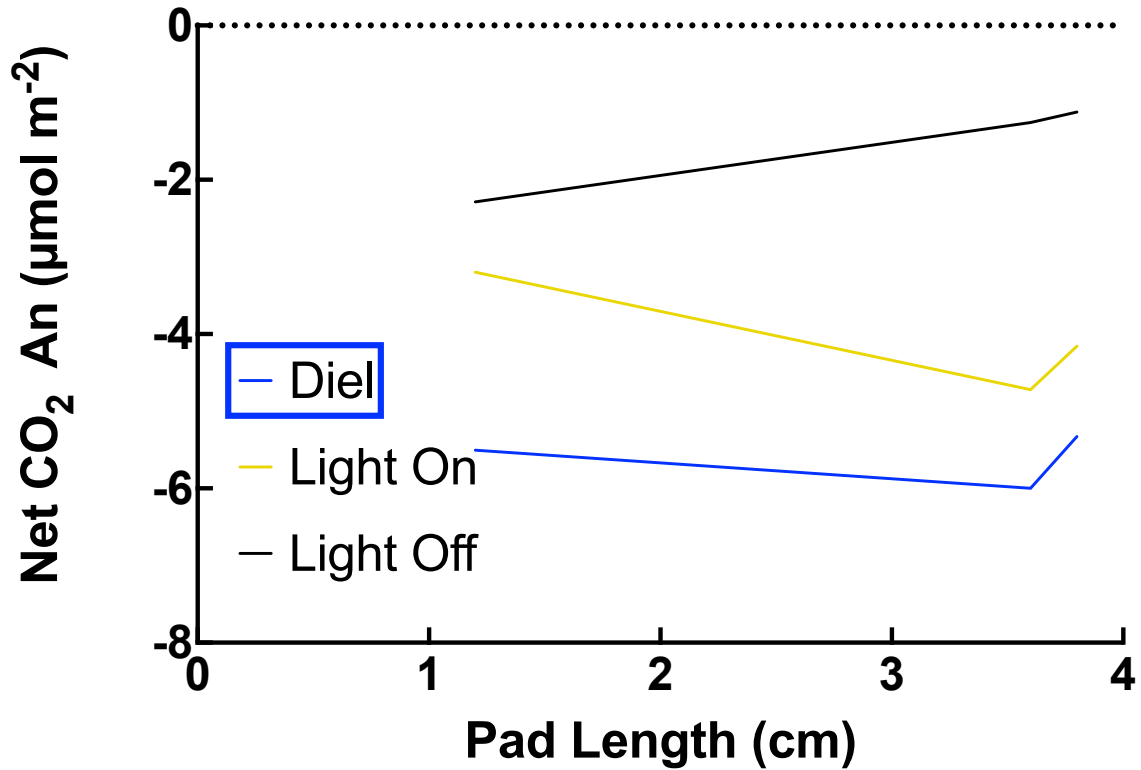


*Figure 9:* The diel (blue line), light (yellow line), and dark (black line) net assimilated CO<sub>2</sub> (µmol m<sup>-2</sup>) vs. cladode length (cm) in seedling 4 grown at PAR of 100 µmol m<sup>-2</sup> s<sup>-1</sup> at 20 °C in well-watered conditions. This seedling had chlorosis from tightly packed soil and was not used to calculate the AUC for net gas exchange of well-watered plants in PAR 100.

## Seedling 5 - PAR 100 - Watered

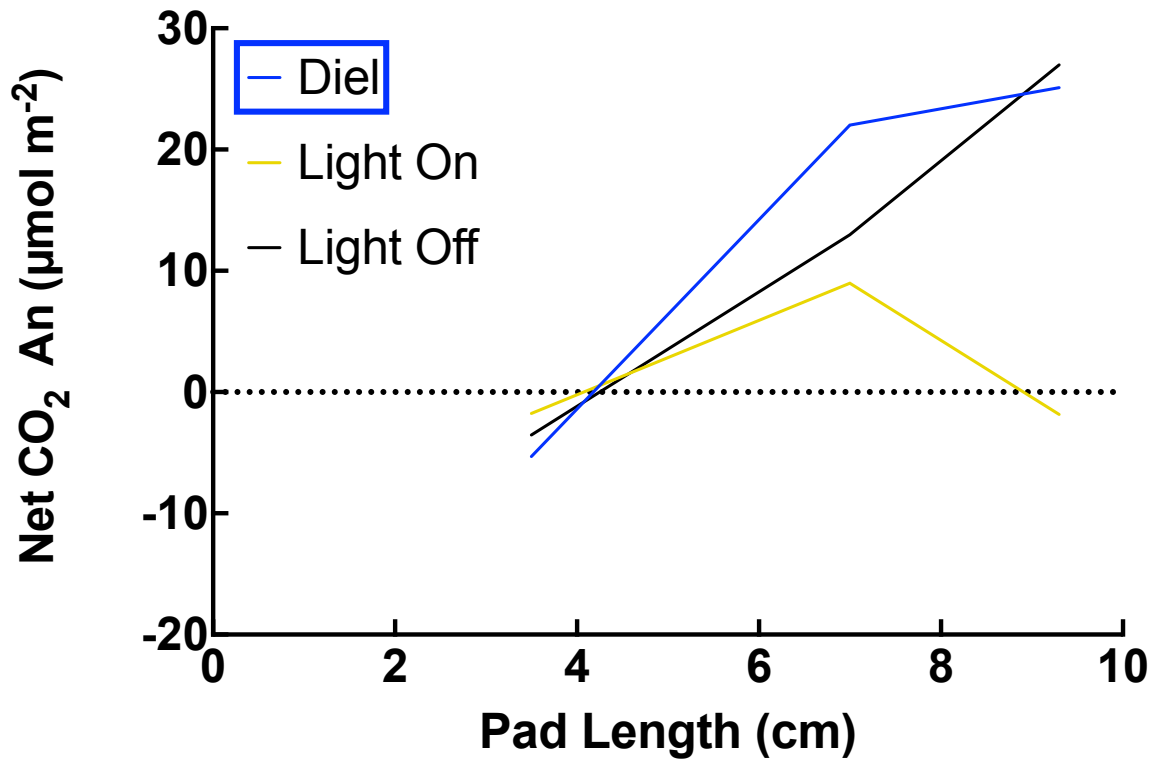


*Figure 40:* The diel (blue line), light (yellow line), and dark (black line) net assimilated CO<sub>2</sub> (µmol m<sup>-2</sup>) vs. cladode length (cm) in seedling 5 grown at PAR of 100 µmol m<sup>-2</sup> s<sup>-1</sup> at 20 °C in well-watered conditions.

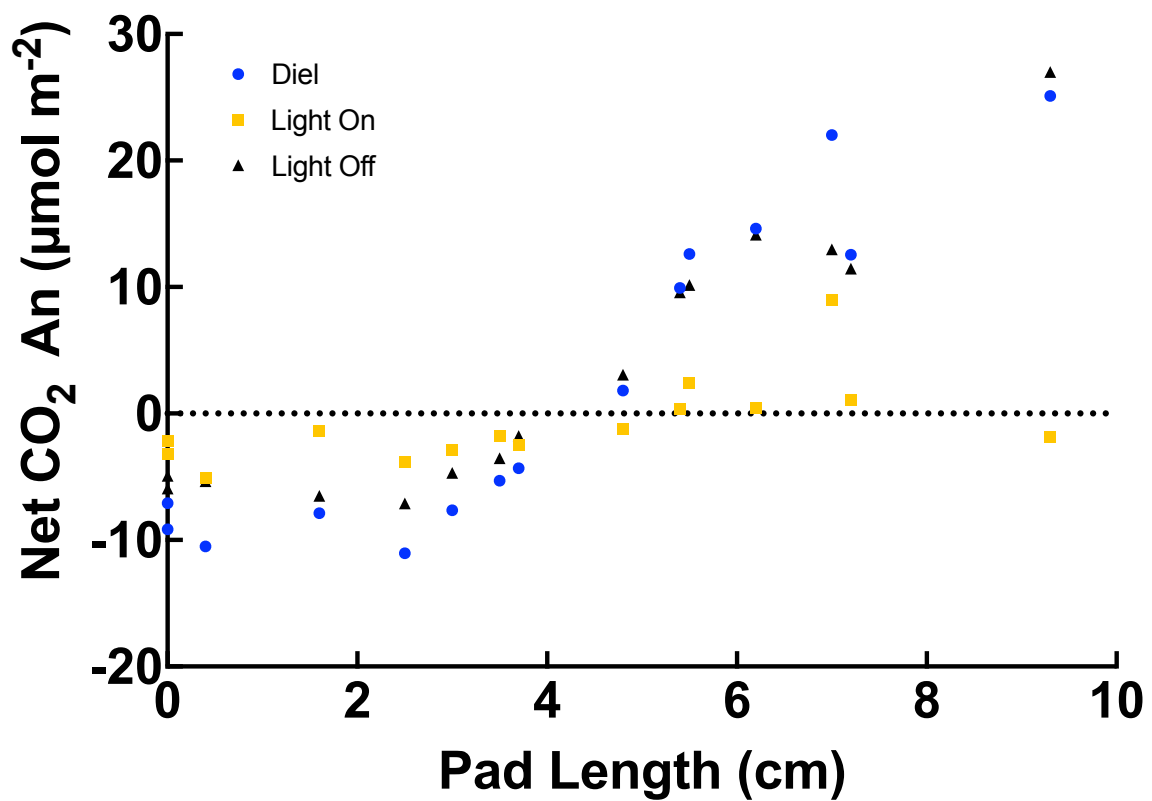


*Figure 11:* The combined diel (blue line), light (yellow line), and dark (black line) net assimilated CO<sub>2</sub> (μmol m<sup>-2</sup>) vs. cladode length (cm) in all seedlings grown at PAR of 100 μmol m<sup>-2</sup> s<sup>-1</sup> at 20 °C in well-watered conditions.

## Seedling 1 - PAR - Drought

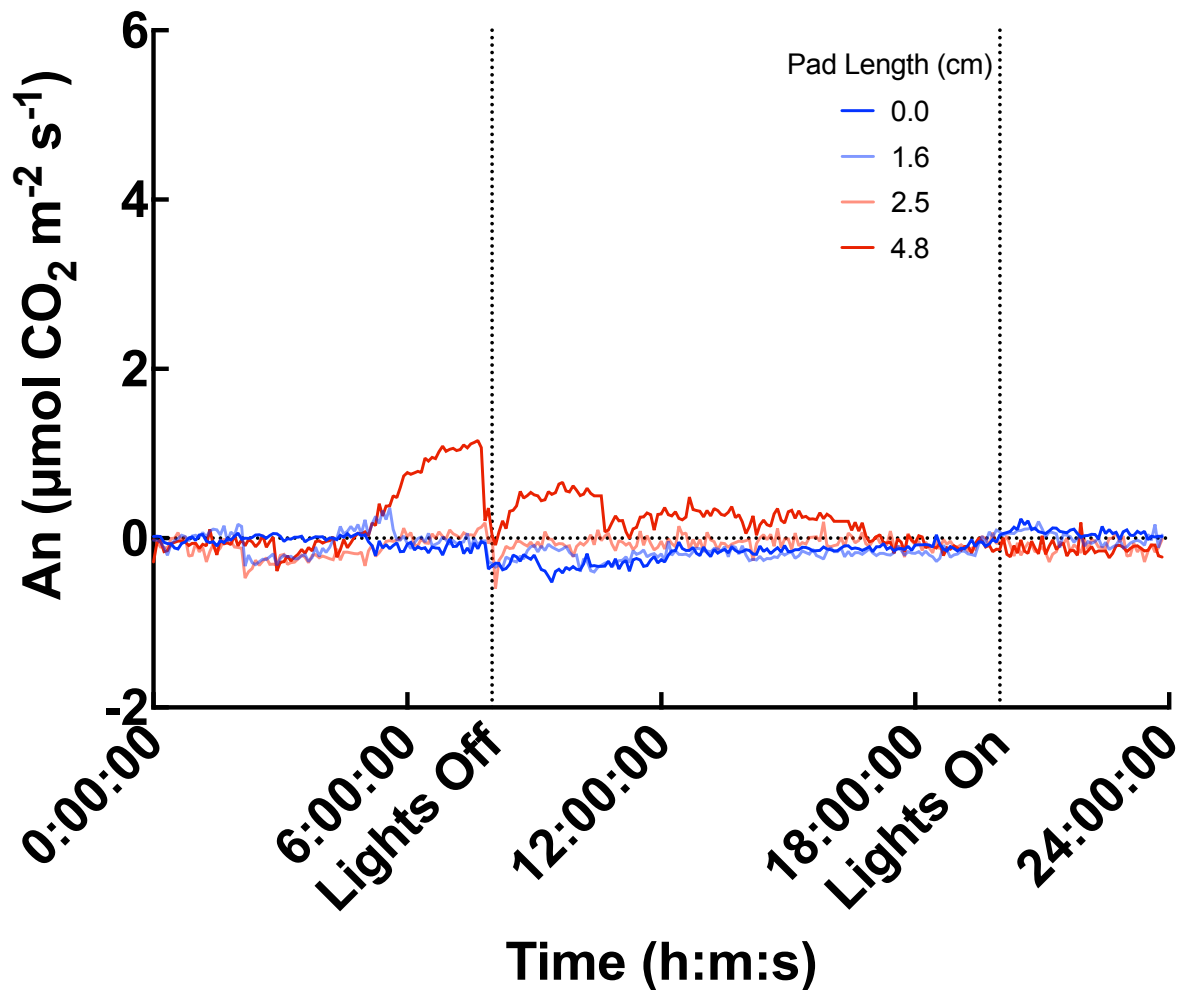


Figure 12: 24-hour gas exchange measurements of *O. ficus-indica* seedling 1 grown at a PAR of  $100 \mu\text{mol m}^{-2} \text{ s}^{-1}$  at  $20^\circ \text{C}$  in well-watered conditions as the central cladode grows (Dark blue to light blue to light red to dark red). The assimilation rate ( $\mu\text{mol CO}_2 \text{ m}^{-2} \text{ S}^{-1}$ ) was logged every 5 minutes. Each measurement was taken after allowing the soil to completely dry out for one day.

## Seedling 2 - PAR 100 - Drought

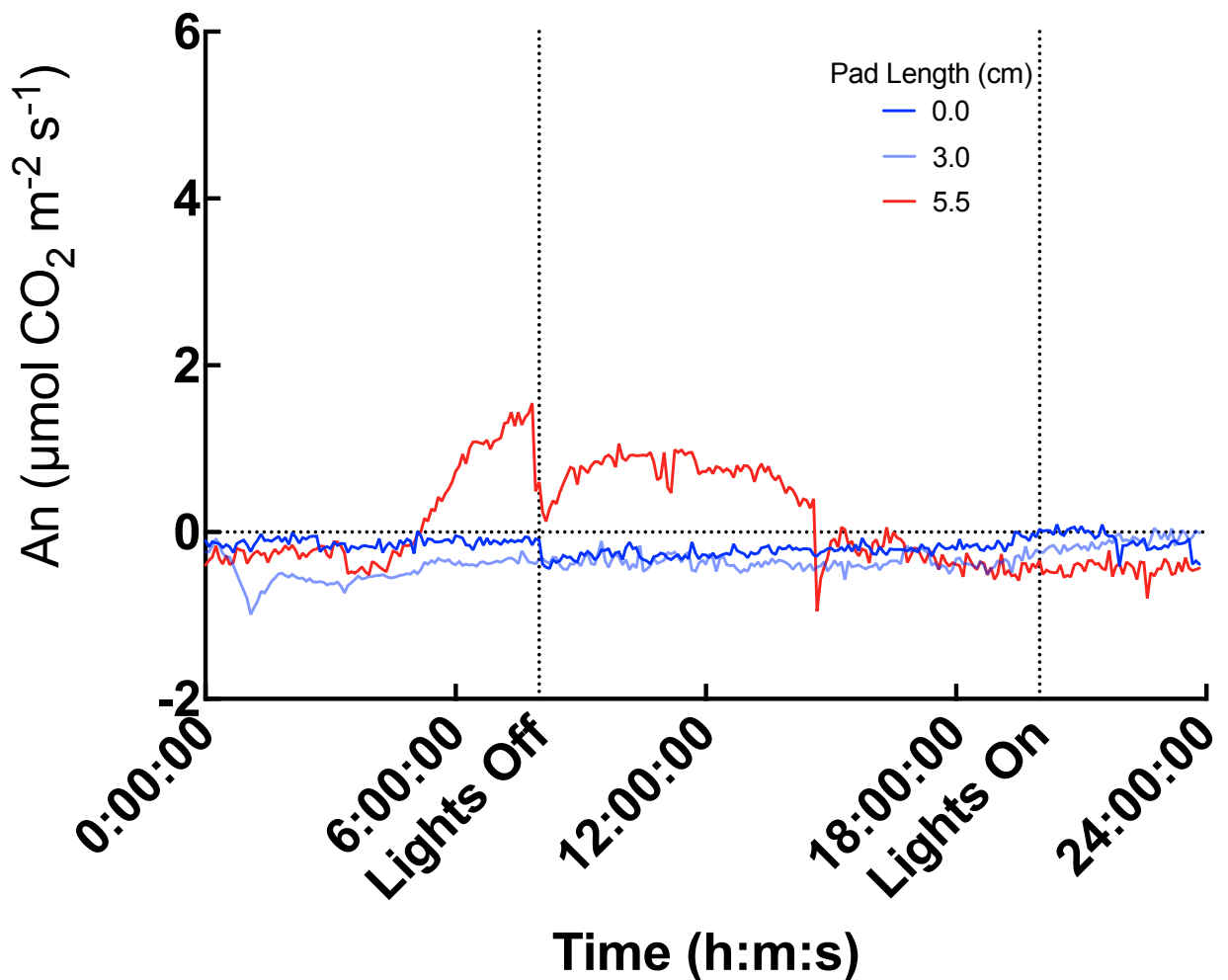


Figure 13: 24-hour gas exchange measurements of *O. ficus-indica* seedling 2 grown at a PAR of  $100 \mu\text{mol m}^{-2} \text{ s}^{-1}$  at  $20^\circ\text{C}$  in well-watered conditions as the central cladode grows (Dark blue to light blue to light red to dark red). The assimilation rate ( $\mu\text{mol CO}_2 \text{ m}^{-2} \text{ S}^{-1}$ ) was logged every 5 minutes. Each measurement was taken after allowing the soil to completely dry out for one day.



## Seedling 4 - Par 100 Drought - Chlorosis

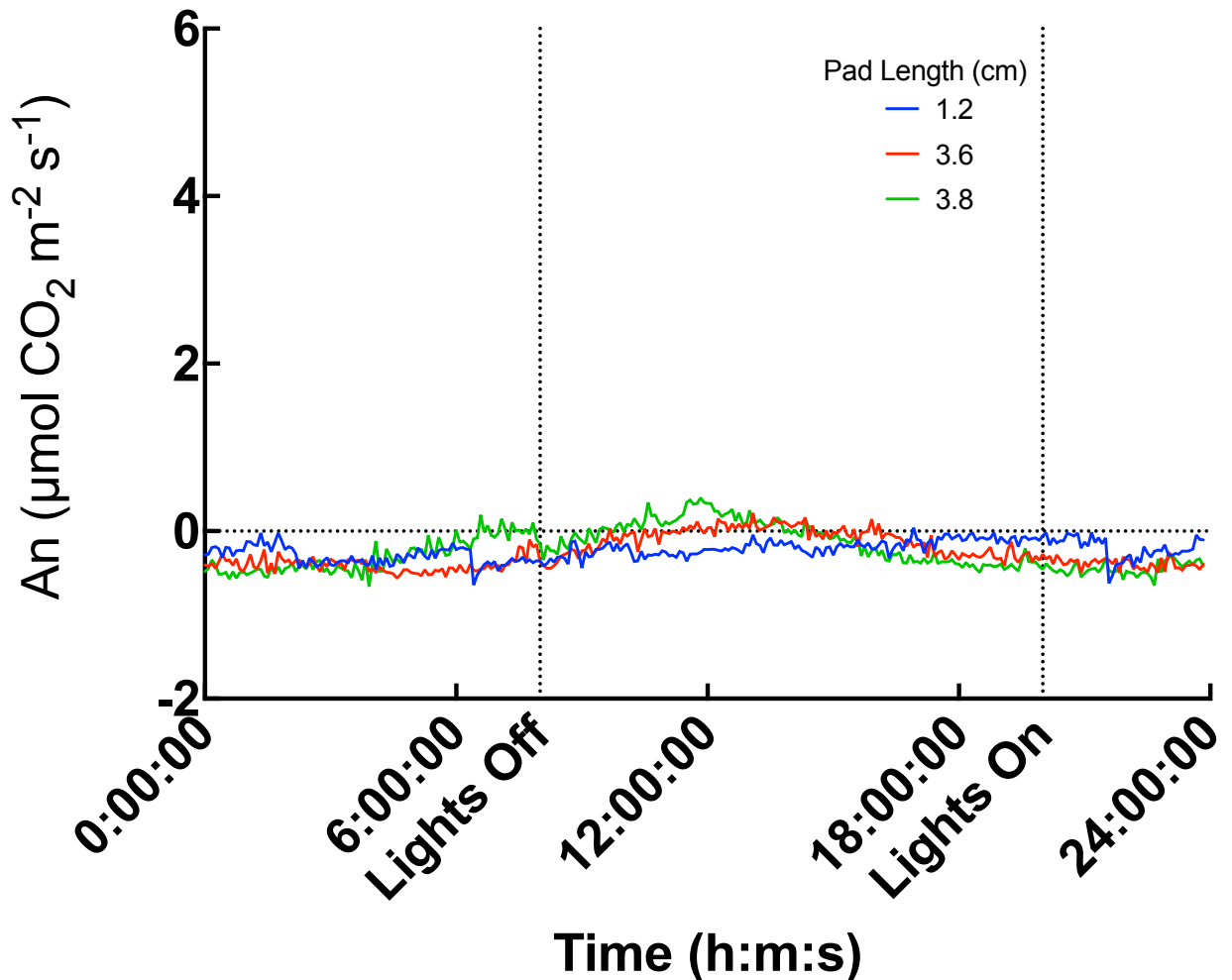


Figure 14: 24-hour gas exchange measurements of *O. ficus-indica* seedling 4 grown at a PAR of  $100 \mu\text{mol m}^{-2} \text{ s}^{-1}$  at  $20^\circ \text{C}$  in well-watered conditions as the central cladode grows. The assimilation rate ( $\mu\text{mol CO}_2 \text{ m}^{-2} \text{ S}^{-1}$ ) was logged every 5 minutes. Each measurement was taken after allowing the soil to completely dry out for one day. This seedling had chlorosis from tightly packed soil and was not used to calculate the AUC for net gas exchange of drought plants in PAR 100.

## Seedling 5 - PAR 100 - Drought

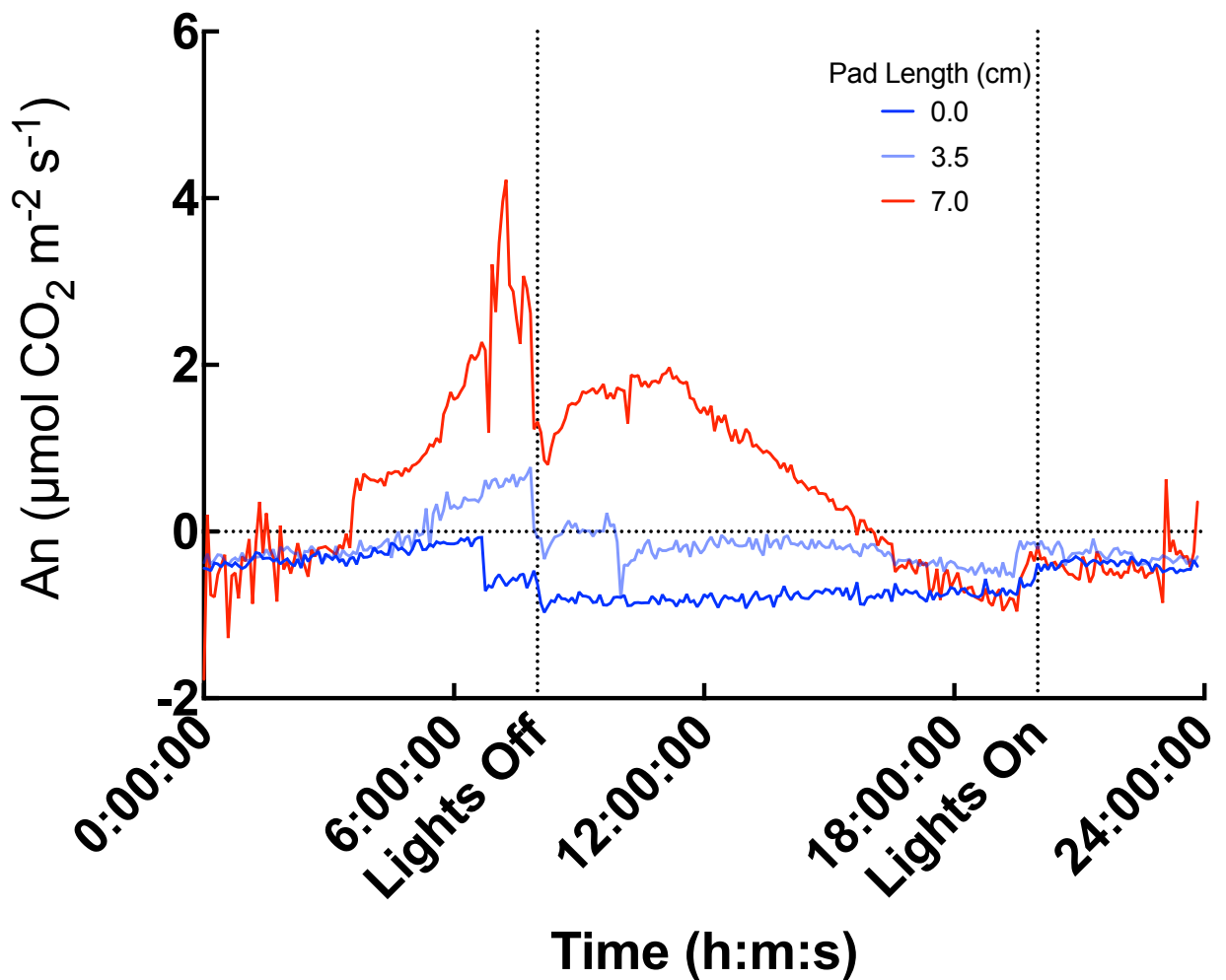
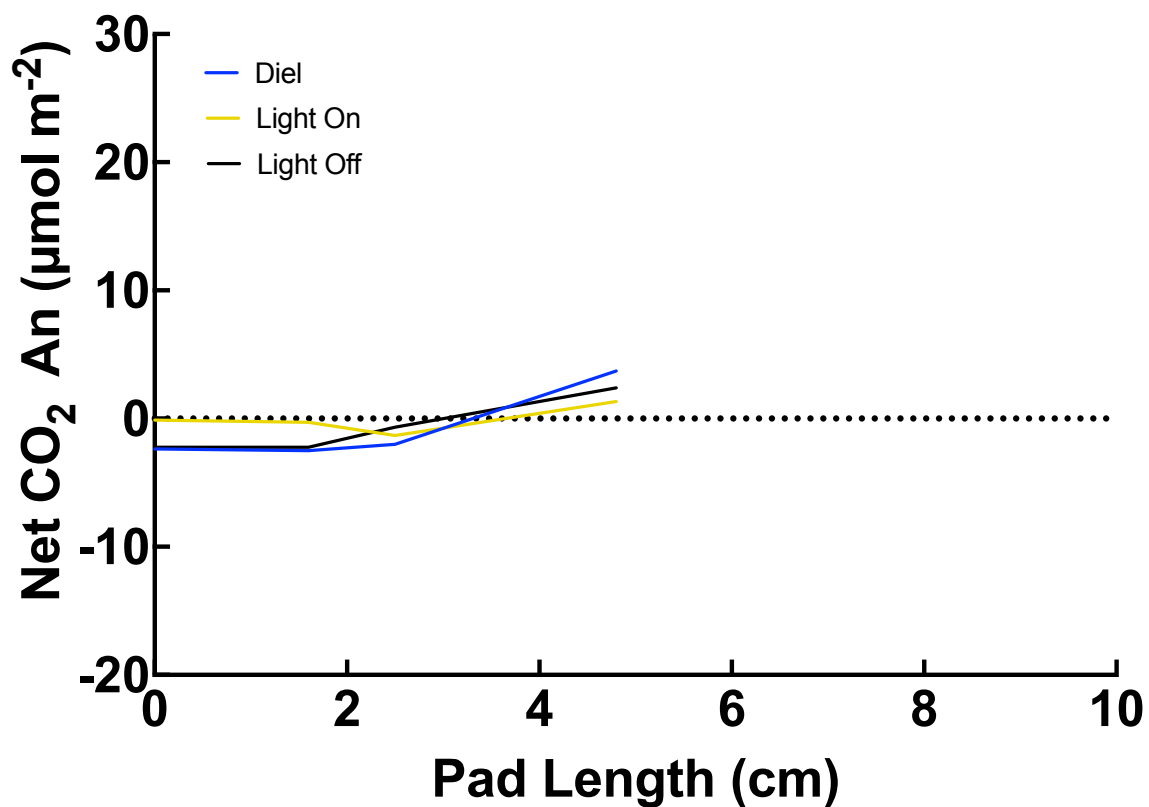
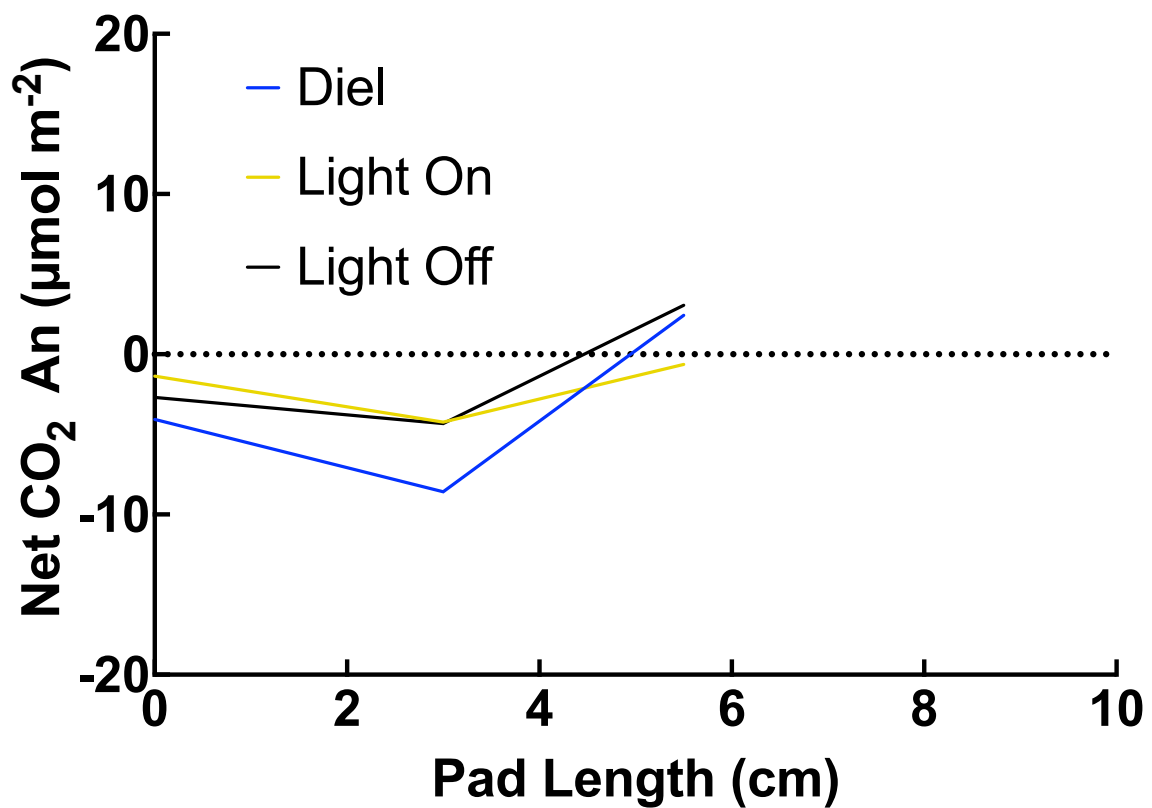


Figure 15: 24-hour gas exchange measurements of *O. ficus-indica* seedling 5 grown at a PAR of  $100 \mu\text{mol m}^{-2} \text{ s}^{-1}$  at  $20^\circ \text{C}$  in well-watered conditions as the central cladode grows (Dark blue to light blue to light red to dark red). The assimilation rate ( $\mu\text{mol CO}_2 \text{ m}^{-2} \text{ S}^{-1}$ ) was logged every 5 minutes. Each measurement was taken after allowing the soil to completely dry out for one day.



*Figure 16:* The diel (blue line), light (yellow line), and dark (black line) net assimilated CO<sub>2</sub> (µmol m<sup>-2</sup>) vs. cladode length (cm) in seedling 1 grown at PAR of 100 µmol m<sup>-2</sup> s<sup>-1</sup> at 20 °C in drought. This seedling had chlorosis from tightly packed soil and was not used to calculate the AUC for net gas exchange of well-watered plants in PAR 100.

## Seedling 2 - Par 100 - Drought



*Figure 17:* The diel (blue line), light (yellow line), and dark (black line) net assimilated CO<sub>2</sub> (µmol m<sup>-2</sup>) vs. cladode length (cm) in seedling 2 grown at PAR of 100 µmol m<sup>-2</sup> s<sup>-1</sup> at 20 °C in drought.

## Seedling 4 - PAR 100 Drought - Chlorosis

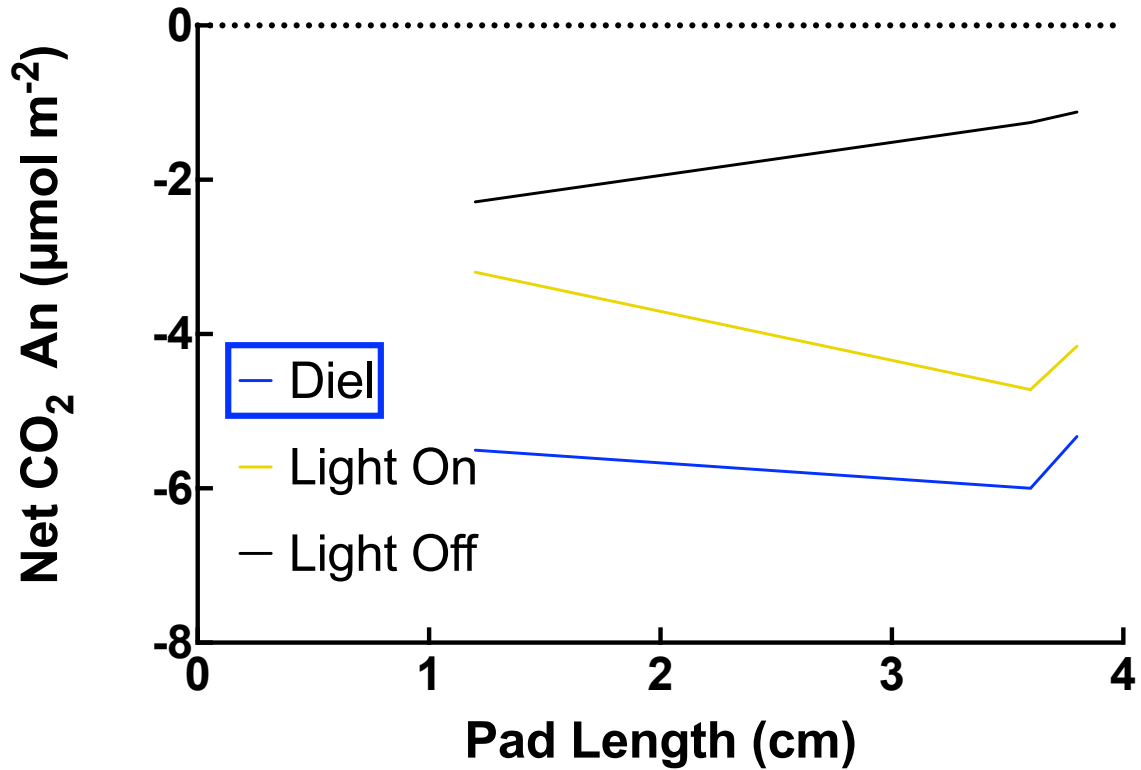


*Figure 18:* The diel (blue line), light (yellow line), and dark (black line) net assimilated CO<sub>2</sub> ( $\mu\text{mol m}^{-2}$ ) vs. cladode length (cm) in seedling 4 grown at PAR of  $100 \mu\text{mol m}^{-2} \text{ s}^{-1}$  at  $20^\circ\text{C}$  in drought. This seedling had chlorosis from tightly packed soil and was not used to calculate the AUC for net gas exchange of well-watered plants in PAR 100.

## Seedling 5 - PAR 100 - Drought

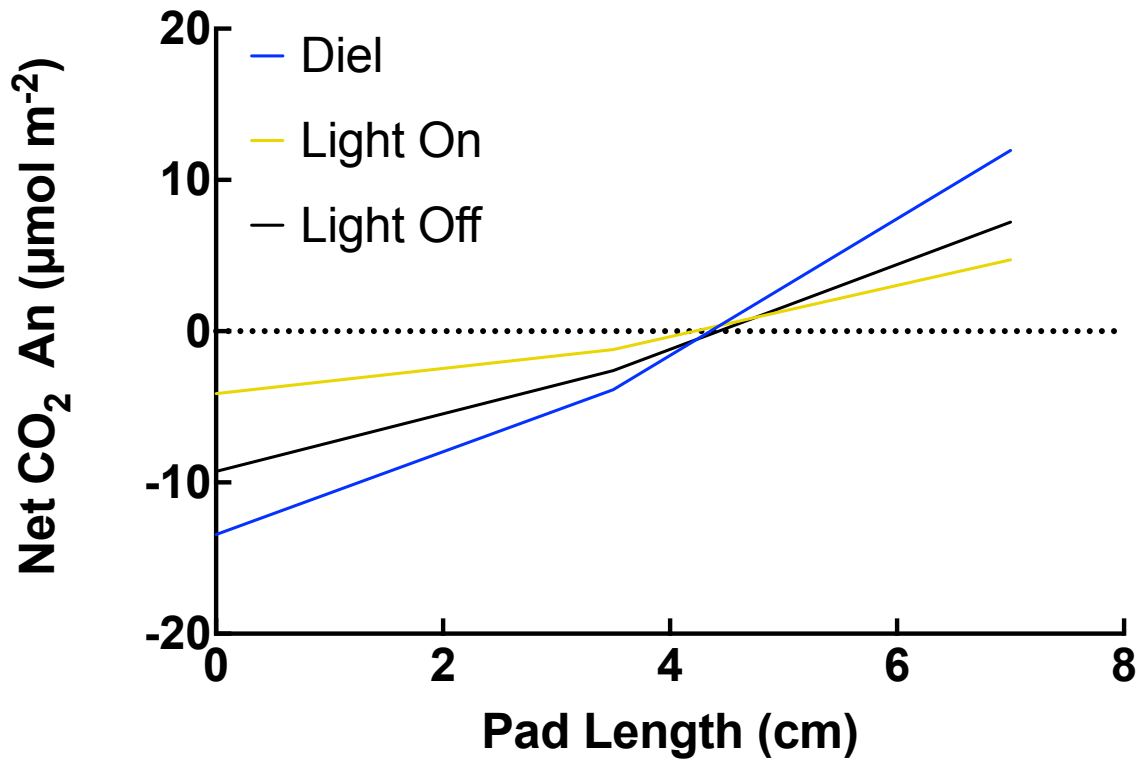


*Figure 19:* The diel (blue line), light (yellow line), and dark (black line) net assimilated CO<sub>2</sub> (µmol m<sup>-2</sup>) vs. cladode length (cm) in seedling 5 grown at PAR of 100 µmol m<sup>-2</sup> s<sup>-1</sup> at 20 °C in Drought.

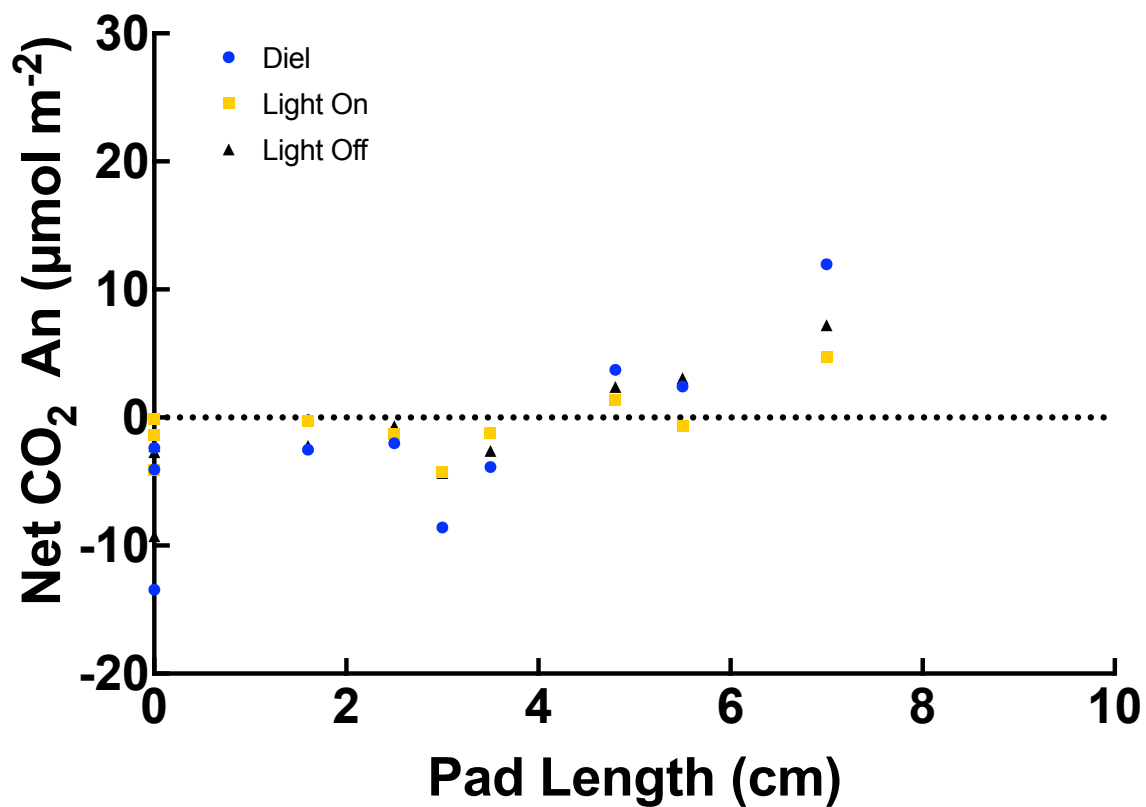


*Figure 20:* The combined diel (blue line), light (yellow line), and dark (black line) net assimilated CO<sub>2</sub> (μmol m<sup>-2</sup>) vs. cladode length (cm) in all seedlings grown at PAR of 100 μmol m<sup>-2</sup> s<sup>-1</sup> at 20 °C in drought.

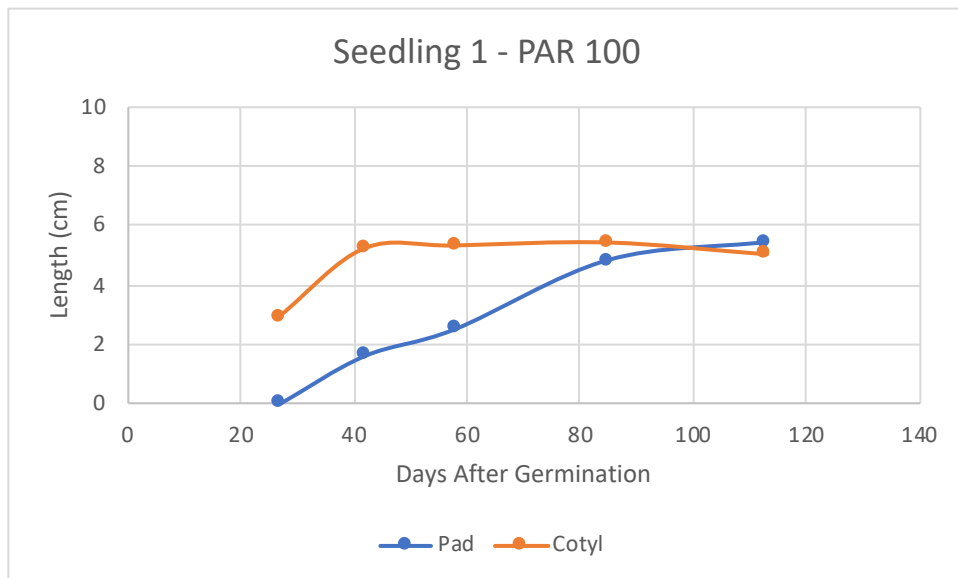


Figure 21: Measured length (cm) of *O. ficus-indica* seedling 1 central cladode (blue dots and line) and combined cotyledons (orange dots and line) within the gas exchange sample period (days after germination). Grown at PAR of 100  $\mu\text{mol m}^{-2} \text{s}^{-1}$  at 20 °C in well-watered conditions.

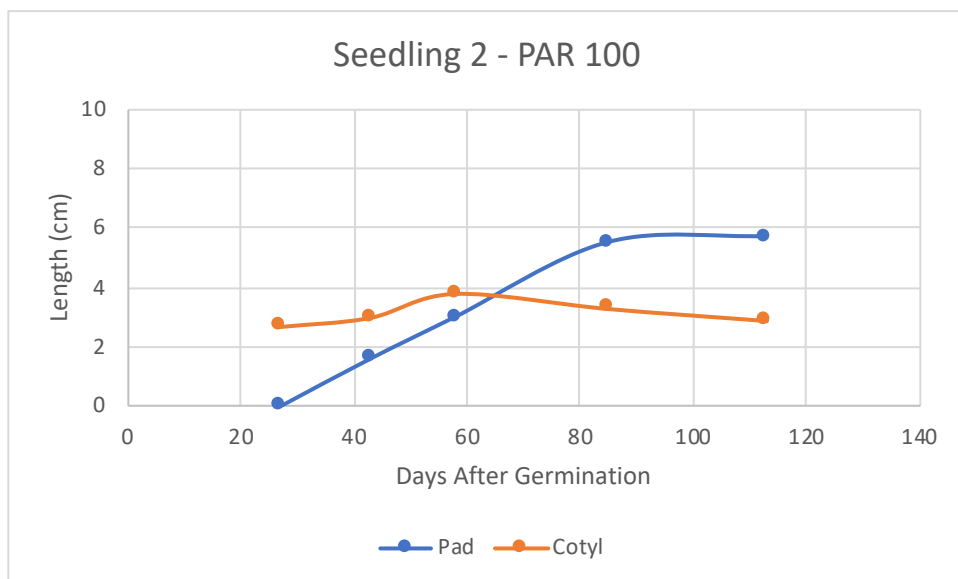
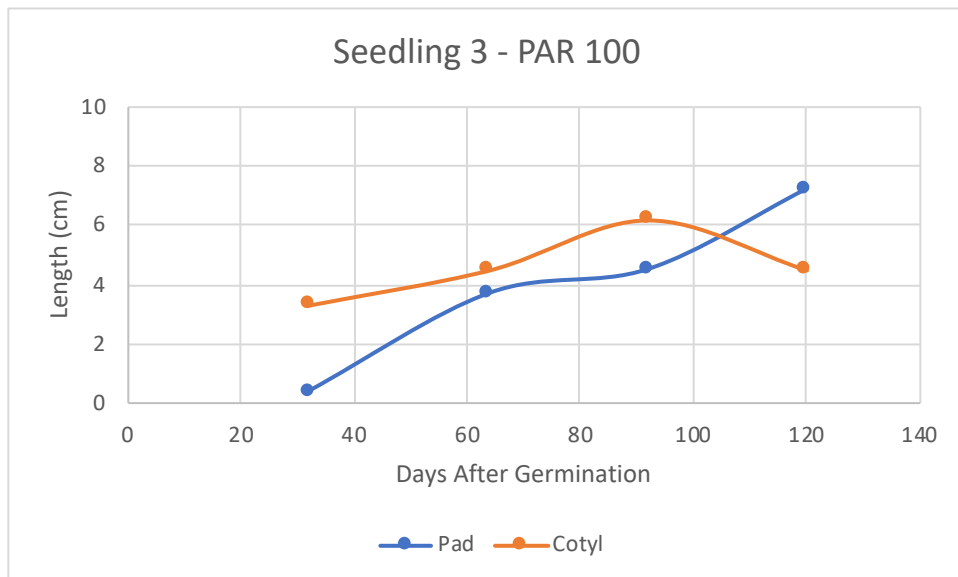


Figure 22: Measured length (cm) of *O. ficus-indica* seedling 2 central cladode (blue dots and line) and combined cotyledons (orange dots and line) within the



gas exchange sample period (days after germination). Grown at PAR of  $100 \mu\text{mol m}^{-2} \text{s}^{-1}$  at  $20 \text{ }^\circ\text{C}$  in well-watered conditions.



*Figure 23:* Measured length (cm) of *O. ficus-indica* seedling 3 central cladode (blue dots and line) and combined cotyledons (orange dots and line) within the gas exchange sample period (days after germination). Grown at PAR of  $100 \mu\text{mol m}^{-2} \text{s}^{-1}$  at  $20 \text{ }^\circ\text{C}$  in well-watered conditions.

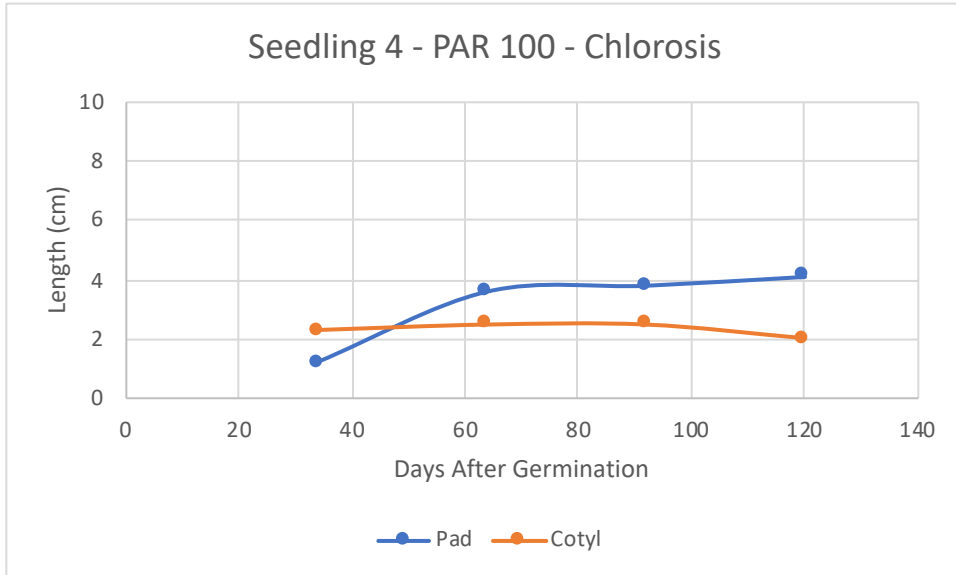


Figure 24: Measured length (cm) of *O. ficus-indica* seedling 4 central cladode (blue dots and line) and combined cotyledons (orange dots and line) within the gas exchange sample period (days after germination). Grown at PAR of 100  $\mu\text{mol m}^{-2} \text{s}^{-1}$  at 20 °C in well-watered conditions.

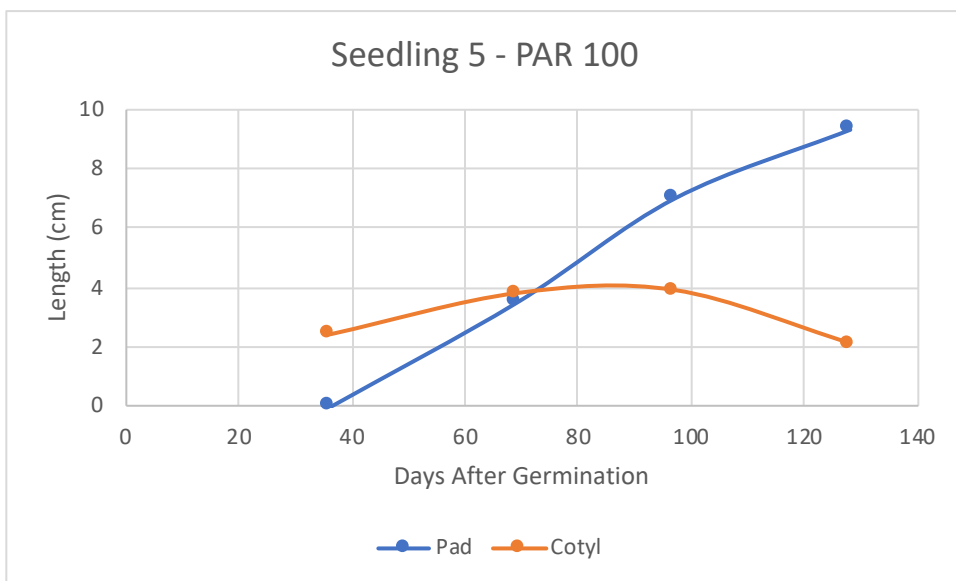
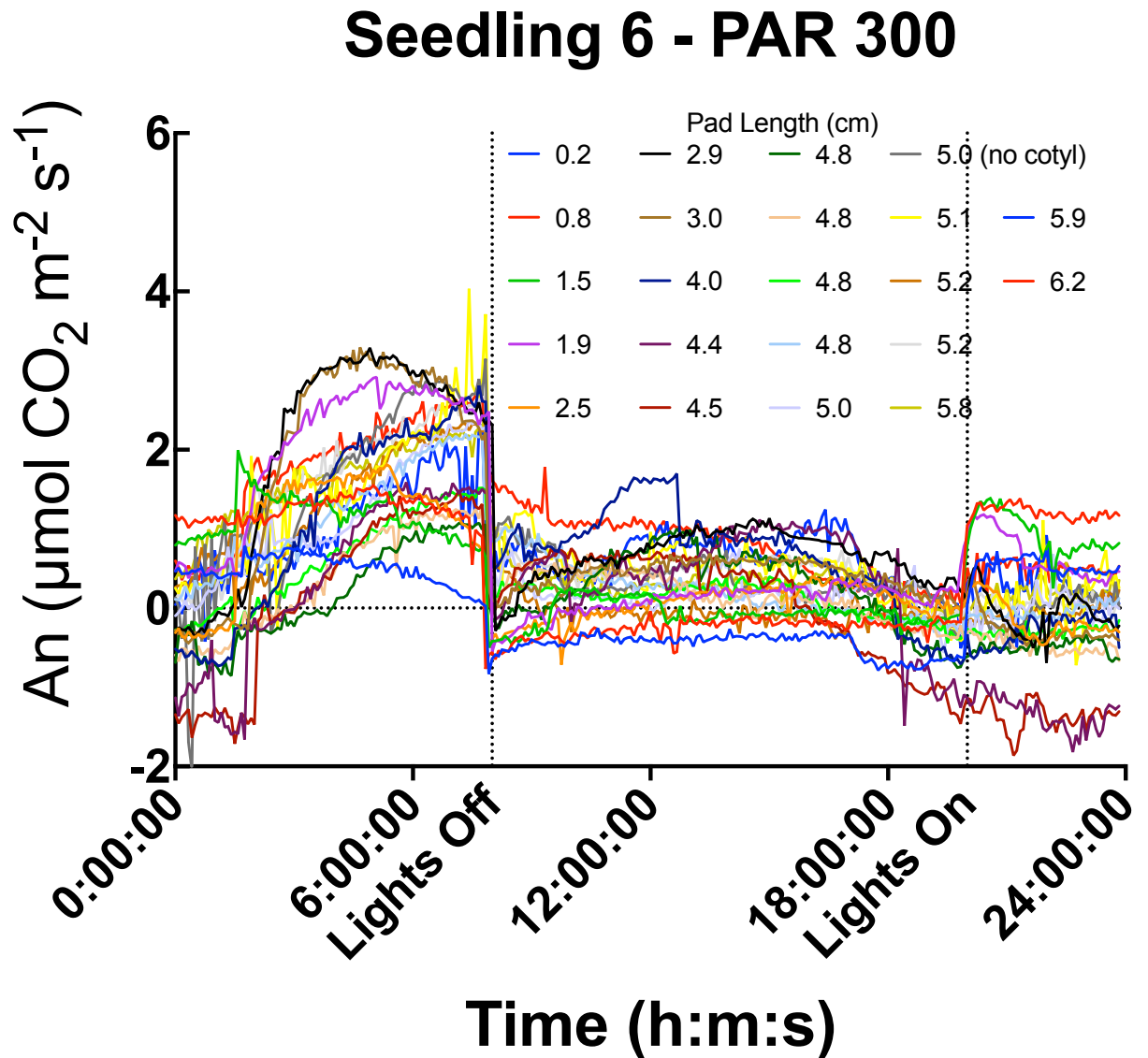


Figure 25: Measured length (cm) of *O. ficus-indica* seedling 1 central cladode (blue dots and line) and combined cotyledons (orange dots and line) within the

gas exchange sample period (days after germination). Grown at PAR of 100  $\mu\text{mol m}^{-2} \text{s}^{-1}$  at 20 °C in well-watered conditions.



*Figure 5:* 24-hour gas exchange measurements of *O. ficus-indica* seedling 6 grown at a PAR of 300  $\mu\text{mol m}^{-2} \text{s}^{-1}$  at 20 °C in well-watered conditions as the central cladode grows. The assimilation rate ( $\mu\text{mol CO}_2 \text{m}^{-2} \text{S}^{-1}$ ) was logged every 5 minutes.

## Seedling 6 - PAR 300 - 1st Set

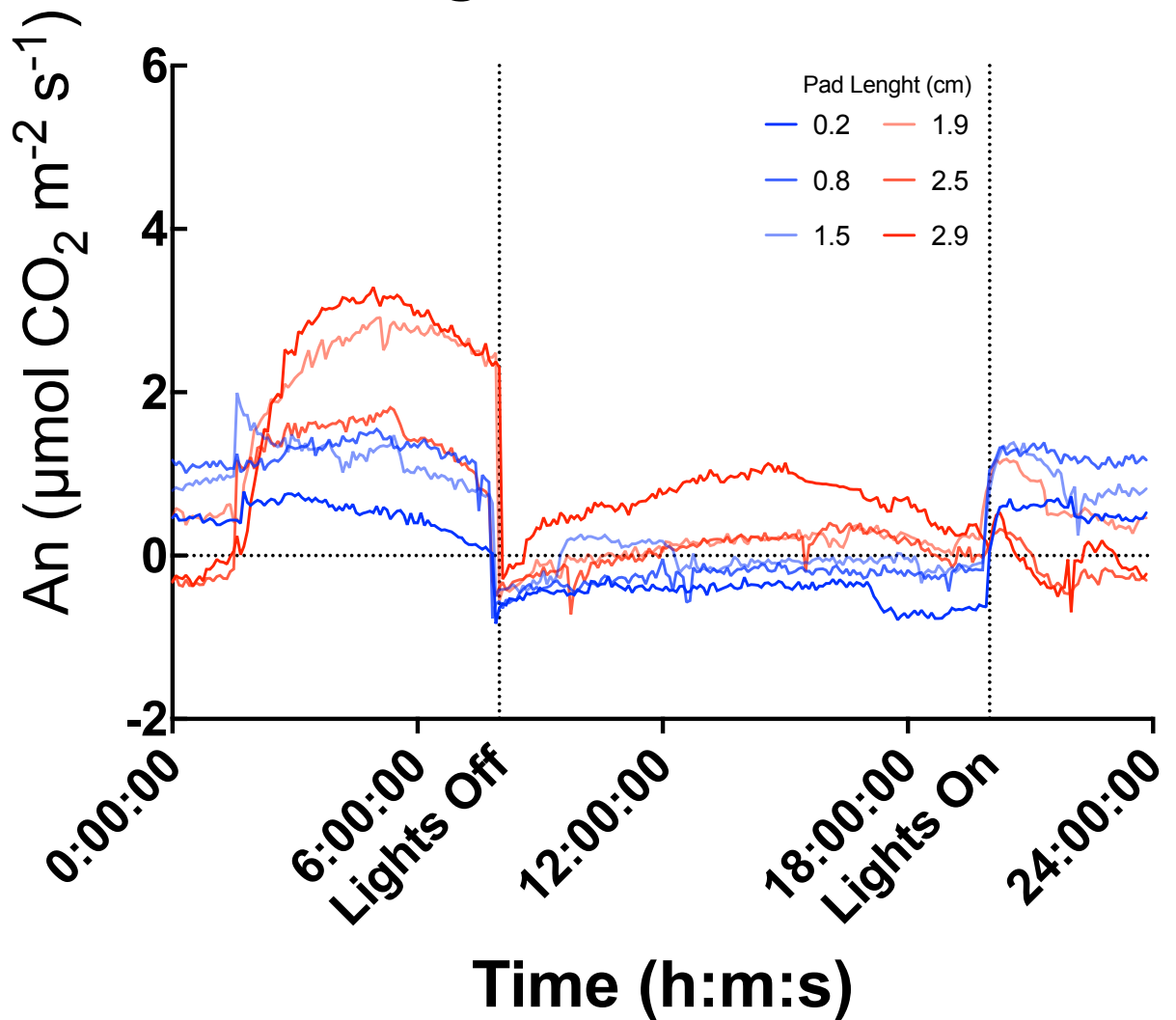


Figure 27: 1<sup>st</sup> set of 6 24-hour gas exchange measurements of *O. ficus-indica* seedling 6 grown at a PAR of  $300 \mu\text{mol m}^{-2} \text{ s}^{-1}$  at  $20^\circ\text{C}$  in well-watered conditions as the central cladode grows (Dark blue to light blue to light red to dark red). The assimilation rate ( $\mu\text{mol CO}_2 \text{ m}^{-2} \text{ S}^{-1}$ ) was logged every 5 minutes.

## Seedling 6 - PAR 300 - 2nd Set

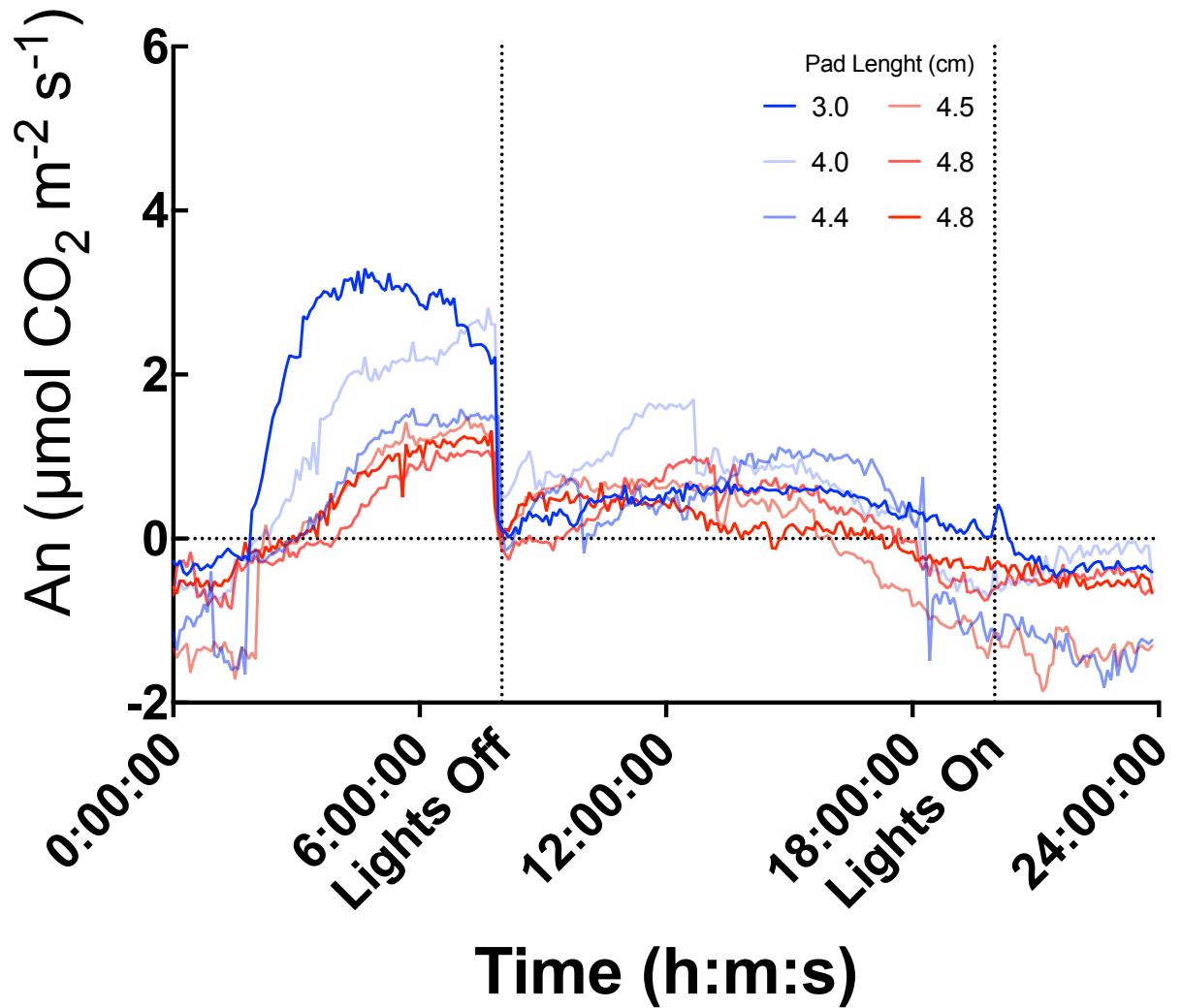


Figure 28: 2<sup>nd</sup> set of 6 24-hour gas exchange measurements of *O. ficus-indica* seedling 6 grown at a PAR of  $300 \mu\text{mol m}^{-2} \text{ s}^{-1}$  at  $20^\circ\text{C}$  in well-watered conditions as the central cladode grows (Dark blue to light blue to light red to dark red). The assimilation rate ( $\mu\text{mol CO}_2 \text{ m}^{-2} \text{ S}^{-1}$ ) was logged every 5 minutes.

## Seedling 6 - PAR 300 - 3rd Set

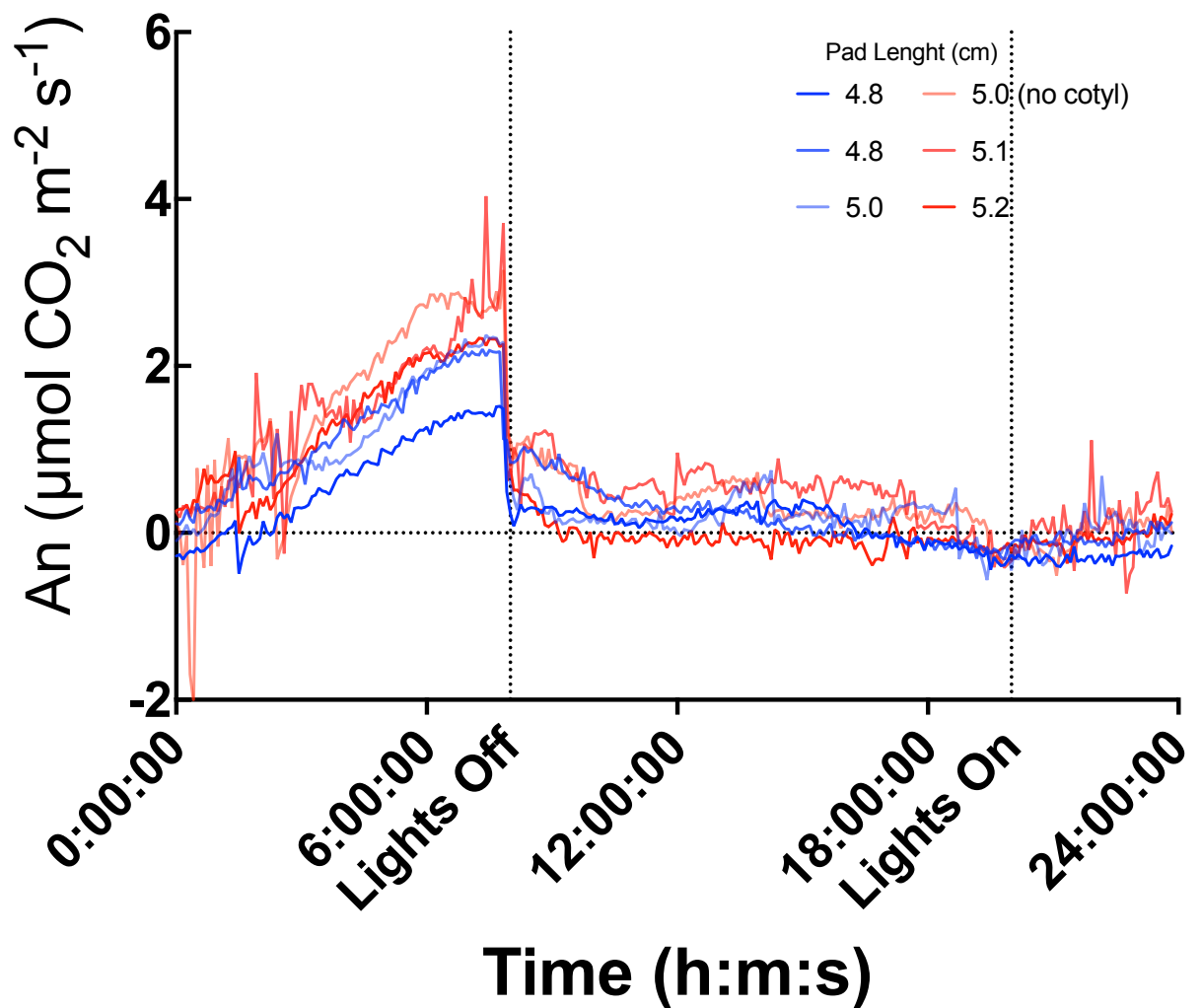


Figure 29: 3<sup>rd</sup> set of 6 24-hour gas exchange measurements of *O. ficus-indica* seedling 6 grown at a PAR of  $300 \mu\text{mol m}^{-2} \text{ s}^{-1}$  at  $20^\circ\text{C}$  in well-watered conditions as the central cladode grows (Dark blue to light blue to light red to dark red). The assimilation rate ( $\mu\text{mol CO}_2 \text{ m}^{-2} \text{ S}^{-1}$ ) was logged every 5 minutes.

## Seedling 6 - PAR 300 - 4rth Set

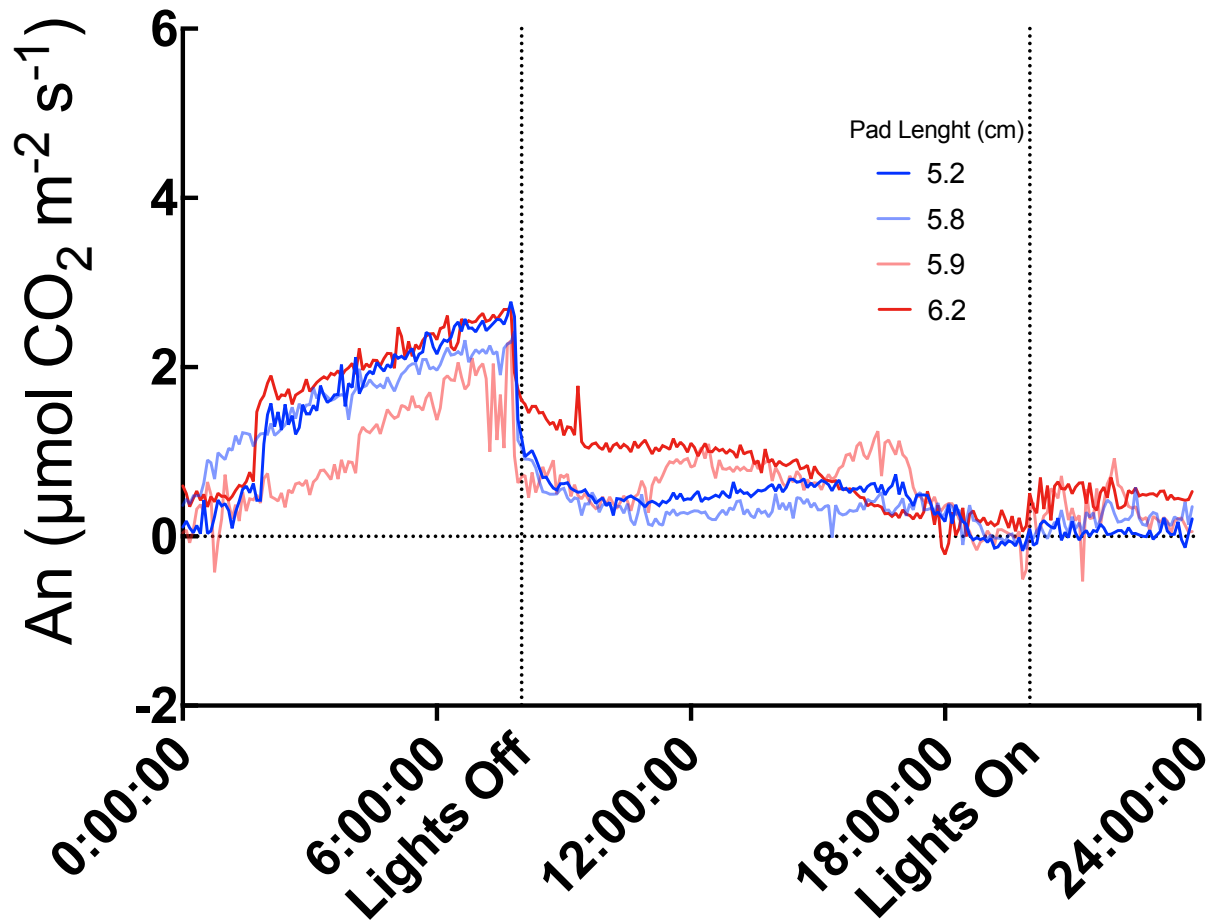


Figure 30: 4rth set of 6 24-hour gas exchange measurements of *O. ficus-indica* seedling 6 grown at a PAR of  $300 \mu\text{mol m}^{-2} \text{ s}^{-1}$  at  $20^\circ\text{C}$  in well-watered conditions as the central cladode grows (Dark blue to light blue to light red to dark red). The assimilation rate ( $\mu\text{mol CO}_2 \text{ m}^{-2} \text{ S}^{-1}$ ) was logged every 5 minutes.

## Seedling 7 - PAR 300

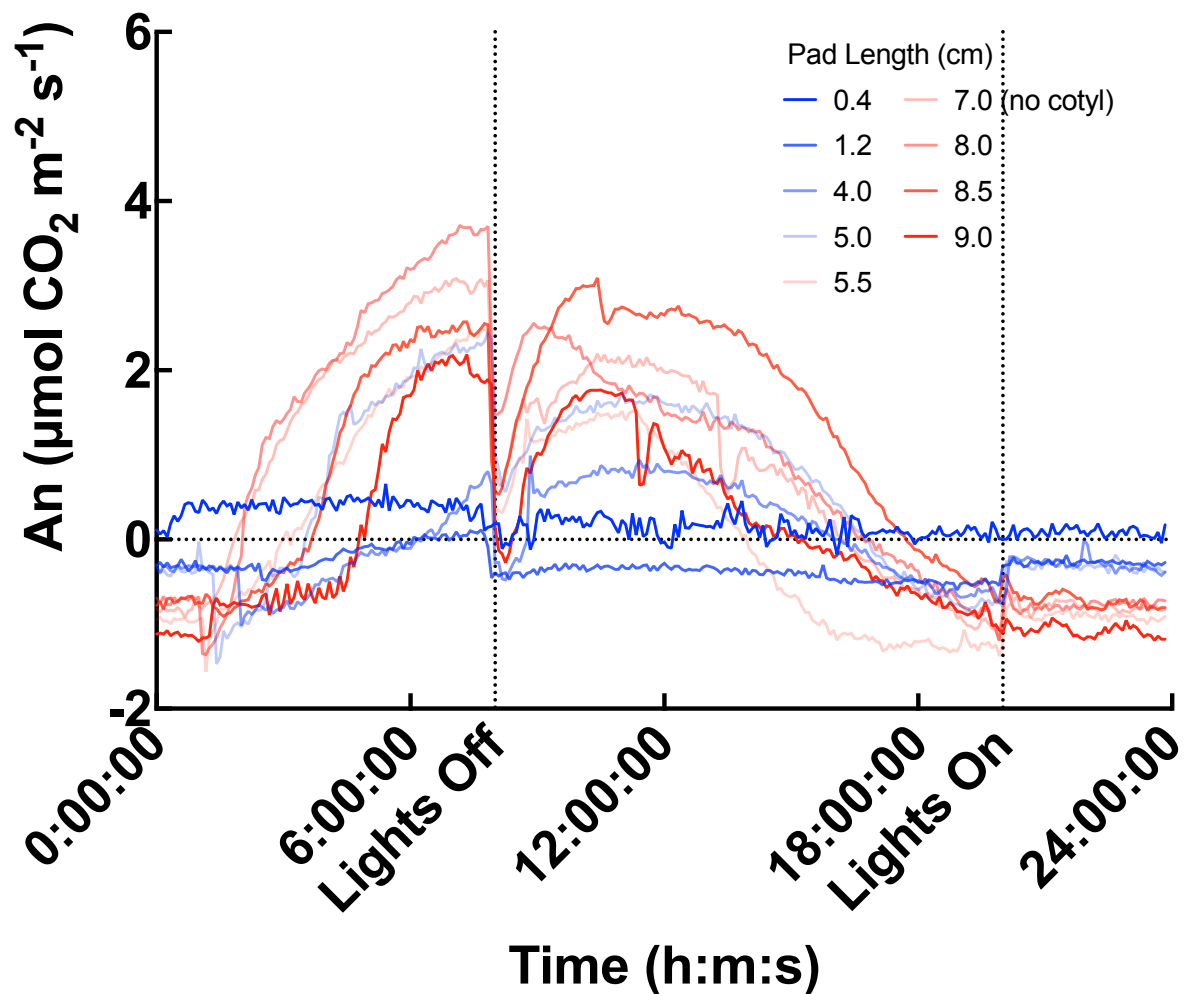


Figure 31: 24-hour gas exchange measurements of *O. ficus-indica* seedling 7 grown at a PAR of  $300 \mu\text{mol m}^{-2} \text{ s}^{-1}$  at  $20^\circ\text{C}$  in well-watered conditions as the central cladode grows (Dark blue to light blue to light red to dark red). The assimilation rate ( $\mu\text{mol CO}_2 \text{ m}^{-2} \text{ S}^{-1}$ ) was logged every 5 minutes.



## Seedling 8 - PAR 100

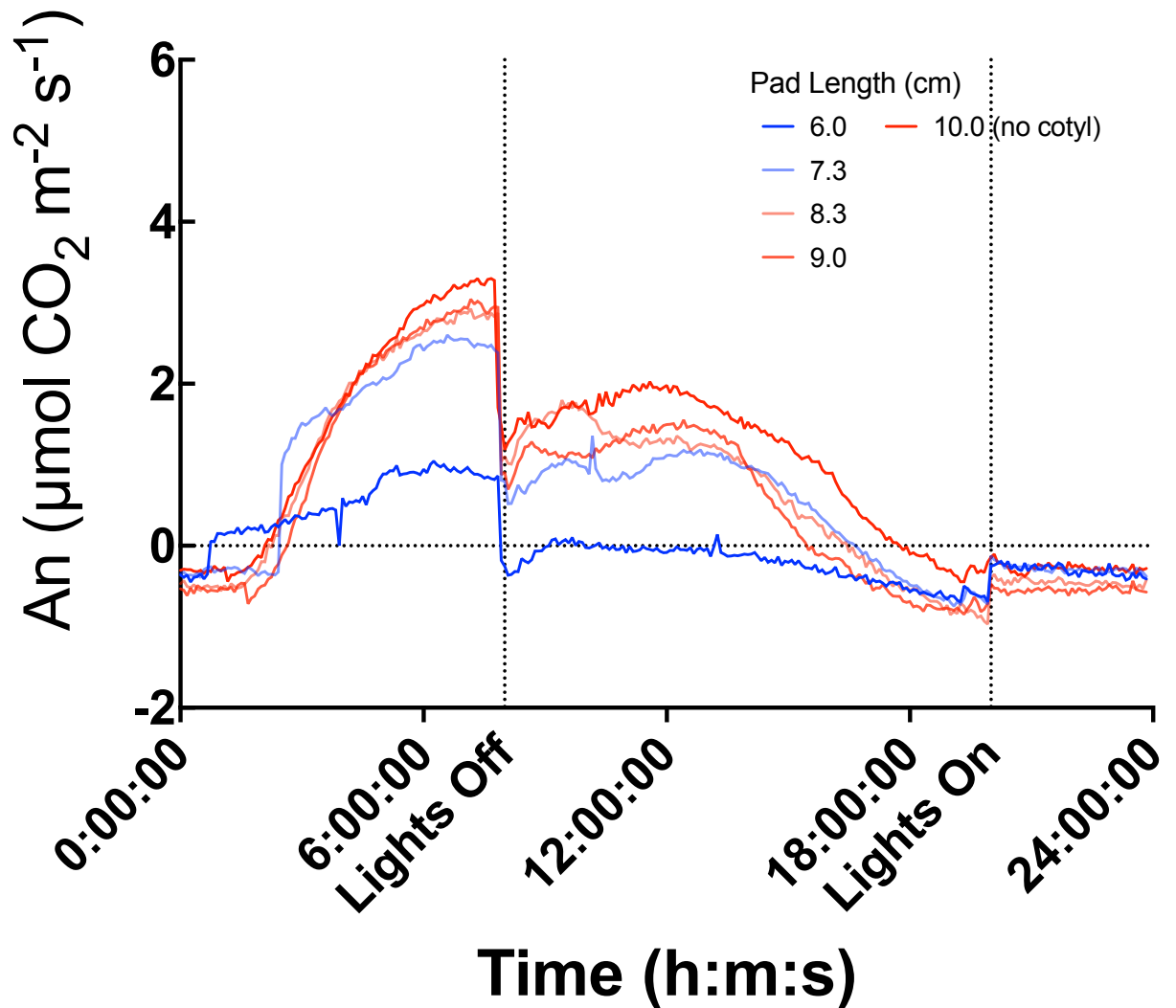
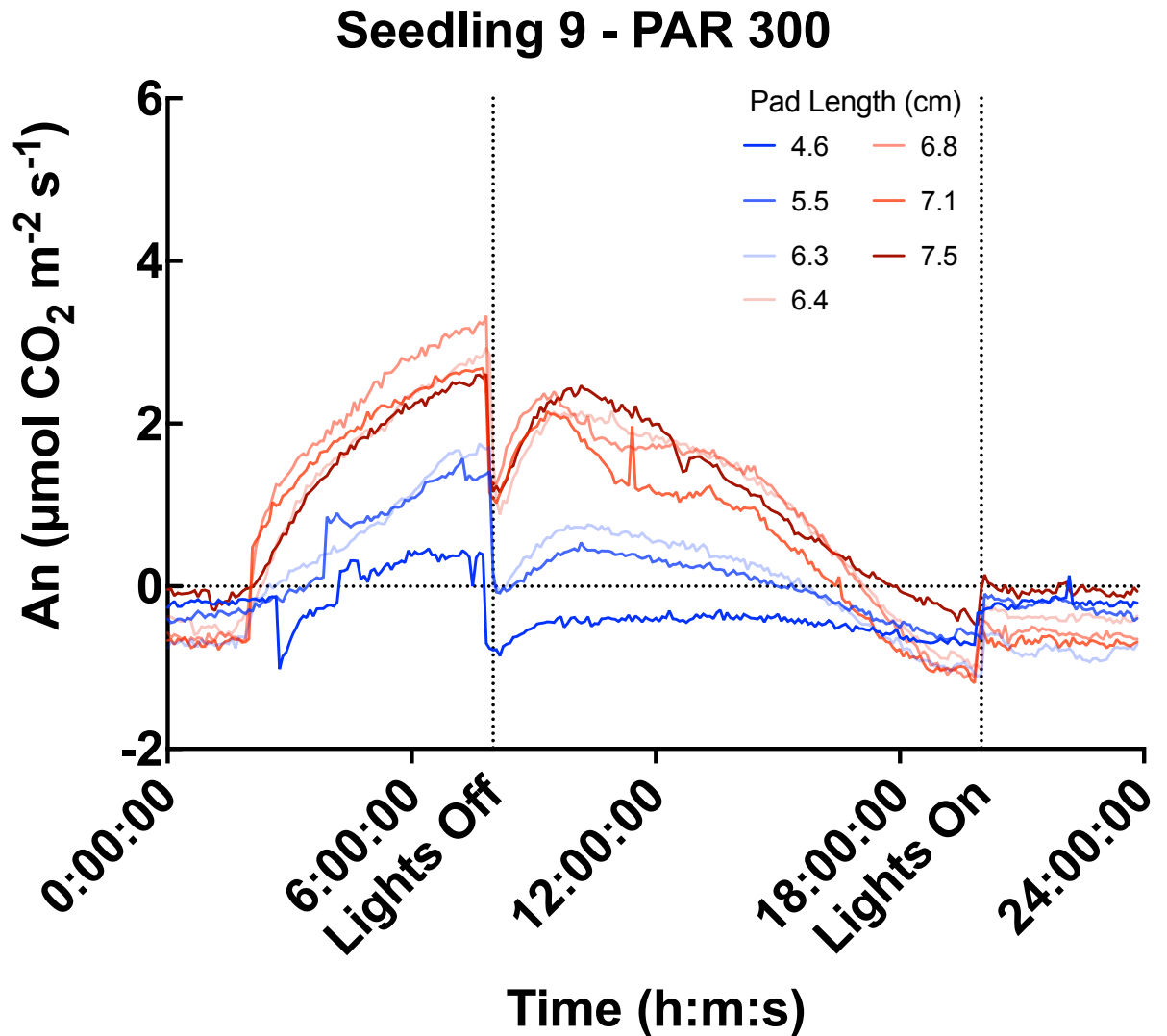


Figure 32: 24-hour gas exchange measurements of *O. ficus-indica* seedling 8 grown at a PAR of  $300 \mu\text{mol m}^{-2} \text{ s}^{-1}$  at  $20^\circ \text{C}$  in well-watered conditions as the central cladode grows (Dark blue to light blue to light red to dark red). The assimilation rate ( $\mu\text{mol CO}_2 \text{ m}^{-2} \text{ S}^{-1}$ ) was logged every 5 minutes.



*Figure 33:* 24-hour gas exchange measurements of *O. ficus-indica* seedling 9 grown at a PAR of  $300 \mu\text{mol m}^{-2} \text{s}^{-1}$  at  $20^\circ\text{C}$  in well-watered conditions as the central cladode grows (Dark blue to light blue to light red to dark red). The assimilation rate ( $\mu\text{mol CO}_2 \text{m}^{-2} \text{S}^{-1}$ ) was logged every 5 minutes.

## Seedling 6 - PAR 300

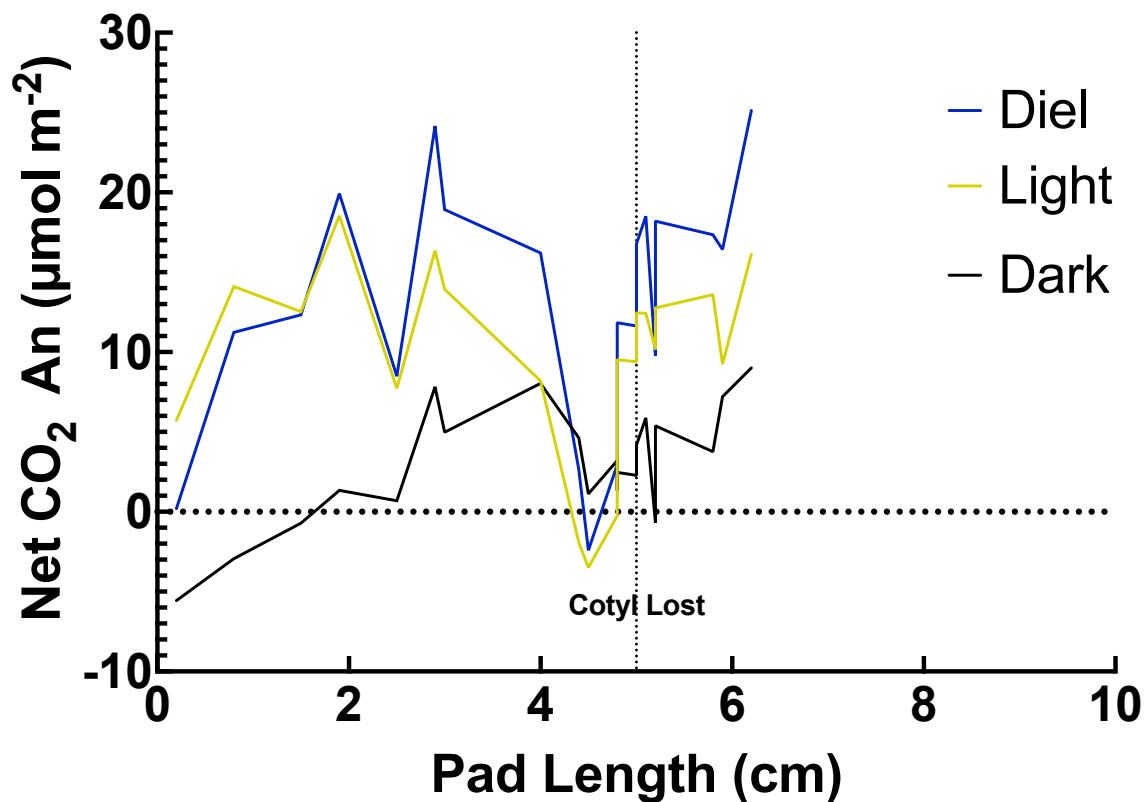


Figure 34: The diel (blue line), light (yellow line), and dark (black line) net assimilated CO<sub>2</sub> (µmol m<sup>-2</sup>) vs. cladode length (cm) in *O. ficus-indica* seedling 6 grown at PAR of 300 µmol m<sup>-2</sup> s<sup>-1</sup> at 20 °C in well-watered conditions.

## Seedling 7 - PAR 300

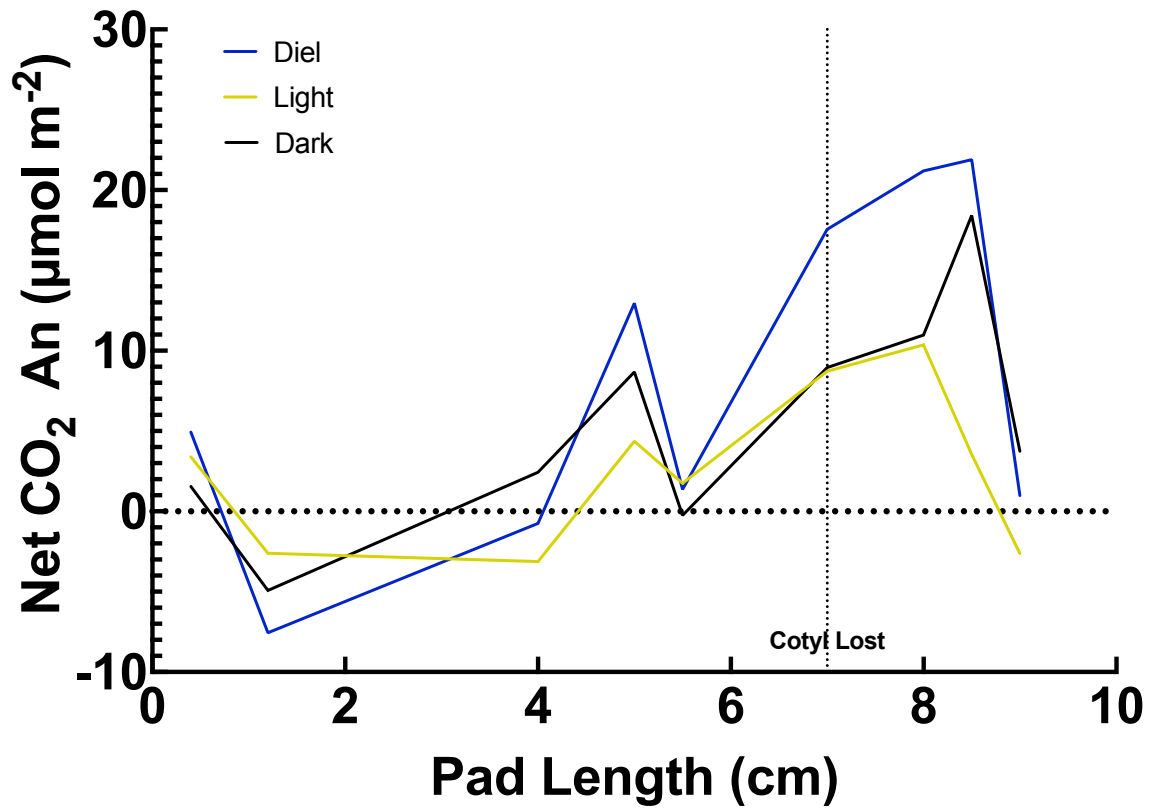


Figure 35: The diel (blue line), light (yellow line), and dark (black line) net assimilated CO<sub>2</sub> (µmol m<sup>-2</sup>) vs. cladode length (cm) in *O. ficus-indica* seedling 7 grown at PAR of 300 µmol m<sup>-2</sup> s<sup>-1</sup> at 20 °C in well-watered conditions.

## Seedling 8 - PAR 300

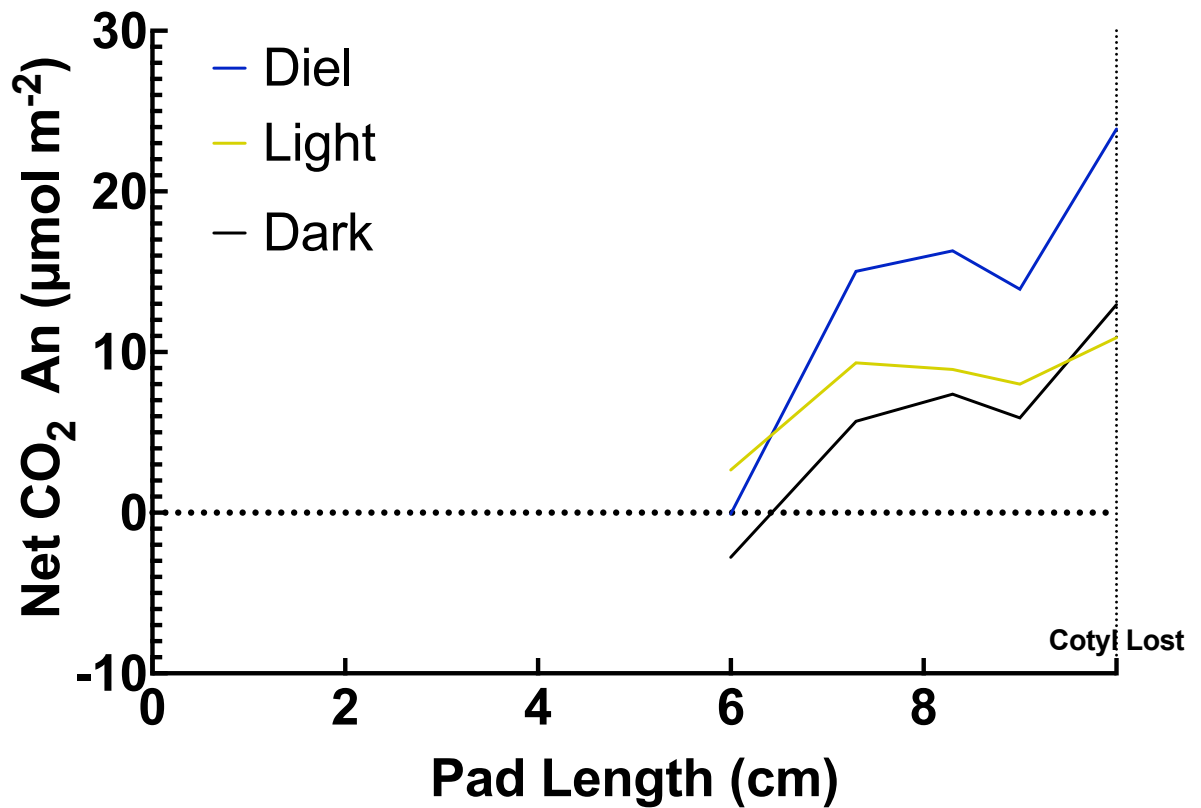
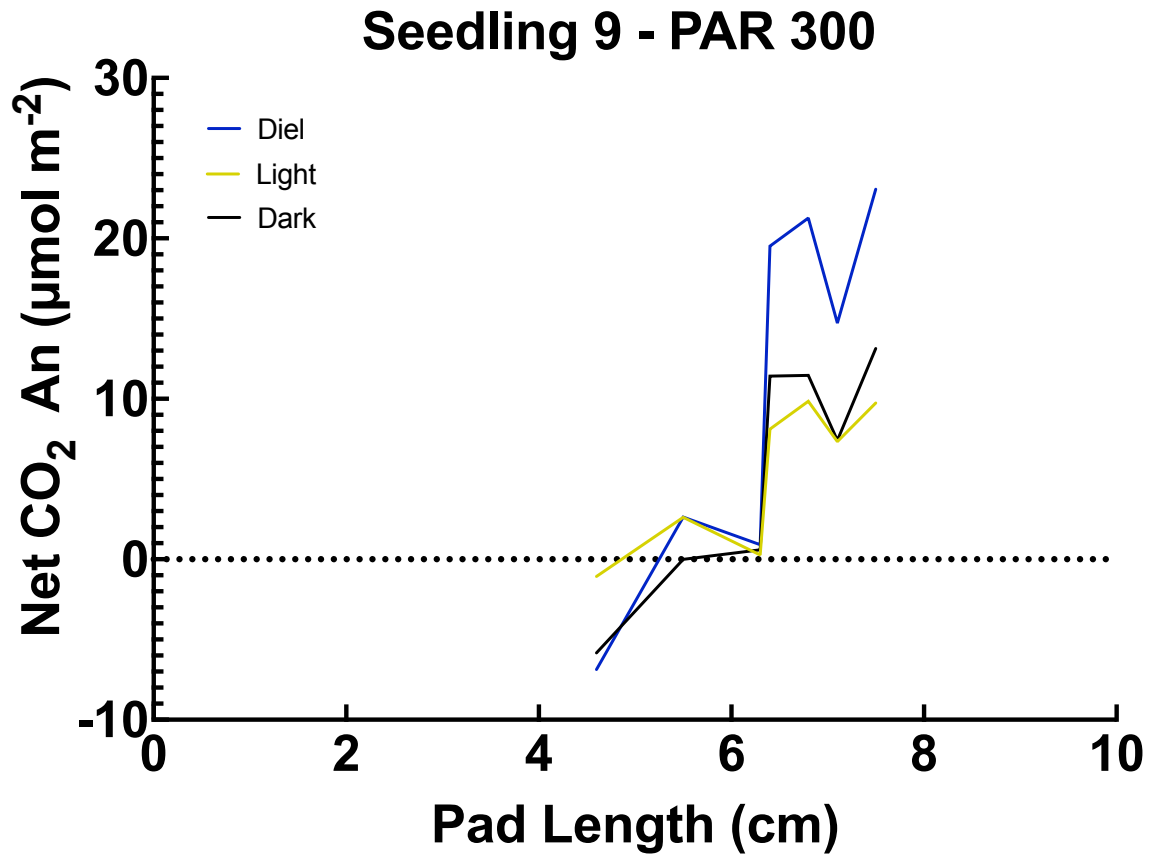


Figure 36: The diel (blue line), light (yellow line), and dark (black line) net assimilated CO<sub>2</sub> (µmol m<sup>-2</sup>) vs. cladode length (cm) in *O. ficus-indica* seedling 8 grown at PAR of 300 µmol m<sup>-2</sup> s<sup>-1</sup> at 20 °C in well-watered conditions.



*Figure 37:* The diel (blue line), light (yellow line), and dark (black line) net assimilated CO<sub>2</sub> (µmol m<sup>-2</sup>) vs. cladode length (cm) in *O. ficus-indica* seedling 9 grown at PAR of 300 µmol m<sup>-2</sup> s<sup>-1</sup> at 20 °C in well-watered conditions.

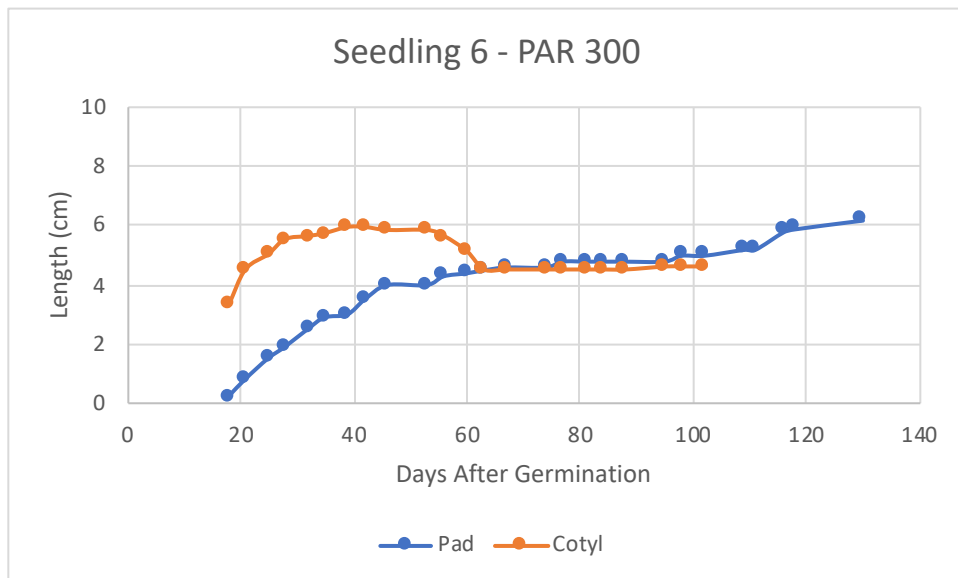


Figure 38: Measured length (cm) of *O. ficus-indica* seedling 6 central cladode (blue dots and line) and combined cotyledons (orange dots and line) within the gas exchange sample period (days after germination). Grown at PAR of 300  $\mu\text{mol m}^{-2} \text{s}^{-1}$  at 20 °C in well-watered conditions.

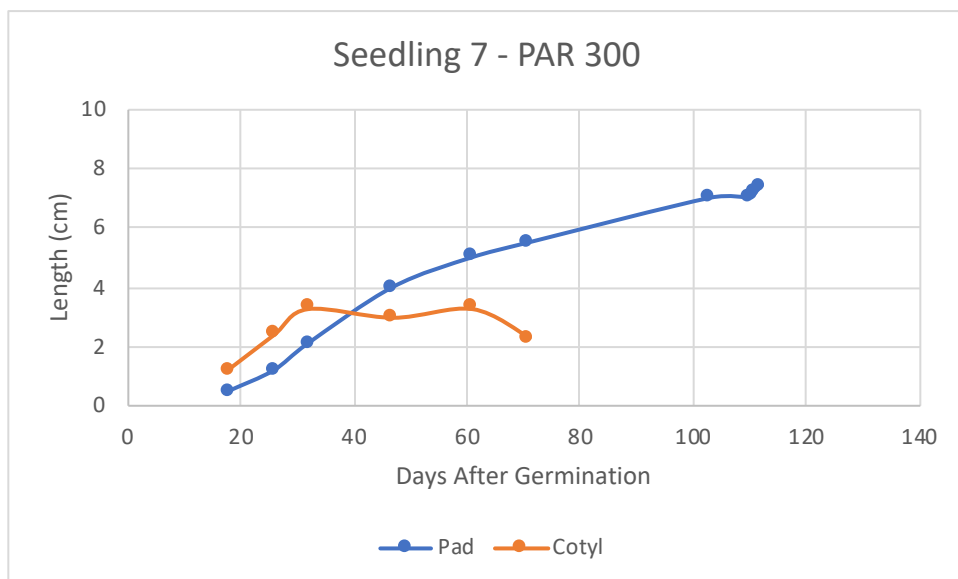
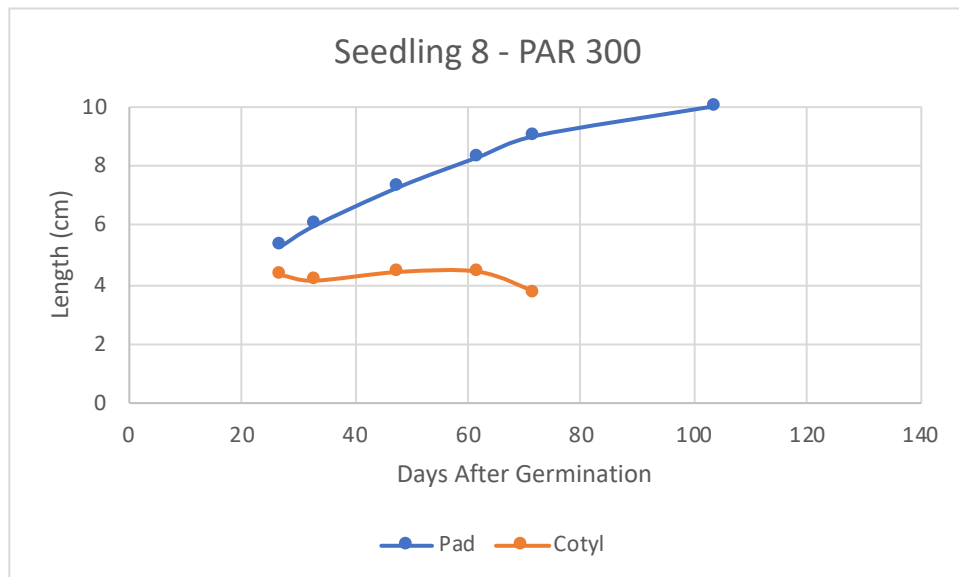


Figure 39: Measured length (cm) of *O. ficus-indica* seedling 7 central cladode (blue dots and line) and combined cotyledons (orange dots and line) within the

gas exchange sample period (days after germination). Grown at PAR of  $300 \mu\text{mol m}^{-2} \text{s}^{-1}$  at  $20 \text{ }^\circ\text{C}$  in well-watered conditions.



*Figure 40:* Measured length (cm) of *O. ficus-indica* seedling 8 central cladode (blue dots and line) and combined cotyledons (orange dots and line) within the gas exchange sample period (days after germination). Grown at PAR of  $300 \mu\text{mol m}^{-2} \text{s}^{-1}$  at  $20 \text{ }^\circ\text{C}$  in well-watered conditions.



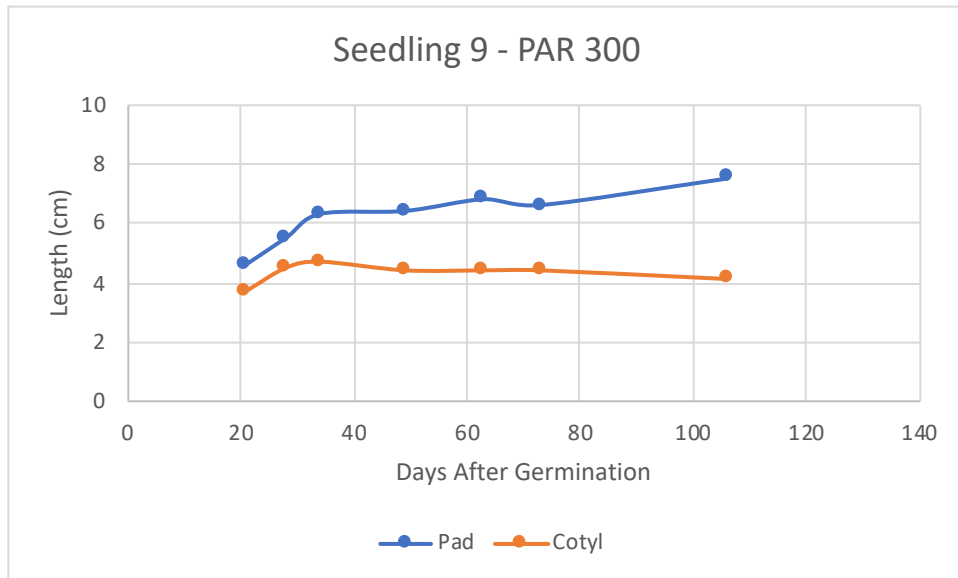


*Figure 41:* Measured length (cm) of *O. ficus-indica* seedling 9 central cladode (blue dots and line) and combined cotyledons (orange dots and line) within the gas exchange sample period (days after germination). Grown at PAR of 300  $\mu\text{mol m}^{-2} \text{s}^{-1}$  at 20 °C in well-watered conditions.

# Daughter Pad 1

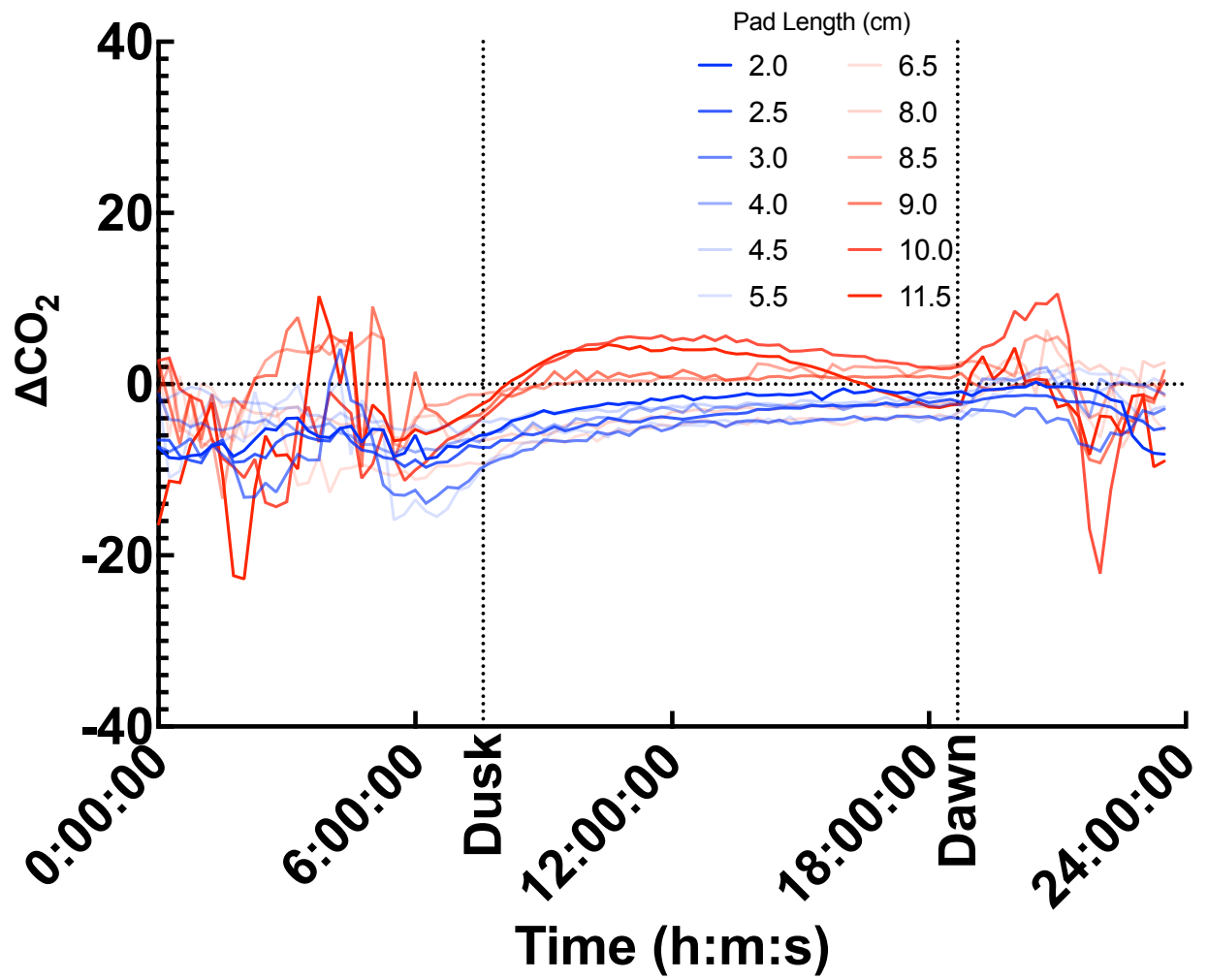
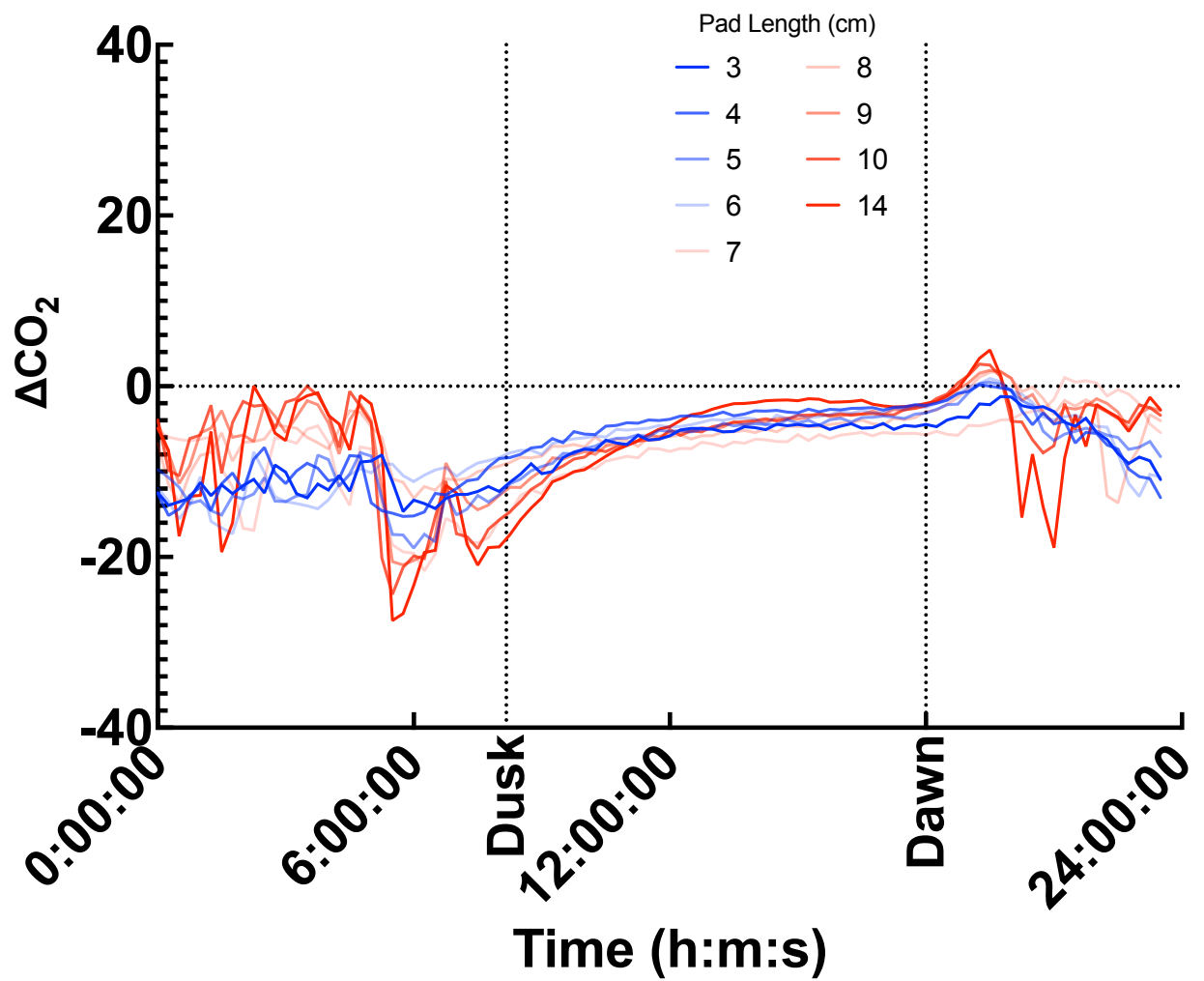


Figure 42: 24-hour gas exchange measurements of *O. ficus-indica* daughter cladode 1 in the custom-built chamber as the cladode grows (Dark blue to light blue to light red to dark red) under standard greenhouse conditions with natural light at approx.  $1,100\text{-}1,500 \mu\text{mol m}^{-2} \text{s}^{-1}$  and temperature at  $28\text{-}32 \text{ }^\circ\text{C}$  day/ $17\text{-}18 \text{ }^\circ\text{C}$  night. The  $\Delta\text{CO}_2$  (ppm) is equal to the sample chamber subtracted by the reference chamber and was logged every 10 minutes.

## Daughter Pad 2



*Figure 43:* 24-hour gas exchange measurements of *O. ficus-indica* daughter cladode 2 in the custom-built chamber as the cladode grows (Dark blue to light blue to light red to dark red) under standard greenhouse conditions with natural light at approx.  $1,100-1,500 \mu\text{mol m}^{-2} \text{s}^{-1}$  and temperature at  $28-32 \text{ }^\circ\text{C}$  day/ $17-18 \text{ }^\circ\text{C}$  night. The  $\Delta\text{CO}_2$  (ppm) is equal to the sample chamber subtracted by the reference chamber and was logged every 10 minutes.

## Daughter Pad 3

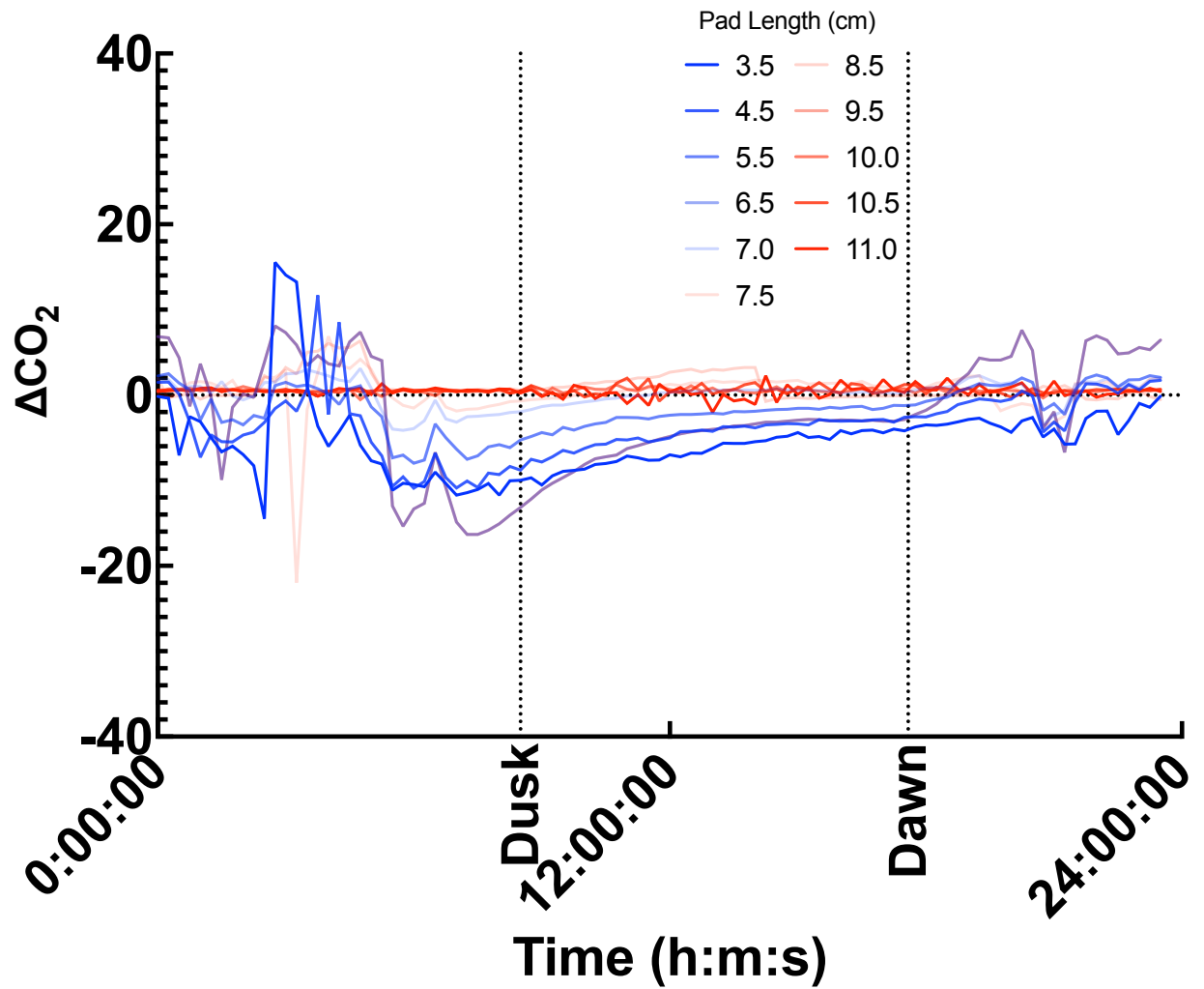
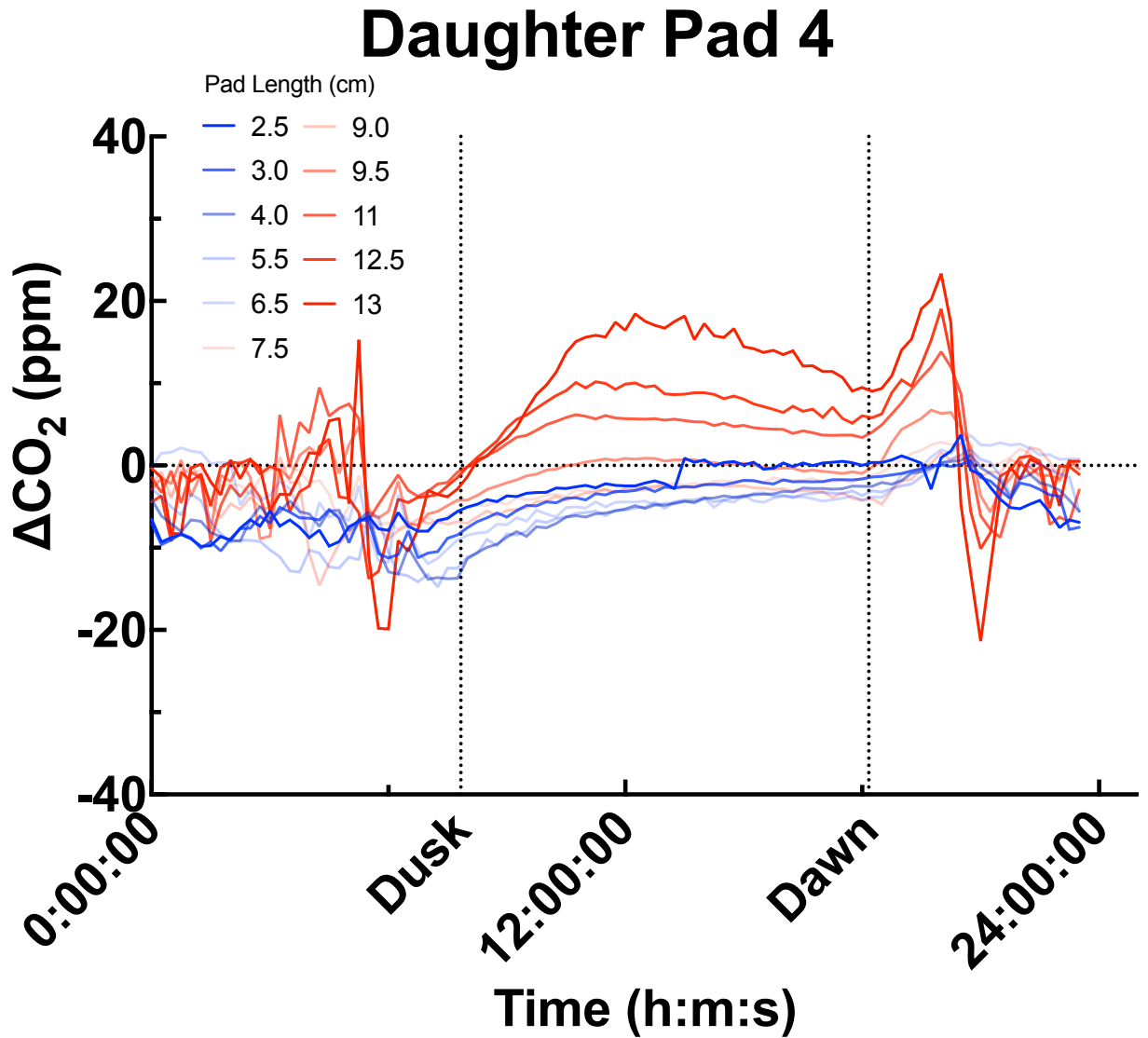


Figure 44: 24-hour gas exchange measurements of *O. ficus-indica* daughter cladode 3 in the custom-built chamber as the cladode grows (Dark blue to light blue to light red to dark red) under standard greenhouse conditions with natural light at approx.  $1,100\text{-}1,500 \mu\text{mol m}^{-2} \text{s}^{-1}$  and temperature at  $28\text{-}32 \text{ }^\circ\text{C}$  day/ $17\text{-}18 \text{ }^\circ\text{C}$  night. The  $\Delta\text{CO}_2$  (ppm) is equal to the sample chamber subtracted by the reference chamber and was logged every 10 minutes.



*Figure 45:* 24-hour gas exchange measurements of *O. ficus-indica* daughter cladode 4 in the custom-built chamber as the cladode grows (Dark blue to light blue to light red to dark red) under standard greenhouse conditions with natural light at approx.  $1,100\text{-}1,500 \mu\text{mol m}^{-2} \text{s}^{-1}$  and temperature at  $28\text{-}32 \text{ }^\circ\text{C}$  day/ $17\text{-}18 \text{ }^\circ\text{C}$  night. The  $\Delta\text{CO}_2$  (ppm) is equal to the sample chamber subtracted by the reference chamber and was logged every 10 minutes.

## Daughter Pad 5

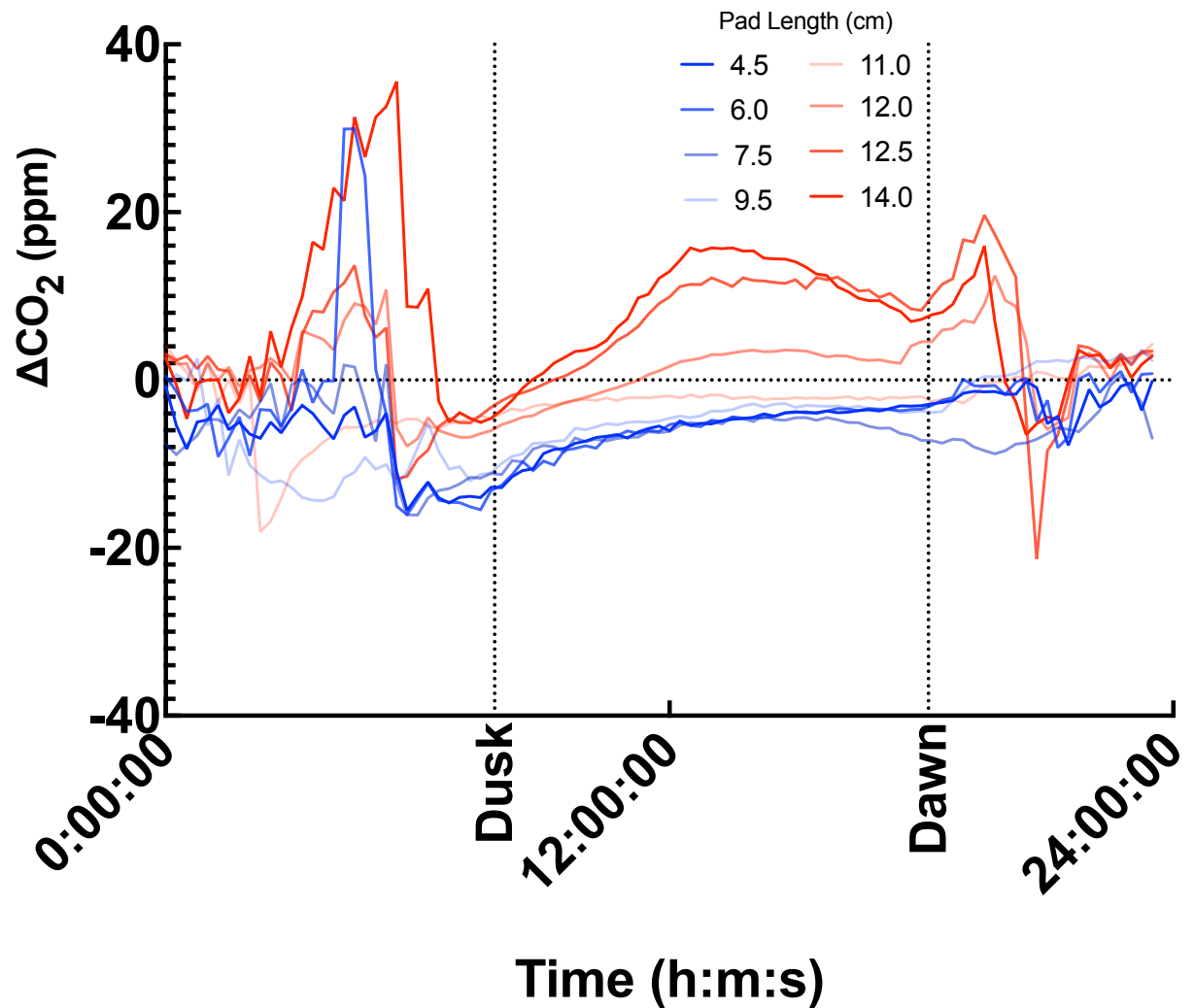


Figure 46: 24-hour gas exchange measurements of *O. ficus-indica* daughter cladode 5 in the custom-built chamber as the cladode grows (Dark blue to light blue to light red to dark red) under standard greenhouse conditions with natural light at approx.  $1,100\text{-}1,500 \mu\text{mol m}^{-2} \text{s}^{-1}$  and temperature at  $28\text{-}32 \text{ }^\circ\text{C}$  day/ $17\text{-}18 \text{ }^\circ\text{C}$  night. The  $\Delta\text{CO}_2$  (ppm) is equal to the sample chamber subtracted by the reference chamber and was logged every 10 minutes.

## Daughter Pad 1

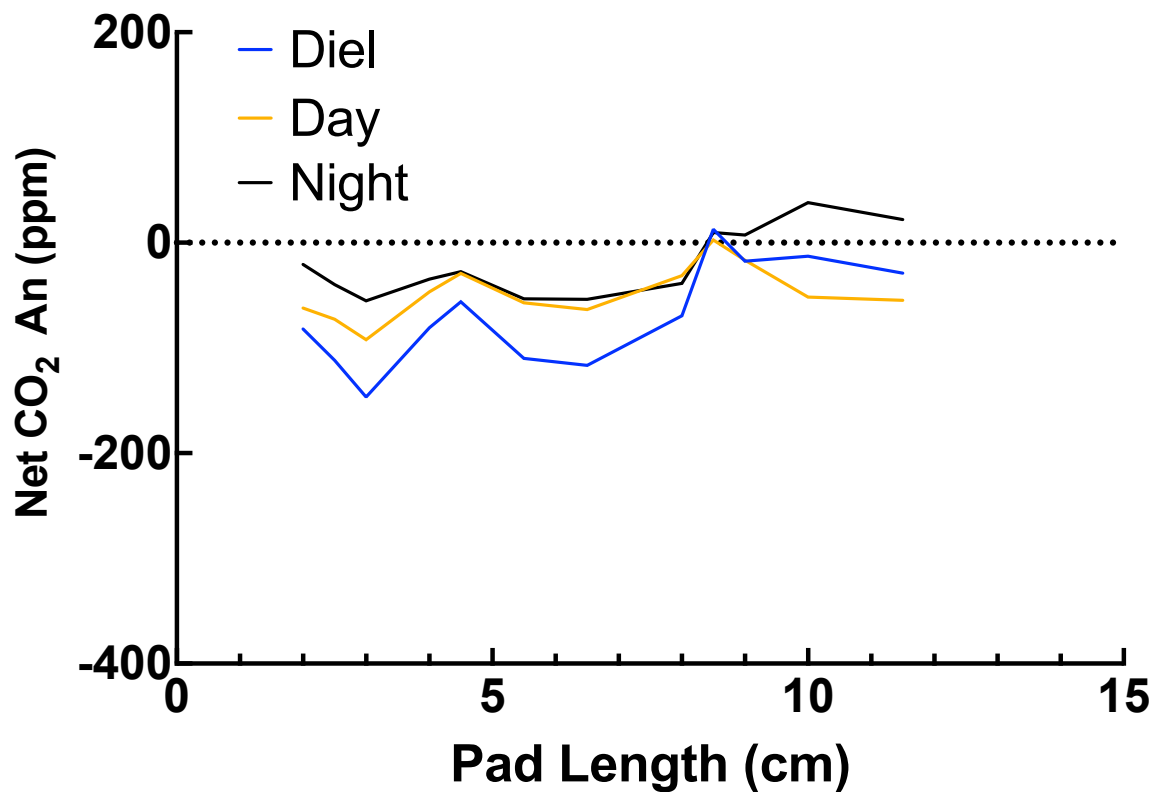


Figure 47: The diel (blue line), light (yellow line), and dark (black line) net assimilated CO<sub>2</sub> (ppm) vs. cladode length (cm) in *O. ficus-indica* daughter cladode 1 grown under standard greenhouse conditions with natural light at approx. 1,100-1,500  $\mu\text{mol m}^{-2} \text{s}^{-1}$  and temperature at 28-32 °C day/17-18 °C night.

## Daughter Pad 2

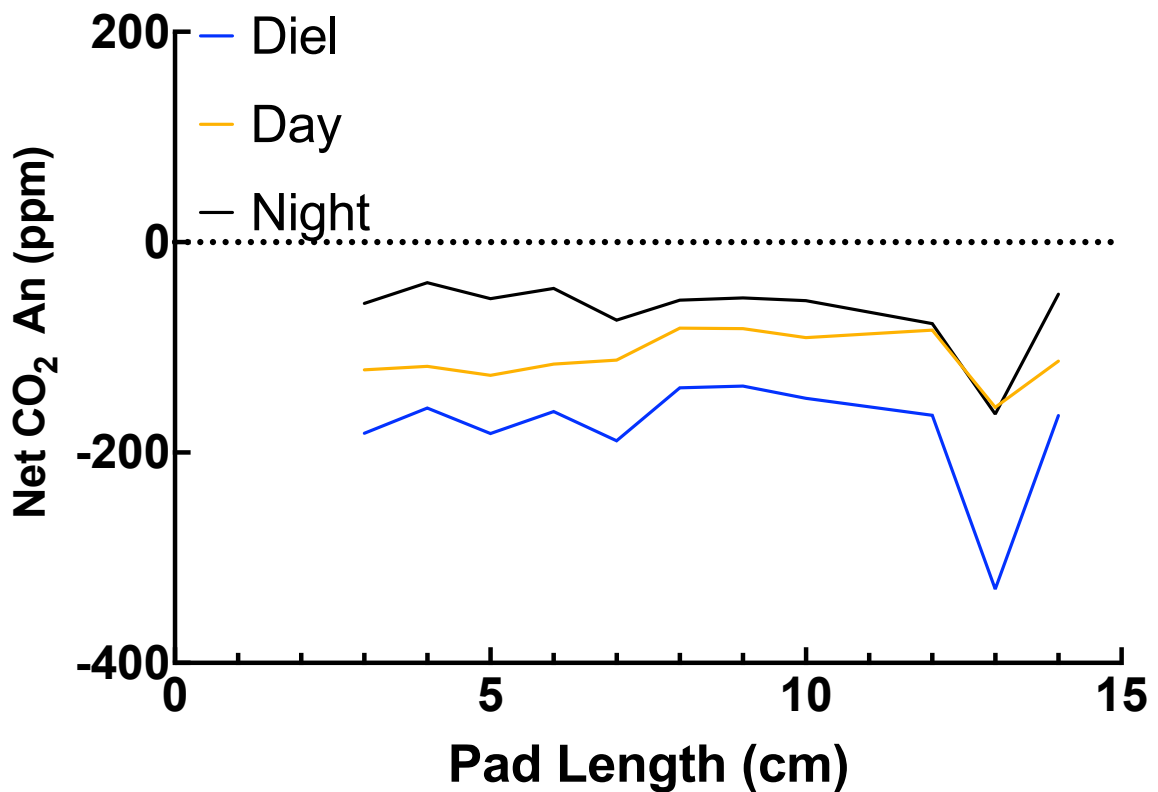


Figure 48: The diel (blue line), light (yellow line), and dark (black line) net assimilated CO<sub>2</sub> (ppm) vs. cladode length (cm) in *O. ficus-indica* daughter cladode 2 grown under standard greenhouse conditions with natural light at approx. 1,100-1,500  $\mu\text{mol m}^{-2} \text{s}^{-1}$  and temperature at 28-32 °C day/17-18 °C night.



## Daughter Pad 3

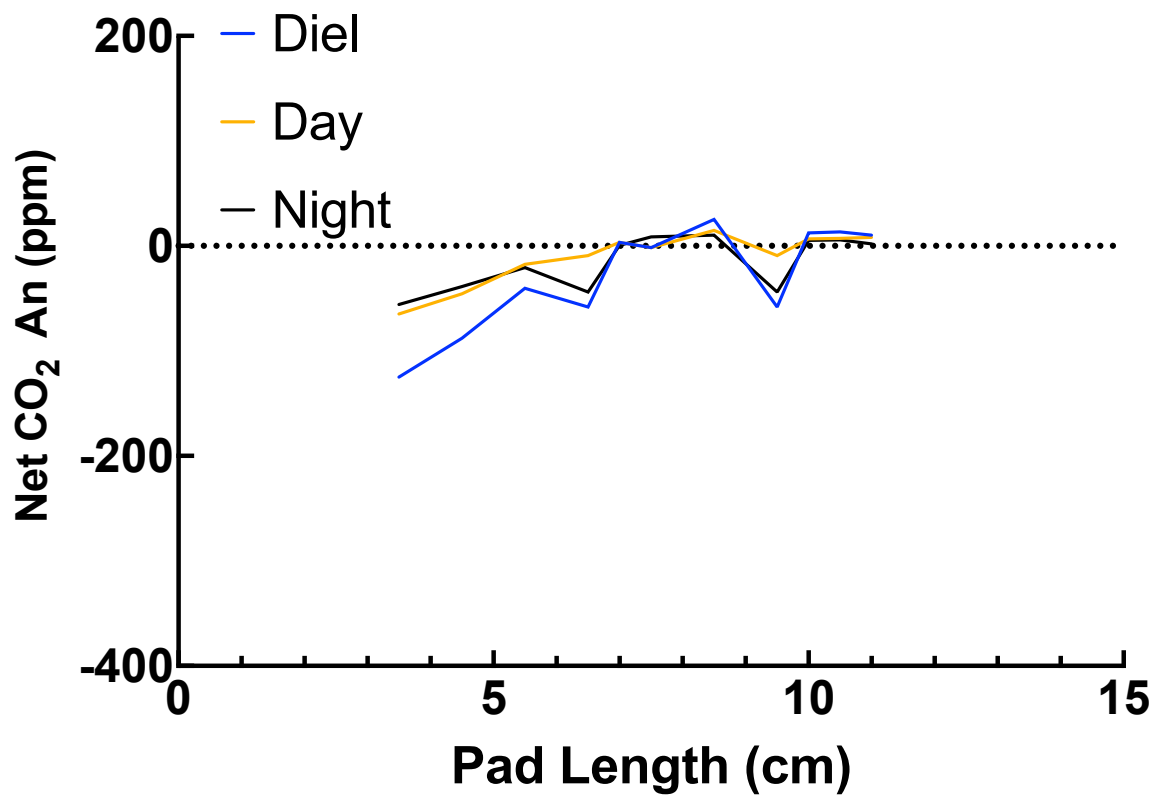
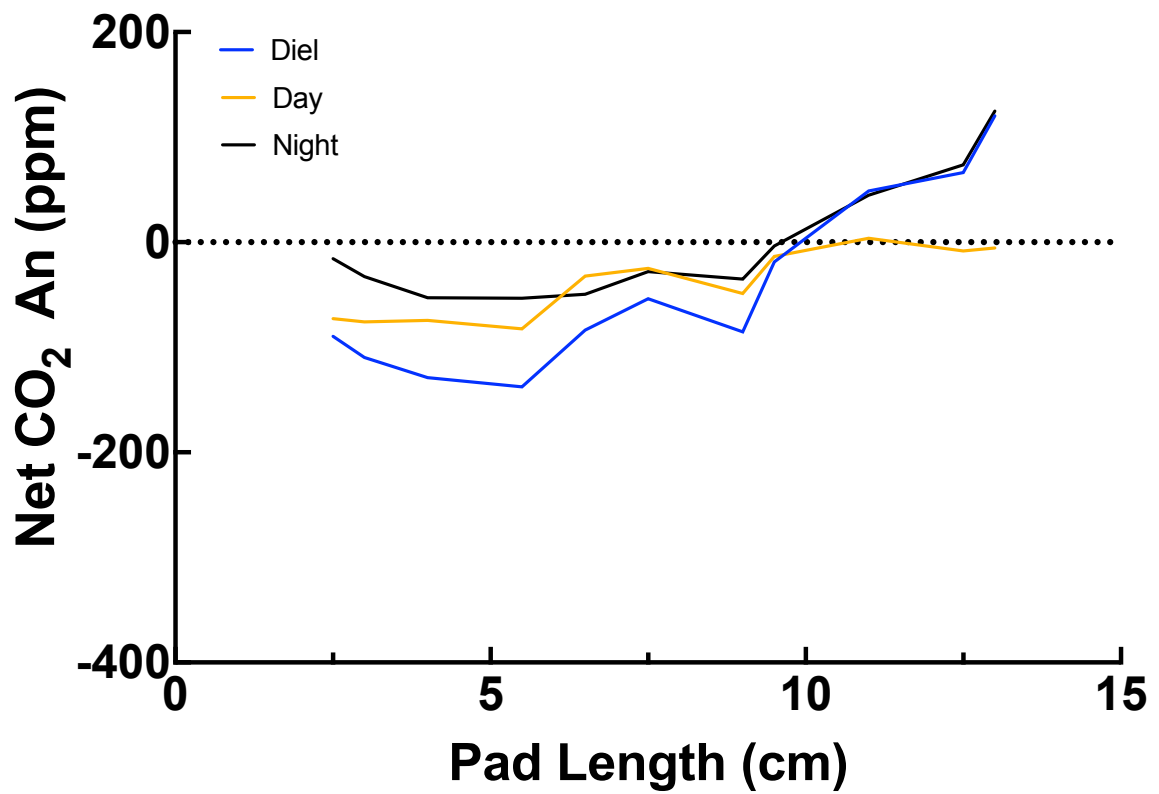


Figure 49: The diel (blue line), light (yellow line), and dark (black line) net assimilated CO<sub>2</sub> (ppm) vs. cladode length (cm) in *O. ficus-indica* daughter cladode 3 grown under standard greenhouse conditions with natural light at approx. 1,100-1,500  $\mu\text{mol m}^{-2} \text{s}^{-1}$  and temperature at 28-32 °C day/17-18 °C night.

## Daughter Pad 4



*Figure 50:* The diel (blue line), light (yellow line), and dark (black line) net assimilated CO<sub>2</sub> (ppm) vs. cladode length (cm) in *O. ficus-indica* daughter cladode 4 grown under standard greenhouse conditions with natural light at approx. 1,100-1,500  $\mu\text{mol m}^{-2} \text{s}^{-1}$  and temperature at 28-32 °C day/17-18 °C night.

## Daughter Pad 5

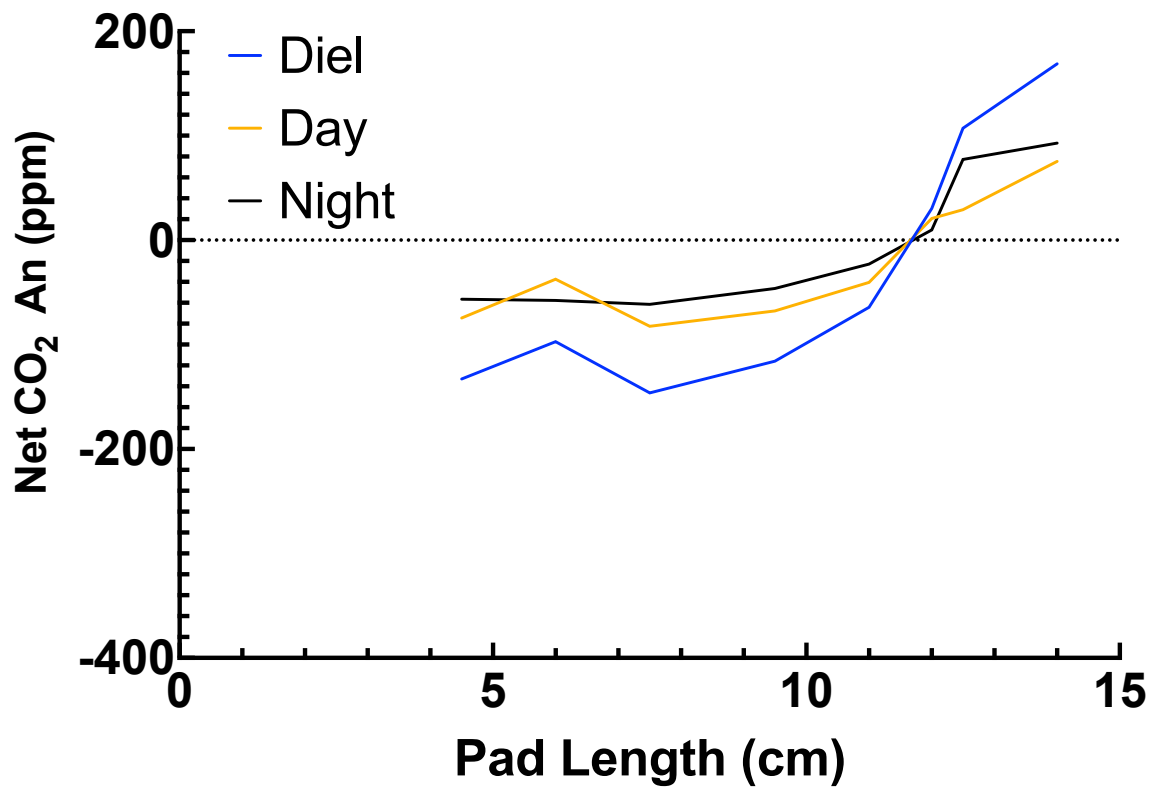


*Figure 51:* The diel (blue line), light (yellow line), and dark (black line) net assimilated CO<sub>2</sub> (ppm) vs. cladode length (cm) in *O. ficus-indica* daughter cladode 5 grown under standard greenhouse conditions with natural light at approx. 1,100-1,500  $\mu\text{mol m}^{-2} \text{s}^{-1}$  and temperature at 28-32 °C day/17-18 °C night.

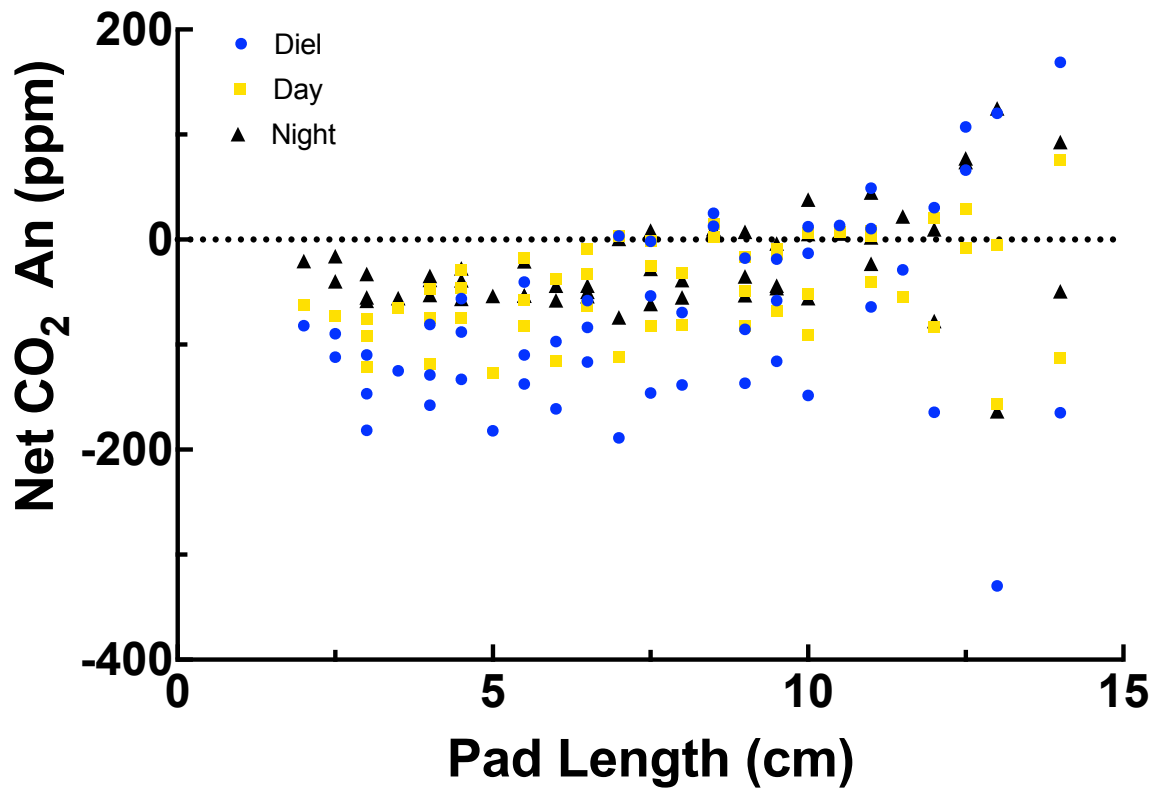
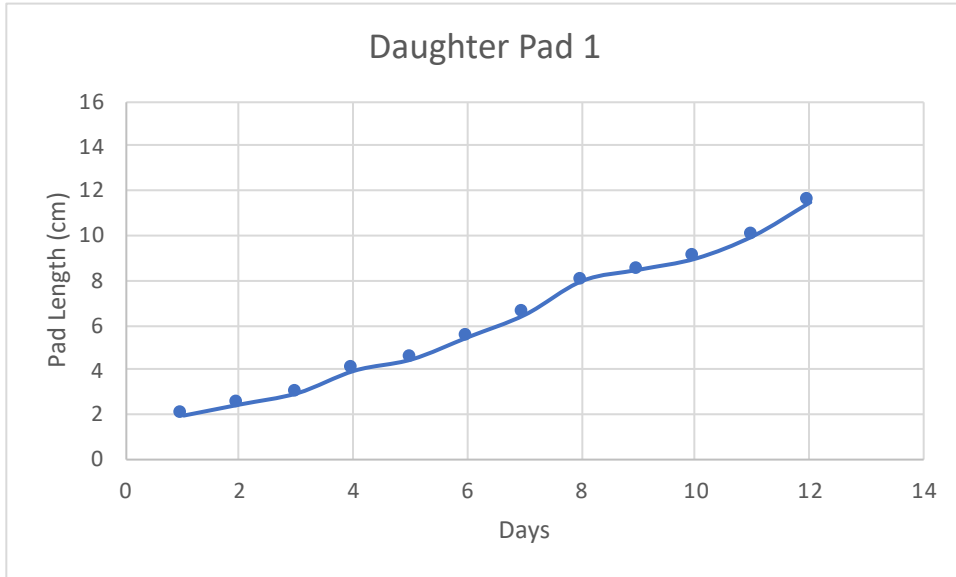


Figure 52: Combined diel (blue circle), light (yellow square), and dark (black triangle) net assimilated CO<sub>2</sub> (ppm) vs. cladode length (cm) in *O. ficus-indica* daughter cladodes grown under standard greenhouse conditions with natural light at approx. 1,100-1,500  $\mu\text{mol m}^{-2} \text{s}^{-1}$  and temperature at 28-32 °C day/17-18 °C night.



*Figure 53:* Measured length (cm) of *O. ficus-indica* daughter cladode 1 (blue dots and line) within the gas exchange sample period (days in chamber) under standard greenhouse conditions with natural light at approx.  $1,100\text{-}1,500 \mu\text{mol m}^{-2} \text{s}^{-1}$  and temperature at  $28\text{-}32 \text{ }^\circ\text{C}$  day/ $17\text{-}18 \text{ }^\circ\text{C}$  night.

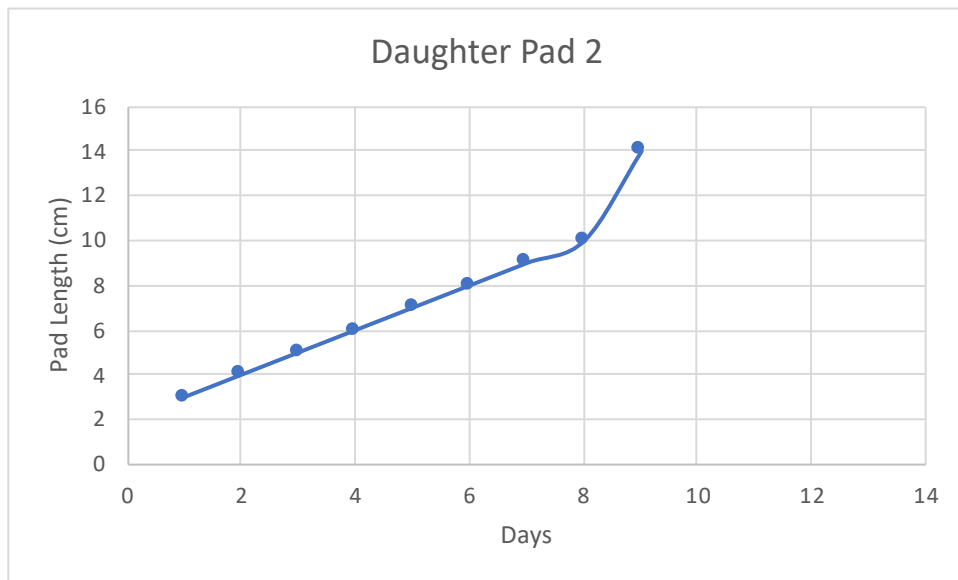


Figure 54: Measured length (cm) of *O. ficus-indica* daughter cladode 2 (blue dots and line) within the gas exchange sample period (days in chamber) under standard greenhouse conditions with natural light at approx.  $1,100-1,500 \mu\text{mol m}^{-2} \text{s}^{-1}$  and temperature at  $28-32 \text{ }^\circ\text{C}$  day/ $17-18 \text{ }^\circ\text{C}$  night.

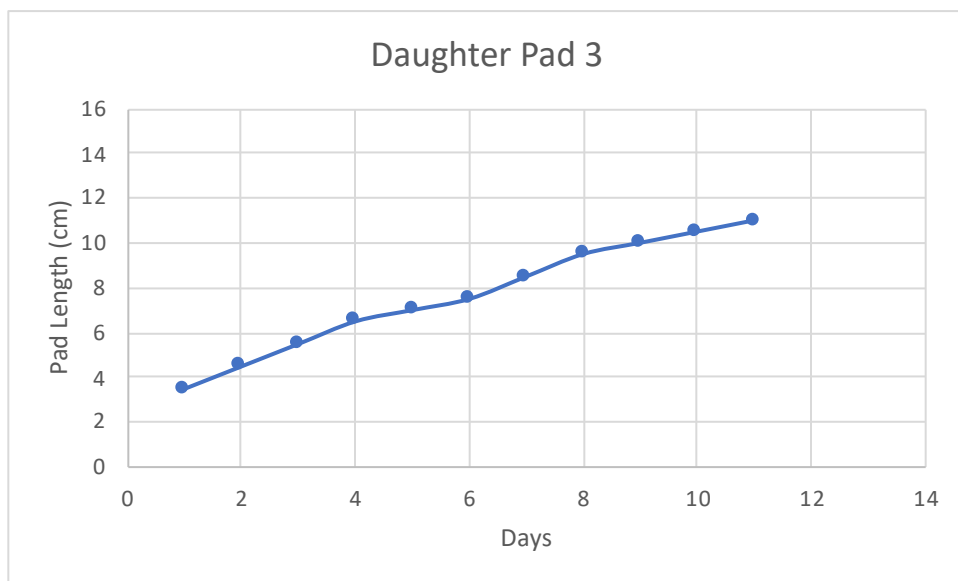
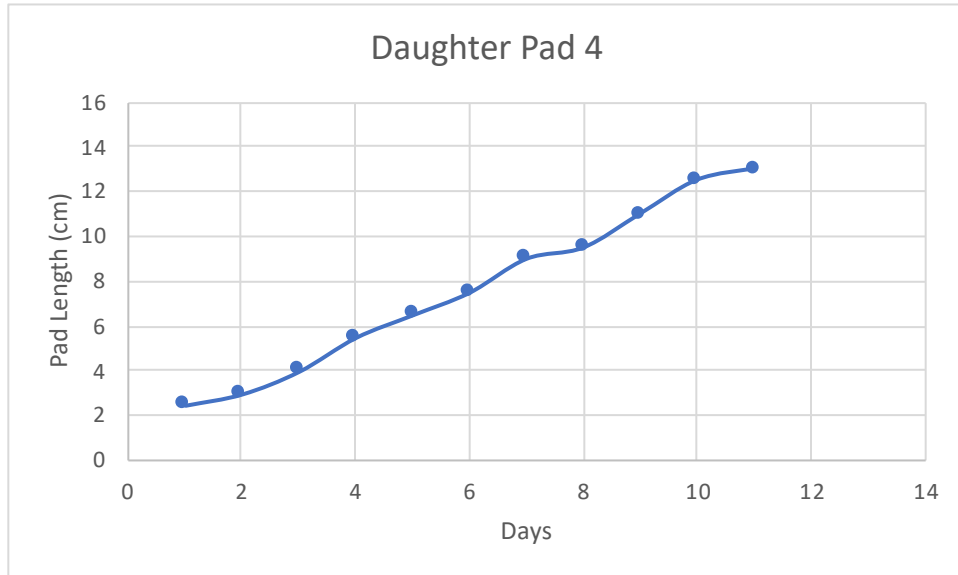
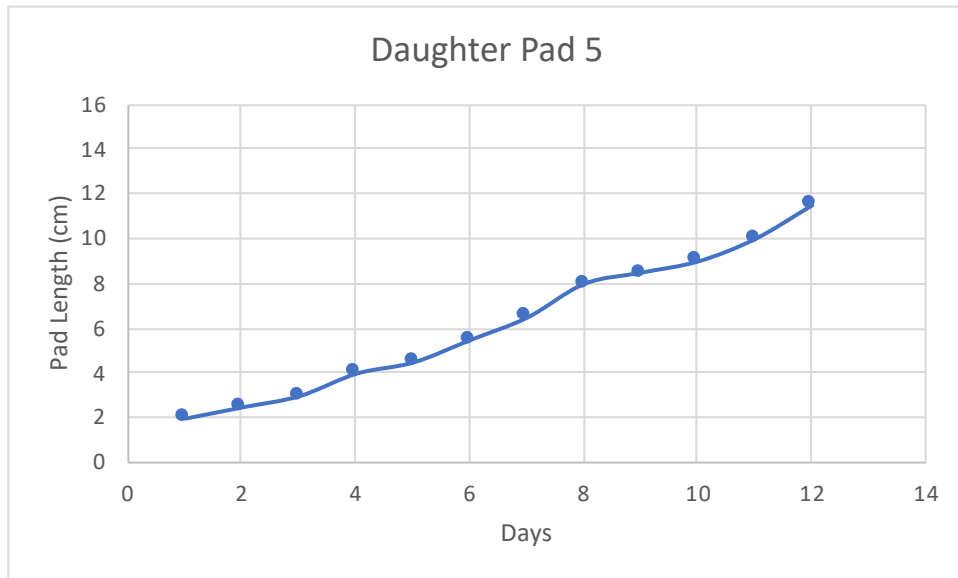


Figure 55: Measured length (cm) of *O. ficus-indica* daughter cladode 3 (blue dots and line) within the gas exchange sample period (days in chamber) under standard

greenhouse conditions with natural light at approx.  $1,100\text{-}1,500\ \mu\text{mol m}^{-2}\ \text{s}^{-1}$  and temperature at  $28\text{-}32\ ^\circ\text{C}$  day/ $17\text{-}18\ ^\circ\text{C}$  night.



*Figure 56:* Measured length (cm) of *O. ficus-indica* daughter cladode 4 (blue dots and line) within the gas exchange sample period (days in chamber) under standard greenhouse conditions with natural light at approx.  $1,100\text{-}1,500\ \mu\text{mol m}^{-2}\ \text{s}^{-1}$  and temperature at  $28\text{-}32\ ^\circ\text{C}$  day/ $17\text{-}18\ ^\circ\text{C}$  night.



*Figure 57:* Measured length (cm) of *O. ficus-indica* daughter cladode 5 (blue dots and line) within the gas exchange sample period (days in chamber) under standard greenhouse conditions with natural light at approx.  $1,100-1,500 \mu\text{mol m}^{-2} \text{s}^{-1}$  and temperature at  $28-32 \text{ }^\circ\text{C}$  day/ $17-18 \text{ }^\circ\text{C}$  night.



## Daughter Pad in Growth Chamber

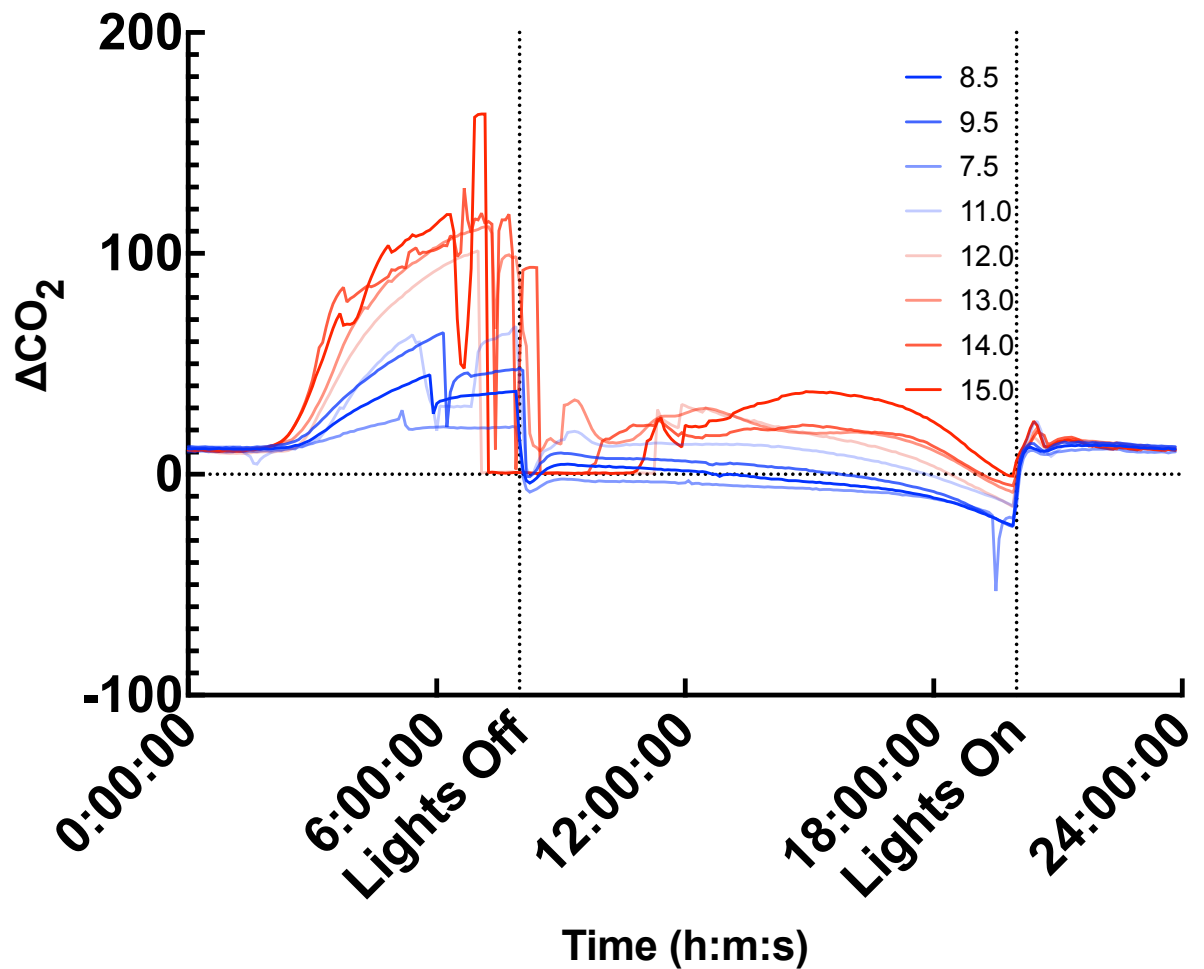


*Figure 58:* 24-hour gas exchange measurements of *O. ficus-indica* daughter cladode in the custom-built chamber as the cladode grows (dark blue to light blue to light red to dark red) within a Conviron growth chamber with a measured PAR at the canopy level of  $367 \mu\text{mol m}^{-2} \text{s}^{-1}$  and temperature at  $25 \text{ }^{\circ}\text{C}$  day and night. The  $\Delta\text{CO}_2$  (ppm) is equal to the sample chamber subtracted by the reference chamber and was logged every 10 minutes.

## Daughter Pad in Growth Chamber

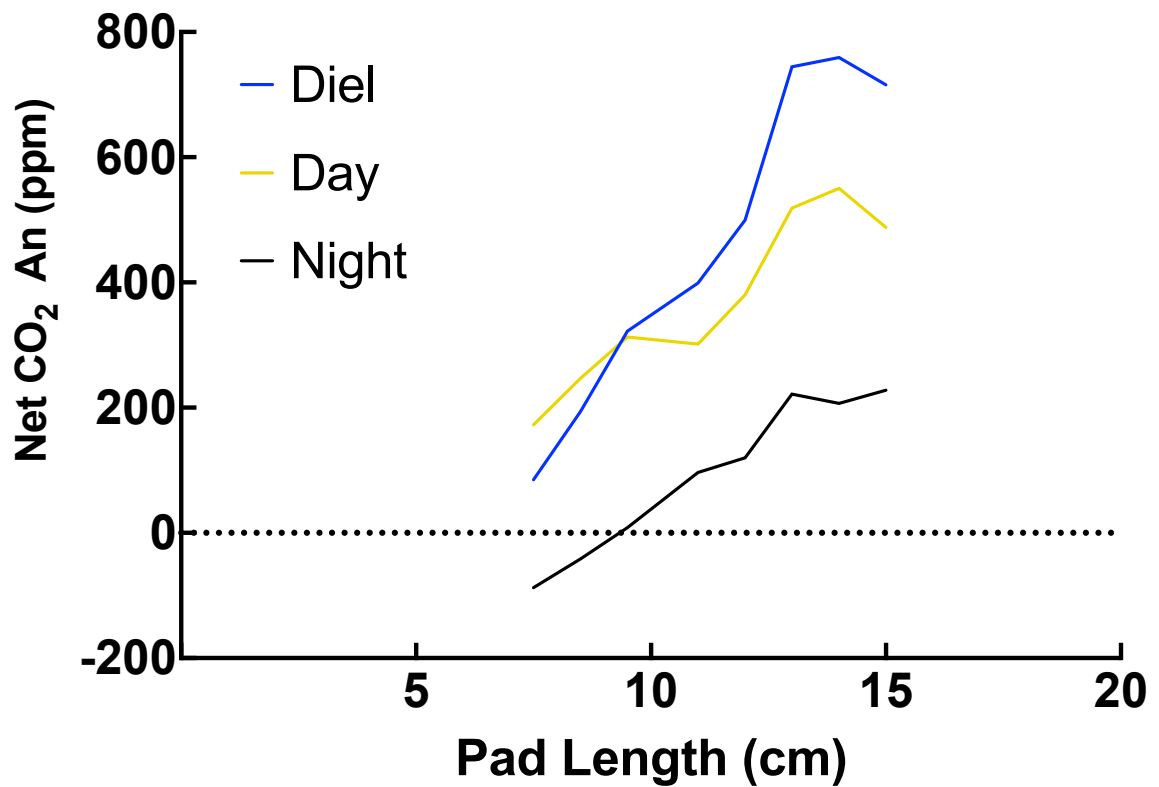


*Figure 59:* The diel (blue line), light (yellow line), and dark (black line) net assimilated CO<sub>2</sub> (ppm) vs. cladode length (cm) in *O. ficus-indica* daughter cladode on an individual growing within a Conviron growth chamber with a measured PAR at the canopy level of  $367 \mu\text{mol m}^{-2} \text{s}^{-1}$  and temperature at  $25 \text{ }^{\circ}\text{C}$  day and night.

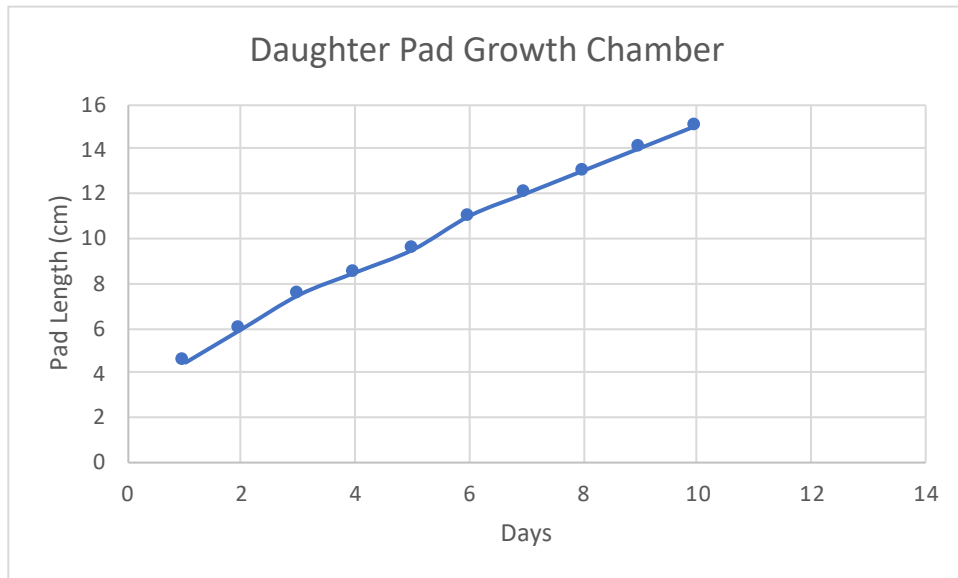


*Figure 60:* Measured length (cm) of *O. ficus-indica* daughter cladode (blue dots and line) within the gas exchange sample period (days in chamber) within a Conviron growth chamber with a measured PAR at the canopy level of  $367 \mu\text{mol m}^{-2} \text{s}^{-1}$  and temperature at  $25 \text{ }^\circ\text{C}$  day and night.

## Germination with and without sucrose

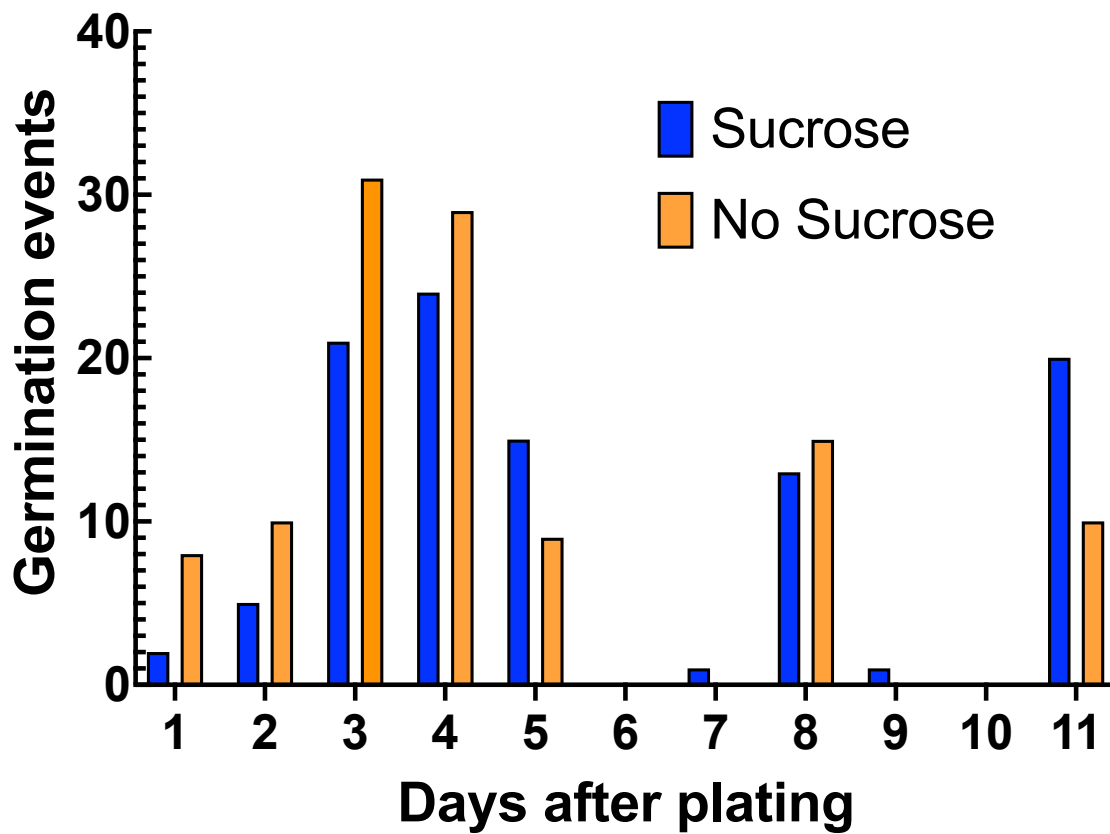


*Figure 61:* Timing and frequency of germination events in *Opuntia ficus-indica* plated in either 3.0% sucrose, 0.6% plant agar, 0.5% Murashige & Skoog medium with Gamborg's B5 vitamins, and a 10mM Gibberellic acid concentration or the same media containing no sucrose. 94 out of 150 seeds germinated in sucrose, and 95 out of 150 seeds germinated in no sucrose. There were no germination events after 11 days.



*Figure 62: Observed *O. ficus-indica* Seedling phenotypes included those with roots emerging from where the cladodes made contact with the hypocotyl (A), tricotyledonous seedling (B), polyembryonic seedlings (C), and di-cladode individuals (D). None of these abnormal phenotypes were used in the experimentation in this study.*

## Curriculum vitae

### Nicholas Alexander Niechayev

*Professional address:*

University of Reno, Nevada  
Department of Biochemistry and Molecular Biology  
1664 North Virginia Street, Reno, NV 89557

*Home address:*

3176 Achilles Dr.  
Reno, NV 89512

(951) 212-6642

nniechayev@nevada.unr.edu

---

#### EDUCATION

University of Nevada, Reno | Reno, NV

**Ph.D. in Biochemistry 2017-present**

Ohio University | Athens, OH

**M.S. in Environmental Studies 2014-2016**

California State University of San Bernardino | San Bernardino, CA

**B.S. in Biology 2010-2014**

#### GRANTS, AWARDS, AND STIPENDS

USDA NIFA Grant awarded 2018

Second place at Ohio University's student research expo 2016

Ohio University Graduate Assistantship Stipend 2014

CSUSB Student Research Competition Award 2014

Dean's List 2013 & 2014

OSR Stipend Awarded 2013

ASI Materials Grant Awarded 2012

ASI Travel Grant Awarded 2012

#### TEACHING EXPERIENCE

University of Nevada, Reno | Reno, NV

**Biochemistry Teaching Assistant 2017**

Led discussion sections, and graded exams.

California State University of San Bernardino | San Bernardino, CA

**Biology Tutor 2011-2014**

Tutored cellular biology courses and graded exams

#### RELATED EXPERIENCE

University of Nevada, Reno | Reno, NV

2017-present

**Research Assistant in Dr. John Cushman's Biochemistry Lab**

Conducting research related to the development, transformation, and productivity of the potential biofuel feedstock *O. ficus-indica*.

Ohio University | Athens, OH  
2014-2016

**Graduate Assistant in Dr. Sarah Davis' Bioenergy and Ecology Lab**

Assisted with the construction and operation of an experimental anaerobic digester, farming of potential biofuel crops, and lab and field experimentation of the potential biofuel feedstock *Agave americana*.

California State University of San Bernardino | San Bernardino, CA  
2011-2014

**Research Assistant in Dr. John Skillman's Plant Eco Physiology Lab**

Provided assistance in the study of seasonal variation in microclimate, plant phenology, and leaf physiology for *Carpobrotus edulis* and *Dudleya edulis* in the San Clemente coastal bluff vegetation, requiring techniques used in Chemistry, Biology, and Statistics.

**WORKS AND PUBLICATIONS**

- Niechayev NA, Mayer JA, Cushman JC. (2021) Developmental dynamics of crassulacean acid metabolism (CAM) in *Opuntia ficus-indica*, an obligate CAM species. *in preparation*.
- Niechayev NA, Pereira PN, & Cushman JC. (2021) The nitrate vs.. ammonium preference of *Opuntia ficus-indica*: a sand culture snapshot. *in preparation*.
- Niechayev NA, & Cushman JC. (2021). The economic and environmental viability of *Opuntia ficus-indica* in the southwestern United States. *in preparation*.
- Ferris C, King N, Niechayev NA, Mayer JA, & Cushman JC. (2021) An optimized Biolistic® and *Agrobacterium* mediated transformation of *Opuntia ficus-indica*. *in preparation*.
- Angres G, Niechayev NA, & Cushman JC. (2021) A field validated cladode area index (CAI) model for *Opuntia spp.* indirect measurements. *in preparation*.
- Neupane D, Mayer JA, Niechayev NA, Bishop CD, & Cushman JC. (2021). Five-year field trial of the biomass productivity and water input response of cactus pear (*Opuntia spp.*) as a bioenergy feedstock for arid lands. *GCB Bioenergy*, 13(4), 719-741. DOI: 10.1111/gcbb.12805
- Pereira, PN, Niechayev, NA, Blair BB., & Cushman JC. (2021). Climate change responses and adaptations in Crassulacean Acid metabolism (CAM) plants. In *Photosynthesis, Respiration, and Climate Change* (pp. 283-329). Springer, Cham. DOI: 10.1007/978-3-030-64926-5\_10
- Davis SC, Simpson J, Gil-Vega KDC, Niechayev NA, Tongerlo EV, Castano NH, Dever LV, & Búrquez, A. (2019). Undervalued potential of crassulacean acid metabolism for current and future agricultural production. *Journal of Experimental Botany*, 70(22), 6521-6537. DOI:10.1093/jxb/erz223
- Niechayev NA, Pereira PN, & Cushman JC. (2019). Understanding trait diversity associated with crassulacean acid metabolism (CAM). *Current opinion in plant biology*, 49, 74-85. DOI: 10.1016/j.pbi.2019.06.004

Niechayev NA, Jones AM, Rosenthal DM, & Davis SC. (2019). A model of environmental limitations on production of *Agave americana* L. grown as a biofuel crop in semi-arid regions. *Journal of Experimental Botany*, 70(22), 6549-6559. DOI:10.1093/jxb/ery383

Davis SC, Kuzmick ER, Niechayev NA, & Hunsaker DJ. (2017). Productivity and water use efficiency of *Agave americana* in the first field trial as bioenergy feedstock on arid lands. *GCB Bioenergy*. 9:314-325. DOI: 10.1111/gcbb.12324

## POSTERS AND TALKS

Niechayev NA, Mayer JA, Henitz C, Bishop C, Neupane D, Pereira P, Angres G, Faris C, King N, Enriquez, Petrusa L, Cushman JC (2021). Development of *Opuntia ficus-indica* for commercial production in the United States. International Virtual Mini-Symposium. Cactacea: Phylogenetics, Evolution and Conservation in the Genomics Era. Phoenix, AZ. September 1-3, 2021.

Neupane D, Niechayev N, Mayer JA, Bishop CD, Cushman JC. Biomass productivity of prickly pear cactus (*Opuntia* spp.) under different irrigation regimes. American Society of Plant Biologists annual meeting, Washington, D.C. July 27-31, 2020.

Niechayev N, Mayer JA, Cushman JC. Developmental dynamics of crassulacean acid metabolism (CAM) in *Opuntia ficus-indica*. American Society of Plant Biologists annual meeting, San Jose, CA. August 4-7, 2019.

Niechayev N, Mayer JA, Cushman JC. Developmental dynamics of crassulacean acid metabolism (CAM) in *Opuntia ficus-indica*. Biology of CAM Plants, Desert Botanical Garden, Phoenix, AZ. March 18-22, 2018.

Niechayev N, Mayer JA, Yim, WC, Cushman JC. Developmental dynamics of crassulacean acid metabolism (CAM) in *Opuntia ficus-indica*. 26<sup>th</sup> Plant and Animal Genome Conference, San Diego, CA. January 12-17, 2018.

Niechayev NA., Beechko AN., Skillman JB. Seasonal variation in microclimate, plant phenology, and leaf physiology for *Carpobrotus edulis* and *Dudleya edulis* in the San Clemente coastal bluff vegetation. Conference paper and poster session presented at the 34<sup>th</sup> New Phytologist Symposium on Systems Biology and Ecology of CAM Plants, Tahoe City, CA. July 14, 2014.

## RELEVANT SKILLS

Completed an in-person factory certified 3-day LI-COR LI-6400XT portable photosynthesis training course, and highly experienced with the LI-COR 6800 portable photosynthesis machine.

Experienced with R, R-studio, PRISM and Matlab statistical programs.

Proficient with Microsoft Office.

Hands on research experience with equipment and techniques involved in field and lab experimentation such as:

- Soil microbe Gas Chromatography
- LI-COR LI-6400 portable photosynthesis systems and light sensors



- Tissue sample titrations
- RT-QPCR and relative expression analysis of target genes
- Isotopic mass spectrometric analysis
- Water potential determination via pressure bomb
- DNA, RNA, protein, and specific metabolite extraction from plant tissues
- Colorimetric assays
- LECO FP928 combustion analyzer operation for N:C ratio determination
- Field trial design and experimentation
- Indirect measurement modeling
- Agricultural/environmental production modeling
- Tissue culture and greenhouse techniques for restoring and maintaining collections
- Seed germination
- Flow cytometry and microscopy for ploidy counting
- Plasmid cloning and plant transformation (*Agrobacterium* and biolistic) protocols
- Oxygen electrodes for photosynthetic and dark respiration rate measurements
- Collection and analysis of soil moisture, texture, and cation exchange capacity
- Growth and life/size stage censuring
- Slide Prep and Microscopy

Possess a Nevada Driver's License and completed a California defensive driving course for the purpose of safely transporting hazardous chemicals.

Years of hands-on experience restoring, maintaining, and operating tractors, automobiles, motorcycles, and small engines.

Avid gardener.

World Tae Kwon Doe Federation certified 1<sup>st</sup> dan black belt.